

**N^ε-Acryloyllysine piperazides as irreversible inhibitors of
transglutaminase 2 – synthesis, structure-activity relationships and
pharmacokinetic profiling**

Wodtke, R.; Hauser, C.; Ruiz-Gómez, G.; Jäckel, E.; Bauer, D.; Lohse, M.; Wong, A.;
Pufe, J.; Ludwig, F.-A.; Fischer, S.; Hauser, S.; Greif, D.; Pisabarro, M. T.; Pietzsch, J.;
Pietsch, M.; Löser, R.;

Originally published:

May 2018

Journal of Medicinal Chemistry 61(2018)10, 4528-4560

DOI: <https://doi.org/10.1021/acs.jmedchem.8b00286>

Perma-Link to Publication Repository of HZDR:

<https://www.hzdr.de/publications/Publ-27127>

Release of the secondary publication
on the basis of the German Copyright Law § 38 Section 4.

N^ε-Acryloyllysine piperazides as irreversible inhibitors of transglutaminase 2 – synthesis, structure-activity relationships and pharmacokinetic profiling[‡]

Robert Wodtke^{a,e,f}, Christoph Hauser^b, Gloria Ruiz-Gómez^c, Elisabeth Jäckel^{a,e},
David Bauer^{a,f}, Martin Lohse^{a,e}, Alan Wong^a, Johanna Pufe^a,
Friedrich-Alexander Ludwig^d, Steffen Fischer^d, Sandra Hauser^a, Dieter Greif^e,
M. Teresa Pisabarro^c, Jens Pietzsch^{a,f}, Markus Pietsch^{b,*}, Reik Löser^{a,f,*}

[a] Helmholtz-Zentrum Dresden-Rossendorf, Institut für Radiopharmazeutische Krebsforschung, Bautzner Landstraße 400, 01328 Dresden, Germany

[b] Zentrum für Pharmakologie, Medizinische Fakultät, Universität zu Köln, Gleueler Straße 24, 50931 Köln, Germany

[c] Structural Bioinformatics, BIOTEC, TU Dresden, Tatzberg 47-51, 01307 Dresden, Germany

[d] Helmholtz-Zentrum Dresden-Rossendorf, Institut für Radiopharmazeutische Krebsforschung, Forschungsstelle Leipzig, Permoserstraße 15, 04318 Leipzig, Germany

[e] Fakultät Natur- und Umweltwissenschaften, Hochschule Zittau/Görlitz, Theodor-Körner-Allee 16, 02763 Zittau, Germany

[f] Fakultät Chemie und Lebensmittelchemie, Technische Universität Dresden, Mommsenstraße 4, 01062 Dresden, Germany

[‡] Dedicated to Profs. Drs. Michael Gütschow and Jörg Steinbach, on the occasion of their 60th and 65th birthdays, respectively, in gratefulness for their past and continuing support.

Abstract:

Transglutaminase 2 (TGase 2)-catalysed transamidation represents an important posttranslational mechanism for protein modification with implications in physiological and pathophysiological conditions including fibrotic and neoplastic processes. Consequently, this enzyme is considered a promising target for the diagnosis and therapy of these diseases. In this study, we report on the synthesis and kinetic characterisation of *N*^ε-acryloyllysine piperazides as irreversible inhibitors of TGase 2. Systematic structural modifications on 54 new compounds were performed with a major focus on fluorine-bearing substituents due to the potential of such compounds to serve as radiotracer candidates for positron emission tomography. The determined inhibitory activities ranged from 100-10 000 M⁻¹s⁻¹, which resulted in comprehensive structure-activity relationships. Structure-activity correlations using various substituent parameters accompanied by covalent docking studies provide an advanced understanding of the molecular recognition for this inhibitor class within the active site of TGase 2. Selectivity profiling of selected compounds for other transglutaminases demonstrated an excellent selectivity towards transglutaminase 2. Furthermore, an initial pharmacokinetic profiling of selected inhibitors was performed including the assessment of potential membrane permeability and liver microsomal stability.

Introduction

Transglutaminases have been discovered 60 years ago in guinea pig liver.¹ Even though initially identified in mammals, their occurrence has been confirmed for all kingdoms of eukaryotic organisms including plants and fungi.²⁻⁴ In addition, transglutaminases are found in bacteria, which indicates the fundamental importance of these enzymes for biological processes.

The human transglutaminases constitute a family of nine homologues, which comprises the transglutaminases 1-7, the blood coagulation factor XIIIa and the catalytically inactive erythrocyte protein band 4.2. All human family members represent multidomain proteins consisting of a β -sandwich, the central α/β transamidase domain which harbours the acyl transferase active site and exhibits similarity to papain-like cysteine proteases, and two C-terminal β -barrels.⁵

Transglutaminase 2 (TGase 2), which is also referred to as tissue transglutaminase, represents the most intensively studied family member. Its acyltransferase site is constituted by the residues Cys277, His335, Asp358 and Trp241 (numbering according to the human enzyme), which directly participate in catalysis. The central α/β transamidase domain catalyses the γ -glutamyl transfer between protein-bound glutamine residues and a variety of primary amines. In particular, protein-bound lysine residues, low-molecular weight polyamines, e.g. cadaverine, spermidine and spermine, and biogenic monoamines can comprise the latter category of substrates. Beside its eponymous acyl transferase activity, TGase 2 can bind to fibronectin and exhibits GTPase activity, functions which have been ascribed to the N-terminal β -sandwich and the C-terminal β -barrel domains, respectively. Due to its multidomain structure the enzyme exists in two distinguished conformational states: a stretched open one and a compact closed conformation. In the closed state, which is induced and stabilised by GTP, the C-terminal β -barrels block the access to the active site of the transamidase domain. The open conformation, in which TGase 2 is fully active with regards to its acyl transferase activity, is induced and stabilised by Ca^{2+} ions.⁶⁻⁷

TGase 2 is ubiquitously expressed and is mainly located in the cytoplasm under physiological conditions. This implies that under these conditions the enzyme is mainly inactive due to the high levels of GTP and GDP and the low concentration of Ca^{2+} ions in the cytosol. Under certain circumstances, TGase 2 can occur in other cell organelles such as the nucleus and

mitochondria and can be released to the extracellular milieu. Despite higher levels of Ca^{2+} and low concentrations of GTP and GDP, the enzyme is largely inactive in that latter compartment as well. Activation can occur under the influence of certain pathogenic stimuli, such as local injury,⁸ pro-inflammatory mediators or hypoxia.⁹⁻¹⁰ Extracellular inactivity of the enzyme has been mainly attributed to the formation of a vicinal disulphide bridge between Cys370 and Cys371, which renders TGase 2 inactive regarding acyl transfer catalysis. Thioredoxin-catalysed reduction of this disulphide bond can activate TGase 2, which is stimulated by inflammatory signals such as the cytokine interferon- γ .¹¹

Even though strictly regulated and largely suppressed under physiological conditions, increased acyl transferase activity by TGase 2 has been shown to contribute to the pathogenesis of several diseases such as celiac disease,¹²⁻¹⁴ neurodegenerative disorders,¹⁵⁻¹⁶ diseases related to fibrotic processes,¹⁷⁻²⁰ and cancer.²¹⁻²³ While the extent of γ -glutamyl transfer catalysis clearly correlates to the disease state for kidney fibrosis,¹⁷ the function of TGase 2 in neoplastic diseases is less clear. However, it becomes more and more apparent that TGase 2 is a key player for the progression of several kinds of cancer, including breast carcinoma²⁴, renal cell carcinoma²⁵ and malignant melanoma²⁶. In this context, the elevated levels of TGase 2 expression are directly correlated with poor prognostic indicators for survival, e.g. metastatic phenotype and drug resistance of the cancer cells. Moreover, recent studies identified TGase 2 as a survival factor for cancer stem cells from different tumour entities,²⁷⁻³¹ even though its detailed function at the molecular level is not completely understood. Direct evidence for the involvement of extracellular TGase 2-catalysed acyl transfer in tumour progression has been obtained by studying the enzyme's function in pancreatic ductal adenocarcinoma. According to this work, the expression of TGase 2 is highly increased in the malignant pancreatic tissue and immunohistochemical staining for the enzyme is accompanied by *N* ϵ -(γ -glutamyl)-lysine isopeptide cross-links in the extracellular matrix and basement membrane. Furthermore, investigations at the cellular level have demonstrated the efficient crosslinking of collagen by TGase 2 secreted from cancer cells, which stimulates fibroblasts for further matrix deposition. In turn, proliferation of tumour cells through mechanical stimuli is elicited. In line with these results, siRNA-mediated knockdown of TGase 2 led to the attenuation of tumour growth in an orthotopic xenograft mouse model of pancreatic cancer.³² Similar results were obtained for the invasive ductal carcinoma-type of breast cancer.³³ Besides extracellular crosslinking, the posttranslational modification of potentially oncogenic intracellular proteins, such as I κ B α ,³⁴⁻³⁵ phospholipase A₂³⁶ and aconitase 2,³⁷ by TGase 2-mediated transamidation is discussed in the context of tumour progression. Moreover, the release of ammonia through TGase 2-catalysed hydrolytic deamidation of protein-bound

glutamine residues was identified as a potential mechanism for counteracting the acidification of the tumour microenvironment associated with increased aerobic glycolysis of tumour cells.³⁸ Further tumour-promoting functions of TGase 2 independent of its acyl transferase activity have been attributed to its capability of acting as intracellular GTP-binding protein³⁹ and its role as extracellular adapter protein,⁴⁰ both of which involve the closed conformation of the enzyme.⁷

In consequence of its obvious involvement in the progression of different tumours and further pathogenic processes, TGase 2 represents an interesting target for pharmacological inhibition to treat these diseases. Furthermore, considering the remaining open questions with regards to its detailed functions – particularly in cancer – compounds that can be employed as molecular probes for imaging this enzyme in vivo are highly desirable and their development receives increasing interest.⁴¹⁻⁴² In addition, appropriate imaging agents which allow for quantitative assessment of target occupancy and dose selection will support the clinical translation of inhibitors. Based on its quantitative character and its sensitivity, positron-emission tomography (PET) is often considered as the most advantageous imaging modality for such purposes.⁴³⁻⁴⁷

Based on the motivation to develop ¹⁸F-labelled radiotracers for PET studies, the present study focusses on the synthesis and kinetic characterisation of fluorinated irreversible inhibitors for targeting TGase 2. Irreversible inhibitors ranging from small molecules to peptidic compounds with different electrophilic warheads, which form a covalent bond with the active cysteine residue, represent the most intensively studied class of TGase 2 inhibitors.⁴⁸⁻⁴⁹ Radiotracers derived from such irreversibly acting inhibitors appear to be favourable for imaging purposes due to the absent elimination from the target tissue, which potentially results in a high signal/noise ratio as demonstrated for PET tracers targeting monoamine oxidase B and fatty acid amide hydrolase.⁵⁰⁻⁵¹ Despite directed against the α/β transamidase domain, irreversible TGase 2 inhibitors have been shown to attenuate tumour proliferation even when acyl transferase-independent functions are mainly involved.⁵²⁻⁵³ This finding is attributed to the presence of a dynamic equilibrium between the open and closed conformations of TGase 2.⁵⁴

An important subclass of irreversible inhibitors is represented by Michael acceptors, which react with the active cysteine residue according to a 1,4-addition. In this context, Signorini *et al.* observed the inhibition of the transamidase activity of TGase 2 from erythrocytes by acrylamide.⁵⁵ Later, Marrano *et al.* incorporated the acrylamide moiety as electrophilic warhead in different diaminocarboxylic acid derivatives and identified *N*-acryloyllysines as potent inhibitors of TGase 2.⁵⁶⁻⁵⁷

Based on these results, Wityak et al. investigated structure-activity relationships (SARs), which led to the identification of the phenylacetyl and arylpiperazine moieties as favourable substituents at the α -amino and carboxyl group of lysine, respectively.⁵⁸ The most potent compound of this study is compound **6a**, which exhibits an excellent selectivity for TGase 2 within the transglutaminase family. Furthermore, this compound is amenable to structural modifications with fluorine, particularly via its phenylacetyl and pyridylpiperazine moieties (see Figure 1). Therefore, **6a** was chosen as lead compound for the development of potential fluorinated radiotracers in the present study.

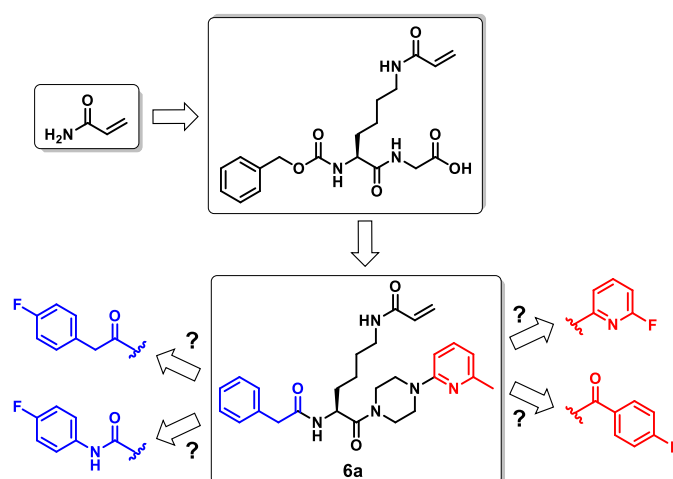


Figure 1. Course of development within acrylamide-based TGase 2 inhibitors and selected fluorinated derivatives envisaged in this study

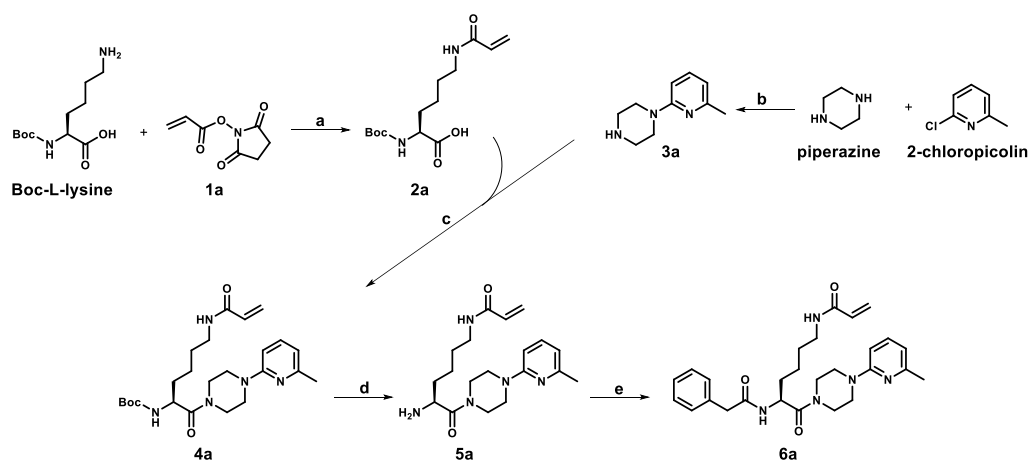
In addition to fluorination, further structural modifications were considered to uncover novel SARs. On the one hand, this will support radiotracer design by combining reactivity-conferring and fluorinated moieties. On the other hand, SAR studies supported by *in silico* molecular docking could give insights into the molecular basis for recognition of these inhibitors. To assess the inhibitory potential of the synthesised *N*^F-acryloyllysines, two TGase 2 activity assays recently developed by us were used.⁵⁹⁻⁶⁰ Furthermore, covalent docking studies together with structure-activity relationships concluded from the kinetic data shed light on the binding mode of the *N*^F-acryloyllysines. Regarding the suitability of compounds as potential radiotracers, both their reactivity towards the desired molecular target and their pharmacokinetic properties are important. Therefore, an initial *in vitro* pharmacokinetic characterisation of the novel *N*^F-acryloyllysines was carried out. These studies included the assessment of the compound's potential membrane permeability, their stability towards oxidative metabolism and their potential unspecific binding, using appropriate analytical assays and computational methods.

Results and Discussion

Synthetic strategies for the *N*^ε-acryloyllysine piperazides

Synthesis of *N*^ε-Boc-*N*^ε-acryloyllysine

Structural modifications of lead compound **6a** were primarily focused on the introduction of fluorine at different sites, but also other functional groups were considered to uncover SARs. According to retrosynthetic considerations, compound **6a** can be fragmented into three main parts: the central *N*^ε-acryloyl-L-lysine, the N-terminal phenyl acetic acid and the C-terminal 6-methylpyridin-2-ylpiperazine. For chemical modifications, the C- and N-terminal moieties seem to be most appropriate. Based on the principles of amino acid and peptide chemistry, incorporation of the phenylacetyl group at the α-amino group should be conducted after incorporation of the piperazinyl moiety at the α-carboxyl group (Scheme 1). Furthermore, *N*^ε-acryloylation was accomplished as first step, which allows for a modular synthetic approach. As the positions for structural modifications are at two different moieties of the inhibitors, the inhibitory potential can be finally further increased by combination of advantageous substituents. It should be mentioned that the synthetic strategy for the inhibitors in this study basically corresponds to the published method, but it varies in the conditions for distinct steps.^{58,61}



Scheme 1. General synthesis steps for the *N*^ε-acyl-*N*^ε-acryloyllysine piperazides using the example of reference compound **6a**

Reagents and conditions: **a)** TEA, CH₃OH, 2 h; **b)** *n*-BuOH, 130°C, 5 d; **c)** PyBOP, DIPEA, THF, 5 h; **d)** TFA/CH₂Cl₂ (1/1, v/v), 2 h; **e)** phenylacetyl chloride, TEA, CH₂Cl₂, 5 h.

For the synthesis of *N*^ε-Boc-*N*^ε-acryloyllysine, *N*^ε-acryloylation was performed by the use of *N*-acryloxysuccinimide (**1a**), which was synthesised from acryloyl chloride and *N*-

hydroxysuccinimide according to published methods.⁶²⁻⁶⁴ In this context, *N*-acryloxysuccinimide appeared to be advantageous over acryloyl chloride, as the latter one led to the formation of the condensation product of *N*^t-Boc-*N*^ε-acryloyllysine and *N*^t-Boc-lysine as side product. The high solubility of the desired product in water caused challenges during processing and purification of the reaction mixture. Therefore, initially the crude product was used for the subsequent coupling reaction with the piperazine building blocks. Residual *N*-hydroxysuccinimide and triethylamine should not have detrimental effects on that reaction. However, ongoing attempts to purify the crude product (without processing) revealed a method for column chromatography which uses CH₂Cl₂ with gradually increasing content of isopropanol (from 5 to 8%) containing a constant portion of acetic acid (2%) as eluent. To avoid formation of acetamide during the subsequent coupling reaction, residual acetic acid was removed by repeated azeotropic evaporations of the product in the presence of toluene.⁶⁵ Compound **2a** was obtained in 50% yield by this method.

Syntheses of the piperazine building blocks

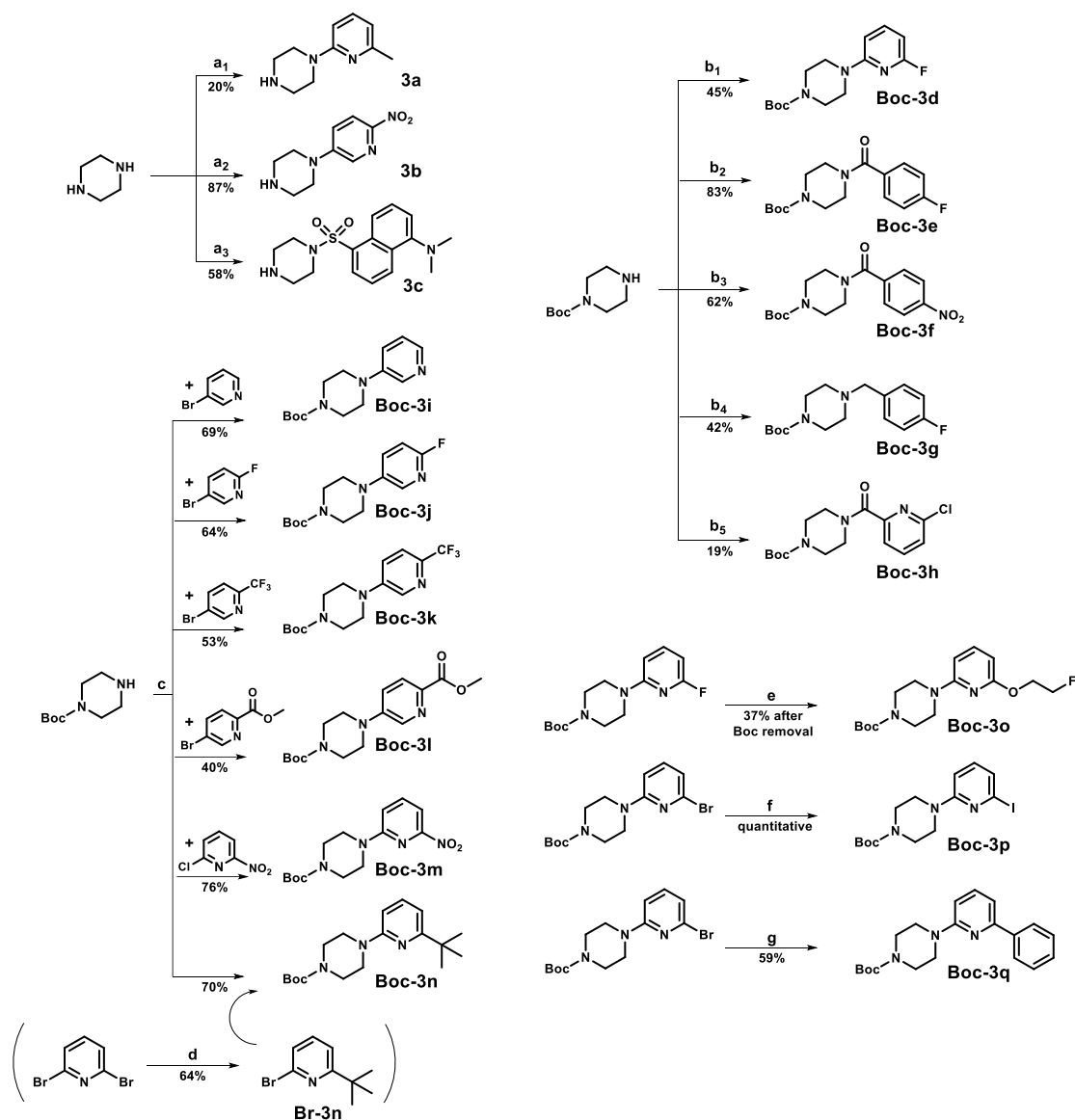
Most of the piperazine building blocks used in this study were synthesised by the reaction of piperazine or Boc-piperazine with the respective pyridine, benzoic acid and sulfonic acid derivatives (Scheme 2). For compounds **3a** and **3b**, the thermal substitution at 2-chloropicoline (in *n*-butanol⁶⁶) and 3-bromo-6-nitropyridine (in acetonitrile⁶⁷), respectively, with piperazine was used without the addition of a further base. Due to the high reactivity of 2,6-difluoropyridine, the procedure of Prante *et al.* was adopted for the synthesis of **Boc-3d**, which uses Boc-piperazine instead of piperazine, triethylamine as base and DMF instead of *n*-butanol as solvent.⁶⁸ A series of pyridyl-substituted piperazines (**Boc-3i-Boc-3n**) was obtained by Buchwald-Hartwig amination of Boc-piperazine with the respective bromo-substituted pyridine derivatives,⁶⁹ with the exception of the 6-nitropyridin-2-yl derivative, which was synthesised by the use of 2-chloro-6-nitropyridine. The coupling reactions furnished the desired piperazine building blocks in good yields (40-76%) after purification by column chromatography. 2-Bromo-6-*tert*-butylpyridine (**Br-3n**), which was needed for the synthesis of **Boc-3n**, was accessible by a novel Cu(I)-catalysed coupling reaction of tertiary Grignard reagents with azacyclic electrophiles.⁷⁰⁻⁷¹ The other pyridine derivatives were commercially available. A structural variation, which was not intended arose during the reaction of Boc-piperazine with 2-chloro-6-trichloromethylpyridine under the conditions of a Buchwald-Hartwig amination. Instead of the intended 6-trichloromethylpyridyl moiety, the incorporation of the 6-chloropicolinoyl moiety occurred, which was confirmed by NMR and ESI-MS analyses (compound **Boc-3h**). The substitution of the ring chlorine is known,⁷² however, even under different conditions (NaOH/TEA as bases and CH₃CN/DMF/CH₃OH as solvents), the formation of the picolinic acid

derivative was exclusively observed. Such reaction products have been identified for the reaction of β -trichloromethylpyridines with nucleophiles as well as for the hydrolysis of 2-chloro-6-trichloromethylpyridine.⁷²⁻⁷³

For the selective mono-acylation with the 4-fluorobenzoyl- and 4-nitrobenzoyl groups, Boc-piperazine was reacted with the respective benzoyl chlorides. After processing of the reaction mixtures (especially washing with 1 M HCl), a purification step for both compounds (**Boc-3e** and **Boc-3f**) could be omitted. The incorporation of the dansyl moiety was managed according to the procedure by Sashuk et al. using piperazine and dansyl chloride without the need for purification (**3c**).⁷⁴ The synthesis of the 4-fluorobenzyl-substituted piperazine **Boc-3g** was realised by reductive amination between Boc-piperazine and 4-fluorobenzaldehyde using sodium triacetoxyborohydride as reducing agent.⁷⁵ After purification by column chromatography, this piperazine derivative was obtained in moderate yield (42%).

Some variations in the piperazine building blocks were achieved by direct modification of pyridyl-substituted piperazines (Scheme 2). In this context, the fluoroethoxy group was introduced via nucleophilic aromatic substitution of 1-Boc-4-(6-fluoropyridin-2-yl)piperazine and 2-fluoroethanol.⁷⁶ Worth of note, the fluoroethoxy-substituted product **Boc-3o** could not be separated from its fluoro-substituted educt **Boc-3d**, neither by RP-HPLC nor by conventional normal-phase column chromatography. Analysis of the crude product by NMR revealed a proportion of 40% of the product in the mixture. As the extent of conversion could not be increased by different conditions (CaH₂ instead of NaH and longer reaction time), subsequent Boc deprotection of the crude product was performed followed by purification via RP-HPLC. The commercially available 1-Boc-4-(6-bromopyridin-2-yl)piperazine served as starting material for two further piperazine building blocks. The 1-Boc-6-iodopyridin-2-ylpiperazine (**Boc-3p**) was obtained quantitatively via copper-catalysed „aromatic Finkelstein reaction“ with NaI.⁷⁷ For the synthesis of 1-Boc-6-phenylpyridin-2-ylpiperazine (**Boc-3q**, 59%), a Suzuki coupling with phenylboronic acid in aqueous environment was selected, according to the procedure for the Suzuki coupling of β -chloroacroleins with boronic acid described by Hesse and Kirsch.⁷⁸

Starting from the final inhibitor bearing a picolinic acid methyl ester moiety (compound **8f**), two further structural variations were obtained. Hydrolysis of the ester bond furnished the respective picolinic acid derivative **8e**, which was subsequently used for the conversion to the primary amide **8g**.



Scheme 2. Synthetic methods for the preparation of the piperazine building blocks **3**

Boc removal from Boc-piperazine derivatives **Boc-3d-Boc-3q** to yield **3d-3q** was performed using a mixture of TFA/CH₂Cl₂ as outlined in the main text and in the Chemistry Section in Supporting Information. Compounds **3r-3x** are not shown in the scheme as they are commercially available. **Reagents and conditions:** **a₁**) 2-chloropicoline, *n*-butanol, 130°C, 5 d; **a₂**) 3-bromo-6-nitropyridine, CH₃CN, 95°C, 6 h; **a₃**) dansyl chloride, CH₂Cl₂, 15 min; **b₁**) 2,6-difluoropyridine, TEA, DMF, 150°C, 24 h; **b₂**) 4-fluorobenzoyl chloride, TEA, CH₂Cl₂, 2 h; **b₃**) 4-nitrobenzoyl chloride, TEA, THF, 2 h; **b₄**) 4-fluorobenzaldehyde, sodium triacetoxyborohydride, THF, N₂, 5 h; **b₅**) nitrapyrin, Cs₂CO₃, xantphos, Pd₂(dba)₃, Ar, 70°C, 24 h; **c**) respective bromopyridine derivative, Cs₂CO₃, xantphos, Pd₂(dba)₃, THF, Ar, 70°C, 5-12 h; **d**) CuI, *tert*-butylmagnesium chloride, THF, Ar, <0°C → 30°C, 3 h; **e**) fluoroethanol, NaH, DMSO, Ar, 100°C, 2 d; **f**) CuI, NaI, TMEDA, 1,4-dioxane, Ar, 100°C, 44 h; **g**) phenylboronic acid, Pd(OAc)₂, (C₄H₉)₄NBr, K₂CO₃, H₂O/THF (5:2, v/v), 100°C, 6h.

In the case of the Boc-protected piperazine derivatives, the Boc group had to be removed prior to coupling with *N^R*-Boc-*N^F*-acryloylslysine. To this end, the Boc-piperazine derivatives were

treated with a mixture of TFA/CH₂Cl₂ (1:1, v/v) for 2 h. To avoid excessive use of base for the amide coupling reactions, the resulting TFA salts were neutralised with aqueous NaOH and extracted into the organic phase to obtain the free secondary amines. This procedure was omitted for the picolinic acid methyl ester derivative **Boc-3I** due to its susceptibility to basic hydrolysis.

Amide coupling between N^t-Boc-N^f-acryloyllysine and the piperazine building blocks

The formation of the amide bond was realised using PyBOP as a coupling agent in the presence of DIPEA as base. All coupling products (compounds **4**) were purified by column chromatography. The conversion of the crude product of N^t-Boc-N^f-acryloyllysine resulted in only slightly diminished yields compared to the purified product (20-90% and 50-90%), which justifies the initial approach omitting the purification after N^f-acryloylation.

Boc removal and functionalisation at the α-amino group

The removal of the Boc group from the coupling products was conducted as described for the Boc-protected piperazine building blocks (TFA/CH₂Cl₂ (1:1, v/v), 2 h). However, the neutralisation of the TFA salts (compounds **5**) was not accomplished. Therefore, additional equivalents of base had to be considered for the next reaction step. The last step to the final inhibitors (compounds **6-21**) comprised the functionalisation at the α-amino group. The incorporation of the different substituents was achieved by three different ways: reaction of activated carboxylic acid derivatives or analogues, PyBOP-mediated reaction with carboxylic acids and reductive amination.

In the course of the last reaction step several side reactions were observed. When possible, the respective side products (**6c**, **16a-d**, **14n-q**) were separated and characterised by NMR and ESI-MS. The results are discussed in the Supporting Information (Discussion S1).

Transglutaminase assays

Fluorimetric assay method

For the characterisation of the *N*^F-acryloyllysines towards inhibition of hTGase 2 (human transglutaminase 2), a continuous fluorimetric assay method was used, which was recently developed by our group.⁵⁹ This assay is based on the measurement of an increase in fluorescence over time due to the TGase 2-catalysed hydrolysis of the water-soluble fluorogenic acyl donor **Z-Glu(HMC)-Gly-OH** resulting in the formation of HMC and Z-Glu-Gly-OH. Due to significant spontaneous hydrolysis of **Z-Glu(HMC)-Gly-OH** at higher pH values, kinetic characterisation of inhibitors was performed at pH 6.5 using six different concentrations of inhibitor. Analysis of the progress curves was done under the formalism of slow-binding inhibition providing finally values for the performance constants k_{inact}/K_i .⁵⁹ In case of hyperbolically decreasing initial velocities with increasing inhibitor concentration, the dissociation constants (K_i) of the non-covalent enzyme-inhibitor complex were also derived.

In addition to the characterisation of the desired drug-target interaction, assessment of specificity and selectivity of drug candidates is fundamental. As the family of transglutaminases consists of eight enzymatically active proteins, the development of selective hTGase 2 inhibitors is challenging. To address the issue of selectivity, assay methods for the characterisation of transglutaminases beside hTGase 2 are necessary. For the characterisation of the selectivity (based on k_{inact}/K_i values) of irreversible inhibitors with 3-bromo-4,5-dihydroisoxazol warhead, Klöck *et al.*⁷⁹ utilised the well-known GDH-coupled assay method⁸⁰ with appropriate small glutamine-containing peptides for the respective transglutaminases (Z-QG-OH for hTGase 2 and mTGase 2, Z-QS-OH for hTGase 1 and hTGase 3, H-QEQVSPLSLLK-OH for hfXIIIa). Inspired by the results of this study, we hypothesised that the fluorogenic acyl donor **Z-Glu(HMC)-Gly-OH**, which is a good substrate for gpTGase 2 (guinea pig transglutaminase 2) and hTGase 2,⁵⁹ could be also used to characterise further TGases. Thus, the enzymatic hydrolysis of **Z-Glu(HMC)-Gly-OH** by mTGase 2 (murine transglutaminase 2), hTGase 1, hTGase 3, hTGase 6 and hfXIIIa was investigated at pH 6.5. Worth of note, acyl donor **Z-Glu(HMC)-Gly-OH** is also a suitable substrate for all other TGases studied (Figure 2 and Table 1). While the kinetic parameter towards mTGase 2 are comparable to gpTGase 2 and hTGase 2, the substrate properties towards hTGase 1, hTGase 3, hTGase 6 and hfXIIIa are significantly diminished. The performance constants (k_{cat}/K_m) for these TGases are reduced to 1/18 or less compared to hTGase 2. Considering the off-target TGases, **Z-Glu(HMC)-Gly-OH** exhibits the most favourable properties towards hTGase 6, followed by hTGase 1, hfXIIIa and hTGase 3. In a recent study, Akbar *et al.*⁸¹ kinetically characterised the well-known TGase 2 substrate Z-

Glu(*p*NP)-Gly-OH ($k_{\text{cat}}/K_M=11\,833\text{ M}^{-1}\text{s}^{-1}$ for hTGase 2) towards hTGase 1 and hTGase 6 at pH=6.5. Similar to its coumarinylester analogue, this compound is also a suitable substrate for these TGases even though the performance constants are significantly reduced compared to hTGase 2. In contrast to **Z-Glu(HMC)-Gly-OH**, Z-Glu(*p*NP)-Gly-OH is better tolerated by hTGase 1 ($k_{\text{cat}}/K_M=1\,333\text{ M}^{-1}\text{s}^{-1}$) than by hTGase 6 ($k_{\text{cat}}/K_M=500\text{ M}^{-1}\text{s}^{-1}$), which might indicate differences in the recognition of these substrates within the active sites of the different TGases.

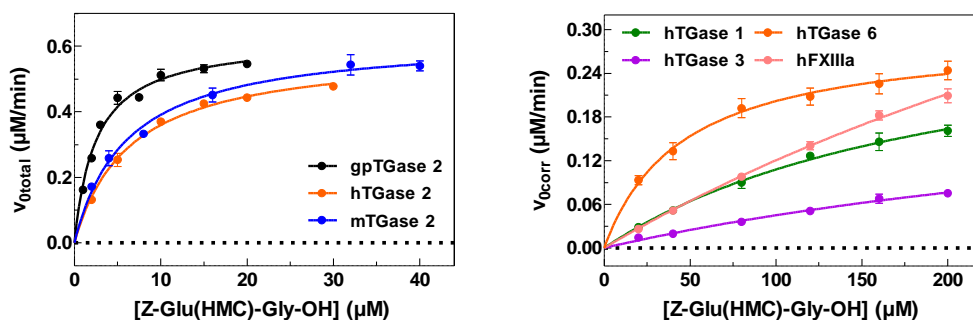


Figure 2. Enzymatic hydrolysis of Z-Glu(HMC)-Gly-OH by different TGases at pH 6.5

Plots of $V_{0\text{total}}=f([Z\text{-Glu(HMC)-Gly-OH}])$ for gpTGase 2, hTGase 2 and mTGase 2 and plots of $V_{0\text{corr}}=f([Z\text{-Glu(HMC)-Gly-OH}])$ for hTGase 1, hTGase 3, hTGase 6 and hFXIIIa including nonlinear regressions according to equation VI (Experimental Section). Data shown are mean values \pm SEM of three separate experiments, each performed in duplicate. When not apparent, error bars are smaller than the symbols. Plots for gpTGase 2 and hTGase 2 have already been shown in a previous study.⁵⁹ Conditions: pH 6.5, 30 °C, 5% DMSO, 500 μM TCEP, 3 $\mu\text{g/mL}$ TGase.

Table 1. Kinetic parameters for the enzymatic hydrolysis of acyl donor Z-Glu(HMC)-Gly-OH by different TGases at pH 6.5 and 30 °C

Enzym	regression analysis			numerical integration		
	K_m (μM)	k_{cat} (s^{-1})	k_{cat}/K_m ($\text{M}^{-1}\text{s}^{-1}$)	K_m (μM)	k_{cat} (s^{-1})	k_{cat}/K_m ($\text{M}^{-1}\text{s}^{-1}$)
gpTGase 2*	2.53 (0.18)	0.33 (0.01)	130 000	2.67 (0.20)	0.34 (0.01)	129 000
hTGase 2*	6.60 (1.06)	0.32 (0.02)	48 500	5.78 (1.03)	0.32 (0.02)	57 600
mTGase 2	6.10 (0.26)	0.29 (0.01)	47 500	5.55 (0.34)	0.28 (0.01)	50 500
hTGase 1	183 (39) 226 [#]	0.17 (0.02) 0.19 [#]	929 841 [#]	190 (52)	0.18 (0.03)	947
hTGase 3	202 (25) 506 [#]	0.07 (0.01) 0.06 [#]	347 119 [#]	-	-	-
hTGase 6	46.1 (2.7)	0.13 (0.01)	2 820	44.1 (2.4)	0.14 (0.01)	3 170
hFXIIIa	498 (148) 772 [#]	0.34 (0.08) 0.48 [#]	683 622 [#]	441 (104)	0.33 (0.07)	748

For details on the calculation of the kinetic parameters, see Experimental Section. Data shown are mean values (\pm SEM) of three separate experiments, each performed in duplicate. Active concentrations of mTGase 2, hTGase 1, hTGase 3, hTGase 6 and hFXIIIa were calculated from Zedira's activity data. *Kinetic data for gpTGase 2 and hTGase 2 have previously been published.⁵⁹ [#]Data obtained by the method of Cornish-Bowden and Eisenthal.⁸²

The same data sets were also analysed by numerical regression⁵⁹ providing kinetic parameters that are in good agreement to those of the classical regression analyses (Table 1). However, no fit traces could be obtained for the data of hTGase 3. The high proportion of spontaneous reaction of **Z-Glu(HMC)-Gly-OH**⁵⁹ might be problematic for the accurate analysis of the data for this enzyme by numerical integration.

Due to the low rates of substrate conversion by hTGase 1, hTGase 3, hTGase 6 and hFXIIIa, the progression curves for each substrate concentration are linear. Therefore, acyl donor **Z-Glu(HMC)-Gly-OH** can be applied for the kinetic characterisation of irreversible inhibitors within its solubility limit (<250 μM) towards these TGases, even though the enzymes are not saturated by the substrate.

Fluorescence anisotropy assay

Another assay method, which was recently described by our group,⁶⁰ is based on the measurement of an increase in fluorescence anisotropy (FA) during the TGase 2-catalysed transamidation of a fluorophore-conjugated cadaverine derivative with DMC. Out of the three investigated cadaverine derivatives towards gpTGase 2-catalysed transamidation, rhodamine B-isonipecotyl-cadaverine (**R-I-Cad**) exhibits the most favourable substrate properties. With respect to the potential usefulness of this assay method for characterising cellular TGase 2's transamidation activity, the characterisation of the substrate pair **R-I-Cad** and DMC towards hTGase 2 was envisaged. Furthermore, the characterisation of selected

inhibitors by this assay method was sought to compare the results with those of the fluorimetric assay method. This enabled the evaluation of the inhibitory properties of the *N*^F-acryloyllysines at different pH values (6.5 *versus* 8.0) as well as towards different enzymatic activities (hydrolase *versus* transamidase activity).

Initial investigations on the dependence between the activity and concentration of hTGase 2 provided similar results compared to gpTGase 2 as linearity predominates over a wide range of enzyme concentrations (0.5-5 µg/mL, Figure S1 in Supporting Information). The results obtained by varying the concentration of one substrate in the presence of the other substrate at a fixed concentration are shown in Table 2 and Figure S2 in Supporting Information. Compared to gpTGase 2, a similar kinetic behaviour of both substrates can be observed towards hTGase 2, especially with regards to the maximum velocities. However, the K_m value of DMC towards hTGase 2 is significantly reduced (2.78 µM) compared to gpTGase 2 (27.5 µM). Concerning the characterisation of irreversible inhibitors, the potential of the FA assay method was also recently demonstrated.⁶⁰ Due to the high rate of hTGase 2-catalysed incorporation of **R-I-Cad** in DMC it was decided to reduce the enzyme concentration from 5 µg/mL to 2 µg/mL for inhibitor characterisation. Compared to gpTGase 2, the time for preincubation of enzyme and inhibitor had to be reduced for hTGase 2 from 30 to 5 min due to the significantly higher reaction rate of most of the *N*^F-acryloyllysines towards the human enzyme (see below).

Table 2. Kinetic parameters for the substrate pairs DMC/F-Cad towards gpTGase 2 and DMC/R-I-Cad towards gpTGase 2 and hTGase 2

Enzym		K_m (µM)	V_{max} (mA s ⁻¹)	K_i (µM)
gpTGase 2	DMC	3.05 (0.44)	0.027 (0.002)	-
	F-Cad	2.22 (1.40) × 10 ⁻⁴	0.018 (0.001)	9.15 (3.11)
gpTGase 2	DMC	27.5 (6.4)	0.176 (0.028)	135 (32)
	R-I-Cad	2.42 (0.69) × 10 ⁻⁴	0.113 (0.013)	7.14 (2.20)
hTGase 2	DMC	2.78 (0.10)	0.132 (0.001)	174 (16)
	R-I-Cad	3.43 (0.02) × 10 ⁻⁴	0.121 (0.002)	6.81 (0.45)

For details on the calculation of the kinetic parameters, see Experimental Section. Data shown are mean values (±SEM) of three (gpTGase 2) or two (hTGase 2) experiments, each performed in duplicate (hTGase 2) or triplicate (gpTGase 2). Kinetic data for gpTGase 2 have previously been published.⁶⁰

Taken together, two reliable assay methods based on fluorescence intensity and fluorescence anisotropy were established for inhibitor characterisation, which facilitate investigations of the inhibitory behaviour at different pH values towards different enzymatic activities as well as towards different TGase enzymes. Due to the known similarity between gpTGase 2 and

hTGase 2, which has often justified the use of gpTGase 2 as cost-efficient alternative to the human variant in the past,⁸³ there was a special interest on the behaviour of the *N*^ε-acryloyllysines towards both enzymes. Even though the settings of both assay methods were basically identical for these TGases, it should be mentioned that for gpTGase 2 fluorescein-labelled cadaverine (**F-Cad**) was chosen as acyl acceptor for the measurements by the FA assay method while **R-I-Cad** was used for experiments on hTGase 2 (kinetic plots and data are also shown for the purpose of comparison in Table 2 and Supporting Information). This difference in the composition of the assay mixture should, however, be unproblematic, as **F-Cad** and **R-I-Cad** were shown to provide reasonably comparable results for the characterisation of irreversible inhibitors.⁶⁰

To confirm the irreversibility of the inhibition of gpTGase 2 and hTGase 2 by the *N*^ε-acryloyllysines, a jump-dilution experiment according to Copeland⁸⁴ was exemplarily performed for the inhibition of gpTGase 2 by lead compound **6a**. As expected, no enzymatic activity has been restored after 1:100 dilution of a pre-incubated mixture of enzyme and inhibitor (both 100-fold concentrated) into the assay mixture, which clearly confirms the irreversible inhibition of TGase 2 by *N*^ε-acryloyllysines (Figure S3 in Supporting Information).

In order to determine the active enzyme concentrations, the FA-based assay has recently been shown to be a reliable and fast method for active-site titration of gpTGase 2 by using iodoacetamide in a concentration range stoichiometric to the enzyme.⁶⁰ However, when TCEP instead of DTT was used as antioxidant for hTGase 2, the active-site titration with iodoacetamide led to false results for that enzyme due to the known reactivity of the inhibitor with TCEP.⁸⁵ Therefore, one of the most potent *N*^ε-acryloyllysines in this study, compound **8d** (see below), was applied for the active-site titration hTGase 2. By using a preincubation time of 40 min, the concentration of catalytically active hTGase 2 could be determined (with **R-I-Cad** and DMC as substrates; Figure S4 in Supporting Information). Furthermore, a comparable result was obtained for hTGase 2 with the fluorimetric assay following the hydrolysis of **Z-Glu(HMC)-Gly-OH** in the presence of **8d** after a preincubation period of 40 min (Figure S4).

Molecular docking studies

Computational methods that are available for the modelling of covalent enzyme-inhibitor complexes were considerably improved over the recent years.⁸⁶ Within this study, covalent docking was carried out to predict the binding mode of the synthesised irreversible covalent inhibitors towards hTGase 2 and rationalise the differences in enzymatic activity which were experimentally observed at atomic detail. The crystal structure of the open conformation of hTGase 2 in complex with a peptide-like irreversible inhibitor developed by Khosla's group was

used for this purpose (PDB ID 2Q3Z).⁸⁷ In this structure, two hydrophobic pockets are well defined. The entrance to pocket 1 through the catalytic site is flanked by Lys176 and Met252 and its tunnel-like shape involves the residues Gln169, Ile178, Trp180, and the backbone of Trp254. Pocket 2 is deeper and comprises Asn302, Ala304, Leu312, Ile313, Phe316, Met330, Ile331 and Leu420. In the crystal structure, there is no electron density for residues 307-308 and 319-327, which are located proximal to the catalytic site. Due to the potential role of these missed residues on defining proximal binding sites for the newly developed inhibitors, they were modelled before performing the docking studies (see Experimental Section, Figure S5 in Supporting Information). A similar approach was previously undertaken by Badarau et al. with good results regarding the predictions.⁸⁸ The energy-refined 3D molecular model of hTGase 2 in the open conformation suggested an additional pocket 3 proximal to the pocket 2 flanked by Arg317 and Asn308 (Figure 3A), whose existence has been proposed before even though no experimental or computational proof was provided.⁴⁹ Covalent docking studies were first performed with the lead compound **6a**. Binding poses were predicted either with the phenylacetyl group or the pyridylpiperazinyl moiety occupying the hydrophobic pocket 2. The first scenario with the phenylacetyl in pocket 2 (Figure 3A) has revealed three H bonds involving the hTGase 2 residues Trp241, Ile331 and Asn333. In this case, the methyl group of the pyridylpiperazinyl moiety was forming van-der-Waals contacts with Arg317. In the second scenario with the pyridylpiperazinyl moiety located in pocket 2 (Figure S6 in Supporting Information), multiple binding modes⁸⁹ were predicted in which the phenyl group could either be oriented towards Arg317, Phe320 or Phe334. The latter binding mode was more favourable than the other two, being stabilised by three H bonds (Trp241, Cys277 and Asn333). Hence, the hTGase 2-**6a** complex might be represented by a dynamic ensemble of multiple binding poses with the phenylacetyl group occupying pocket 2 or interacting with Phe334. Residues Arg317 and Phe320 might act as intermediate anchor points for the dynamic interconversion between the two binding modes.

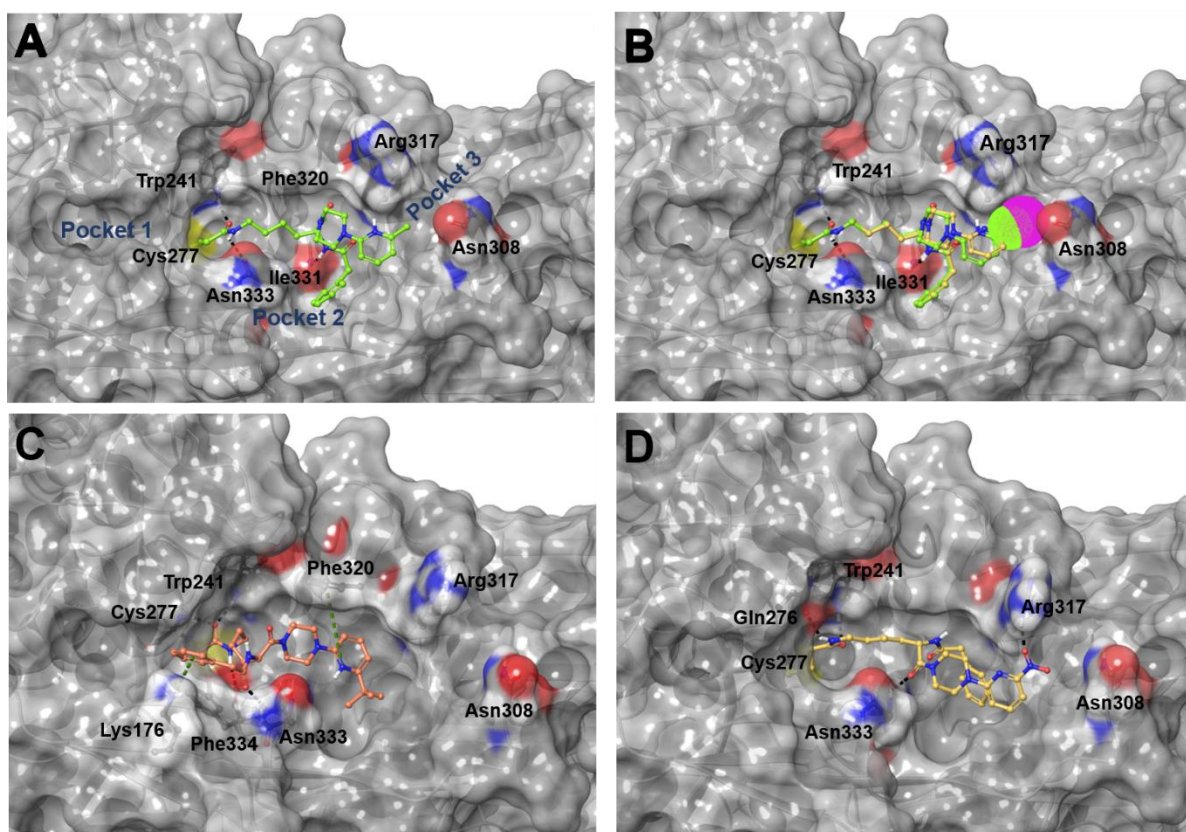


Figure 3. Molecular modelling of the interaction of hTGase 2 with covalent inhibitors

The enzyme is shown in gray surface with relevant residues coloured by atom type and inhibitors are shown in sticks and colored by atom type. Intermolecular H bonds and cation- π interactions are depicted by black and green dashed lines, respectively. **A)** **6a** (green), **B)** **7e** (yellow, iodine atom highlighted in magenta surface) superimposed with **6a** (methyl substitution in pyridine ring highlighted in green surface), **C)** **7f** (orange) and **D)** **7i** (light orange). Figure generated in Maestro (Schrödinger).⁹⁰

Structure-activity relationships for human TGase 2

Enantiomeric purity of the N^f-acryloyllysine piperazides

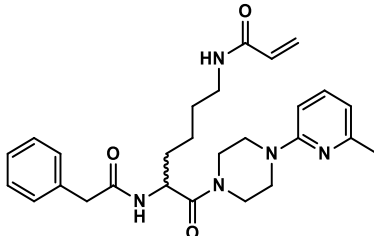
Concerning the enantiomeric purity of the inhibitors, the amide coupling between the lysine main-chain carbonyl and the piperazine building blocks is the most crucial step. However, due to the low electron withdrawing effect of the lysine side chain as well as the protection of the α -amino group as urethane, enantiomerisation is strongly hindered. To further support the conservation of the configuration at the C $_{\alpha}$ atom, the moderately strong base DIPEA and the moderately polar solvent THF were used.⁹¹ Finally, the enantiomeric purity of the inhibitors was analysed exemplarily for compound **6a** by CD spectroscopy and HPLC using a chiral stationary phase (chiral HPLC). In addition to the appropriate analytical method, both enantiomers are needed. Therefore, compound **6b** was synthesised starting from Boc-D-lysine. The CD spectra

confirmed that both compounds are enantiomers (Figure S7 in Supporting Information). Analysis of mixtures of **6a** with increasing amounts of **6b** by chiral HPLC revealed that the enantiomeric purity is greater than 98% (Figure S8 in Supporting Information). Therefore, the stereochemical integrity was not affected during the synthesis of the compounds. As the procedure for the amide coupling was similarly performed for all compounds, the enantiomeric purity of **6a** can be considered as representative for all inhibitors.

Influence of configuration at C $^{\alpha}$

Even though *N*^ε-acryloyllysines are known for a long time to act as potent inhibitors of TGase 2,⁵⁶ the influence of the configuration at C $^{\alpha}$ on their inhibitory behaviour has not been investigated so far. The focus on the L-enantiomer is probably a result from studies on substrates for gpTGase 2 where peptides containing L-glutamine exhibit a significantly higher substrate potential than peptides with D-glutamine.⁹² However, to confirm this assumption the D-enantiomer (**6b**) of compound **6a** was kinetically characterised towards hTGase 2 (Table 3). The change of the configuration leads to a marked decrease in the inhibitory potential. The ratio of the inactivation constants of both enantiomers ($(k_{\text{inact}}/K_i)_S/(k_{\text{inact}}/K_i)_R$, eudismic ratio) is 24. Consequently, this verifies the focus on the L-configuration in the past and justifies the synthesis of all inhibitors in this work starting from Boc-L-lysine.

Table 3. Influence of the configuration at C $_{\alpha}$ on the inhibition of hTGase 2

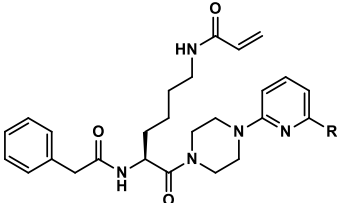
			
compound	configuration	k_{inact}/K_i (M ⁻¹ s ⁻¹)	K_i (μM)
6a [#]	S	4 880 (20)	5.73 (0.77)
6b	R	206 (8)	-
Data shown are mean values (±SEM) of two separate experiments, each performed in duplicate. [#] Kinetic data for compound 6a have previously published. ⁵⁹			

Substitution at position 6 of pyridine-2-ylpiperazines

As discovered by Wityak et al., the methyl group in position 6 of the pyridine ring significantly increases the inhibitory potential compared to the unsubstituted pyridine (as investigated for compounds **4o** and **4p** by Wityak et al., which differ from **7a** and **6a** in the way that the phenylacetyl group is replaced by a Z group as *N*^α-substituent).⁵⁸ Therefore, we initially

focussed on the systematic variation of the substituent in this position. The kinetic data of the respective series of analogues are shown in Table 4.

Table 4. Influence of the substituents in position 6 of the pyridin-2-yl moiety on the inhibition of hTGase 2

			
compound	R	k_{inact}/K_i ($\text{M}^{-1}\text{s}^{-1}$)	K_i (μM)
6a[#]	CH ₃	4 880 (20)	5.73 (0.77)
7a	H	2 980 (80)	8.42 (1.29)
7b	F	3 850 (240)	6.28 (0.33)
7c	Cl	4 910 (160)	4.43 (0.25)
7d	Br	5 200 (180)	5.65 (0.69)
7e	I	7 350 (200)	2.92 (0.02)
7f	<i>tert</i> -butyl	6 140 (140)	3.50 (0.05)
7g	phenyl	4 560 (220)	7.76 (2.43)
7h	2-fluoroethoxy	3 020 (160)	7.32 (0.36)
7i	NO ₂	10 200 (100)	2.26 (0.10)

Data shown are mean values (\pm SEM) of two separate experiments, each performed in duplicate. [#]Kinetic data for **6a** have already been listed in Table 3.

In accordance with the results by Wityak et al., the unsubstituted pyridine derivative **7a** ($k_{\text{inact}}/K_i=2\,980\text{ M}^{-1}\text{s}^{-1}$) is less potent than the reference compound **6a**, even though the phenylacetyl group is present at the α -amino group instead of the Z group.⁵⁸ Incorporation of fluorine in compound **7b** ($k_{\text{inact}}/K_i=3\,850\text{ M}^{-1}\text{s}^{-1}$) leads to a slight increase of the inactivation constant compared to **7a**, however, the level of **6a** is not restored. Subsequent substitution by the other halogen atoms Cl, Br and I (compounds **7c**, **7d** and **7e**) further increases the inhibitory potential with the iodine derivative ($k_{\text{inact}}/K_i=7\,350\text{ M}^{-1}\text{s}^{-1}$) being even more potent than the reference compound **6a**. This trend indicates that the inactivation constant increases with the size of the substituents. Concerning quantitative structure-activity relationships, there are parameters available describing the sterical demand of a substituent. These substituent parameters include the Taft parameter E_s ⁹³⁻⁹⁵ and the differential van-der-Waals radius v (Charton values⁹⁶⁻⁹⁷). As shown in Figure 4, there are linear relationships between these substituent parameters and the logarithmically transformed inactivation constants ($R^2\approx 0.9$). In this context, the potential bioisosteric behaviour of Cl and CH₃ based on their similar sterical demand has already been observed in other SAR studies, both at sp^2 and sp^3 carbon atoms.⁹⁸⁻

¹⁰⁰ For example, 3-aminopyrazinone-derived thrombin inhibitors with 4-chloropyridin-2-yl and 4-methylpyridin-2-yl moieties show similar K_i values for the inhibition of thrombin.⁹⁹

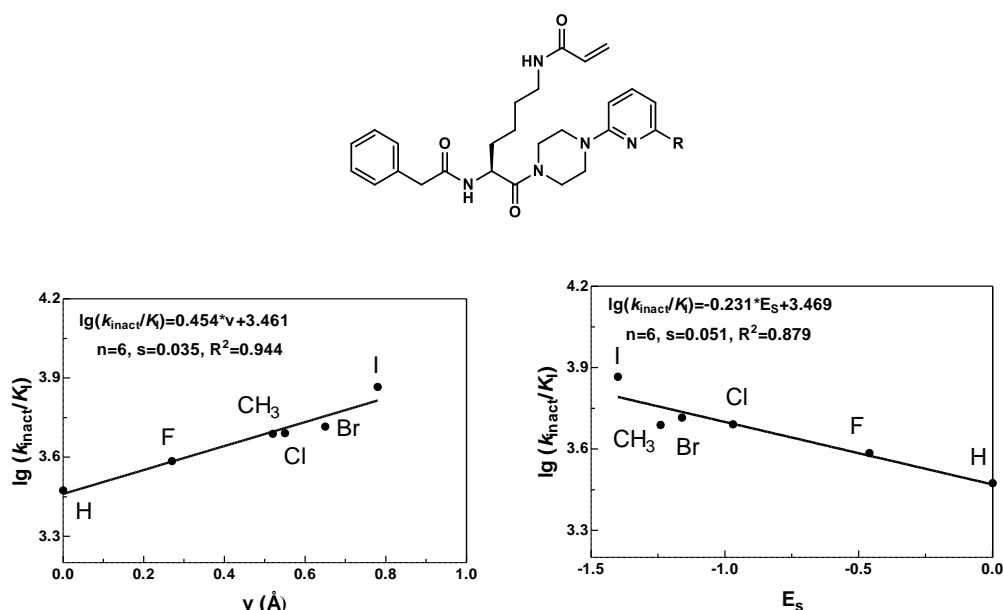


Figure 4. Relationship between the size of the substituent in position 6 of the pyridin-2-yl moiety and the inactivation constants of the inhibitors 6a and 7a-e

Plots of $\lg(k_{\text{inact}}/K_i)=f(v)$ (left) and $\lg(k_{\text{inact}}/K_i)=f(E_s)$ (right) using the mean values of the inactivation constants of compounds **6a** and **7a-e** (Table 4) and the following values for $v(\text{\AA})$ ^{97,101-102}: 0.00 (H), 0.27 (F), 0.52 (CH₃), 0.55 (Cl), 0.65 (Br) and 0.78 (I) and E_s ¹⁰¹⁻¹⁰²: 0.00 (H), -0.46 (F), -1.24 (CH₃), -0.97 (Cl), -1.16 (Br) and -1.40 (I). Regression analysis was performed by linear regression; n denotes to the amount of data points, s to the standard deviation of the regression equation and R^2 to the coefficient of determination.¹⁰³⁻¹⁰⁴

In addition to steric parameters, the presence of the different substituents strongly influences the pK_a values of the respective pyridinium ions (Table 13). However, a linear relation to the logarithmic transformed inactivation constants can not be derived (Figure S9 Supporting Information), which underlines the importance of the sterical demand for the inhibitory potential. Therefore, there might be a hydrophobic pocket within the catalytic centre which could be occupied by the substituents in position 6 of the pyridine ring allowing a more favourable binding of larger substituents. This is further supported by the obtained dissociation constants, K_i , of the reversible enzyme-inhibitor complex (Table 4). These values decrease with increasing size of the substituents illustrating the contribution of the substituents to non-covalent interactions.

Interestingly, covalent docking studies indeed predicted a common recognition region for the functionalised fragment pyridine-2-yl in **7a-e** and **7i** around pocket 3 flanked by the side chains of Arg317 and Asn308, which resembles the binding mode found for **6a** (Figure 3B).

To assess the limits of the size of substituents in position 6, substituents with even greater sterical demand than iodine were introduced. As a result of the incorporation of the *tert*-butyl ($v=1.24 \text{ \AA}$, $E_S=-2.78$)^{97,102} and phenyl groups ($E_S=-3.82$; value is referred to the width)¹⁰², the inhibitory potential of **7f** ($k_{\text{inact}}/K_i=6\,140 \text{ M}^{-1}\text{s}^{-1}$) und **7g** ($k_{\text{inact}}/K_i=4\,560 \text{ M}^{-1}\text{s}^{-1}$) decreases compared to **7e**. The decrease is even more pronounced for compound **7h**, although the 2-fluoroethoxy might be of similar size as iodine ($v(\text{ethoxy})=0.48 \text{ \AA}$, $v(\text{F})=0.27 \text{ \AA}$)⁹⁷, but the asymmetric character is obviously less advantageous.

In contrast to the pyridine-2-yl derivatives **6a** and **7a-e**, covalent docking results suggested a different binding mode for **7f-h** in which the pyridine-2-yl moiety functionalised with the bulky *tert*-butyl, phenyl and 2-fluoroethoxy groups, respectively, occupy pocket 2 by making contacts with the protein residues Ile313, Phe316, Ile331 and Leu420, and the phenylacetyl moiety being either solvent-exposed or engaged in contacts with Lys176 or Phe334, which resembles the alternative binding mode predicted for **6a** (Figure 3C and Figure S6).

As ¹⁸F-labelled pyridines are accessible via the respective nitropyridine-derived precursors,¹⁰⁵⁻¹⁰⁶ compound **7i** was synthesised as a potential precursor for radiolabelling and characterised. Considering the SARs so far, compound **7i** ($k_{\text{inact}}/K_i=10\,200 \text{ M}^{-1}\text{s}^{-1}$) surprisingly exhibits the highest inhibitory potential within this series of analogues, which is twice as high as the inhibitory potential of reference compound **6a**. Concomitantly to the increase of the inactivation constant, the K_i value decreases from $5.73 \text{ }\mu\text{M}$ for **6a** to $2.26 \text{ }\mu\text{M}$ for **7i** indicating that the increased inhibitory potential is driven by more favourable non-covalent interactions. As the sterical demand of the nitro group ($E_S=-2.52$)¹⁰² is similar to that of the *tert*-butyl group, the reason for the increased inhibitory potential might be independent of the size. However, the nitro group could participate in polar interactions, particularly as hydrogen bond acceptor. Using the Eyring equation and the Van't Hoff isotherm the relation between the equilibrium constant of a reaction and the free enthalpy of a transition state can be expressed with equation I.

$$\ln k = \ln \left(\frac{\kappa k_B T}{h} \right) - \frac{\Delta G_0^\ddagger}{RT} \quad (\text{I})$$

k ...rate constant κ ...transmission coefficient
 k_B ...BOLTZMANN'S-constant R ...gas constant
 T ...temperature (303,15 K)
 h ...PLANCK'S constant
 K^\ddagger ...equilibrium constant of transition state
 ΔG_0^\ddagger ...free enthalpy of transition state

Accordingly, to quantify the contribution of the nitro group to lowering of the free enthalpy of the transition state, the difference of the k_{inact}/K_i values of **7i** and **7a** can be used (equation II).

$$\Delta\Delta G_0^\ddagger = -RT \ln \frac{(k_{\text{inact}}/K_i)_{7i}}{(k_{\text{inact}}/K_i)_{7a}} \quad (\text{II})$$

This results in an energy gain of 3.1 kJ/mol (0.74 kcal/mol) due to the presence of the nitro group compared to H. A similar value (3.31 kJ/mol, 0.79 kcal/mol) is obtained by the use of the K_i instead of the k_{inact}/K_i values. Typical energy gains of H bonds are in between 4 to 12 kJ/mol and for ionic interactions up to 20 kJ/mol,¹⁰⁷ but strongly depend in both cases on desolvation effects accompanied by the effect of enthalpy-entropy compensation.¹⁰⁸⁻¹¹¹ In view of a possible H bond, the nitro group generally represents a weak H bond acceptor ($pK_a(-\text{NO}_2\text{H}^+) = -11$, Ref. ¹¹²). However, the potential of aromatic nitro groups is higher than that of aliphatic ones.¹¹³ Covalent docking results on **7i** are supporting this assumption. The nitro group establishes side-on interactions with the guanidine group of Arg317 (Figure 3D). Interestingly, this charged residue located proximal to the catalytic site constitutes an exclusive feature of hTGase 2 (and also gpTGase 2) in comparison to all other human transglutaminases, which might confer certain selectivity towards hTGase 2 to those covalent inhibitors forming polar contacts with the side chain of Arg317 (see Figure S10 in Supporting Information).

Substitution at position 6 of pyridine-3-ylpiperazines

In addition to the favourable influence of the methyl group in *meta* position to the piperazine ring, Wityak et al. discovered also an increase of the inhibitory potential by incorporation of a trifluoromethyl group in *para* position to the piperazine ring (compounds **4o** and **4s** in Ref.⁵⁸, with the Z group as *N*-substituent and a pyridine-2-ylpiperazine moiety in **4s**). These results as well as the SARs from 2,6-disubstituted pyridine rings led to the idea of investigating substituents in position 6 of the pyridine-3-ylpiperazine in more detail (Table 5). The influence

of the ring position of the pyridine nitrogen atom, which was moved from *ortho* to *meta* position in this series, was separately investigated as discussed below.

Surprisingly, inhibitor **8a** ($k_{\text{inact}}/K_i=6\,520\text{ M}^{-1}\text{s}^{-1}$) bearing the unsubstituted pyridine-3-yl group exhibits a two times higher inhibitory potential than its regioisomer **7a** and is even more potent than reference compound **6a**. Because the pyridine nitrogen in **8a** has a similar spatial orientation as the nitro group in **7i**, polar interactions might again be responsible for the increase in the inhibitory potential. The low K_i value of $2.60\text{ }\mu\text{M}$ is in accordance with this hypothesis. However, the interactions of the pyridine nitrogen atom are obviously less favourable than those of the nitro group as the inhibitory potential of **8a** is still lower than that of **7i**. In agreement with these experimental observations, the binding mode predicted for **8a** enables interactions in which the nitrogen of the pyridine-3-yl group acts as H bond acceptor towards Arg317 in pocket 3 in a similar manner as the nitro group of **7i** but showing a different orientation of the piperazine group. Although both derivatives were also supported by additional H bonds with Trp241 and Asn333, **7i** was forming one additional favourable interaction with Gln276 (Figure 3D and Figure 5A).

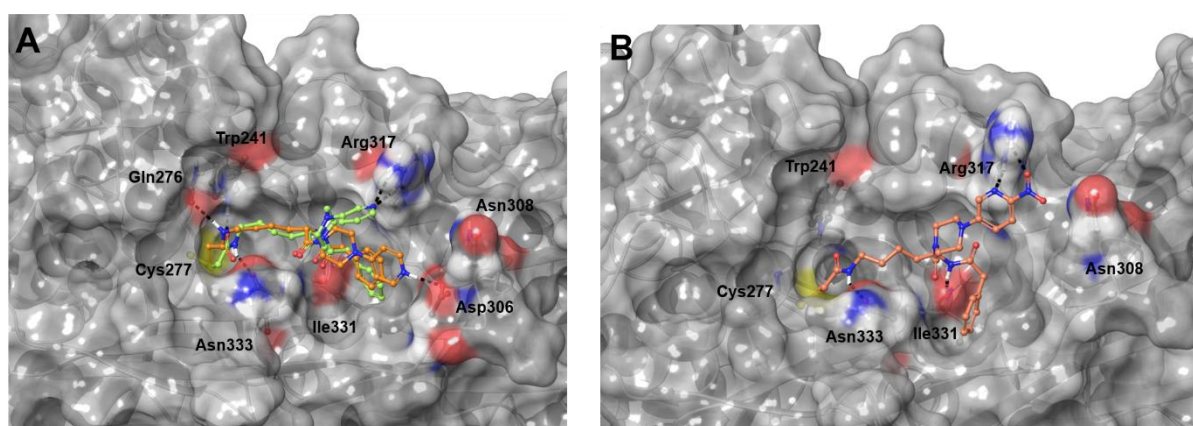


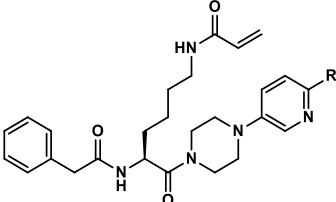
Figure 5. Molecular modelling of the interaction of hTGase 2 with covalent inhibitors.

The enzyme is shown in gray surface with relevant residues coloured by atom type and inhibitors are shown in sticks and colored by atom type. Intermolecular H bonds are depicted by black dashed lines. **A**) **8a** (green) and **10** (light orange) superimposed, **B**) **8d**. Figure generated in Maestro (Schrödinger).⁹⁰

The incorporation of F and CF_3 in position 6, especially with regards to potential radioligands, considerably diminishes the inhibitory potential of **8b** and **8c** in comparison to **8a** (Table 5). While the trifluoromethyl derivative **8c** is equipotent to the pyridine-2-yl derivative **7a**, the fluoropyridyl derivative **8b** is even less tolerated by hTGase 2. A sterical hindrance by the substituents can therefore be excluded. The reason for the reduced inhibitory potencies might be the dramatically diminished electron density at the pyridine nitrogen due to the strong

electron withdrawing effect of F and CF₃. This is reflected by the calculated pK_a values of the respective pyridinium ions (cpK_a(**8a**)=7.0; cpK_a(**8b**)=1.3; cpK_a(**8c**)=2.3, see Table 13 and Table S1 in Supporting Information). In turn, this lowers the suitability of the pyridine nitrogen as H bond acceptor. Even though the nitro group further decreases the electron density at the pyridine nitrogen (cpK_a=2.15), the inhibitory potential of compound **8d** ($k_{\text{inact}}/K_i=8\,460\text{ M}^{-1}\text{s}^{-1}$) is higher than that of compound **8a**. Consequently, the nitro group is able to compensate for the interactions of the pyridine nitrogen and can even increase the inhibitory potential. In contrast, the substituents F and CF₃ are weak H bond acceptors⁴⁸ and have therefore no compensatory function. The slightly higher inhibitory potential of **7i** compared to **8d** might indicate a more favourable orientation of the nitro group in *meta* position to the piperazine ring compared to the *para* position, in case they would interact with identical amino acid residues on the hTGase 2 protein. The predictions from covalent docking studies indicated side-on interactions of the nitro group and the pyridine nitrogen of **8d** with Arg317. However, **8d** showed one H bond less with the protein than **7i**, which would explain the lower inhibitory potency for **8d** (Figure 5B).

Table 5. Influence of the substituents in position 6 of the pyridin-3-yl moiety on the inhibition of hTGase 2

			
compound	R	$k_{\text{inact}}/K_i\text{ (M}^{-1}\text{s}^{-1}\text{)}$	$K_i\text{ (}\mu\text{M)}$
8a	H	6 520 (40)	2.60 (0.22)
8b	F	2 040 (120)	10.9 (2.1)
8c	CF ₃	2 700 (90)	6.77 (0.45)
8d	NO ₂	8 460 (710)	2.45 (0.09)
8e	COOH	1 750 (290)	-
8f	COOCH ₃	2 650 (150)	7.12 (0.82)
8g	CONH ₂	2 700 (20)	5.72 (0.22)
Data shown are mean values (\pm SEM) of two separate experiments, each performed in duplicate.			

Subsequently, to further characterise the supposed polar interactions of the nitro group, the three picolinic acid derivatives **8e**, **8f** and **8g** were synthesised. The isoelectronic substitution of the nitro group by the carboxylate group in compound **8e** reduced the inactivation constant to 1/5 of the value of **8d**. Notably, both methyl ester **8f** and primary amide **8g** are more potent

than **8e** resulting in inactivation constants similar to that of the CF₃ derivative **8c**. Comparable to the F and CF₃ substituents, the COO⁻, COOCH₃ and CONH₂ groups lower the electron density at the pyridine nitrogen (cpK_a values for the respective pyridinium ions 6.4 (**8e**), 3.4 (**8f**) and 4.3 (**8g**)). Although the potential of these groups for polar interactions can be rated higher than that of F, CF₃ and NO₂, they are obviously not able to compensate for the interactions of the pyridine nitrogen.¹¹³⁻¹¹⁶

The supposed polar interactions of the substituents in position 6 should be crucially influenced by their electron withdrawing character. To analyse this relation quantitatively, Hammett sigma constants can be used.¹¹⁷⁻¹¹⁸ Indeed, as shown in Figure 6, the logarithmically transformed inactivation constants of the inhibitors increase with the intensity of the electron withdrawing character of the substituents as defined by their σ_p values ($R^2=0.76$). In this context, the unsubstituted pyridine-3-yl derivative **8a** deviates from that relation as the pyridine nitrogen of this compound exerts strong interactions to the enzyme, which is not the case for the other inhibitors according to the docking predictions. As a specific characteristic in this series of analogues, the pyridine ring represents a *push-pull* system due to the *para* arrangement of the piperazine ring (+M effect) and the electron withdrawing substituents. A more appropriate parameter for the substituents in such systems is referred to as σ_p^- , which also considers occurrent resonance effects.¹¹⁹⁻¹²⁰ For the inhibitors **8c-8g**, there is a linear relation ($R^2=0.99$) between the σ_p^- and the logarithmically transformed inactivation constants (Figure 6).

The deviation of the derivative **8b** from that correlation in addition to compound **8a** might originate from the limited interaction potential of fluorine due to its smaller size compared to the other substituents. The significantly improved correlation for the substituents CF₃, NO₂, COO⁻, COOCH₃ and CONH₂ using their σ_p^- constants confirms the influence of the electron donating piperazine ring. The increased propensity of the nitro group for polar interactions in such *push-pull* systems, especially as H bond acceptor, is known.^{113,121} Nevertheless, the distinct predominance of NO₂ over COO⁻, CONH₂ and COOCH₃ is surprising and might indicate a more complex relation. A similar tendency between these substituents to act as H bond acceptors was discovered by Tan et al. for structure-activity relationships of dual cyclooxygenase 2/5-lipoxygenase inhibitors.¹²² However, in case of these inhibitors the substituents were bound to a phenyl group.

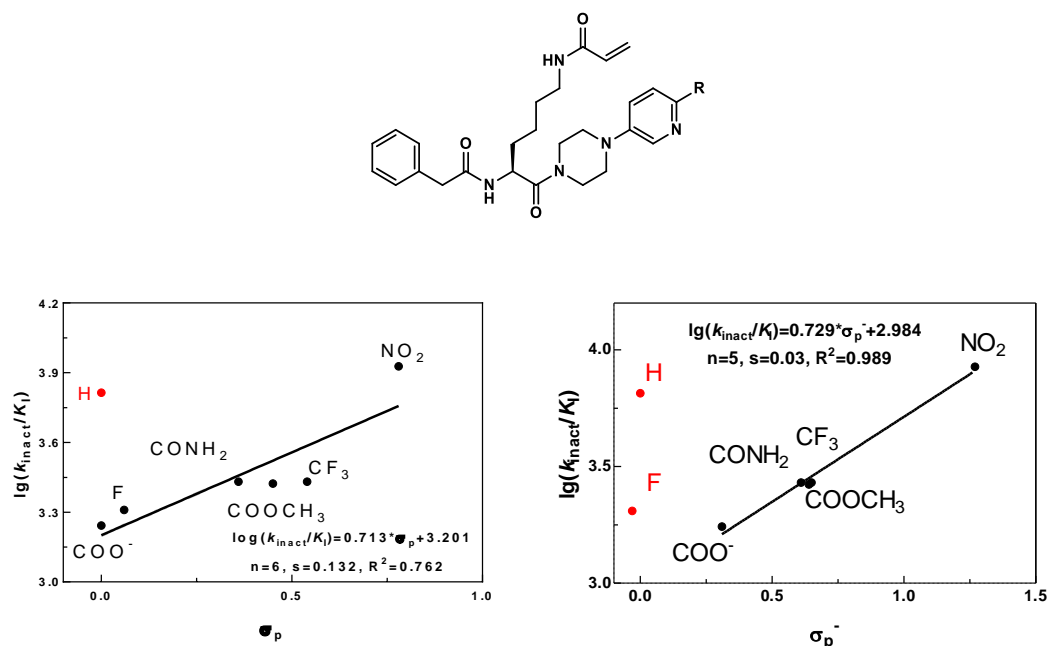


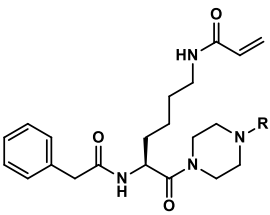
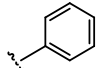
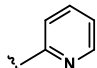
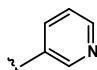
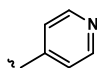
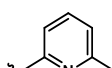
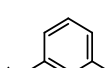
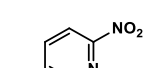
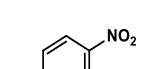
Figure 6. Relationship between the electronic properties (σ_p and σ_p^-) of the substituents in position 6 of the pyridin-3-yl moiety and the inactivation constants of the inhibitors 8a-g

Plots of $\lg(k_{\text{inact}}/K_i)=f(\sigma_p)$ (left) and $\lg(k_{\text{inact}}/K_i)=f(\sigma_p^-)$ (right) using the mean values of the inactivation constants of compounds **8a-8g** (Table 5) and the following values for $\sigma_p^{119,123}$: 0.00 (H), 0.06 (F), 0.00 (COO⁻), 0.36 (CONH₂), 0.45 (COOCH₃), 0.54 (CF₃) and 0.78 (NO₂) and σ_p^{-119} : 0.00 (H), -0.03 (F), 0.31 (COO⁻), 0.61 (CONH₂), 0.64 (COOCH₃), 0.65 (CF₃) and 1.27 (NO₂). Regression analysis was performed by linear regression. Data points in red were not considered for regression analysis. See text for the respective explanation.

Influence of the pyridine nitrogen

Previous SARs in this study indicated that the pyridine nitrogen influences the inhibitory potential in addition to the influence of the substituents at the pyridine ring. To further investigate this assumption, a series of phenylpiperazines and pyridylpiperazines (**9-12**) were synthesised and kinetically characterised (Table 6).

Table 6. Influence of the pyridine nitrogen on the inhibition of hTGase 2

			
compound	R	k_{inact}/K_i ($\text{M}^{-1}\text{s}^{-1}$)	K_i (μM)
9		2 970 (80)	-
7a^a		2 980 (80)	8.42 (1.29)
8a^a		6 520 (40)	2.60 (0.22)
10		10 500 (100)	2.55 (0.08)
6a^a		4 880 (20)	5.73 (0.77)
11		4 050 (40)	7.55 (0.79)
8d^a		8 460 (710)	2.45 (0.09)
12		7 700 (130)	2.52 (0.08)
Data shown are mean values (\pm SEM) of two separate experiments, each performed in duplicate. ^a Kinetic data for these compounds are already listed in Table 3, Table 4 and Table 5.			

Firstly, it was realised that the pyridine nitrogen in *ortho* position to the piperazine ring exerts no interactions to the enzyme as the pyridine-2-yl derivatives **7a** and **6a** exhibit similar inactivation constants as their deaza analogues **9** and **11**, respectively. Within the series of unsubstituted pyridine derivatives, the shift of the pyridine nitrogen from *ortho* to *meta* leads to a two-fold increase of the inactivation constants. A further doubling of the inhibitory potential is achieved by shifting the nitrogen to the *para* position ($k_{\text{inact}}/K_i=10\,500\,\text{M}^{-1}\text{s}^{-1}$) with the resulting compound **10** being equipotent to compound **7i**.

Due to the high pK_a value of the respective pyridinium ion in **10** ($cpK_a=10.7$, Table 13), the pyridine nitrogen might be mainly protonated at pH 6.5 (pH value applied in the fluorimetric assay). In turn, this means that the NH^+ group functions as an H bond donor instead of an H bond acceptor as in the case of the nitro group. Consequently, compounds **10** and **7i** are probably interacting with different residues within the binding site of hTGase 2. Covalent docking studies suggested two different binding modes for **10**, resembling previous findings. In the top-ranked pose, Asp306 could act as H bond acceptor towards the pyridine NH^+ when the phenylacetyl group is located in pocket 2 (Figure 5A). Alternatively, the pyridine NH^+ could form an H bond with the backbone of Phe316, while the phenylacetyl moiety is engaged in cation- π interactions with Lys176 (Figure S11 in Supporting Information).

The compensatory function of the nitro group in compound **8d** concerning the diminished interaction potential of the pyridine nitrogen was also confirmed as **8d** and its deaza analogue **12** exhibit similar inactivation constants ($8\,460\,M^{-1}s^{-1}$ and $7\,700\,M^{-1}s^{-1}$, respectively) and showed similar binding modes.

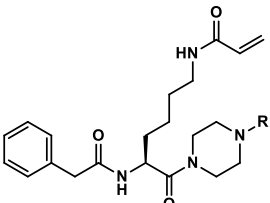
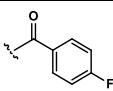
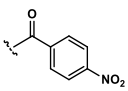
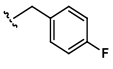
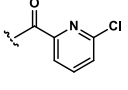
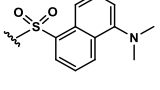
Benz(o)yl and sulfonyl substituents at piperazine

With respect to the synthesis of potential radiotracer candidates, the piperazine ring enables the incorporation of prosthetic groups containing fluorine, e.g. the 4-fluorobenzoyl group via *N*-succinimidyl-4- $[^{18}F]$ fluorobenzoate¹²⁴⁻¹²⁵ or the 4-fluorobenzyl group via reductive alkylation with 4- $[^{18}F]$ fluorobenzaldehyde.¹²⁶ Accordingly, the influence of benz(o)yl substituents on the inhibitory potential was investigated (Table 7).

The exchange of the 6-methylpyridin-2-yl moiety in reference compound **6a** by a 4-fluorobenzoyl group in **13a** leads to a reduction of the k_{inact}/K_i value from $4\,880$ to $1\,620\,M^{-1}s^{-1}$. Noteworthy, this difference in the inactivation constant is similar to that between **6a** and **8b** even though the structural variations differ significantly, which indicates a certain tolerance of hTGase 2 towards different aromatic groups at the piperazine ring. Due to the favourable impact of the nitro group attached to the pyridine ring on the inhibitory potential, the 4-nitrobenzoyl derivative **13b** was synthesised. Furthermore, this compound could act as a precursor for ^{18}F -fluorinations.¹²⁷ The kinetic characterisation revealed a twofold higher inhibitory potential of **13b** compared to its fluorine analogue **13a**, which demonstrates that the positive effect of the nitro group does also exist when it is attached to structurally different moieties. However, the potential polar interactions are obviously less favoured compared to **7i** and **8d**. In line with these observations, covalent docking results predicted mainly two different binding modes for **13b**. Thus, the nitro group could establish salt bridge or/and π -cation interactions with Arg317 instead of side-on H bonds, as observed for **7i** and **8d**, and the

phenylacetyl group might participate in π - π interactions with Trp278. Alternatively, the carbonyl oxygen of the 4-nitrobenzoyl group could make contacts with Arg317, while the phenylacetyl group could be located in pocket 2 (Figure S12 in Supporting Information). The lower number of H bonds between **13b** and hTGase 2 observed for these binding modes in comparison to those obtained for **7i** and **8d** is also in good agreement with the lower inhibitory capacity of **13b**.

Table 7. Influence of benz(o)yl and sulfonyl substituents at the piperazine ring on the inhibition of hTGase 2

			
compound	R	k_{inact}/K_i ($\text{M}^{-1}\text{s}^{-1}$)	K_i (μM)
13a		1 620 (190)	13.4 (2.7)
13b		2 950 (470)	7.71 (0.19)
13c		3 030 (120)	7.60 (0.07)
13d		1 340 (80)	-
13e		1 980 (70)	-
Data shown are mean values (\pm SEM) of two separate experiments, each performed in duplicate.			

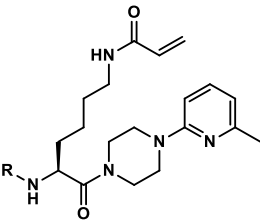
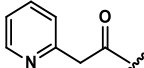
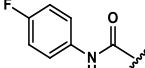
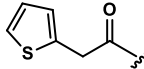
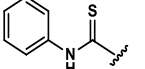
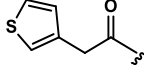
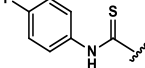
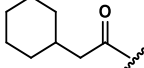
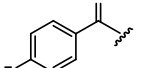
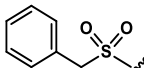
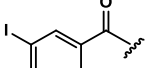
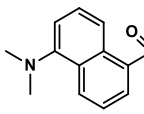
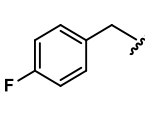
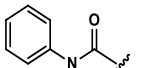
Formal reduction of the benzoyl-piperazine amide bond in **13a** led to the tertiary amine **13c**, which exhibits a twofold higher inhibitory potential than its amidic parent. Compound **13c** might benefit from increased conformational flexibility, which facilitates an advantageous orientation of the 4-fluorophenyl group within the binding site. The 6-chloropicolinic acid derivative **13d** belongs also to this group of compounds. Its k_{inact}/K_i value is slightly lower than that of the 4-fluorobenzoyl derivative **13a**. Therefore, as the interaction potential of the pyridine nitrogen might be negligible ($\text{cp}K_a$ value of 0.8 for the respective pyridinium ion, Table S1 in Supporting Information), the *meta* substitution by chlorine at the benzoyl group appears to be less well tolerated than the *para* substitution by fluorine.

Due to the good compatibility of the dansyl group as fluorescent moiety in TGase 2 inhibitors enabling diverse *in vitro* experiments,^{88,128} the dansyl group was also installed at the piperazine ring. Although this fluorophore has a significantly greater steric demand than the 6-methylpyridin-2-yl moiety of reference compound **6a**, the inhibitory potential of **13e** declines only to 40% of that from **6a**. Therefore, compound **13e** is even more potent than **13a** and **13d**. Interestingly, covalent docking results predicted a good tolerance for the dansyl group in pocket 2 while the phenylacetyl moiety would make contacts with Tyr245 and Met252 (Figure S13 in Supporting Information). This tolerance towards sterically demanding substituents at the piperazine ring was already demonstrated by Wityak et al., as compounds containing a 2-naphthyl or pyridine-2-yl moiety at the piperazine ring exhibit similar inhibitory capacity (compounds **4n** and **4o** in Ref.⁵⁸, with the Z group as *N*²-substituent). Furthermore, Akbar et al. recently reported an extensive SAR study for *N*²-Z-*N*¹-acryloyllysine piperazides with a primary focus on different sterically demanding acyl and sulfonyl groups at the piperazine ring.⁸¹ Worth of note, all structural modifications led to comparably potent hTGase 2 inhibitors with inactivation constants ranging from 582 M⁻¹s⁻¹ to 1 883 M⁻¹s⁻¹ (measured at pH=6.5 using Z-Glu(*p*NP)-Gly-OH as substrate). These results clearly emphasise the tolerance of hTGase 2 towards structurally different substituents at the piperazine ring.

Variations of the N² substituent

As mentioned above, systematic structural variations were also performed at the α-amino group of the lysine moiety (Table 8).

Table 8. Influence of different *N*^a-substituents on the inhibition of hTGase 2

					
cpd.	R	k_{inact}/K_i ($\text{M}^{-1}\text{s}^{-1}$)	cpd.	R	k_{inact}/K_i ($\text{M}^{-1}\text{s}^{-1}$)
14a		676 (61)	14h		278 (25)
14b[#]		3 480 (270)	14i		79 (1)
14c		1 680 (63)	14j		113 (10)
14d		232 (14)	14k		423 (22)
14e		362 (39)	14l		349 (21)
14f		95 (12)	14m		127 (11)
14g		287 (13)			
Data shown are mean values (\pm SEM) of two separate experiments, each performed in duplicate. [#] $K_i=5.56$ (0.02) μM					

Pyridyl and thienyl groups are often employed as bioisosteric replacements for phenyl groups,¹²⁹⁻¹³⁰ which is due to the similar steric and electronic properties of $-\text{CH}=\text{}$ and $-\text{N}=\text{}$ as well as $-\text{CH}=\text{CH}-$ and $-\text{S}-$, respectively.¹³¹⁻¹³² However, exchange of the phenylacetyl group by a pyridin-2-ylacetyl moiety results in a dramatic reduction of the inactivation constant for compound **14a** to 13% of the value for reference compound **6a**. The other two regioisomeric pyridylacetyl derivatives were also synthesised, however, their kinetic characterisation had to be omitted due to the observed macrocyclisation between the respective pyridine nitrogens and the acrylamide group (Discussion S1 in Supporting Information). A significantly higher reactivity towards hTGase 2 is achieved by the two regioisomeric thienylacetyl derivatives **14b** ($k_{\text{inact}}/K_i=3\,480\text{ M}^{-1}\text{s}^{-1}$) and **14c** ($k_{\text{inact}}/K_i=1\,680\text{ M}^{-1}\text{s}^{-1}$), which exhibit 68 and 33% of the activity of the phenylacetyl derivative **6a**, respectively. As benzene, pyridine and thiophene are similar

in their sterical demand, the size of the different aromatic systems might not be causative for the different inhibitory potential. In contrast to their similar size, their logP values differ significantly indicating a possible reason for the observed differences in reactivity. Indeed, the relationship between the respective Hansch's π values and the logarithmically transformed inactivation constants reveals a trend to higher inhibitory potential with increasing hydrophobicity of the substituents (Figure S14 in Supporting Information). This indicates that the aromatic rings might occupy a shared hydrophobic pocket, which simultaneously accounts for the differences in reactivity of the isomeric thienylacetyl derivatives. In agreement with this finding, docking studies indicate that the binding modes of **6a**, **14b** and **14c** are similar. However, it was observed that the phenyl- and 3-thienylacetyl groups of **6a** and **14c** were occupying pocket 2 more efficiently than the 2-thienylacetyl moiety in **14b**, which lost van-der-Waals contacts with Leu420. Nevertheless, the pyridyl group in **14b** establishes van-der-Waals interactions with Arg317, while this contact is not formed with **14c**, which might explain the different inhibitory potencies of the two regioisomers (Figure S15 in Supporting Information). Alternative binding modes were predicted exhibiting the pyridine ring positioned in pocket 2 and the phenyl- and thienylacetyl groups making contacts with Phe334 and Met252 or Phe320. Under these circumstances, the phenylacetyl group of **6a** fills the available space in pocket 2 better than the thienylacetyl derivatives. The electron density at the sulphur atom is slightly increased compared to the carbon atoms and this might be less advantageous when the sulphur atom extends deeper into the hydrophobic pocket. An even higher hydrophobicity is exhibited by the cyclohexylacetyl group, however, the formal saturation of the phenyl group also increases the sterical demand. This is probably the reason for the dramatically reduced inhibitory potential of **14d** to 5% of the value of reference compound **6a**.

The further structural modifications performed at the α -amino group comprise sulfonyl, carbamoyl, thiocarbamoyl and benz(o)yl groups, which all resulted in compounds with a significantly reduced inhibitory potential ($k_{\text{inact}}/K_i < 500 \text{ M}^{-1}\text{s}^{-1}$) compared to lead compound **6a** (for a more detailed discussion see Discussion S2 in Supporting Information). Consequently, rigidisation and shortening of the substituent at the α -amino group is detrimental for the inhibitory potential and the most favourable interactions are still exerted by the phenylacetyl group. In this regard, the binding modes predicted for this series of compounds appeared to be diverse. The newly incorporated functionalities could be disposed either along pocket 2 in a non-optimal manner, mostly only via interactions with Phe316, or making contacts with Phe320 or Phe334. The pyridine ring substituted with a methyl group in position 6 could be positioned either in pocket 2 forming van-der-Waals contacts with Ala304 at the surface of pocket 2 or being located in the proximity of Arg317.

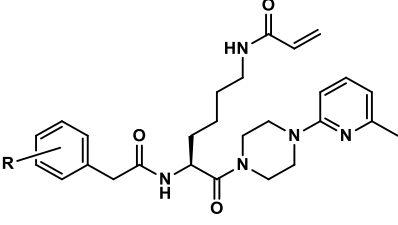
Substituents at the phenyl group of the phenylacetyl moiety

None of the phenylacetyl substitutions at the α -amino group resulted in a more potent inhibitor than reference compound **6a**. Consequently, a series of compounds was envisaged to investigate the influence of substituents at the phenyl group of the phenylacetyl moiety (Table 9).

For this purpose, a series of analogues varying in position 4 of the phenyl group was taken into focus. Incorporation of a methyl group, as done in compound **15a** ($k_{\text{inact}}/K_i=2\,940\text{ M}^{-1}\text{s}^{-1}$), reduced the inhibitory potential to almost 50% of the value of **6a**, whereas the presence of the halogen atoms F (**15b**), Cl (**15c**), Br (**15d**) and I (**15e**) is even worse tolerated. Compared to the analogous substitution at position 6 of the pyridine ring (compounds **6a**, **7a-7e**), a dependence of the inhibitory potential on the size of the substituents cannot be derived (Figure S16 in Supporting Information). Similarly, π -values as parameters for the hydrophobicity of the substituents are not suitable to describe the observed trend within compounds **6a** and **15a-15e** (Figure S17 in Supporting Information). However, with respect to the different inactivation constants of the thienylacetyl derivatives **14b** and **14c**, the electronic properties of the substituents might be pivotal for the observed trend of the inhibitory potential. The relationship between Hammett's σ_p values and the logarithmically transformed inactivation constants (Figure 7) reveals a linear increase of the inhibitory potential for **15a-15e** with increasing electron withdrawing effect of the substituents. Clearly, the hydrogen atom lies well above the regression line, which indicates that substitution of the 4-position at the phenylacetyl group could change the binding mode. This conclusion is supported by the results obtained from covalent docking. The 4-methylphenyl ring of compound **15a** is predicted to form cation- π interactions with the guanidino group of Arg317, while the 6-methylpyridyl moiety is positioned in pocket 2 (Figure 8A). This docking result is in line with the striking correlation between $\lg(k_{\text{inact}}/K_i)$ and σ_p shown in Figure 7, as the observed substituent effects resemble those that have been found for the cation- π interaction in supramolecular complexes between the tetramethylammonium ion and uranyl-salophen receptors bearing substituted benzyloxy arms.¹³³⁻¹³⁴ Docking results for the 4-halophenyl derivatives **15b-e** indicate similar interactions with Arg317 as predicted for **15a**. In turn, the obtained docking results explain the deviation of **6a** from the correlation in Figure 7 as the presence of substituents in the *para* position of the phenyl ring obviously induces a different binding mode compared to the unsubstituted derivative (phenylacetyl moiety preferably goes to pocket 2; Figure 3A), which is associated with the loss of one H bond. One H bond is also lost in alternative docking poses predicted for the enzyme-inhibitor complexes derived from the **15** series, in which the substituted phenylacetyl group is placed in the hydrophobic pocket 2 (Figure 8B). In general, the loss of

one H bond for the **15** series of compounds with respect to **6a** in both observed binding modes is consistent with their lower inhibitory capacity.

Table 9. Influence of substituents at the phenylacetyl moiety on the inhibition of hTGase 2

			
compound	R	k_{inact}/K_i ($\text{M}^{-1}\text{s}^{-1}$)	K_i (μM)
6a [#]	H	4 880 (20)	5.73 (0.77)
15a	4-CH ₃	2 940 (90)	-
15b	4-F	1 530 (50)	-
15c	4-Cl	1 050 (90)	-
15d	4-Br	1 130 (40)	-
15e	4-I	1 080 (10)	-
15f	2-F	3 770 (30)	4.49 (0.12)
15g	3-F	2 000 (170)	-

Data shown are mean values (\pm SEM) of two separate experiments, each performed in duplicate. [#]Kinetic data for **6a** are already listed in Table 3.

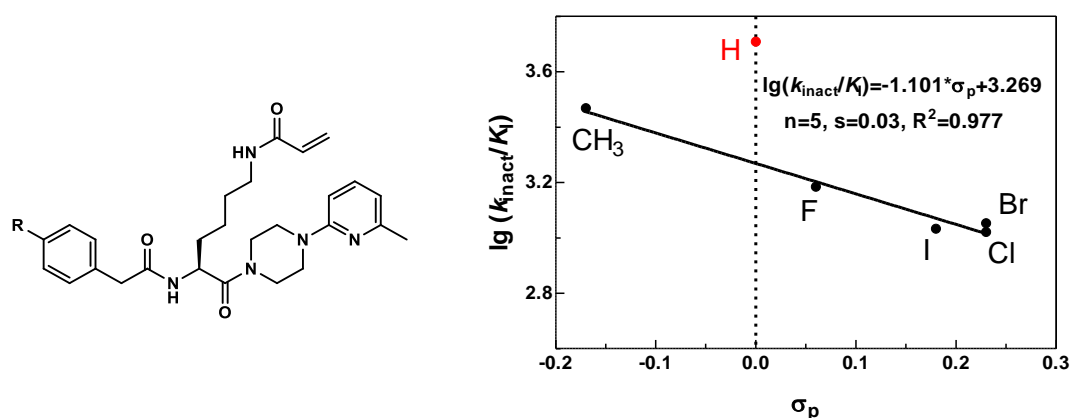


Figure 7. Relationship between the electronic properties (σ_p) of the substituents in position 4 of the phenylacetyl moiety and the inactivation constants of the inhibitors 6a and 15a-e

Plots of $\lg(k_{\text{inact}}/K_i) = f(\sigma_p)$ using the mean values of the inactivation constants of compounds **6a** and **15a-e** (Table 9) and the following values for σ_p^{119} : 0.00 (H), -0.17 (CH₃), 0.06 (F), 0.23 (Cl), 0.23 (Br), 0.18 (I). Regression analysis was performed by linear regression. Compound **6a** (data point in red) was not considered for regression analysis. See text for the respective explanation.

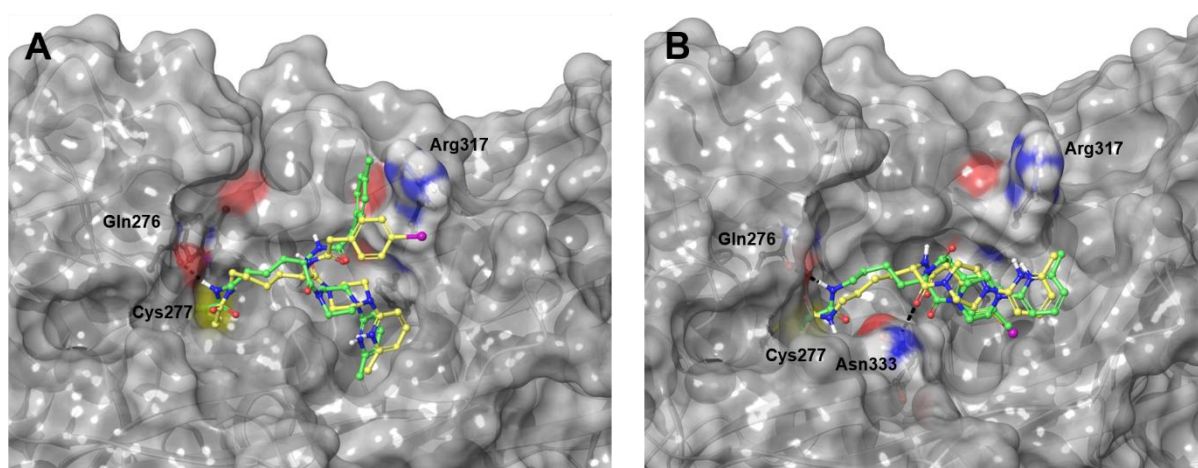


Figure 8. Different binding modes of the interaction of hTGase 2 with 15a (green) and 15e (yellow)

hTGase 2 is shown in gray surface with relevant residues coloured by atom type and inhibitors are shown in sticks and colored by atom type. Intermolecular H bonds and salt bridges are depicted by black and magenta dashed lines, respectively. Figure generated in Maestro (Schrödinger).⁹⁰

To investigate the dependence of the inhibitory potential on the position of substituents at the phenyl group, compounds **15f** and **15g** bearing a 2-fluorophenylacetyl and 3-fluorophenylacetyl moiety, respectively, were synthesised. According to their kinetic characterisation, substitution by fluorine in position 2 and 3 is better tolerated than in position

4; however, the 2-fluorophenylacetyl derivative **15f** is even twice as potent than the 3-fluorophenylacetyl derivative **15g**. Noteworthy, a similar trend was observed by Wityak et al. for CF₃ instead of F at the phenyl group in *N*^ε-Z-*N*^ε-acryloyllysine (IC₅₀ values of 3.5 μM (2-CF₃), 10 μM (3-CF₃) and 33 μM (4-CF₃)).⁵⁸

*Combination of selected pyridylpiperazinyl and *N*^ε substituents*

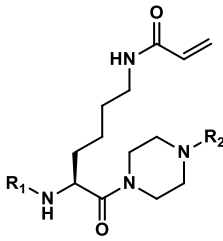
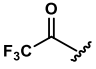
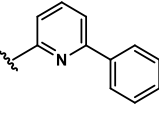
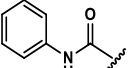
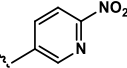
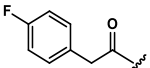
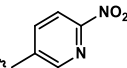
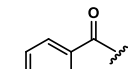
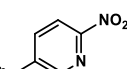
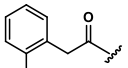
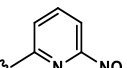
In addition to structural modifications, which were either performed at the piperazine ring or the α-amino group, compounds with variations at both sites were also envisaged to study whether the different moieties contribute additively to the inhibitory potential (Table 10).

In this context, compound **16c** bearing a 6-phenylpyridin-2-yl and a trifluoroacetyl group represents rather an accidentally obtained product as the trifluoroacetylation at the α-amino group was a side reaction during the phenylacetylation (Discussion S1 in Supporting Information). However, compared to the phenylacetyl analogue **7g** ($k_{\text{inact}}/K_{\text{I}}=4\,560\text{ M}^{-1}\text{s}^{-1}$), the presence of the trifluoroacetyl group ($k_{\text{inact}}/K_{\text{I}}=1\,600\text{ M}^{-1}\text{s}^{-1}$) is detrimental for the inhibitory potential but better tolerated than most of the other variations at the α-amino group (Table 8).

To investigate the favourable effect of the 6-nitropyridin-3-yl moiety (present in **8d**), this group also combined with three other substituents at the α-amino group (compounds **17a-c**). The inhibitory potentials of these inhibitors increase compared to their 6-methylpyridin-2-yl analogues by factors of 1.1-3.2 for the inactivation constants (Figure S18 in Supporting Information). The propensity of the nitro group to engage in non-covalent interactions is also reflected by the systematic variations of the initial velocities v_{i} observed for **17a-c**, which accounts for the determination of their K_{I} values in contrast to compounds **14g**, **14k** and **15b**. A similar result was obtained using the 6-nitropyridin-2-yl moiety (present in **7i**). Compound **18** bearing this pyridyl group and a 2-fluorophenylacetyl group at *N*^ε is two times more potent than its 6-methylpyridin-2-yl derivative **15f**. Consequently, the detrimental effect of the *N*^ε substituent is partially compensated by the nitropyridyl moiety, independently of the kind of substituent.

Further inhibitors obtained by combination of different pyridylpiperazinyl and *N*^ε substituents are included in Figure S19 in Supporting Information.

Table 10. Inhibition of hTGase 2 by double modified *N*^F-acryloyllysines

				
compound	R ₁	R ₂	k_{inact}/K_i (M ⁻¹ s ⁻¹)	K_i (μM)
16c			1 600 (200)	14.3 (3.79)
17a			932 (80)	7.96 (0.01)
17b			3 570 (380)	5.02 (0.18)
17c			470 (31)	14.0 (0.18)
18			8 220 (170)	1.98 (0.02)
Data shown are mean values (±SEM) of two separate experiments, each performed in duplicate.				

*Reactivity of *N*^F-acryloyllysines towards different enzymatic activities and different pH values*

Concerning the issue of assay comparability as well as dependence of inhibitory activity on pH value, selected *N*^F-acryloyllysines were screened with both assay methods towards both enzymes. The relationships between values of k_{inact}/K_i and IC₅₀ for both enzymes are shown in Figure 9. Worth of note, an apparent linear correlation can be obtained for both enzyme species even though the two assay methods use different pH values (6.5 versus 8.0) and measure different enzymatic activities (hydrolase versus transamidase activity). Consequently, the same trend in inhibitory activity is retained under both assay conditions (whereas the absolute reactivity might be different) and - eventually even more interesting - the inhibitory behaviour towards enzymatic hydrolysis and transamidation are essentially comparable. However, compound **7b** significantly deviates from the correlation for the human enzyme as it has higher inhibitory potential at pH 8.0 (or lower potential at pH 6.5) compared to the expected value based on the tendency for the other compounds.

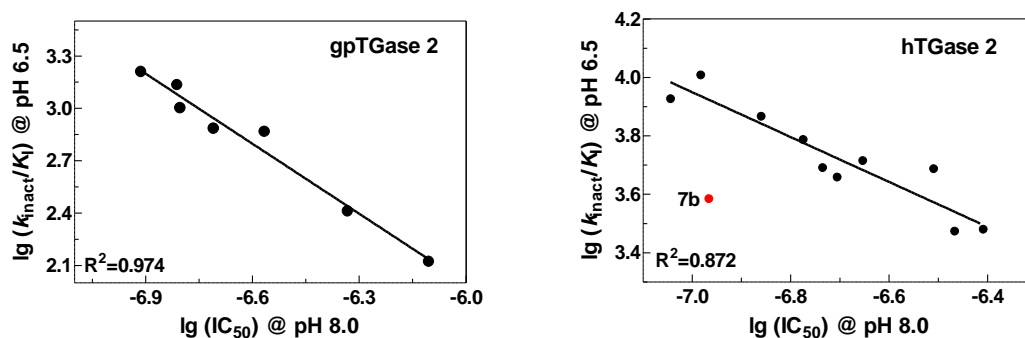


Figure 9. Relationship between IC_{50} values from FA assay (pH 8.0) and k_{inact}/K_i values from fluorimetric assay (pH 6.5)

Plots of $\lg(\text{IC}_{50})=f(\lg(k_{\text{inact}}/K_i))$ for gpTGase 2 (inhibitors **6a**, **6b**, **7b**, **7i**, **8d**, **14h** and **15e**) (left) and hTGase 2 (**6a**, **7a-i** and **8d**) (right) using selected inhibitors. The coefficients of determination resulting from the regression analyses by linear regression are shown. Data point in red (**7b**) (right) was not considered for regression analysis. See text for the respective explanation.

N^F-propionyllysine piperazides as reversible inhibitors

According to the two-step inhibition mechanism of TGase 2 by the *N^F*-acryloyllysine piperazides, which was concluded based on the observed systematic reduction of the initial velocities v_i in the substrate conversion curves with increasing inhibitor concentration, there is a non-covalent enzyme inhibitor complex prior to the final covalent complex. Consequently, inhibition of the activity of hTGase 2 should also be observed for the case that the acrylamide warhead is replaced by a similar group which does not form a covalent bond with the active cysteine residue. To prove this hypothesis, the respective *N^F*-propionyl analogues **21a** and **21b** (Figure 10) of lead compound **6a** and the nitropyridyl derivative **8d**, respectively, were synthesised and kinetically characterised. Moreover, an analogue of a potential radiotracer which does not form a covalent bond with hTGase 2 could act as a control compound for PET studies to get information on the envisaged target binding of the radiotracer *in vivo*.

The formal saturation of the C-C double bond within the acryloyl group leads to an inert group, but simultaneously the respective propionyl group exhibits a slightly greater sterical demand, which might influence the interactions with the enzyme. As expected, the enzymatic conversion of **Z-Glu(HMC)-Gly-OH** in the presence of **21a** or **21b** yielded linear progression curves where the slopes decrease with increasing inhibitor concentrations (Figure S20 in Supporting Information). Analysis of the recorded data on the basis of a competitive inhibition mechanism provided K_i values of 64.3 and 15 μM for **21a** and **21b**, respectively. These values are significantly higher than those for **6a** (5.73 μM) and **8d** (2.45 μM), which might not only result

from the different sterical demand of the *N*^ε-substituents but also from the fact that the K_i values determined for **6a** and **8d** are kinetically defined, whereas those of **21a** and **21b** represent equilibrium constants.

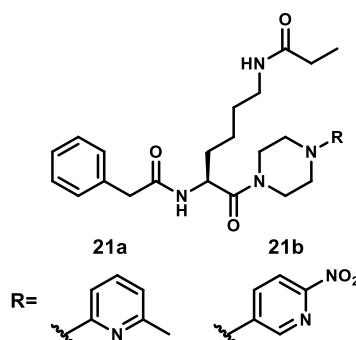


Figure 10. Structures of the reversible inhibitors 21a and 21b

Reactivity of *N*^ε-acryloyllysines towards guinea pig TGase 2 in comparison to their reactivity towards human TGase 2

In the course of the kinetic characterisation of the *N*^ε-acryloyllysines towards hTGase 2 we were also interested in their reactivity towards gpTGase 2, which was used for a long time as cost-efficient alternative to the human enzyme.⁸³ In this context, a recent study demonstrated that several substrates and inhibitors exhibit similar kinetic parameters towards both enzymes.⁸³ However, as shown in our previous study, the reactivity of **6a** by means of k_{inact}/K_i values towards hTGase 2 is by a factor of ≈ 7 higher when compared with gpTGase 2, which indicates a difference in the binding of **6a** within the catalytic centres of both isoforms. In addition to reference compound **6a**, its D-enantiomer **6b** was also characterised towards gpTGase 2 using the fluorimetric assay. Similar to the human isoform, the L-configuration is preferred by gpTGase 2 as compound **6b** ($k_{\text{inact}}/K_i=133 \text{ M}^{-1}\text{s}^{-1}$) exhibits a lower inhibitory potential than **6a** ($k_{\text{inact}}/K_i=740 \text{ M}^{-1}\text{s}^{-1}$). However, as the inhibitory activity of **6a** (eutomer) towards gpTGase 2 is lower compared to hTGase 2, the eudismic ratio is also lower (24 and 5 for hTGase 2 and gpTGase 2, respectively).

In accordance to the lower reactivity of **6a**, the inactivation constants k_{inact}/K_i of compounds **7b**, **7i** and **8d** are reduced towards gpTGase 2 by factors of ≈ 5 -7. This difference in reactivity was further proven by determination of IC_{50} values using the fluorescence anisotropy assay for the compound series **7** as well as compounds **6a** and **8d** towards both enzymes (Table 11). Even though the pre-incubation period for gpTGase 2 was six times longer than for hTGase 2 (30 min *versus* 5 min), the IC_{50} values are similar or even lower for the human enzyme. Concerning SARs for the gpTGase 2, the nitropyridyl derivatives **7i** and **8d** are again

significantly more potent than the lead compound **6a** as reflected by their high inactivation constants and low IC₅₀ values. Generally, this indicates similar interactions of these compounds with gpTGase 2 and hTGase 2. However, the productivity of binding is considerably higher at the humane enzyme. Apart from that analogy, the trend within the series of compounds **7** (see IC₅₀ values) is less distinct for gpTGase 2 compared to hTGase 2. Substitutions in position 6 of the pyridine-2-yl moiety are obviously well tolerated but no explicit relation could be derived.

Table 11. Reactivity of selected *N*^ε-acryloyllysines towards hTGase 2 and gpTGase 2

cpd.	<i>k</i> _{inact} / <i>K</i> _i (M ⁻¹ s ⁻¹)		IC ₅₀ (μM)	
	hTGase 2	gpTGase 2	hTGase 2	gpTGase 2
6a	4 880	740	0.31	0.27
6b	206	133	-	0.79
7a	2 980	-	0.34	0.31
7b	3 850	771	0.11	0.20
7c	4 910	-	0.18	0.16
7d	5 200	-	0.22	0.20
7e	7 350	-	0.14	-
7f	6 140	-	0.17	0.17
7g	4 560	-	0.20	0.15
7h	3 020	-	0.39	0.27
7i	10 200	1 630	0.10	0.12
8d	8 460	1 370	0.09	0.15
14h	278	259	-	0.46
15e	1 080	1 010	-	0.16

For details on the calculation of the kinetic parameters, see Experimental Section. Data shown for hTGase 2 and gpTGase 2 are mean values of at least two separate experiments, each performed in duplicate.

In contrast to these results, compounds **14h** (4-fluorophenylcarbamoyl group at *N*^ε) and **15e** (4-iodophenylacetyl group at *N*^ε) exhibit similar inactivation constants towards both enzymes. Interestingly, **15e** is even more potent than **6a** towards gpTGase 2 indicating other structural requirements for the substituents at the α-amino group. A model of gpTGase 2 was built to investigate the binding mode of **6a** and **15e** and shed light on the molecular basis for recognition that could rationalise their inhibitory activities towards this enzyme with respect to hTGase 2. First, the comparison of the active sites modelled for hTGase 2 and gpTGase 2 suggested differences in pocket 2 and pocket 3 (Figure S21 in Supporting Information). Pocket 2 appears slightly more closed in hTGase 2 because of the disposition of Phe320, which corresponds to Ser320 in gpTGase 2, and leave Met330 more exposed. On the other hand, pocket 3 seems to be broader in the guinea pig homologue. These structural differences could affect the inhibitory capacity of the developed inhibitors on these two orthologous enzymes.

Further covalent docking of **6a** on the gpTGase 2 revealed a lack of important interactions with the protein compared to the human enzyme, which is consistent with the kinetic data. The pyridyl moiety was positioned in pocket 2, the phenylacetyl was oriented towards Arg317 and only one H bond with Trp241 was predicted. In contrast, the predicted binding mode for **15e** is similar for both orthologues, which is reflected by similar inhibitory potencies towards gpTGase 2 and hTGase 2 (Figure S22 in Supporting Information).

Selectivity and initial pharmacokinetic profiling of selected inhibitors

In addition to the kinetic characterisation towards hTGase 2 and gpTGase 2, selected inhibitors were subjected to selectivity and pharmacokinetic analyses to obtain more information with regards to their suitability for in vivo application. For selectivity studies, compounds **7b** and **7i** were chosen as they represent one of the most potent fluorinated inhibitors and one of the most potent inhibitors in this study in general, respectively. The kinetic characterisation towards hTGase 1, hTGase 3, hTGase 6 and hfXIIIa using the fluorogenic acyl donor **Z-Glu(HMC)-Gly-OH** revealed an excellent selectivity of both compounds for hTGase 2 with selectivity factors between 275 and 1925 (Table 12). Therefore, the substitution of the methyl group by fluorine or a nitro group does not seem to influence the reactivity towards these human TGase-isoforms, even though the given selectivity for reference compound **6a** by Wityak et al. was not re-assessed.⁵⁸ Due to the use of mouse models for preclinical evaluations of biological active compounds, especially radiotracers, the inhibitory potentials of **6a**, **7b** and **7i** were also determined towards mTGase 2. In accordance to the similar substrate properties of **Z-Glu(HMC)-Gly-OH** towards human and mTGase 2, the k_{inact}/K_i values of these three inhibitors are similar between the two enzyme isoforms, which indicates a high similarity within their active sites.

To demonstrate the reactivity of the *N*^F-acryloyllysines towards TGase 2 in a biological matrix, the inhibitory potencies of **6a**, **7b** and **7i** were characterised in cell lysates from A375 human melanoma cells. These cells exhibit a significant expression of hTGase 2 as determined by Western blot analyses (Figure S23 in Supporting Information). hTGase 2 activity in cell lysates was measured by using the fluorescence anisotropy assay with DMC and **R-I-Cad** as substrates. Notably, the increase in the fluorescence anisotropy originates exclusively from the hTGase 2-catalysed incorporation of **R-I-Cad** into DMC as no signal increase can be detected in the presence of the selective inhibitors **6a**, **7b** and **7i** or in the absence of DMC (Figure S24 and Figure S25 in Supporting Information). Furthermore, lysates from MeWo cells, which show virtually no expression of hTGase 2, did not lead to any measurable signal either (Figure S24). The inhibitory activity of the three *N*^F-acryloyllysines was quantified by the determination of IC₅₀

values. As shown in Table 12, the inhibitors largely retain the submicromolar activity as observed for the isolated target enzyme. Compound **7i** is the most potent inhibitor (0.40 μM), even though the IC_{50} values in cell lysates (see Figure S25 for the respective curves) are considerably higher compared to the values obtained for the recombinant enzyme. It should be mentioned that due to the rather artificial assay conditions (3 mM CaCl_2) applied in these experiments, the detected hTGase 2 activity corresponds to the amount of activatable hTGase 2 and does not reflect hTGase 2 activity in intact cells. Nevertheless, such assay methods provide evidence for target reactivity in a biologically more relevant assay setting for the respective inhibitors.¹³⁵

Table 12. Selectivity and cellular lysate activity of inhibitors 6a, 7b and 7i

cpd.	k_{inact}/K_i ($\text{M}^{-1}\text{s}^{-1}$) ^a						hTGase 2 IC_{50} (μM) ^b	A375-hTGase 2 IC_{50} (μM) ^c
	hTGase 2	mTGase 2	hTGase 1	hTGase 3	hTGase 6	hFXIIIa		
6a	4 880	3 420	<i>n. d.</i>	<i>n. d.</i>	<i>n. d.</i>	<i>n. d.</i>	0.31	0.79
7b	3 850	3 990	9	<i>n. d.</i>	14 ^d	2	0.11	1.10
7i	10 200	8 900	23	<13	13 ^d	13	0.10	0.40

For details on the calculation of the kinetic parameters, see Experimental Section. ^aThe following concentrations of acyl donor **Z-Glu(HMC)-Gly-OH** were used: 25 μM (gpTGase 2), 30 μM (hTGase), 35 μM (mTGase 2), 40 μM (hTGase 1, hTGase 3, hTGase 6, hFXIIIa). Data shown for hTGase 2 and mTGase 2 are mean values of two separate experiments, each performed in duplicate. Data shown for hTGase 1, hTGase 3, hTGase 6 and hFXIIIa are mean values of one experiment, which was performed in duplicate. ^bhTGase 2 was preincubated with inhibitor for 5 min, DMC (30 μM) and **R-I-Cad** (0.81 μM) were used as substrates. ^cSame conditions as described under b with a protein concentration of the lysate of 2 g/l (corresponds to a TGase 2 activity of approx. 1 $\mu\text{g}/\text{mL}$). IC_{50} values shown are mean values of two to three experiments, each performed in duplicate. ^dCalculated value based on the k_{obs} value at $[I]=200$ μM . *n. d.* denotes to not determined.

One of the biggest challenges during drug development is often faced by the gastrointestinal absorption of the drug after oral administration. Even though this barrier is not relevant for potential radiotracers, the knowledge about their cell and tissue penetration is essential, which for most of the small molecules takes place via passive diffusion.¹³⁶ The physicochemical parameters influencing the passive diffusion of molecules include acid-base character, lipophilicity, solubility, and membrane permeability. To obtain these parameters, appropriate experimental as well as computational methods exist.¹³⁷

To characterise the *N*^ε-acryloyllysines regarding their membrane permeability, the PAMPA (parallel artificial membrane permeability assay) method was used, which allows for the screening of a library of compounds.^{136,138} Using this method, the passive diffusion of compounds through an artificial membrane can be characterised. The PAMPA method was performed in a 96-well plate format with subsequent spectrophotometric determination of the compound concentrations in donor and acceptor wells. A mixture of 1,2-dioleoyl-*sn*-glycero-3-phosphocholine (DOPC, 10%, w/v) and cholesterol (5%, w/v) in dodecane was used as artificial membrane.^{136,139-140} Finally, to quantify the membrane permeability, the effective

permeability P_e (in nm/s) was calculated for each compound considering the respective membrane retention R_M .¹⁴¹ Initially, the validity of the PAMPA method and the differentiable range of P_e values was characterised using reference compounds of known membrane permeability. To this end, hydrochlorothiazide (poorly permeable), metoprolol (moderately permeable) and verapamil (highly permeable) were chosen¹⁴² and the expected tendency of their P_e values was confirmed (Table 13, range from 0.6 to 520 nm/s). However, it should be mentioned that the PAMPA method as performed here does not consider the phenomenon of unstirred water layers (UWLs), which are adjacent to both sides of the membrane.¹⁴³⁻¹⁴⁵ These UWLs particularly influence the permeation rate of highly permeable compounds where the permeation through the UWLs becomes rate-limiting, which results in an upper limit for P_e .¹⁴⁶ Therefore, structure-property relationships within a group of well permeable compounds cannot be derived.

Similar to the reference compounds, the P_e values for the *N*^ε-acryloyllysines range from 3 to 220 nm/s revealing significant differences in the permeation rates. The majority of compounds appears to be well permeable exhibiting P_e values between 100-220 nm/s. The narrow range of P_e values might reflect the aforementioned limitations for the characterisation of well permeable compounds due to the present UWLs.

Considering the P_e values of hydrochlorothiazide and metoprolol, a series of compounds with poor or moderate permeability was identified. This is of particular importance with respect to the selective targeting of intra- and extracellular TGase 2, especially by radiotracers in vivo. The picolinic acid derivatives **8e** and **8g** and the pyridine-4-yl derivative **10** can be classified as poorly permeable. The low P_e value of **10** (5.1 nm/s) might originate from the high pK_a value of the respective pyridinium ion ($cpK_a=10.7$, Table 13) resulting in a positively charged molecule at pH 7.5. Accordingly, due to the lower pK_a value of the pyridinium ion, the regioisomeric pyridine-3-yl derivative **8a** ($cpK_a=7.0$, Table S1) exhibits a higher P_e value than compound **10** (12.9 nm/s). However, the highest P_e value within the regioisomeric pyridine derivatives was determined for the pyridine-2-yl derivative **7a** (61.3 nm/s) even though the pK_a value of the pyridinium ion ($cpK_a=8.4$, Table S1) lies between that of **10** and **8a**. In accordance with this result, compounds bearing a 6-methylpyridine-2-yl moiety exhibit high P_e values, which was not expected based on the pK_a value of the pyridinium ion ($cpK_a=9.1$, Table S1). In this context, Chen et al.¹⁴⁷ recently showed within their mechanistic study on the permeability of meta-substituted pyridines that not membrane partitioning but rather aqueous desolvation of these compounds dictates the permeation rate. Consequently, an unfavourable solvation of the pyridine-2-yl moieties could be the reason for the relatively high permeation rates of the respective *N*^ε-acryloyllysines.

Noteworthy, the group of compounds with moderate permeability comprises amongst others the 6-nitropyridin-3-yl derivatives **8d** and **17a-17c**, while the 6-nitropyridine-2-yl derivatives (**7i** and **18**) exhibit significantly higher P_e values. The difference in the permeation rates for the nitropyridine derivatives might originate from the aforementioned *push-pull* effect within the 6-nitropyridine-3-yl substituents, which increases the polar character of these compounds.

During the calculation of the P_e values, the membrane retention R_M (portion of compound which remains in the membrane) can be derived. This parameter is given in Table 13 as molar fraction (%) of the applied amount of substance. With respect to the development of radiotracers, high non-specific binding of compounds is often a problem and a common reason for the failure of promising candidates.¹⁴⁸⁻¹⁴⁹ Therefore, an in vitro method which can predict the potential degree of non-specific binding is highly desirable. In this context, Jiang et al. observed that the chromatographic hydrophobicity index values (CHI IAM, determined at an immobilised artificial membrane) correlate well with data from in vitro non-specific binding obtained by equilibrium dialysis ($R^2=0.79$).¹⁴⁸ Due to the similar origin, R_M values should contain similar information as CHI IAM_{7.4} values. To this end, for a series of compounds including all fluorinated inhibitors, the CHI IAM_{7.4} values were measured and compared to the R_M values (Table 13). Indeed, a similar trend between both parameters can be observed. Whereas most of the compounds exhibit R_M values of <30%, some of them show significantly higher values including the 6-*tert*-butyl-pyridine-2-yl derivative **7f** ($R_M=69\%$) and the 6-phenyl-pyridine-2-yl derivative **7g** ($R_M=64\%$). Accordingly, the CHI IAM_{7.4} values for most of the compounds are around 30, whereas **7f** and **7g** exhibit values of ≈ 39 .

In addition to the calculation of $\log D_{7.4}$ values, these parameters were also experimentally determined for several fluorinated inhibitors by using a novel ^{19}F -NMR-based method developed by Linclau et al.¹⁵⁰ This method is basically a variation of the classical shake-flask method in which the proportion of the fluorinated compound in the octanol and aqueous phase were measured by ^{19}F -NMR spectroscopy with trifluoroethanol as internal standard. As seen in Table 13, the tendency for the calculated $\log D_{7.4}$ values is in accordance with the experimental values. However, the absolute experimental values are 0.32 to 1.21 log units higher than the calculated values, clearly demonstrating the limits of computational methods.

As mentioned above, solubility is a further parameter which co-determines their passive diffusion as it characterises the concentration a compound can reach in a distinct solution.¹⁵¹ For compounds **7b** and **7i**, the thermodynamic solubility in PBS (pH 7.4 and 22°C over 26 h and 39 h, respectively) was measured revealing values of 645 and 452 μM , respectively. These values will guide in vitro and in vivo experiments in which the addition of organic co-

solvents to increase the solubility is more limited than in experiments using recombinant enzymes.

Table 13. Determined and calculated physicochemical parameters of selected *N*^ε-acryloyllysines

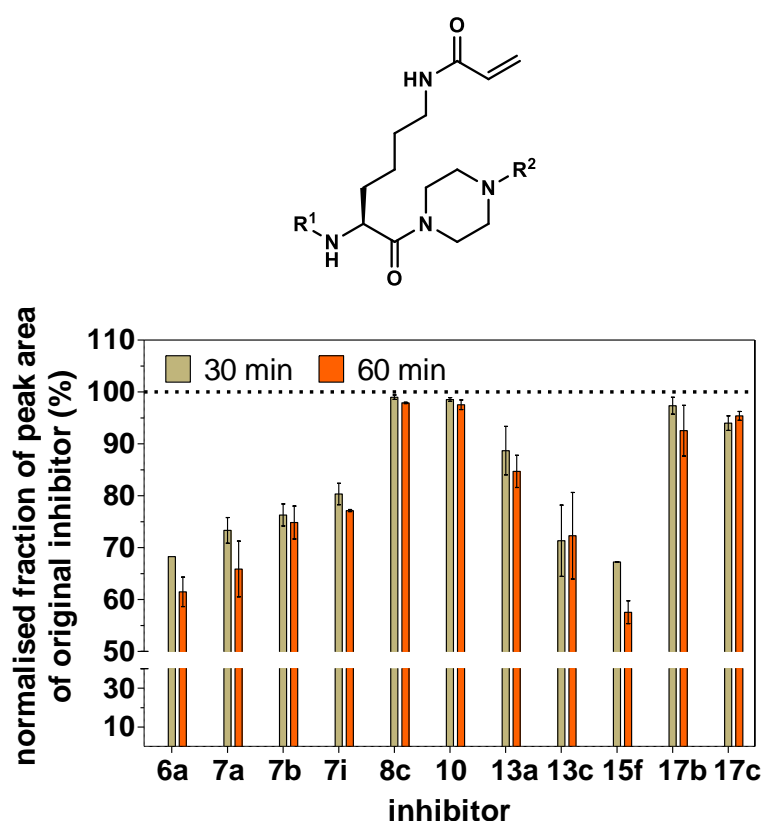
cpd.	cpK _a ^a	logD _{7.4}	clogD _{7.4}	P _{e(7.5)} (nm/s)	R _M (%)	CHI IAM _{7.4}
6a	9.1	-	-0.36	87.7 (3.9)	-1	29.4
7b	2.8	2.10	1.27	133 (19)	14	31.8
7f	8.9	-	2.77	219 (28)	69	39.5
7g	7.6	-	2.79	219 (57)	64	39.0
7i	0.6	-	1.02	91.6 (8.1)	10	30.7
8b	1.3	1.66	1.05	35.4 (3.2)	4	26.8
8c	2.3	2.13	1.81	89.8 (3.1)	11	31.8
10	10.7	-	-0.37	5.1 (0.8)	31	25.4
13a	-	1.60	1.18	30.5 (5.2)	-3	25.0
13c	6.2 ^b	2.65	1.98	103 (13)	12	32.0
13e	4.1 ^c	-	3.08	76.8 (4.8)	38	37.7
14h	9.1	0.47	-0.32	125 (31)	11	34.3
14k	9.1	0.28	-0.10	127 (27)	16	31.4
15b	9.1	0.36	-0.32	114 (7.0)	10	32.4
15f	9.1	-	-0.32	114 (9.0)	21	30.1
15g	9.1	-	-0.32	125 (3.2)	24	30.9
17b	-2.5	1.85	1.04	19.7 (3.1)	9	28.3
17c	-2.5	2.21	1.17	40.8 (5.7)	12	28.5
18	0.6	2.25	1.04	87.4 (5.4)	12	30.7

Fluorinated compounds are coloured in blue. P_{e(7.5)} values for the reference compounds are as follows: hydrochlorothiazide (0.6 ± 0.1), metoprolol (40.4 ± 5.1), verapamil (520 ± 80). Further information to the calculated parameter cpK_a, clogD_{7.4} and the experimentally determined parameter logD_{7.4}, P_{e(7.5)}, R_M and CHI IAM_{7.4} can be found within the Experimental Section and in Table S1 of the Supporting Information. ^aIf not otherwise stated, the cpK_a value corresponds to the pK_a value of the respective pyridinium ion. ^bValue corresponds to the piperazinium ion. ^cValue corresponds to the dimethylammonio group of the dansyl moiety.

Evidence towards the susceptibility of compounds against oxidative in vivo metabolism can be obtained by investigating their stability in the presence of liver microsomes.¹⁵² Data from such studies for the lead compound **6a** reported by Wityak et al. suggest that it is insufficiently stable against oxidative metabolism.⁵⁸ To get more detailed information, **6a** and a series of selected inhibitors, mainly fluorinated compounds, were tested towards their stability in mouse liver microsomes. Therefore, compounds were incubated with mouse liver microsomes in the presence of NADPH and the resulting mixtures were analysed after 30 and 60 min by HPLC-UV analysis. Finally, the portion of residual intact inhibitor was determined and is graphically depicted in Figure 11. As control measurements, each compound was incubated with mouse liver microsomes in the absence of NADPH. In accordance to Wityak et al., **6a** is metabolised relatively fast with 62% of original compound remaining after 60 min.⁵⁸ The substitution of the methyl group by hydrogen or fluorine in compounds **7a** and **7b**, respectively, does not

significantly alter the metabolic degradation rate. In contrast, compound **10** containing a pyridyl moiety with a *para* orientation of pyridine nitrogen and piperazine ring is virtually fully stable over 60 min. At a first glance, this allows for the conclusion that the site for oxidation reactions is mainly the respective pyridine-2-yl ring. However, compound **13a** in which the pyridine ring is substituted by a 4-fluorobenzoyl is more stable than the lead compound **6a** (85% intact compound after 60 min) but less stable than compound **10**. These observations taken together with enhanced-product ion (EPI) mass spectra of compound **7b** (Figure S26 in Supporting Information) suggest the pyridylpiperazine moiety as major site of metabolic transformation, even though it cannot be stated clearly whether the pyridine or the piperazine ring is more prone to hydroxylation. Data on the metabolism of established piperazine-containing drugs, such as the tricyclic neuroleptic clozapine, indicate that the piperazine ring undergoes CYP(cytochrome P450)-mediated semiaminal formation, which can give rise to reactive iminium ions.¹⁵³⁻¹⁵⁴ Generally, hydroxylation catalysed by CYP monooxygenases at sp³-hybridised carbon atoms adjacent to nitrogen is strongly dependent on the electron-donating capacity of the latter atom.¹⁵⁵ Hence, electron-deficient pyridine rings should attenuate the propensity for metabolic hydroxylation at potential aromatic sites and – via mesomeric effects involving the piperazine nitrogen – also at aliphatic sites. Accordingly, substitution of the 6-methylpyridine-2-yl ring in **6a** by the pyridine-4-yl ring in **10** increases the stability of the pyridylpiperazine moiety towards oxidative metabolism. A possible explanation for that could be the aforementioned push-pull effect due to the *para* orientation of the piperazine ring and pyridine nitrogen, which might lead to a strong shift of the electron density to the pyridine nitrogen. This hypothesis is further supported as compounds **17b**, **17c** and **8c** bearing 6-nitropyridine-3-yl and 6-trifluoropyridine-3-yl moieties, respectively, exhibit a comparable stability to **10**.

Even though potential metabolically labile moieties were identified, it should be mentioned that for most of the compounds no significant further metabolisation occurs between 30 and 60 min. This might indicate a potential inhibition of the CYP enzymes by the original compounds or formed metabolites, which could lead to an underestimation of the overall stability of the compounds.



cpd	R ¹	R ²
6a		
7a		
7b		
7i		
8c		
10		
13a		
13c		
15f		
17b		
17c		

Figure 11. Stability of selected inhibitors in mouse liver microsomes

Determined fractions of peak areas of original compound at 30 and 60 min were normalised to the fraction of peak area of original compound determined after incubation for 60 min without NADPH, microsomal protein and substrates. Data shown are mean values (\pm SD) of one experiment which was performed in duplicate.

Conclusions

Based on the *N*^ε-acryloyllysine piperazide core structure, we synthesised more than 50 new inhibitors by varying either the substituent at the α -amino group or at the piperazine ring or both. Their kinetic characterisation, which considered both hTGase 2-catalysed hydrolysis and transamidation, allowed for the derivation of comprehensive structure-activity relationships. The observed inhibitory potencies based on inactivation constants k_{inact}/K_i comprised two orders of magnitude ranging from 100 to 10 000 M⁻¹s⁻¹. Activity data generated by systematic structural variations allowed for correlation analyses considering different substituent parameters. Furthermore, to facilitate the interpretation of the SAR data, covalent docking studies were conducted using an hTGase 2 molecular model based on a recent crystal structure of this protein in the open conformation and completed by modelling of a flexible loop

close to the catalytic centre. The predicted binding modes of the inhibitors within the active site of hTGase 2 are in agreement with experimentally obtained kinetic data. The obtained docking results in combination with SAR data led to the identification of amino acid residues that are crucial for inhibitor binding and shed light on the principles of molecular recognition for the chemotype of acryloyllysine-derived hTGase 2 inhibitors. The rationale established in our studies indicate that *N*-acryloyllysine piperazides are characterised by multiple binding modes that are sensitive to subtle structural changes rather than a strictly defined targeting of subsites by distinct moieties. These results will direct future design of inhibitors for hTGase 2.

Evaluation of selected potent analogues against other human transglutaminases has revealed an excellent selectivity profile in favour to hTGase 2. In addition to their interaction with the target enzyme, compounds were profiled with regards to their membrane permeability using the PAMPA method, which supports prediction of the pharmacokinetic behavior. Furthermore, selected inhibitors were assessed concerning their stability against oxidative microsomal degradation. Considering the determined inhibitory potencies in combination with these pharmacokinetic in vitro data and inhibitor characterisation in complex biological matrix (cell lysates) provides valuable hints for the development of radiotracers for TGase 2 imaging. Some promising candidates for labelling with fluorine-18 were already identified within this study (i.e. compounds **7b**, **8c**, **13c**, **17b**, **18**).

Experimental Section

Fluorimetric assay⁵⁹

All measurements were conducted at 30 °C over 900 s (interval of 20 s) with a Synergy 4 Multi-Mode Microplate Reader (BioTek Instruments, Software Gen 5, Winooski, VT, USA,) and black 96- well BRANDplates with transparent bottoms (BRAND, Wertheim, Germany). Fluorescence was detected in bottom read mode. To detect released HMC, a combination of optical filters adjusted to 365/40 nm and 465/40 nm as ranges of wavelengths for excitation and emission, respectively, were used. Measurements at pH 6.5 were conducted with a sensitivity of 45. The assay mixture (200 µL) contained aqueous solution (190 µL) and DMSO (5%, v/v, 10 µL). The following two buffer systems were used: assay buffer (100 mM MES, 3 mM CaCl₂, 50 µM EDTA, adjusted to pH 6.5 with 1 M NaOH) and enzyme buffer (100 mM MES, 3 mM CaCl₂, 10 mM TCEP, 20% (v/v) glycerol). The buffers were stored at 0 °C for periods of up to two weeks and freshly prepared after that period. The concentrations of the enzyme stock solutions were 0.5 mg/mL or 1 mg/mL. All regression analyses were done with GraphPad Prism (version 5.02, GraphPad Software, San Diego, CA, USA). To provide values of means and SEMs, the

corresponding regression analyses were separately performed for each experiment, and the obtained fit values were collected and statistically analysed. Analysis by numerical integration was done as described previously by our group.⁵⁹ The kinetic characterisation of **Z-Glu(HMC)-Gly-OH** (including its synthesis) towards enzymatic hydrolysis by hTGase 2 and gpTGase 2 and that of inhibitor **6a** towards hTGase 2 and gpTGase 2 using acyl donor **Z-Glu(HMC)-Gly-OH** were also conducted within the aforementioned study. All TGase isoforms (gpTGase 2 (T006), hTGase 2 (T022), mTGase 2(T040), hTGase 1 (T009), hTGase 3 (T013), hTGase 6 (T021), hFXIIIa (T070) and the inhibitors Z006 and Z013 were purchased from Zedira® (Darmstadt, Germany).

*Characterisation of **Z-Glu(HMC)-Gly-OH** towards enzymatic hydrolysis by different TGases*

For investigations of enzyme-catalysed hydrolysis reactions of acyl donor **Z-Glu(HMC)-Gly-OH**, six or eight different concentrations of **Z-Glu(HMC)-Gly-OH** were used (three separate experiments, each performed in duplicate). The corresponding stock solutions were prepared in DMSO. DMSO (5 µL) and the acyl donor stock solution (5 µL) were added to assay buffer (180 µL). The reactions were initiated by addition of TGase stock solution (10 µL, 60 µg/mL for each TGase isoform, TGase 3 was preincubated for 30 min at 30 °C (Figure S27 in Supporting Information)). For measurements of the spontaneous reactions, the solution of the respective TGase isoform was replaced by enzyme buffer. The recorded time courses of type (RFU-RFU₀)=f(t) for the enzymatic conversion were analysed either by nonlinear (equation III) or linear regression to the experimental data over the first 300 s, depending on the shape of the curve. For the case of nonlinear regression, the first derivative of equation III at t=0 (equation IV) afforded the initial slopes, which are equal to the values of v_{0total} (units of RFU/s).

$$\text{RFU} - \text{RFU}_0 = \text{Plateau} * (1 - e^{-k*t}) \quad (\text{III})$$

$$\text{RFU}_0: \text{RFU}_{t=0} \quad \text{Plateau: RFU}_{t \rightarrow \infty}$$

k: rate constant to reach the plateau

$$v_{0\text{total}} = k * \text{Plateau} \quad (\text{IV})$$

For analysis of the spontaneous reactions, the recorded time courses of type (RFU-RFU₀)=f(t) were analysed by linear regression to the experimental data over the first 300 s. The respective slopes are equal to the values of v_{0control} (units of RFU/s).

All fluorescence rates (RFU/s) were converted into molar rates (µM/min) by dividing by the corresponding fluorescence coefficients.⁵⁹ Subsequently, the two sets of initial rates

($V_{0total}=f([Z\text{-Glu(HMC)-Gly-OH}])$ and $V_{0control}=f([Z\text{-Glu(HMC)-Gly-OH}])$) were globally analysed by use of the model of total and nonspecific binding as implemented in GraphPad Prism to determine the kinetic parameters for the enzymatic conversion. Accordingly, the following rule was defined (equation V):

$$V_{0total} = V_{0corr} + V_{0control} \quad (V)$$

where V_{0corr} represents the rates for the enzymatic conversions. Within this model, the portion of $V_{0corr}=f([Z\text{-Glu(HMC)-Gly-OH}])$ and $V_{0control}=f([Z\text{-Glu(HMC)-Gly-OH}])$ were analysed by nonlinear regression by use of equation VI (Michaelis-Menten equation) and linear regression ($V_{0control}=k_{obs}*[Z\text{-Glu(HMC)-Gly-OH}]$), respectively.

$$V_{0corr} = \frac{V_{max}*[S]}{K_m+[S]} \quad (VI)$$

Because of the negligible spontaneous reaction of compound **Z-Glu(HMC)-Gly-OH** within the range of concentrations for mTGase 2, plots of $V_{0total}=f([Z\text{-Glu(HMC)-Gly-OH}])$ were directly analysed by nonlinear regression to the data by use of equation VI. The evaluation of the data sets for hTGase 1, hTGase 3 and hFXIIIa were also performed by the method of Cornish-Bowden and Eisenthal.⁸²

Characterisation of irreversible inhibitors

For the characterisation of irreversible inhibitors towards gpTGase 2, hTGase 2 and mTGase 2 at pH 6.5, six or eight different concentrations of the inhibitors were used (two separate experiments, each performed in duplicate). In contrast to this, four different concentrations were investigated (one experiment, each concentration in duplicate) for the inhibition of hTGase 1, hTGase 3, hTGase 6 and hFXIIIa. Compound **Z-Glu(HMC)-Gly-OH** was chosen as acyl donor. The appropriate stock solutions were prepared in DMSO. Stock solutions of inhibitor (5 μ L) and **Z-Glu(HMC)-Gly-OH** (5 μ L, 1 or 1.2 mM for gpTGase 2, 1.2 or 1.4 mM for hTGase 2, 1.4 mM for mTGase 2, 1.6 mM for hTGase 1, hTGase 3, hTGase 6 and hFXIIIa) were added to assay buffer (180 μ L). The reactions were initiated upon addition of the respective TGase stock solution (10 μ L, 60 μ g/mL for hTGase 2, mTGase 2, gpTGase 2, hTGase 6 and 120 μ g/mL for hTGase 1, hTGase 3, hFXIIIa). The recorded time courses of type $(RFU-RFU_0)=f(t)$ were analysed by nonlinear regression to the experimental data over the entire measurement period (900 s) by use of equation VII:

$$RFU - RFU_0 = v_s * t + \frac{(V_i - V_s) * (1 - e^{-k_{obs} * t})}{k_{obs}} \quad (VII)$$

v_s : steady state velocity

v_i : initial velocity

k_{obs} =pseudo-first-order rate constant for the transition of v_i into v_s

For the case, that the initial velocities do not vary significantly with increasing concentrations of inhibitor, the plots of $k_{obs}=f([I])$ were analysed by linear regression. To obtain the value of k_{inact}/K_i , the corresponding slope ($k_{obs}/[I]=k_{inact}/K_i'$) was multiplied by $(1+[Z-Glu(HMC)-Gly-OH]/K_m)$ (except for hTGase 3 and hFXIIIa, where $k_{obs}/[I]$ reflects k_{inact}/K_i as $[Z-Glu(HMC)-Gly-OH]/K_m < 1$). For the case, that the initial velocities vary significantly with increasing concentrations of inhibitor, the double reciprocal plots $1/k_{obs}=f(1/[I])$ were analysed by linear regression according to equation IX. The obtained values $k_{obs}/[I]$ were also converted into k_{inact}/K_i by multiplication by $(1+[Z-Glu(HMC)-Gly-OH]/K_m)$. The respective value of K_i was calculated by analysis of the plot $v_i=f([I])$ by equation X and equation XI.

$$k_{obs} = \frac{k_{inact} * [I]}{K_i' + [I]} \quad (VIII)$$

$$\frac{1}{k_{obs}} = \frac{K_i'}{k_{inact}} * \frac{1}{[I]} + \frac{1}{k_{inact}} \quad (IX)$$

$$v_i = \frac{V_0}{1 + \frac{[I]}{K_i'}} + v_{0control} \quad (X)$$

$$K_i = \frac{K_i'}{1 + \frac{[Z-Glu(HMC)-Gly-OH]}{K_m}} \quad (XI)$$

Characterisation of *N*^F-propionyllysines

For the characterisation of the *N*^F-propionyllysines **21a** and **21b** towards hTGase 2 at pH 6.5, the enzymatic hydrolysis of acyl donor **Z-Glu(HMC)-Gly-OH** (35 μ M) was followed in the presence of six different concentrations of the inhibitors (0, 10, 20, 40, 80 and 100 μ M; one to two separate experiments, each performed in duplicate). The appropriate stock solutions were prepared in DMSO. Stock solutions of inhibitor (5 μ L) and **Z-Glu(HMC)-Gly-OH** (5 μ L, 1.4 mM) were added to assay buffer (180 μ L). The reactions were initiated upon addition of the hTGase 2 stock solution (10 μ L, 60 μ g/mL). The recorded time courses of type $(RFU - RFU_0)=f(t)$ were analysed by linear regression to the experimental data over 180 s. K_i values were determined as described for the irreversible inhibitors.

Active site titration using **8d** and **Z-Glu(HMC)-Gly-OH**

For the active site titration at pH 6.5, the enzymatic hydrolysis of acyl donor **Z-Glu(HMC)-Gly-OH** (30 μ M) was followed after preincubation of hTGase 2 with inhibitor **8d** (5, 10, 15, 20, 25, 60, 80 and 100 nM; four separate experiments, each performed in duplicate). The appropriate stock solutions for **Z-Glu(HMC)-Gly-OH** and **8d** were prepared in DMSO and 1% DMSO/assay buffer, respectively. Stock solutions of inhibitor **8d** (10 μ L) and hTGase 2 (10 μ L, 60 μ g/mL) were added to assay buffer (10 μ L) and the mixture was incubated for 40 min at 30 °C. Afterwards, assay buffer (160 μ L) and DMSO (5 μ L) were added. The reactions were initiated upon addition of **Z-Glu(HMC)-Gly-OH** (5 μ L, 1.2 mM). The recorded time courses of type $(RFU-RFU_0)=f(t)$ were analysed by linear regression to the experimental data over 300 s. Within the obtained plots of $v_{0total}=f([8d])$, linear regressions were separately performed for data below and above the applied enzyme concentration (38.5 nM) and the active enzyme concentration was determined as x value of the intersection point of the two lines.

Fluorescence anisotropy assay⁶⁰

All measurements were conducted at 30 °C over 900 s (interval of 30 s) using Synergy 2 and Synergy 4 Multi-Mode Microplate Readers (BioTek Instruments, Software Gen 5, Winooski, VT, USA) and black 96- well BRANDplates with F-bottom wells (BRAND, Wertheim, Germany). Experiments were done at excitation wavelengths of 485 nm (**F-Cad**) and 540 nm (**R-I-Cad**) and emission wavelengths of 528 nm (**F-Cad**) and 620 nm (**R-I-Cad**), respectively. The FA (r) was calculated by the Gen 5 software from the measured parallel and perpendicular fluorescence intensities ($I_{||}$ and I_{\perp} , respectively) according to the equation XII

$$r = \frac{I_{||} - G \times I_{\perp}}{I_{||} + 2G \times I_{\perp}} \quad (XII)$$

using a G factor of 0.87 (preset value).^{60,156} All further data analyses including calculation of rates by linear regression of the FA over time, curve fitting, and statistics were conducted with GraphPad Prism (version 5.02 or version 5.04, GraphPad Software, San Diego, CA, USA). The assay mixture (200 μ L) contained aqueous solution (190 μ L) and DMSO (5%, v/v, 10 μ L). The following four buffer systems were used: assay buffer A (100 mM MOPS, 3 mM $CaCl_2$, 50 μ M EDTA, adjusted to pH 8.0 with 1 M NaOH), assay buffer B (as A but 6 mM $CaCl_2$), enzyme buffer for hTGase 2 (100 mM MOPS, 3 mM $CaCl_2$, 10 mM TCEP, 20% (v/v) glycerol) and enzyme buffer for gpTGase 2 (100 mM MOPS, 3 mM $CaCl_2$, 10 mM DTT, 20% (v/v) glycerol). The buffers were stored at 0 °C for periods of up to two weeks and freshly prepared after that period. The concentrations of the enzyme stock solutions were 0.5 mg/mL or 1 mg/mL. To

provide values of means and SEMs, the corresponding regression analyses were separately accomplished for each experiment, and the obtained fit values were collected and statistically analysed. The kinetic characterisation of the substrate pair **F-Cad** and DMC and of inhibitor **6a** towards gpTGase 2 was already performed in a previous study of our group.⁶⁰

*Characterisation of substrate pair **R-I-Cad** and DMC towards hTGase 2*

For the kinetic characterisation of DMC in the presence of a fixed concentration of **R-I-Cad** (0,81 μM), eight different concentrations of DMC (0.3-300 μM) were used (two separate experiments, each performed in duplicate). The corresponding stock solutions of DMC and **R-I-Cad** were prepared in assay buffer A and DMSO, respectively. DMC (50 μL), **R-I-Cad** (5 μL) and DMSO (5 μL) were added to assay buffer A (130 μL) and the mixture was preincubated for 30 min at 30 °C. The reactions were initiated by addition of hTGase 2 stock solution (10 μL , 100 $\mu\text{g/mL}$) or enzyme buffer. The recorded time courses of type $FA=f(t)$ were analysed by linear regression to the experimental data over 900 s. K_m , K_i and V_{\max} were calculated according to the equation of substrate inhibition (XIII).¹⁵⁷

$$v = \frac{V_{\max} * [S]}{K_m + [S] * (1 + \frac{[S]}{K_i})} \quad (\text{XIII})$$

For the kinetic characterisation of **R-I-Cad** in the presence of a fixed concentration of DMC (30 μM), nine different concentrations of **R-I-Cad** (0.000162-4.06 μM) were used (two or three separate experiments, each performed in duplicate). DMC (50 μL), **R-I-Cad** (5 μL) and DMSO (5 μL) were added to assay buffer A (130 μL) and the mixture was preincubated for 30 min at 30 °C. The reactions were initiated by addition of hTGase 2 stock solution (10 μL , 100 $\mu\text{g/mL}$) or enzyme buffer. Data analysis was done as described above.

To investigate the dependence of the enzyme activity on hTGase 2 concentration, 30 μM DMC, 0.81 μM **R-I-Cad**, and seven different concentrations of hTGase 2 (0-5 $\mu\text{g/mL}$) were used. **R-I-Cad** (5 μL), DMSO (5 μL) and hTGase 2 (10 μL) or enzyme buffer (10 μL) were added to assay buffer A (130 μL) and the mixture was preincubated for 30 min at 30 °C. The reactions were initiated by addition of DMC. The recorded time courses of type $FA=f(t)$ were analysed by linear regression to the experimental data over 420 s.

Characterisation of irreversible inhibitors towards hTGase 2 and gpTGase 2

For the characterisation of irreversible inhibitors towards hTGase 2 and gpTGase 2 at a fixed preincubation time, 7 and 10 different concentrations of the inhibitors were used, respectively (two to four separate experiments, each performed in duplicate). The appropriate stock solutions of the inhibitors were prepared in DMSO. For hTGase 2, DMC (30 μM) and **R-I-Cad**

(0.81 μM) were chosen as acyl donor and acyl acceptor, respectively, whereas for gpTGase 2, **F-Cad** (0.81 μM) was chosen as acyl acceptor and DMC was used in a concentration of 10 μM . Inhibitor (5 μL), **R-I-Cad/F-Cad** (5 μL) and TGase 2 (10 μL , 40 $\mu\text{g/mL}$ for hTGase 2 and 100 $\mu\text{g/mL}$ for gpTGase 2) were added to assay buffer A (130 μL) and the mixture was incubated for 5 min (hTGase 2) or 30 min (gpTGase 2) at 30 $^{\circ}\text{C}$. The reactions were initiated by addition of DMC (50 μL). The recorded time courses of type $\text{FA}=\text{f}(\text{t})$ were analysed by linear regression to the experimental data over 900 s. The inhibitor concentration, $[\text{I}]$, causing 50% inhibition, IC_{50} , and the Hill slope, n_{H} , were calculated according to equation XIV

$$\text{rate} = \text{Bottom} + \frac{(\text{Top} - \text{Bottom}) \times [\text{I}]^{n_{\text{H}}}}{[\text{I}]^{n_{\text{H}}} + \text{IC}_{50}^{n_{\text{H}}}} \quad (\text{XIV})$$

with Bottom and Top representing the lower and upper plateaus of the sigmoid dose–response curve, respectively.

*Active site titration using **8d** and the substrate pair **R-I-Cad** and DMC*

For the active site titration at pH 8.0, the hTGase 2-catalysed reaction between **R-I-Cad** (0.81 μM) and DMC (30 μM) was followed after preincubation (40 min) of hTGase 2 with inhibitor **8d** at eight different concentrations (10, 20, 30, 40, 50, 60, 120, 240 nM; three separate experiments, each performed in duplicate). Reaction rates of concentrations below and above the expected enzyme concentrations were subjected to a linear regression with the abscissa value of the intersection point of the two lines resulting in the active concentration of the enzyme.

*Confirmation of irreversible binding of **6a** to gpTGase 2*

To confirm the irreversible mode of action of **6a** towards gpTGase 2, a jump dilution experiment according to Copeland⁸⁴ was performed. Here, 500 $\mu\text{g/mL}$ TGase 2 (100x the assay concentration) and 30 μM inhibitor **6a** ($\approx 100\times \text{IC}_{50}$) were preincubated for 30 min before being diluted 1:100 into assay buffer and **F-Cad** (0.81 μM), with the reaction being subsequently started by the addition of DMC (10 μM). As a control, the inhibition of 5 $\mu\text{g/mL}$ TGase 2 (1x) by 300 nM **6a** ($\approx 1\times \text{IC}_{50}$) was investigated as described. The remaining activities are given as percentage values (mean values \pm SEM of three separate experiments, each performed in triplicate) relative to the reaction rates in absence of inhibitor.

Determination of TGase 2 activity in cell lysates from A375 and MeWo cells

The human metastatic melanoma cell lines A375 and MeWo were obtained from the ATCC. They were cultured in Dulbecco's modified Eagle's medium (DMEM) supplemented with 10 vol-% fetal calf serum (FCS) and 1 U/mL penicillin/streptomycin (P/S, all reagents from

Biochrom, Berlin, Germany) at 37°C in a humidified atmosphere with 5% CO₂. Cells were monthly tested to be mycoplasma negative with Venor® GeM Mycoplasma Detection Kit (Minerva Biolabs, Berlin, Germany). Cell pellets were collected by detaching cells, grown in a 75 cm² culture flask (Greiner Bio-One, Kremsmünster, Austria), with 2 mM EDTA in PBS, afterwards cell suspension was centrifuged (3 min, 300×g) and the pellet was washed with PBS twice. For cell lysis, pellets were resuspended in 50 µL modified RIPA buffer (150 mM NaCl, 50 mM Tris pH 8.0, 1 µg/mL Leupeptin, 1 mM PMSF, 5 mM NaF, 1 mM NaVO₄, 1 mM DTT), incubated on ice for 30 min and applied to ultrasound. Subsequently, cell lysates were spinned for 15 min at 4°C at 15 000×g and the supernatant was transferred into a fresh tube. The protein content was determined with a BCA protein assay (ThermoFisher, Waltham, MA, USA) according to the manufacturer's protocol. Lysates were stored at -60°C.

For determination of TGase 2 activity in cell lysates (2 g protein/l), DMC (30 µM) and **R-I-Cad** (0.81 µM) were chosen as acyl donor and acyl acceptor, respectively, and the volume of the assay mixture was reduced to 100 µL compared to measurements using the recombinant enzymes. For control measurements, inhibitor **6a** (10 µM) was used or DMC was omitted. Assay buffer B (20 µL) and DMSO or inhibitor **6a** (2.5 µL) were added to the solution of cell lysate (50 µL) and the mixture was incubated for 10 min at 30 °C. The reactions were initiated upon addition of **R-I-Cad** (2.5 µL) and DMC (25 µL). The recorded time courses of type FA=f(t) were analysed by linear regression to the experimental data over 900 s.

*Characterisation of compounds **6a**, **7b** and **7i** towards A375 cell lysates*

For the characterisation of irreversible inhibitors towards A375 cell lysates at a fixed preincubation time, 7 different concentrations of the inhibitors were used (two to three separate experiments, each performed in duplicate). Assay buffer B (20 µL), inhibitor (2.5 µL), and **R-I-Cad** (2.5 µL) were added to the solution of cell lysate (50 µL) and the mixture was incubated for 5 min at 30 °C. The reactions were initiated by addition of DMC (25 µL). The recorded time courses of type FA=f(t) were analysed by linear regression to the experimental data over 900 s. The inhibitor concentration, [I], causing 50% inhibition, IC₅₀, was calculated as described above.

Molecular modelling

Comparative modelling

The 3D structure of gpTGase 2 was modelled taking the crystal structure of the homologous hTGase 2 (PDB ID 2Q3Z, 2.0 Å) as template.⁸⁷ The covalently bound irreversible inhibitor was removed. Both orthologues share 83% sequence identity and 91% sequence similarity. The

programme Modeller as implemented in Discovery Studio (Accelrys, San Diego, CA, USA)¹⁵⁸ was used for the modeling. The missed loops of hTGase 2 were also modelled using this programme.

Molecular docking

Protein preparation: Previous to the docking studies, the modelled structures of hTGase 2 and gpTGase 2 were prepared with Protein Preparation Wizard from Schrödinger¹⁵⁹ (Schrödinger, New York, NY, USA) keeping His335 in its protonated state.

Ligand preparation: Ligands were prepared with the LigPrep¹⁶⁰ in Maestro suite.⁹⁰ Epik¹⁶¹⁻¹⁶² was used to generate ionization state at pH 7.0 ± 2.0. The OPLS2005 and OPLS3 force fields were used.¹⁶³

Covalent docking: Covalent docking studies were carried out with Glide by using the workflow CovDock v1.2.¹⁶⁴ The grid box was set up around residues Trp241, Ile313 and Asn333 with an inner and outer boxes of 10 Å × 10 Å × 10 Å and 30 Å × 30 Å × 30 Å, respectively. The sulphur of Cys277 was defined as the site to form a covalent bond to the acrylate group of the designed inhibitors. The OPLS2005 and OPLS3 force fields were used.¹⁶³ Docking results were ranked according to their Prime energy and MM-GBSA¹⁶⁵ binding energies.

PAMPA method^{136,139-140}

<i>Buffer:</i>	50 mM HEPES, adjusted to pH 7.5 with 1 M NaOH
<i>Membrane forming solution:</i>	1,2-dioleoyl- <i>sn</i> -glycero-3-phosphocholine (25 mg, final 10%, w/v) and cholesterol (1.25 mg, final 5%, w/v) in <i>n</i> -dodecane (250 µL), the mixture was sonicated for 20 min at 37 °C to obtain a clear solution
<i>Reference compounds:</i>	hydrochlorothiazide (not permeable), metoprolol (as metoprolol tartrate, moderate permeable) and verapamil (as (±)-verapamil hydrochloride, well permeable)
<i>96-well plates:</i>	MultiScreen® 96-well Transport Receiver Plate, not sterile (Merck, Cat. No. MATRNPS50; used as donor plates) MultiScreen-IP, 0.45 µm, transparent, not sterile (Merck, Cat. No. MAIPNTR10; used as acceptor plates)

UV-Star® Microplate, 96 Well, F-Bottom (Chimney Well),
 µClear® (Greiner Bio-One, Item No. 655801, used for
 measurements of UV absorption)

The determination of the effective permeability P_e was conducted in triplicate. Stock solutions of the reference compounds and TGase 2 inhibitors were prepared in DMSO (0.4-4 mM). 70 µL of these stock solutions were diluted with 1330 µL buffer (5% DMSO, v/v, 20-200 µM, depending on solubility). 300 µL of these solutions were added into the wells of the donor plate and 150 µL into the wells of the UV-Star® Microplate. 7 µL of the preheated membrane forming solution were carefully added on the filter of the acceptor plate. Then, the acceptor plate was inserted into the donor plate. Subsequently, 200 µL of a mixture of HEPES buffer and DMSO (5%, v/v) were added into the wells of the acceptor plate. The incubation of the plates was conducted in a sealed, wet chamber for 6 or 24 h at 37 °C. After that time, 150 µL out of the wells of the donor and acceptor plate were transferred into the UV-Star® Microplate. To determine the amount of compound in the donor and acceptor wells, the absorption spectra were recorded between 200 and 700 nm using a Synergy 4 Multi-Mode Microplate Reader (BioTek Instruments). These absorption spectra were corrected for the absorption of the HEPES/DMSO (5%, v/v) mixture and, subsequently, the maximum of absorption was determined between 260 and 700 nm. Finally, equation XV (bi-directional permeation model with consideration of mass retention in the membrane)¹⁴¹ was used for the calculation of the effective permeability P_e .

$$c_A(t) = \frac{M-m}{V_D+V_A} + \left(c_A(0) - \frac{M-m}{V_D+V_A} \right) * e^{-P_e * S * \left(\frac{1}{V_A} + \frac{1}{V_D} \right) * t}$$

$$c_D = c_0 * \frac{A_D - A_{buffer}}{A_0 - A_{buffer}}$$

$$c_A = c_0 * \frac{A_A - A_{buffer}}{A_0 - A_{buffer}}$$

$$P_e = -\ln \left[\frac{c_A(t) - \frac{M-m}{V_D+V_A}}{c_0 - \frac{M-m}{V_D+V_A}} \right] * \frac{1}{S * \left(\frac{1}{V_D} + \frac{1}{V_A} \right) * t} \quad (XV)$$

S: area of membrane (0,24 cm²)

t: permeation time

M: total amount of compound (mol)

m: amount of compound lost to membrane (mol)

c_0 : initial concentration of compound

c_D : concentration of compound in donor well

$c_A(t)$: concentration of compound in acceptor well at time t

V_D: volume of donor well (300 µl)

V_A: volume of acceptor well (200 µl)

A_D: absorption of donor well

A_A: absorption of acceptor well

A₀: absorption of the initial concentration

A_{buffer}: absorption of HEPES/DMSO (5%, v/v)

Determination of logD_{7.4} of fluorinated inhibitors by ¹⁹F-NMR

According to Linclau et al.¹⁵⁰

The test compound (at least 5 mg) was dissolved in 800 µL n-octanol and 800 µl PBS (0.01 M sodium phosphate pH 7.4, NaCl; each phase was saturated with the other by shaking the neat media vigorously in a separating funnel) in a 2 mL Eppendorf tube. Trifluoroethanol (TFE, preferably equimolar to test compound, at least 0.5 µL) and the mixture was vortexed until the test compound was completely dissolved and then shaken in a thermomixer at 1 200 rpm at 25°C for 2 h. If necessary, the mixture centrifuged at 15 000 rpm at 25°C for 10 min. 500 µL of each layer were transferred via syringe to separate NMR tubes; transfer of the aqueous phase needs special caution according to Linclau et al.¹⁵⁰ Acetone-*d*₆ (100 µL) was added to each NMR tube and carefully mixed with the phase contents. The ¹⁹F NMR spectra were recorded for each layer, the relaxation delay times were 30 s and 60 s for octanol and aqueous phase, respectively, as suggested by Linclau et al.¹⁵⁰ The acquisition times were adjusted in order to assure sufficient S/N ratios, typically between 200 and 800 scans. The peak areas (AUC) for the ¹⁹F signals of trifluoroethanol and the ¹⁹F signal of the test compound were determined using the integration function implemented in the MestReNova programme, and the area of the trifluoroethanol peak was set to 100. Finally, the logD_{7.4} value was calculated using equation XVI.

$$\log D_{7.4} = \log D_{7.4(\text{TFE})} + \log \left(\frac{\rho_{\text{oct}}}{\rho_{\text{aq}}} \right) \quad (\text{XVI})$$

with $\rho = \text{AUC}(\text{test compound}) / \text{AUC}(\text{TFE})$

$\log D_{7.4(\text{TFE})} = \log P(\text{TFE}) = +0.36$

HPLC-based determination of chromatographic hydrophobicity indices (CHI) at an immobilised artificial membrane (IAM)

According to Valko et al.¹⁶⁶

For analysis of the CHI-IAM values, an analytical HPLC system from Agilent (1100 Series, Santa Clara, CA, USA) was used. A Regis IAM PC DD2 column (10×4.6 cm) was used as

stationary phase. A binary gradient of NH_4OAc buffer (pH=7.4, solvent A) and CH_3CN (solvent B) was used at a flow rate of 1 mg/mL. The programme for elution was as follows: 0-9 min gradient from 100% A to 100% B, 9-9.5 min 100% B, 9.5-10.5 min gradient back to 100% A. The wavelength for detection was 254 nm. To obtain a calibration curve where the gradient retention times of the inhibitors can be converted to CHI-IAM values, a set of reference compounds (benzoic acid, acetanilide, acetophenone, 1,4-dinitrobenzene, anisole, propiophenone, valerophenone and octaphenone)¹⁶⁶ of known CHI-IAM values was analysed by the system above. For HPLC analysis, the inhibitors were dissolved in a mixture of CH_3CN /water 70/30 and their CHI-IAM values were finally calculated using the calibration curve.

Determination of the thermodynamic solubility of compounds **7b and **7i****

The thermodynamic solubility was determined as recently described by Badarau et al.⁸⁸ To the respective inhibitor (1-1.5 mg) in a 2 mL vial was added PBS (0.01 M sodium phosphate pH 7.4, NaCl) to theoretically obtain a 1 mg/mL solution. The suspension was vigorously stirred. After 20 h, the suspension was centrifuged at 4 000 g for 10 min. 100 μL of the supernatant were transferred to a vial containing a PVDF membrane (pore size 0.22 μm , Ultrafree filtration systems from Roth®, Karlsruhe, Germany) and were filtered by centrifugation at 4 000 g for 2 min. 10 μL of the filtrate was transferred to a sample vial for DAD-LC-MS analysis and 80 μL water and 10 μL DMSO were added. 5 μL of that solution were injected into the system. A 4 mM stock solution of the respective inhibitor was prepared in DMSO, which was then diluted to eight solutions between 100 and 2 000 μM with DMSO. Each solution including the stock solution was then diluted with water (1:9, v/v) to obtain a final range of concentration between 10 and 400 μM . 5 μL of each solution were analysed by DAD-LC-MS analysis. A calibration curve was obtained for each inhibitor by determination of the peak areas (at $\lambda=305$ nm and $\lambda=405$ nm for **7b** and **7i**, respectively). Using these calibration curves, the concentration of the inhibitors in PBS could be calculated considering the additional dilution (1:9) of the PBS solution. According to this procedure, the suspension in PBS was also analysed at later time points until the concentration did not further increase indicating the maximum thermodynamic solubility. Mass spectrometry was only used to ensure that the observed UV peak corresponds to the compound of interest.

Stability in liver microsomes

For microsome experiments the following instruments were used: BioShake iQ (QUANTIFOIL Instruments, Jena, Germany) and Centrifuge 5424 (Eppendorf, Hamburg, Germany), UltiMate

3000 UHPLC System (Thermo Scientific, Germering, Germany) including a DAD detector (DAD-3000RS) coupled to an MSQ Plus Single Quadrupole Mass Spectrometer (Thermo Scientific, Austin, Texas, USA), Agilent 1260 Infinity Quaternary LC system (Agilent Technologies, Böblingen, Germany) coupled with a QTRAP 5500 hybrid linear ion-trap triple quadrupole mass spectrometer (AB SCIEX, Concord, Ontario, Canada).

NADPH (nicotinamide adenine dinucleotide phosphate) and testosterone were purchased from Sigma-Aldrich (Steinheim, Germany). GIBCO mouse liver microsomes (MLM, 20 mg/mL) were purchased from Life Technologies (Darmstadt, Germany). Dulbecco's phosphate buffered saline (PBS) (without Ca^{2+} , Mg^{2+}) was purchased from Biochrom (Berlin, Germany).

Incubations had a final volume of 250 μL and were performed in duplicate in PBS (pH 7.4) as follows, with final concentrations as stated in brackets (according to Ludwig et al.¹⁶⁷). PBS, MLM (1 mg/mL) and inhibitors (100 μM) were mixed and preincubated at 37°C for 5 min. Analogously preincubated NADPH (2 mM) was added and mixtures were shaken gently at 37°C. After 30 and 60 min, respectively, 100 μL were taken and added to 100 μL cold acetonitrile (-20°C), followed by vigorous shaking (30 s), cooling at -20°C (0.5 h), and centrifugation at 14 000 rpm (10 min). Supernatants were filtered with Phenex-RC 4 mm Syringe Filters 0.2 μm (Phenomenex, Aschaffenburg, Germany), diluted with water and stored at 4°C until analysed by HPLC-UV. As positive control testosterone was used as substrate and incubated at appropriate concentration, similarly to the protocol described above, to give complete conversion confirmed by HPLC. Furthermore, incubations without NADPH, microsomal protein, and substrates were analysed as negative controls. Microsomal stabilities were calculated from relative peak areas after HPLC-UV analyses on a ReproSil-Pur 120 C18-AQ-column, 125 mm \times 3 mm, 3 μm (Dr. Maisch GmbH, Ammerbuch, Germany) at 40°C. The solvent system consisted of eluent A: 0.1% acetic acid, and eluent B: water/acetonitrile 20/80 (v/v), containing 0.1% acetic acid. Gradient elution (% acetonitrile) at a flow rate of 0.7 mL/min with UV detection at 235 nm (bandwidth 20 nm), unless otherwise stated, for incubation samples from a) **6a**, **7a**, **10**, **15f**: 0-1.5 min, 10%; 1.5-10 min, 10-35%; 10-13 min, 80%; 13-17 min, 10% (detection at 284 nm for **10**), b) **7b**, **7i**, **8c**, **13a**, **13c**: 0-1.5 min, 20%; 1.5-10 min, 20-60%; 10-13 min, 80%; 13-17 min, 20% (detection at 270 nm for **8c**), and c) **17b**, **17c**: 0-1.5 min, 20%; 1.5-10 min, 20-50%; 10-13 min, 80%; 13-17 min, 20%. Conditions for subsequent analyses using the MSQ Plus single quadrupole mass spectrometer were: probe temperature 500°C, needle voltage 3 V, cone voltage 75 V. For further structural elucidation of metabolites, LC conditions were used as described above and enhanced product ion (EPI) and MS^3 spectra were recorded on the QTRAP 5500 hybrid linear ion-trap triple quadrupole

mass spectrometer. Both mass spectrometers were operated in positive electrospray ionisation mode.

Associated Content

Supporting Information

All synthetic methods and analytical data (NMR, ESI-MS) of the compounds as well as additional Figures and Discussions (as mentioned in the text) are included in the Supporting Information.

Author Information

Corresponding Author

*E-mail: markus.pietsch@uk-koeln.de; r.loeser@hzdr.de

Notes

The authors declare no competing financial interest.

Acknowledgments

The authors thank Dr. Torsten Knieß and Andrea Suhr for guiding and assisting in the determination of the CHI-IAM values and Dr. Holger Stephan for calculating $\text{cp}K_{\text{a}}$ and $\log D_{7.4}$ values (all Helmholtz-Zentrum Dresden-Rossendorf, Institute of Radiopharmaceutical Cancer Research) and are grateful to Prof. Marie Urbanová (Institute of Chemical Technology, Prague) for performing the CD measurements. The authors also thank Dr. Georg Schramm (KU Leuven) for continuing assistance in numerical integrations. R.W. and A.W. are grateful for financial support by the RISE (Research Internships in Science and Engineering) programme from DAAD (Deutscher Akademischer Austauschdienst). Partial financial support by the Helmholtz Cross-Programme Initiative “Technology and Medicine – Adaptive Systems” (R.W., E.J., D.B., M.L., J.P., S.H., J.P. and R.L.) and by the Fonds der Chemischen Industrie (R.L.) is gratefully acknowledged. C. H. and M. P. are grateful for support to the Graduate Programme in Pharmacology and Experimental Therapeutics of the University of Cologne and the Bayer Health Care AG (Project No. O23). C.H. acknowledges financial support by the Friedrich-Naumann-Stiftung für die Freiheit (ST 6479/P 622). G.R-G is grateful for the award of a postdoctoral fellowship by the Alexander von Humboldt foundation. Partial support of this work

was provided to M.T.P. and J.P. within the Collaborative Research Center Transregio 67 “Functional biomaterials for controlling healing processes in bone and skin – from material science to clinical application” (TRR 67/3) by the Deutsche Forschungsgemeinschaft (DFG).

Abbreviations Used

hFXIIIa, human Factor XIIIa; gpTGase 2, transglutaminase from guinea pig liver; hTGase, human transglutaminase; mTGase 2, murine transglutaminase 2; SAR, structure-activity relationship; HMC, 7-hydroxy-4-methylcoumarin; *p*NP, *p*-nitrophenylate; PET, positron emission tomography; FA, fluorescence anisotropy; DMC, *N,N*-dimethylcasein; R-I-Cad, rhodamine B-isonipectoyl-cadaverine; CD, circular dichroism; DOPC, 1,2-dioleoyl-*sn*-glycero-3-phosphocholine; CYP, cytochrome P450; PAMPA, parallel artificial membrane permeability assay

References

- (1) Sarkar, N. K.; Clarke, D. D.; Waelsch, H. An enzymatically catalyzed incorporation of amines into proteins. *Biochim. Biophys. Acta* **1957**, *25*, 451-452.
- (2) Shibata, T.; Kawabata, S. In *Transglutaminases*, (Eds.: Hitomi, K.; Kojima, S.; Fésüs, L.), Springer, Tokyo, **2015**, pp. 117-127.
- (3) Serafini-Fracassini, D.; Del Duca, S. Transglutaminases: widespread cross-linking enzymes in plants. *Ann. Bot.* **2008**, *102*, 145-152.
- (4) Duca, S. D.; Serafini-Fracassini, D. Transglutaminases of Higher, Lower Plants and Fungi. *Prog. Exp. Tumor Res.* **2005**, *38*, 223-247.
- (5) Demény, M. A.; Korponay-Szabó, I. R.; Fésüs, L. In *Transglutaminases: Multiple Functional Modifiers and Targets for New Drug Discovery*, (Eds.: Hitomi, K.; Fésüs, L.; Kojima, S.), Springer, Tokyo, **2015**, pp. 1-42.
- (6) Bergamini, C. M.; Collighan, R. J.; Wang, Z.; Griffin, M. Structure and Regulation of Type 2 Transglutaminase in Relation to Its Physiological Functions and Pathological Roles. *Adv. Enzymol. Relat. Areas Mol. Biol.* **2011**, *78*, 1-46.
- (7) Nurminskaya, M. V.; Belkin, A. M. Cellular functions of tissue transglutaminase. *Int. Rev. Cell Mol. Biol.* **2012**, *294*, 1-97.
- (8) Siegel, M.; Strnad, P.; Watts, R. E.; Choi, K.; Jabri, B.; Omary, M. B.; Khosla, C. Extracellular transglutaminase 2 is catalytically inactive, but is transiently activated upon tissue injury. *PLOS ONE* **2008**, *3*, e1861.
- (9) DiRaimondo, T. R.; Klöck, C.; Warburton, R.; Herrera, Z.; Penumatsa, K.; Toksoz, D.; Hill, N.; Khosla, C.; Fanburg, B. Elevated transglutaminase 2 activity is associated with hypoxia-induced experimental pulmonary hypertension in mice. *ACS Chem. Biol.* **2014**, *9*, 266-275.
- (10) Penumatsa, K. C.; Toksoz, D.; Warburton, R. R.; Hilmer, A. J.; Liu, T.; Khosla, C.; Comhair, S. A. A.; Fanburg, B. L. Role of hypoxia-induced transglutaminase 2 in pulmonary artery smooth muscle cell proliferation. *Am J. Physiol. Lung Cell Mol. Physiol.* **2014**, *307*, L576-L585.
- (11) Jin, X.; Stamnaes, J.; Klöck, C.; DiRaimondo, T. R.; Sollid, L. M.; Khosla, C. Activation of extracellular transglutaminase 2 by thioredoxin. *J. Biol. Chem.* **2011**, *286*, 37866-37873.
- (12) Klöck, C.; DiRaimondo, T. R.; Khosla, C. Role of transglutaminase 2 in celiac disease pathogenesis. *Semin. Immunopathol.* **2012**, *34*, 513-522.
- (13) Di Sabatino, A.; Vanoli, A.; Giuffrida, P.; Luinetti, O.; Solcia, E.; Corazza, G. R. The function of tissue transglutaminase in celiac disease. *Autoimmun. Rev.* **2012**, *11*, 746-753.
- (14) Dieterich, W.; Ehnis, T.; Bauer, M.; Donner, P.; Volta, U.; Riecken, E. O.; Schuppan, D. Identification of tissue transglutaminase as the autoantigen of celiac disease. *Nat. Med.* **1997**, *3*, 797-801.
- (15) Jeitner, T. M.; Pinto, J. T.; Krasnikov, B. F.; Horswill, M.; Cooper, A. J. Transglutaminases and neurodegeneration. *J. Neurochem.* **2009**, *109* (Suppl 1), 160-166.
- (16) Ientile, R.; Curro, M.; Caccamo, D. Transglutaminase 2 and neuroinflammation. *Amino Acids* **2015**, *47*, 19-26.
- (17) Johnson, T. S. Tissue Transglutaminase and the Progression of Human Renal Scarring. *J. Am. Soc. Nephrol.* **2003**, *14*, 2052-2062.

- (18) Johnson, T. S.; Fisher, M.; Haylor, J. L.; Hau, Z.; Skill, N. J.; Jones, R.; Saint, R.; Coutts, I.; Vickers, M. E.; El Nahas, A. M.; Griffin, M. Transglutaminase inhibition reduces fibrosis and preserves function in experimental chronic kidney disease. *J. Am. Soc. Nephrol.* **2007**, *18*, 3078-3088.
- (19) Olsen, K. C.; Sapinoro, R. E.; Kottmann, R. M.; Kulkarni, A. A.; Iismaa, S. E.; Johnson, G. V.; Thatcher, T. H.; Phipps, R. P.; Sime, P. J. Transglutaminase 2 and its role in pulmonary fibrosis. *Am. J. Respir. Crit. Care Med.* **2011**, *184*, 699-707.
- (20) Olsen, K. C.; Epa, A. P.; Kulkarni, A. A.; Kottmann, R. M.; McCarthy, C. E.; Johnson, G. V.; Thatcher, T. H.; Phipps, R. P.; Sime, P. J. Inhibition of transglutaminase 2, a novel target for pulmonary fibrosis, by two small electrophilic molecules. *Am. J. Respir. Cell Mol. Biol.* **2014**, *50*, 737-747.
- (21) Mehta, K.; Kumar, A.; Kim, H. I. Transglutaminase 2: a multi-tasking protein in the complex circuitry of inflammation and cancer. *Biochem. Pharmacol.* **2010**, *80*, 1921-1929.
- (22) Kumar, S.; Mehta, K. Tissue transglutaminase, inflammation, and cancer: how intimate is the relationship? *Amino Acids* **2013**, *44*, 81-88.
- (23) Huang, L.; Xu, A.-M.; Liu, W. Transglutaminase 2 in cancer. *Am. J. Canc. Res.* **2015**, *5*, 2756-2776.
- (24) Mehta, K.; Fok, J.; Miller, F. R.; Koul, D.; Sahin, A. A. Prognostic significance of tissue transglutaminase in drug resistant and metastatic breast cancer. *Clin. Cancer Res.* **2004**, *10*, 8068-8076.
- (25) Ku, B. M.; Kim, D. S.; Kim, K. H.; Yoo, B. C.; Kim, S. H.; Gong, Y. D.; Kim, S. Y. Transglutaminase 2 inhibition found to induce p53 mediated apoptosis in renal cell carcinoma. *FASEB J.* **2013**, *27*, 3487-3495.
- (26) Fok, J. Y.; Ekmekcioglu, S.; Mehta, K. Implications of tissue transglutaminase expression in malignant melanoma. *Mol. Cancer Ther.* **2006**, *5*, 1493-1503.
- (27) Kumar, A.; Gao, H.; Xu, J.; Reuben, J.; Yu, D.; Mehta, K. Evidence that aberrant expression of tissue transglutaminase promotes stem cell characteristics in mammary epithelial cells. *PLoS One* **2011**, *6*, e20701.
- (28) Cao, L.; Shao, M.; Schilder, J.; Guise, T.; Mohammad, K. S.; Matei, D. Tissue transglutaminase links TGF- β , epithelial to mesenchymal transition and a stem cell phenotype in ovarian cancer. *Oncogene* **2012**, *31*, 2521-2534.
- (29) Fisher, M. L.; Keillor, J. W.; Xu, W.; Eckert, R. L.; Kerr, C. Transglutaminase Is Required for Epidermal Squamous Cell Carcinoma Stem Cell Survival. *Mol. Cancer Res.* **2015**, *13*, 1083-1094.
- (30) Fisher, M. L.; Adhikary, G.; Xu, W.; Kerr, C.; Keillor, J. W.; Eckert, R. L. Type II transglutaminase stimulates epidermal cancer stem cell epithelial-mesenchymal transition. *Oncotarget* **2015**, *6*, 20525-20539.
- (31) Sullivan, K. E.; Rojas, K.; Cerione, R. A.; Nakano, I.; Wilson, K. F. The stem cell/cancer stem cell marker ALDH1A3 regulates the expression of the survival factor tissue transglutaminase, in mesenchymal glioma stem cells. *Oncotarget* **2017**, *8*, 22325-22343.
- (32) Lee, J.; Condello, S.; Yakubov, B.; Emerson, R.; Caperell-Grant, A.; Hitomi, K.; Xie, J.; Matei, D. Tissue Transglutaminase Mediated Tumor-Stroma Interaction Promotes Pancreatic Cancer Progression. *Clin. Cancer Res.* **2015**, *21*, 4482-4493.
- (33) Assi, J.; Srivastava, G.; Matta, A.; Chang, M. C.; Walfish, P. G.; Ralhan, R. Transglutaminase 2 overexpression in tumor stroma identifies invasive ductal carcinomas of breast at high risk of recurrence. *PLoS ONE* **2013**, *8*, e74437.
- (34) Kim, S.-Y. Transglutaminase 2: A new paradigm for NF κ B involvement in disease. *Adv. Enzymol. Relat. Areas Mol. Biol.* **2011**, *78*, 161-195.
- (35) Brown, K. D. Transglutaminase 2 and NF-kappaB: an odd couple that shapes breast cancer phenotype. *Breast Cancer Res. Treat.* **2013**, *137*, 329-336.
- (36) Curro, M.; Ferlazzo, N.; Risitano, R.; Condello, S.; Vecchio, M.; Caccamo, D.; Ientile, R. Transglutaminase 2 and phospholipase A(2) interactions in the inflammatory response in human Thp-1 monocytes. *Amino Acids* **2014**, *46*, 759-766.
- (37) Ku, B. M.; Lee, C. H.; Lee, S. H.; Kim, S. Y. Increased expression of transglutaminase 2 drives glycolytic metabolism in renal carcinoma cells. *Amino Acids* **2014**, *46*, 1527-1536.
- (38) Katt, W. P.; Antonyak, M. A.; Cerione, R. A. Simultaneously targeting tissue transglutaminase and kidney type glutaminase sensitizes cancer cells to Acid toxicity and offers new opportunities for therapeutic intervention. *Mol. Pharm.* **2015**, *12*, 46-55.
- (39) Kumar, S.; Mehta, K. Tissue Transglutaminase Constitutively Activates HIF-1 α Promoter and Nuclear Factor- κ B via a Non-Canonical Pathway. *PLoS One* **2012**, *7*, e49321.
- (40) Condello, S.; Cao, L.; Matei, D. Tissue transglutaminase regulates β -catenin signaling through a c-Src-dependent mechanism. *FASEB J.* **2013**, *27*, 3100-3112.
- (41) Pietsch, M.; Wodtke, R.; Pietzsch, J.; Löser, R. Tissue transglutaminase: An emerging target for therapy and imaging. *Bioorg. Med. Chem. Lett.* **2013**, *23*, 6528-6543.
- (42) van der Wildt, B.; Lammertsma, A. A.; Drukarch, B.; Windhorst, A. D. Strategies towards in vivo imaging of active transglutaminase type 2 using positron emission tomography. *Amino Acids* **2017**, *49*, 585-595.
- (43) Ametamey, S. M.; Honer, M.; Schubiger, P. A. Molecular imaging with PET. *Chem. Rev.* **2008**, *108*, 1501-1516.
- (44) Pysz, M. A.; Gambhir, S. S.; Willmann, J. K. Molecular imaging: current status and emerging strategies. *Clin. Radiol.* **2010**, *65*, 500-516.
- (45) James, M. L.; Gambhir, S. S. A molecular imaging primer: modalities, imaging agents, and applications. *Physiol. Rev.* **2012**, *92*, 897-965.

- (46) Kalia, M. Personalized oncology: recent advances and future challenges. *Metab. Clin. Exp.* **2013**, 62 Suppl 1, S11-14.
- (47) Jung, K. H.; Lee, K. H. Molecular imaging in the era of personalized medicine. *J. Pathol. Transl. Med.* **2015**, 49, 5-12.
- (48) Keillor, J. W.; Apperley, K. Y. Transglutaminase inhibitors: a patent review. *Expert Opin. Ther. Pat.* **2016**, 26, 49-63.
- (49) Keillor, J. W.; Apperley, K. Y.; Akbar, A. Inhibitors of tissue transglutaminase. *Trends Pharmacol. Sci.* **2015**, 36, 32-40.
- (50) Freedman, N. M. T.; Mishani, E.; Krausz, Y.; Weininger, J.; Lester, H.; Blaugrund, E.; Ehrlich, D.; Chisin, R. In Vivo Measurement of Brain Monoamine Oxidase B Occupancy by Rasagiline, Using ¹¹C-L-Deprenyl and PET. *J. Nucl. Med.* **2005**, 46, 1618-1624.
- (51) Kumata, K.; Yui, J.; Hatori, A.; Maeda, J.; Xie, L.; Ogawa, M.; Yamasaki, T.; Nagai, Y.; Shimoda, Y.; Fujinaga, M.; Kawamura, K.; Zhang, M. R. Development of [¹¹C]MFTC for PET imaging of fatty acid amide hydrolase in rat and monkey brains. *ACS Chem Neurosci* **2015**, 6, 339-346.
- (52) Kerr, C.; Szmazinski, H.; Fisher, M. L.; Nance, B.; Lakowicz, J. R.; Akbar, A.; Keillor, J. W.; Lok Wong, T.; Godoy-Ruiz, R.; Toth, E. A.; Weber, D. J.; Eckert, R. L. Transamidase site-targeted agents alter the conformation of the transglutaminase cancer stem cell survival protein to reduce GTP binding activity and cancer stem cell survival. *Oncogene* **2017**, 36, 2981-2990.
- (53) Ayinde, O.; Wang, Z.; Griffin, M. Tissue transglutaminase induces Epithelial-Mesenchymal-Transition and the acquisition of stem cell like characteristics in colorectal cancer cells. *Oncotarget* **2017**, 8, 20025-20041.
- (54) Mironov, G. G.; Clouthier, C. M.; Akbar, A.; Keillor, J. W.; Berezovski, M. V. Simultaneous analysis of enzyme structure and activity by kinetic capillary electrophoresis-MS. *Nat. Chem. Biol.* **2016**, 12, 918-922.
- (55) Signorini, M.; Dalocchio, F.; Bergamini, C. M. Inhibition of activity and quenching of intrinsic fluorescence of transglutaminase by acrylamide are independent events. *Biochim. Biophys. Acta* **1988**, 957, 168-171.
- (56) Marrano, C.; de Macedo, P.; Keillor, J. W. Evaluation of novel dipeptide-bound α,β -unsaturated amides and epoxides as irreversible inhibitors of guinea pig liver transglutaminase. *Bioorg. Med. Chem.* **2001**, 9, 1923-1928.
- (57) Marrano, C.; de Macedo, P.; Gagnon, P.; Lapierre, D.; Gravel, C.; Keillor, J. W. Synthesis and evaluation of novel dipeptide-bound 1,2,4-thiadiazoles as irreversible inhibitors of guinea pig liver transglutaminase. *Bioorg. Med. Chem.* **2001**, 9, 3231-3241.
- (58) Wityak, J.; Prime, M. E.; Brookfield, F. A.; Courtney, S. M.; Erfan, S.; Johnsen, S.; Johnson, P. D.; Li, M.; Marston, R. W.; Reed, L.; Vaidya, D.; Schaertl, S.; Pedret-Dunn, A.; Beconi, M.; Macdonald, D.; Muñoz-Sanjuan, I.; Dominguez, C. SAR Development of Lysine-Based Irreversible Inhibitors of Transglutaminase 2 for Huntington's Disease. *ACS Med. Chem. Lett.* **2012**, 3, 1024-1028.
- (59) Wodtke, R.; Schramm, G.; Pietzsch, J.; Pietzsch, M.; Löser, R. Synthesis and Kinetic Characterisation of Water-Soluble Fluorogenic Acyl Donors for Transglutaminase 2. *ChemBioChem* **2016**, 17, 1263-1281.
- (60) Hauser, C.; Wodtke, R.; Löser, R.; Pietzsch, M. A fluorescence anisotropy-based assay for determining the activity of tissue transglutaminase. *Amino Acids* **2017**, 49, 567-583.
- (61) Dominguez, C.; Prime, M.; Marston, R.; Brookfield, F. A.; Courtney, S. M.; Macdonald, D.; Wityak, J.; Yarnold, C. J.; Vaidya, D. WO 2014/047288 A2, **2014**.
- (62) Bergbreiter, D. E.; Osburn, P. L.; Li, C. Soluble polymer-supported catalysts containing azo dyes. *Org. Lett.* **2002**, 4, 737-740.
- (63) Mammen, M.; Dahmann, G.; Whitesides, G. M. Effective Inhibitors of Hemagglutination by Influenza-Virus Synthesized from Polymers Having Active Ester Groups - Insight into Mechanism of Inhibition. *J. Med. Chem.* **1995**, 38, 4179-4190.
- (64) Pollak, A.; Blumenfeld, H.; Wax, M.; Baughn, R. L.; Whitesides, G. M. Enzyme Immobilization by Condensation Copolymerization into Cross-Linked Polyacrylamide Gels. *J. Am. Chem. Soc.* **1980**, 102, 6324-6336.
- (65) *CRC Handbook of Chemistry and Physics, 84th Edition*, CRC Press, Boca Raton, **2003**, pp. 6/180-6/183.
- (66) Pavia, M. R.; Taylor, C. P.; Lobbetael, S. J. 6-Alkyl-N,N-Disubstituted-2-Pyridinamines as Anticonvulsant Agents. *J. Med. Chem.* **1989**, 32, 1237-1242.
- (67) Swanson, D. M.; Dubin, A. E.; Shah, C.; Nasser, N.; Chang, L.; Dax, S. L.; Jetter, M.; Breitenbucher, J. G.; Liu, C.; Mazur, C.; Lord, B.; Gonzales, L.; Hoey, K.; Rizzolio, M.; Bogenstaetter, M.; Codd, E. E.; Lee, D. H.; Zhang, S. P.; Chaplan, S. R.; Carruthers, N. I. Identification and biological evaluation of 4-(3-trifluoromethylpyridin-2-yl)piperazine-1-carboxylic acid (5-trifluoromethylpyridin-2-yl)amide, a high affinity TRPV1 (VR1) vanilloid receptor antagonist. *J. Med. Chem.* **2005**, 48, 1857-1872.
- (68) Prante, O.; Tietze, R.; Hocke, C.; Lober, S.; Hubner, H.; Kuwert, T.; Gmeiner, P. Synthesis, radiofluorination, and in vitro evaluation of pyrazolo[1,5-a]pyridine-based dopamine D4 receptor ligands: discovery of an inverse agonist radioligand for PET. *J. Med. Chem.* **2008**, 51, 1800-1810.
- (69) Yin, J.; Buchwald, S. L. Palladium-catalyzed intermolecular coupling of aryl halides and amides. *Org. Lett.* **2000**, 2, 1101-1104.
- (70) Hintermann, L.; Xiao, L.; Labonne, A. A general and selective copper-catalyzed cross-coupling of tertiary Grignard reagents with azacyclic electrophiles. *Angew. Chem. Int. Ed. Engl.* **2008**, 47, 8246-8250.

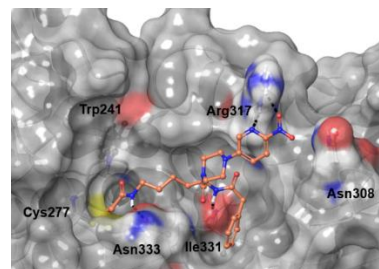
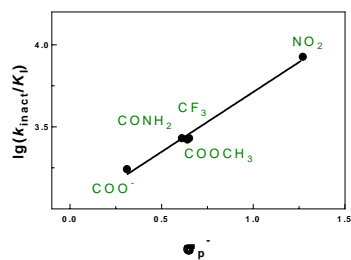
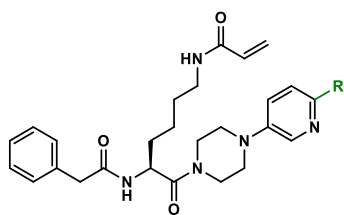
- (71) Henrion, G.; Chavas, T. E.; Le Goff, X.; Gagosz, F. Biarylphosphonite gold(I) complexes as superior catalysts for oxidative cyclization of propynyl arenes into indan-2-ones. *Angew. Chem. Int. Ed. Engl.* **2013**, *52*, 6277-6282.
- (72) Daintier, R. S.; Suschitzky, H.; Wakefield, B. J.; Hughes, N.; Nelson, A. J. Contrasting Reactions of 2,6-Dichloro-4-Trichloromethylpyridine, 2,6-Dichloro-3-Trichloromethylpyridine and Their N-Oxides with Nucleophiles. *J. Chem. Soc. Perkin Trans. 1* **1988**, Doi 10.1039/P19880000227 227-233.
- (73) Meikle, R. W.; Laskowski, D. A.; Regoli, A. J.; Redemann, C. T. The hydrolysis and photolysis rates of nitrapyrin in dilute aqueous solution. *Arch. Environ. Contam. Toxicol.* **1978**, *7*, 149-158.
- (74) Sashuk, V.; Schoeps, D.; Plenio, H. Fluorophore tagged cross-coupling catalysts. *Chem. Commun.* **2009**, 10.1039/b820633c 770-772.
- (75) Abdel-Magid, A. F.; Mehrman, S. J. A review on the use of sodium triacetoxyborohydride in the reductive amination of ketones and aldehydes. *Org. Process Res. Dev.* **2006**, *10*, 971-1031.
- (76) Debien, L.; Braun, M. G.; Quiclet-Sire, B.; Zard, S. Z. Tri- and tetrasubstituted functionalized vinyl sulfides by radical allylation. *Org. Lett.* **2013**, *15*, 6250-6253.
- (77) Klapars, A.; Buchwald, S. L. Copper-catalyzed halogen exchange in aryl halides: an aromatic Finkelstein reaction. *J. Am. Chem. Soc.* **2002**, *124*, 14844-14845.
- (78) Hesse, S.; Kirsch, G. Palladium-Catalyzed C-C Bond Formation from β -Chloroacroleins in Aqueous Media. *Synthesis* **2001**, *5*, 755-758.
- (79) Klöck, C.; Herrera, Z.; Albertelli, M.; Khosla, C. Discovery of potent and specific dihydroisoxazole inhibitors of human transglutaminase 2. *J. Med. Chem.* **2014**, *57*, 9042-9064.
- (80) Day, N.; Keillor, J. W. A continuous spectrophotometric linked enzyme assay for transglutaminase activity. *Anal. Biochem.* **1999**, *274*, 141-144.
- (81) Akbar, A.; McNeil, N. M. R.; Albert, M. R.; Ta, V.; Adhikary, G.; Bourgeois, K.; Eckert, R. L.; Keillor, J. W. Structure-Activity Relationships of Potent, Targeted Covalent Inhibitors That Abolish Both the Transamidation and GTP Binding Activities of Human Tissue Transglutaminase. *J. Med. Chem.* **2017**, *60*, 7910-7927.
- (82) Cornish-Bowden, A., *Fundamentals of enzyme kinetics*, Wiley-Blackwell, Weinheim, **2012**, pp. 45-51.
- (83) Roy, I.; Smith, O.; Clouthier, C. M.; Keillor, J. W. Expression, purification and kinetic characterisation of human tissue transglutaminase. *Protein Expr. Purif.* **2013**, *87*, 41-46.
- (84) Copeland, R. A., *Evaluation of Enzyme Inhibitors in Drug Discovery (Second Edition)*, John Wiley & Sons, Hoboken (New Jersey), **2013**, pp. 318-325.
- (85) Shafer, D. E.; Inman, J. K.; Lees, A. Reaction of Tris(2-carboxyethyl)phosphine (TCEP) with maleimide and alpha-haloacyl groups: anomalous elution of TCEP by gel filtration. *Anal. Biochem.* **2000**, *282*, 161-164.
- (86) Schmidt, T. C.; Welker, A.; Rieger, M.; Sahu, P. K.; Sotriffer, C. A.; Schirmeister, T.; Engels, B. Protocol for rational design of covalently interacting inhibitors. *ChemPhysChem* **2014**, *15*, 3226-3235.
- (87) Pinkas, D. M.; Strop, P.; Brunger, A. T.; Khosla, C. Transglutaminase 2 undergoes a large conformational change upon activation. *PLOS Biol.* **2007**, *5*, 2788-2796.
- (88) Badarau, E.; Wang, Z.; Rathbone, D. L.; Costanzi, A.; Thibault, T.; Murdoch, C. E.; El Alaoui, S.; Bartkeviciute, M.; Griffin, M. Development of Potent and Selective Tissue Transglutaminase Inhibitors: Their Effect on TG2 Function and Application in Pathological Conditions. *Chem. Biol.* **2015**, *22*, 1347-1361.
- (89) Atkovska, K.; Samsonov, S. A.; Paszkowski-Rogacz, M.; Pisabarro, M. T. Multipose binding in molecular docking. *Int. J. Mol. Sci.* **2014**, *15*, 2622-2645.
- (90) Schrödinger Release 2015-2016: Maestro, S., LLC, New York, NY, 2015-2016.
- (91) Romoff, T. T.; Goodman, M. Urethane-protected N-carboxyanhydrides (UNCAs) as unique reactants for the study of intrinsic racemization tendencies in peptide synthesis. *J. Peptide Res.* **1997**, *49*, 281-292.
- (92) Chung, S. I.; Shrager, R. I.; Folk, J. E. Mechanism of action of guinea pig liver transglutaminase. VII. Chemical and stereochemical aspects of substrate binding and catalysis. *J. Biol. Chem.* **1970**, *245*, 6424-6435.
- (93) Taft, R. W. Linear Free Energy Relationships from Rates of Esterification and Hydrolysis of Aliphatic and Ortho-Substituted Benzoate Esters. *J. Am. Chem. Soc.* **1952**, *74*, 2729-2732.
- (94) Taft, R. W. Polar and Steric Substituent Constants for Aliphatic and O-Benzoate Groups from Rates of Esterification and Hydrolysis of Esters. *J. Am. Chem. Soc.* **1952**, *74*, 3120-3128.
- (95) Taft, R. W. Linear steric energy relationships. *J. Am. Chem. Soc.* **1953**, *75*, 4538-4539.
- (96) Charton, M. Steric Effects. 7. Additional ν Constants. *J. Org. Chem.* **1976**, *41*, 2217-2220.
- (97) Charton, M. Steric Effects. I. Esterification and Acid-Catalyzed Hydrolysis of Esters. *J. Am. Chem. Soc.* **1975**, *97*, 1552-1555.
- (98) Bartroli, J.; Turmo, E.; Alguero, M.; Boncompagni, E.; Vericat, M. L.; Conte, L.; Ramis, J.; Merlos, M.; Garcia-Rafanell, J.; Forn, J. New azole antifungals. 3. Synthesis and antifungal activity of 3-substituted-4(3H)-quinazolinones. *J. Med. Chem.* **1998**, *41*, 1869-1882.
- (99) Burgey, C. S.; Robinson, K. A.; Lyle, T. A.; Sanderson, P. E.; Lewis, S. D.; Lucas, B. J.; Krueger, J. A.; Singh, R.; Miller-Stein, C.; White, R. B.; Wong, B.; Lyle, E. A.; Williams, P. D.; Coburn, C. A.; Dorsey, B. D.; Barrow, J. C.; Stranieri, M. T.; Holahan, M. A.; Sitko, G. R.; Cook, J. J.; McMasters, D. R.; McDonough, C. M.; Sanders, W. M.; Wallace, A. A.; Clayton, F. C.; Bohn, D.; Leonard, Y. M.; Detwiler, T. J., Jr.; Lynch, J. J., Jr.; Yan, Y.; Chen, Z.; Kuo, L.; Gardell, S. J.; Shafer, J. A.; Vacca, J. P. Metabolism-directed optimization of 3-aminopyrazinone acetamide thrombin inhibitors. Development of an orally bioavailable series containing P1 and P3 pyridines. *J. Med. Chem.* **2003**, *46*, 461-473.

- (100) Krautwald, S.; Nilewski, C.; Mori, M.; Shiomi, K.; Ōmura, S.; Carreira, E. M. Bioisosteric Exchange of Csp³ - Chloro and Methyl Substituents: Synthesis and Initial Biological Studies of Atpenin A5 Analogues. *Angew. Chem.* **2016**, *128*, 4117-4121.
- (101) Scheler, W., *Grundlagen der allgemeinen Pharmakologie*, VEB Gustav Fischer Verlag, Jena, **1989**, pp. 312-334.
- (102) Hansch, C.; Leo, A., *Exploring QSAR Fundamentals and Applications in Chemistry and Biology*, American Chemical Society, USA, **1995**, pp. 69-96.
- (103) Druckrey, E. Regressionsanalyse von Struktur-Wirkungs-Beziehungen (Hansch-Analyse). *Pharm. unserer Zeit* **1975**, *4*, 145-150.
- (104) Kubinyi, H., *QSAR: Hansch Analysis and Related Approaches*, VCH, Weinheim, **1993**.
- (105) Malik, N.; Solbach, C.; Voelter, W.; Machulla, H.-J. Nucleophilic aromatic substitution by [¹⁸F]fluoride at substituted 2-nitropyridines. *J. Radioanal. Nucl. Chem.* **2009**, *283*, 757-764.
- (106) Dolci, L.; Dolle, F.; Jubeau, S.; Vaufrey, F.; Crouzel, C. 2-[¹⁸F]fluoropyridines by no-carrier-added nucleophilic aromatic substitution with [¹⁸F]FK-K222—a comparative study. *J. Label. Compd. Radiopharm.* **1999**, *42*, 975-985.
- (107) Silverman, R. B., *The Organic Chemistry of Enzyme-Catalyzed Reactions*, Academic Press, San Diego, **2002**, pp. 1-38.
- (108) Bissantz, C.; Kuhn, B.; Stahl, M. A medicinal chemist's guide to molecular interactions. *J. Med. Chem.* **2010**, *53*, 5061-5084.
- (109) Persch, E.; Dumele, O.; Diederich, F. Molecular recognition in chemical and biological systems. *Angew. Chem. Int. Ed. Engl.* **2015**, *54*, 3290-3327.
- (110) Klebe, G. Applying thermodynamic profiling in lead finding and optimization. *Nat. Rev. Drug Discov.* **2015**, *14*, 95-110.
- (111) Martin, Y. C., *Quantitative Drug Design: A critical Introduction*, CRC Press, Boca Raton, **2010**, pp. 15-30.
- (112) Johnstone, R. A. W.; Loureiro, R. M. S.; Cristiano, M. L. S.; Labat, G. Bond energy/bond order relationships for N-O linkages and a quantitative measure of ionicity: the role of nitro groups in hydrogen-bonding. *Arkivoc* **2010**, 142-169.
- (113) Laurence, C.; Berthelot, M.; Lucon, M.; Morris, D. G. Hydrogen-bond Basicity of Nitro-compounds. *J. Chem. Soc. Perkin Trans. 2* **1994**, 491-493.
- (114) Lequestel, J. Y.; Laurence, C.; Lachkar, A.; Helbert, M.; Berthelot, M. Hydrogen-Bond Basicity of Secondary and Tertiary Amides, Carbamates, Ureas and Lactams. *J. Chem. Soc. Perkin Trans. 2* **1992**, 2091-2094.
- (115) Besseau, F.; Laurence, C.; Berthelot, M. Hydrogen-Bond Basicity of Esters, Lactones and Carbonates. *J. Chem. Soc. Perkin Trans. 2* **1994**, 485-489.
- (116) Laurence, C.; Brameld, K. A.; Graton, J.; Le Questel, J. Y.; Renault, E. The pK(BHX) database: toward a better understanding of hydrogen-bond basicity for medicinal chemists. *J. Med. Chem.* **2009**, *52*, 4073-4086.
- (117) Hammett, L. P. The effect of structure upon the reactions of organic compounds benzene derivatives. *J. Am. Chem. Soc.* **1937**, *59*, 96-103.
- (118) Hammett, L. P. Some relations between reaction rates and equilibrium constants. *Chem. Rev.* **1935**, *17*, 125-136.
- (119) Hansch, C.; Leo, A., *Exploring QSAR Fundamentals and Applications in Chemistry and Biology*, American Chemical Society, USA, **1995**, pp. 1-24.
- (120) Anslyn, E. V.; Dougherty, D. A., *Modern Physical Organic Chemistry*, University Science Books, USA, **2006**, pp. 445-453.
- (121) Baitinger, W. F.; Robinson, L.; Schleyer, P. V.; Murty, T. S. Nitro Groups as Proton Acceptors in Hydrogen Bonding. *Tetrahedron* **1964**, *20*, 1635-1647.
- (122) Tan, C. M.; Chen, G. S.; Chen, C. S.; Chang, P. T.; Chern, J. W. Design, synthesis and biological evaluation of benzo[1.3.2]dithiazolium ylide 1,1-dioxide derivatives as potential dual cyclooxygenase-2/5-lipoxygenase inhibitors. *Bioorg. Med. Chem.* **2011**, *19*, 6316-6328.
- (123) Hansch, C.; Leo, A.; Hoekman, D., *Exploring QSAR: Hydrophobic, Electronic, and Steric Constants*, American Chemical Society, USA, **1995**, pp. 217-304.
- (124) Mäding, P.; Füchtner, F.; Wüst, F. Module-assisted synthesis of the bifunctional labelling agent *N*-succinimidyl 4-[¹⁸F]fluorobenzoate ([¹⁸F]SFB). *Appl. Radiat. Isot.* **2005**, *63*, 329-332.
- (125) Kuchar, M.; Pretze, M.; Kniess, T.; Steinbach, J.; Pietzsch, J.; Loser, R. Site-selective radiolabeling of peptides by (18)F-fluorobenzoylation with [(18F)]SFB in solution and on solid phase: a comparative study. *Amino Acids* **2012**, *43*, 1431-1443.
- (126) Mäding, P.; Füchtner, F.; Johannsen, B.; Steinbach, J.; Hilger, C. S.; Friebe, M.; Halks-Miller, M.; Horuk, R.; Mohan, R. 18F-labelling of a potent nonpeptide CCR1 antagonist: synthesis of 1-(5-chloro-2-{2-[(2R)-4-(4-[¹⁸F]fluorobenzyl)-2-methylpiperazin-1-yl]-2-oxoethoxy}phenyl)urea in an automated module. *J. Label. Compd. Radiopharm.* **2006**, *49*, 253-262.
- (127) Wenzel, B.; Hiller, A.; Fischer, S.; Sorger, D.; Deuther-Conrad, W.; Scheunemann, M.; Brust, P.; Sabri, O.; Steinbach, J. In vitro binding profile and radiosynthesis of a novel 18F-labeled azaspirovesamicol analog as potential ligand for imaging of the vesicular acetylcholine transporter. *J. Label. Compd. Radiopharm.* **2011**, *54*, 426-432.

- (128) Choi, K.; Siegel, M.; Piper, J. L.; Yuan, L.; Cho, E.; Strnad, P.; Omary, B.; Rich, K. M.; Khosla, C. Chemistry and biology of dihydroisoxazole derivatives: selective inhibitors of human transglutaminase 2. *Chem. Biol.* **2005**, *12*, 469-475.
- (129) Siebert, C. D. Das Bioisosterie-Konzept: Arzneistoffentwicklung. *Chemie in unserer Zeit* **2004**, *38*, 320-324.
- (130) Meanwell, N. A. Synopsis of some recent tactical application of bioisosteres in drug design. *J. Med. Chem.* **2011**, *54*, 2529-2591.
- (131) Ciapetti, P.; Giethlen, B. In *The Practice of Medicinal Chemistry*, (Eds.: Wermuth, C. G.), Elsevier, Burlington (USA), **2008**, pp. 290-342.
- (132) Klebe, G., *Wirkstoffdesign: Entwurf und Wirkung von Arzneistoffen*, Springer, Heidelberg, **2009**, pp. 114-115.
- (133) Cametti, M.; Dalla Cort, A.; Mandolini, L. Substituent effects in cation- π interactions. Recognition of tetramethylammonium chloride by uranyl-salophen receptors. *Chem. Sci.* **2012**, *3*, 2119.
- (134) Biedermann, F.; Schneider, H. J. Experimental Binding Energies in Supramolecular Complexes. *Chem. Rev.* **2016**, *116*, 5216-5300.
- (135) Prime, M. E.; Andersen, O. A.; Barker, J. J.; Brooks, M. A.; Cheng, R. K.; Toogood-Johnson, I.; Courtney, S. M.; Brookfield, F. A.; Yarnold, C. J.; Marston, R. W.; Johnson, P. D.; Johnsen, S. F.; Palfrey, J. J.; Vaidya, D.; Erfan, S.; Ichihara, O.; Felicetti, B.; Palan, S.; Pedret-Dunn, A.; Schaertl, S.; Sternberger, I.; Ebnet, A.; Scheel, A.; Winkler, D.; Toledo-Sherman, L.; Beconi, M.; Macdonald, D.; Munoz-Sanjuan, I.; Dominguez, C.; Wityak, J. Discovery and structure-activity relationship of potent and selective covalent inhibitors of transglutaminase 2 for Huntington's disease. *J. Med. Chem.* **2012**, *55*, 1021-1046.
- (136) Avdeef, A. The rise of PAMPA. *Expert Opin. Drug Metab. Toxicol.* **2005**, *1*, 325-342.
- (137) Avdeef, A., *Absorption and Drug Development: Solubility, Permeability, and Charge State*, John Wiley & Sons, Hoboken (New Jersey), **2012**.
- (138) Kansy, M.; Senner, F.; Gubernator, K. Physicochemical high throughput screening: parallel artificial membrane permeation assay in the description of passive absorption processes. *J. Med. Chem.* **1998**, *41*, 1007-1010.
- (139) Ruell, J. A.; Tsinman, K. L.; Avdeef, A. PAMPA—a drug absorption in vitro model 5. Unstirred water layer in iso-pH mapping assays and pK_a^{flux} —optimized design (pOD-PAMPA). *Eur. J. Pharm. Sci.* **2003**, *20*, 393-402.
- (140) Avdeef, A.; Strafford, M.; Block, E.; Balogh, M. P.; Chambliss, W.; Khan, I. Drug absorption in vitro model: filter-immobilized artificial membranes. 2. Studies of the permeability properties of lactones in Piper methysticum Forst. *Eur. J. Pharm. Sci.* **2001**, *14*, 271-280.
- (141) Avdeef, A.; Strafford, M.; Block, E.; Balogh, M. P.; Chambliss, W.; Khan, I. Drug absorption in vitro model: filter-immobilized artificial membranes. 2. Studies of the permeability properties of lactones in Piper methysticum Forst. *Eur. J. Pharm. Sci.* **2001**, *14*, 271-280.
- (142) Avdeef, A., *Absorption and Drug Development: Solubility, Permeability, and Charge State*, John Wiley & Sons, Hoboken (New Jersey), **2012**, pp. 448-460.
- (143) Barry, P. H.; Diamond, J. M. Effects of unstirred layers on membrane phenomena. *Physiol. Rev.* **1984**, *64*, 763-872.
- (144) Korjamo, T.; Heikkinen, A. T.; Monkkonen, J. Analysis of unstirred water layer in in vitro permeability experiments. *J. Pharm. Sci.* **2009**, *98*, 4469-4479.
- (145) Sugano, K. Aqueous boundary layers related to oral absorption of a drug: from dissolution of a drug to carrier mediated transport and intestinal wall metabolism. *Mol. Pharm.* **2010**, *7*, 1362-1373.
- (146) Avdeef, A., *Absorption and Drug Development: Solubility, Permeability, and Charge State*, John Wiley & Sons, Hoboken (New Jersey), **2012**, pp. 362-386.
- (147) Chen, I. J.; Taneja, R.; Yin, D.; Seo, P. R.; Young, D.; MacKerell, A. D., Jr.; Polli, J. E. Chemical substituent effect on pyridine permeability and mechanistic insight from computational molecular descriptors. *Mol. Pharm.* **2006**, *3*, 745-755.
- (148) Jiang, Z.; Reilly, J.; Everatt, B.; Briard, E. A rapid vesicle electrokinetic chromatography method for the in vitro prediction of non-specific binding for potential PET ligands. *J. Pharm. Biomed. Anal.* **2011**, *54*, 722-729.
- (149) Auberson, Y. P.; Briard, E.; Sykes, D.; Reilly, J.; Healy, M. Ligand Specific Efficiency (LSE) Index for PET Tracer Optimization. *ChemMedChem* **2016**, *11*, 1415-1427.
- (150) Linclau, B.; Wang, Z.; Compain, G.; Paumelle, V.; Fontenelle, C. Q.; Wells, N.; Weymouth-Wilson, A. Investigating the Influence of (Deoxy)fluorination on the Lipophilicity of Non-UV-Active Fluorinated Alkanols and Carbohydrates by a New log P Determination Method. *Angew. Chem. Int. Ed. Engl.* **2016**, *55*, 674-678.
- (151) Avdeef, A. Physicochemical profiling (solubility, permeability and charge state). *Current topics in medicinal chemistry* **2001**, *1*, 277-351.
- (152) Vose, C. W.; Ings, R. M. In *The Handbook of Medicinal Chemistry: Principles and Practice*, (Eds.: Davis, A.; Ward, S. E.), The Royal Society of Chemistry, Cambridge, **2015**, pp. 184-207.
- (153) Li, F.; Lu, J.; Ma, X. Profiling the reactive metabolites of xenobiotics using metabolomic technologies. *Chem. Res. Toxicol.* **2011**, *24*, 744-751.
- (154) Peterlin Masic, L. Role of Cyclic Tertiary Amine Bioactivation to Reactive Iminium Species: Structure Toxicity Relationship. *Current Drug Metabolism* **2011**, *12*, 35-50.
- (155) Silverman, R. B., *The Organic Chemistry of Enzyme-Catalyzed Reactions*, Academic Press, San Diego, **2002**, pp. 193-219.

- (156) Reindl, W.; Graber, M.; Strebhardt, K.; Berg, T. Development of high-throughput assays based on fluorescence polarization for inhibitors of the polo-box domains of polo-like kinases 2 and 3. *Anal. Biochem.* **2009**, *395*, 189-194.
- (157) Copeland, R. A., *Enzymes: a practical introduction to structure, mechanism, and data analysis*, Wiley-VCH, New York, **2000**, pp. 109-145.
- (158) Accelrys Software Inc., D. S. M. E., Release 3.5, San Diego: Accelrys Software Inc. 2012.
- (159) Sastry, G. M.; Adzhigirey, M.; Day, T.; Annabhimoju, R.; Sherman, W. Protein and ligand preparation: parameters, protocols, and influence on virtual screening enrichments. *J. Comput. Aided Mol. Des.* **2013**, *27*, 221-234.
- (160) Schrödinger Release 2015-2016: LigPrep, S., LLC, New York, NY, 2015-2016.
- (161) Shelley, J. C.; Cholleti, A.; Frye, L. L.; Greenwood, J. R.; Timlin, M. R.; Uchimaya, M. Epik: a software program for pK(a) prediction and protonation state generation for drug-like molecules. *J. Comput. Aided Mol. Des.* **2007**, *21*, 681-691.
- (162) Greenwood, J. R.; Calkins, D.; Sullivan, A. P.; Shelley, J. C. Towards the comprehensive, rapid, and accurate prediction of the favorable tautomeric states of drug-like molecules in aqueous solution. *J. Comput. Aided Mol. Des.* **2010**, *24*, 591-604.
- (163) Harder, E.; Damm, W.; Maple, J.; Wu, C.; Reboul, M.; Xiang, J. Y.; Wang, L.; Lupyan, D.; Dahlgren, M. K.; Knight, J. L.; Kaus, J. W.; Cerutti, D. S.; Krilov, G.; Jorgensen, W. L.; Abel, R.; Friesner, R. A. OPLS3: A Force Field Providing Broad Coverage of Drug-like Small Molecules and Proteins. *J. Chem. Theory Comput.* **2016**, *12*, 281-296.
- (164) Zhu, K.; Borrelli, K. W.; Greenwood, J. R.; Day, T.; Abel, R.; Farid, R. S.; Harder, E. Docking covalent inhibitors: a parameter free approach to pose prediction and scoring. *J Chem Inf Model* **2014**, *54*, 1932-1940.
- (165) Lyne, P. D.; Lamb, M. L.; Saeh, J. C. Accurate prediction of the relative potencies of members of a series of kinase inhibitors using molecular docking and MM-GBSA scoring. *J. Med. Chem.* **2006**, *49*, 4805-4808.
- (166) Valko, K.; Du, C. M.; Bevan, C. D.; Reynolds, D. P.; Abraham, M. H. Rapid-gradient HPLC method for measuring drug interactions with immobilized artificial membrane: comparison with other lipophilicity measures. *J. Pharm. Sci.* **2000**, *89*, 1085-1096.
- (167) Ludwig, F.-A.; Smits, R.; Fischer, S.; Donat, C. K.; Hoepping, A.; Brust, P.; Steinbach, J. LC-MS Supported Studies on the in Vitro Metabolism of both Enantiomers of Flubatine and the in Vivo Metabolism of (+)-[(18)F]Flubatine-A Positron Emission Tomography Radioligand for Imaging alpha4beta2 Nicotinic Acetylcholine Receptors. *Molecules* **2016**, *21*, 1200.

Table of Contents Graphic



Supporting Information

N^ε-Acryloyllysine piperazides as irreversible inhibitors of transglutaminase 2 – synthesis, structure-activity relationships and pharmacokinetic profiling

Robert Wodtke^{a,e,f}, Christoph Hauser^b, Gloria Ruiz-Gómez^c, Elisabeth Jäckel^{a,e},
David Bauer^{a,f}, Martin Lohse^{a,e}, Alan Wong^a, Johanna Pufe^a,
Friedrich-Alexander Ludwig^d, Steffen Fischer^d, Sandra Hauser^a, Dieter Greife^e,
M. Teresa Pisabarro^c, Jens Pietzsch^{a,f}, Markus Pietsch^{b,*}, Reik Löser^{a,f,*}

[a] Helmholtz-Zentrum Dresden-Rossendorf, Institut für Radiopharmazeutische Krebsforschung, Bautzner Landstraße 400, 01328 Dresden, Germany

[b] Zentrum für Pharmakologie, Medizinische Fakultät, Universität zu Köln, Gleueler Straße 24, 50931 Köln, Germany

[c] Structural Bioinformatics, BIOTEC, TU Dresden, Tatzberg 47-51, 01307 Dresden, Germany

[d] Helmholtz-Zentrum Dresden-Rossendorf, Institut für Radiopharmazeutische Krebsforschung, Forschungsstelle Leipzig, Permoserstraße 15, 04318 Leipzig, Germany

[e] Fakultät Natur- und Umweltwissenschaften, Hochschule Zittau/Görlitz, Theodor-Körner-Allee 16, 02763 Zittau, Germany

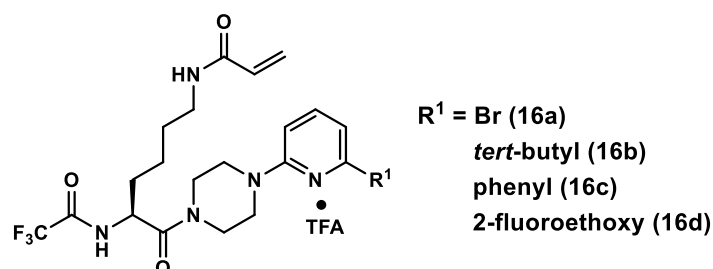
[f] Fakultät Chemie und Lebensmittelchemie, Technische Universität Dresden, Mommsenstraße 4, 01062 Dresden, Germany

Table of Contents

Discussion S1:	Side and degradation products of distinct final inhibitors	4
Discussion S2:	Kinetic characterisation of inhibitors with sulfonyl, carbamoyl, thiocarbamoyl and benz(o)yl residues at the α -amino group	9
Figure S1:	Dependence of enzyme activity on hTGase 2 concentration using the fluorescence polarisation assay	11
Figure S2:	TGase 2-catalysed incorporation of F-Cad and R-I-Cad in DMC at pH 8.0	12
Figure S3:	Confirmation of irreversibility	13
Figure S4:	Active site titration using inhibitor 8d	14
Figure S5:	Modelling of missing residues in the crystal structure of hTGase 2	15
Figure S6:	Molecular modelling of the interaction of hTGase 2 with 6a.....	16
Figure S7:	CD spectroscopy of compounds 6a and 6b	17
Figure S8:	HPLC analysis of compounds 6a and 6b using a chiral stationary phase ..	18
Figure S9:	Relationship between the $\text{cp}K_{\text{a}}$ values of the respective pyridinium ions and the inactivation constants of the inhibitors 6a and 7a-e	19
Figure S10:	Sequence alignment of TGase family members	20
Figure S11:	Alternative binding mode for the interaction of hTGase 2 with 10	21
Figure S12:	Binding modes of the interaction for hTGase 2 with 13b	22
Figure S13:	Molecular modelling of the interaction of hTGase 2 with 13e.....	23
Figure S14:	Relationship between the hydrophobicity of the bioisosteric substituents phenylacetyl, 2-thienylacetyl and 2-pyridylacetyl and the inactivation constants of the inhibitors 6a and 14a-b.....	24
Figure S15:	Molecular modelling of the interaction of hTGase 2 with 14b (A and C) and 14c (B and D).....	25
Figure S16:	Relationship between the size of the substituent in position 4 of the phenylacetyl moiety and the inactivation constants of the inhibitors 6a and 15a-e.....	26
Figure S17:	Relationship between the hydrophobicity of the substituents in position 4 of the phenylacetyl moiety and the inactivation constants of the inhibitors 6a, 15a-e.....	27
Figure S18:	Influence of the 6-nitropyridin-3-yl moiety compared to the 6-methylpyridine-2-yl moiety on the inhibition of hTGase 2.....	28

Figure S19:	Further <i>N</i> ^ε -acryloyllysines obtained by combination of different pyridylpiperazinyll and <i>N</i> ^α residues	29
Figure S20:	Kinetic characterisation of <i>N</i> ^ε -propionyllysines 21a and 21b.....	30
Figure S21:	Molecular modelling of hTGase 2 (A) and gpTGase 2 (B)	31
Figure S22:	Molecular modelling of the interaction of gpTGase 2 with 6a (A) and 15e (B).....	32
Figure S23:	Expression of TGase 2 in A375 and MeWo cells.....	33
Figure S24:	Determination of hTGase 2-activity in cell lysates	34
Figure S25:	Determination of IC ₅₀ values of selected inhibitors towards hTGase 2 using A375 cell lysates	35
Figure S26:	Analysis of potential metabolites of compound 7b.....	36
Figure S27:	Influence of preincubation time on the activity of hTGase 3.....	38
Table S1:	Summary of the determined and calculated physico-chemical parameters of the <i>N</i> ^ε -acryloyllysines	39
Chemistry	41
General		41
Chromatography		41
General synthetic procedures.....		42
<i>N</i> -Acyloxysuccinimide building blocks 1		45
<i>N</i> ^α -Boc- <i>N</i> ^ε -acyllysines 2.....		46
Piperazine building blocks 3		48
<i>N</i> ^α -Boc- <i>N</i> ^ε -acyllysine piperazides 4		65
<i>N</i> ^ε -Acyllysine piperazides (5)		84
Final inhibitors 6-21		102
References	149

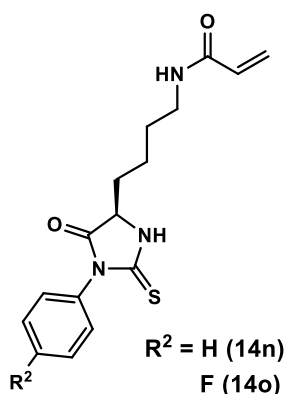
Compounds 16a-d



These side products arose during the phenylacetylation of compounds **5n**, **5o**, **5q** and **5r**. They were formed most likely due to the intermediate activation of residual TFA by phenylacetyl chloride as mixed anhydride. Because of the identical retention times of **16a-d** and their respective phenylacetyl derivatives **7d** and **7f-h** using analytical and preparative RP-HPLC, purification of **7d** and **7f-h** had to be performed by conventional normal-phase column chromatography. In the case of **7g**, the trifluoroacetylated side product **16c** could be isolated in sufficient amounts for analytical and kinetic analyses. Analytical data are only shown for compound **16c**.

The crude product of **16c** was purified *via* column chromatography (isocratic ethyl acetate). The product-containing fractions were combined, evaporated and dried by lyophilisation (from 0.1% TFA/water) to afford **16c** (7.9 mg, 13%) as a white solid. **¹H-NMR (CDCl₃):** δ=8.03–7.97 (m, 2H, H-2,6 of phenyl), 7.61 (dd, ³J=8.3, 7.6 Hz, 1H, H-4 of pyridine), 7.56 (d, ³J=7.5 Hz, 1H, N₆H), 7.48–7.42 (m, 2H, H-3,5 of phenyl), 7.42–7.36 (m, 1H, H-4 of phenyl), 7.19 (d, ³J=7.5 Hz, 1H, H-5 of pyridine), 6.64 (d, ³J=8.4 Hz, 1H, H-3 of pyridine), 6.26 (dd, ³J=17.0 Hz, ²J=1.5 Hz, 1H, CH=CHH), 6.07 (dd, ³J=17.0, 10.3 Hz, 1H, CH=CH₂), 5.70–5.64 (m, 1H, N₆H), 5.62 (dd, ³J=10.2 Hz, ²J=1.5 Hz, 1H, CH=CHH), 4.99–4.92 (m, 1H, C_αH), 3.91–3.59 (m, 8H, 4×CH₂ of piperazine), 3.39–3.30 (m, 2H, C_εH₂), 1.94–1.82 (m, 1H, C_βHH), 1.80–1.52 (m, 3H, C_βHH, C_δH₂), 1.46–1.37 (m, 2H, C_γH₂); **¹³C-NMR (CDCl₃):** δ=168.74, 165.88, 155.39, 139.04 (C-4 of pyridine), 130.85 (CH=CH₂), 129.16 (C-4 of phenyl), 128.73 (C-3,5 of phenyl), 127.02 (C-2,6 of phenyl), 126.64 (CH=CH₂), 111.11 (C-5 of pyridine), 106.21 (C-3 of pyridine), 49.55 (C_α), 45.66 (CH₂ of piperazine), 45.44 (2×CH₂ of piperazine), 42.22 (CH₂ of piperazine), 38.93 (C_ε), 32.46 (C_β), 28.97 (C_δ), 22.06 (C_γ), signals for 4×C_{quaternary} are not visible; **¹⁹F-NMR (CDCl₃):** δ= -75.77 (s, Trifluoroacetyl and TFA); MS (ESI⁺): m/z calculated for C₂₆H₃₁F₃N₅O₃: 518.24 [M+H]⁺, found: 518.2.

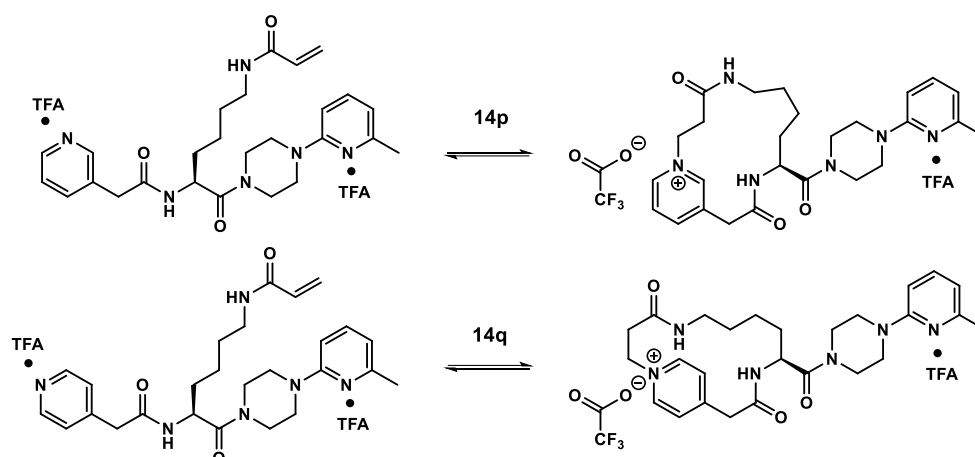
Compounds **14n** and **14o**



Both compounds arose by decomposition of compounds **14i** and **14j** during storage (as solids) at 4 °C. Purification by preparative RP-HPLC afforded 6-methylpyridine-2-ylpiperazine and the respective phenylthiohydantoin derivatives **14n** and **14o**. This decomposition resembles an Edman degradation.¹⁻² Analytical data are only shown for compound **14o**.

Compound **14o** (6.6 mg) was obtained as a white solid. **¹H-NMR (CDCl₃)**: δ =7.92 (broad s, 1H, N_H), 7.33–7.24 (m, 2H, H-2,6 of fluorophenyl), 7.23–7.12 (m, 2H, H-3,5 of fluorophenyl), 6.35 (d, ³*J*=17.2 Hz, 1H, CH=CHH), 6.10 (dd, ³*J*=17.0, 10.3 Hz, 1H, CH=CH₂), 5.83–5.68 (m, 2H, CH=CHH, N_HH), 4.34–4.27 (m, 1H, C_αH), 3.56–3.44 (m, 1H, C_εHH), 3.40–3.26 (m, 1H, C_εHH), 2.22–1.86 (m, 2H, C_βH₂), 1.70–1.60 (m, 2H, C_δH₂), 1.58–1.45 (m, 2H, C_γH₂); **¹³C-NMR (CDCl₃)**: δ =130.31 (d, ³*J*=9.0 Hz, C-2,6 of fluorophenyl), 130.13 (CH=CH₂), 128.11 (CH=CH₂), 116.39 (d, ²*J*=23.1 Hz, C-3,5 of fluorophenyl), 59.67 (C_α), 38.76 (C_ε), 30.51 (C_β), 29.10 (C_δ), 21.17 (C_γ), signals for C-1,4 of fluorophenyl, 2×CO and CS are not visible; **¹⁹F-NMR (CDCl₃)**: δ = -111.47– -111.57 (m, fluorophenyl); MS (ESI⁺): *m/z* calculated for C₁₆H₁₉FN₃O₂S: 336.12 [M+H]⁺, found: 336.3.

Compounds 14p and 14q



After introduction of the regioisomeric pyridylacetyl residues at compound **5a**, further side products were observed. Whereas for the pyridine-2-yl derivative **14a** the desired product was exclusively formed, compounds **14p** and **14q** exist in an equilibrium with the respective macrocycles (determined by NMR analyses), which were probably formed by intramolecular aza-Michael addition. For both mixtures, the equilibrium is located on the side of the macrocycle (e.g. for compound **14q** 16% open form and 84% macrocycle) as determined by integration of the respective C₆H₂ signals from the ¹H-NMR spectra. The reasons for the missing macrocyclisation in **14a** might be the higher sterical shielding of the pyridine nitrogen adjacent to the acetyl residue as well as the higher conformational strain of the respective macrocycle. Aza-Michael additions with aromatic azacycles as nucleophiles are known; however, such reactions usually require catalysis even in the case of highly reactive Michael acceptors such as enones and enals.³ Accordingly, the driving force for the observed macrocyclisation might result from the small spatial distance of both reaction partners, and thus, from a high inherent tendency for cyclisation. Interestingly, macrocyclisations between the acrylamide group and the pyridine rings in compounds **7a**, **8a** and **10** have not been observed. Analytical data are only shown for compound **14q**.

Compound **14q** (27 mg, 64%) was obtained as a yellow oil. Based on the integration of the C₆H₂ signals, 16% of **14q** exists in the open form and 84% as the macrocycle. If not otherwise stated, the NMR data below are primarily listed for the macrocycle. **¹H-NMR** (DMSO-*d*₆): δ=8.95 (d, ³J=6.1 Hz, 2H, H-2,6 of pyridine), 8.81–8.60 (m, 1H, N_aH), 8.13–8.02 (m, 1H, N_eH), 7.97 (d, ³J=6.4 Hz, 2H, H-3,5 of pyridine), 7.63–7.49 (m, 1H, H-4 of methylpyridine), 6.82–6.67 (m, 1H, H-3 of methylpyridine), 6.66–6.53 (m, 1H, H-5 of methylpyridine), 6.18 (dd, ³J=17.1, 10.1 Hz, CH=CH₂ of open form), 6.03 (dd, ³J=17.1 Hz, ²J=2.3 Hz, C=CHH of open form), 5.57–5.52 (m, C=CHH of open form), 4.80–4.65 (m, 3H, C_αH, C_αH₂), 3.96–3.83 (m, 2H, CH₂-

pyridine), 3.72–3.39 (m, 8H, 4×CH₂ of piperazine), 3.14–3.04 (m, C_εH₂ of open form), 3.04–2.91 (m, 2H, C_εH₂), 2.84 (t, ³J=6.3 Hz, 2H, N-C_βH₂), 2.33 (s, 3H, CH₃), 1.71–1.58 (m, 1H, C_βH_H), 1.57–1.45 (m, 1H, C_βH_H), 1.43–1.15 (m, 4H, C_γH₂, C_δH₂); **¹³C-NMR** (DMSO-*d*₆): δ=169.78 (C_αCO), 168.28 (N_εCO), 166.90 (N_αCO), 158.14 (q, ²J_{C,F}=35.7 Hz, CO of TFA), 155.88 (C–1 of pyridine), 144.43 (C–2,6 of pyridine), 139.35, 131.81, 131.60, 128.12 (C–3,5 of pyridine), 112.64 (C–5 of methylpyridine), 56.57 (C_βH₂), 48.71 (C_αH), 44.66 (CH₂ of piperazine), 41.09 (CH₂-pyridine), 38.38 (C_εH₂), 35.37 (C_αH₂), 31.23 (C_β), 28.82 (C_δ), 22.56 (C_γ), signals for 3×CH₂ of piperazine, CH₃, 1×C_{Methylpyridine} are not visible; **¹⁹F-NMR** (DMSO-*d*₆): δ= -74.64 (s, TFA); MS (ESI⁺): m/z calculated for C₂₆H₃₅N₆O₃: 479.28 [M+H]⁺, found: 479.4.

Discussion S2: Kinetic characterisation of inhibitors with sulfonyl, carbamoyl, thiocarbamoyl and benz(o)yl residues at the α -amino group

In addition to the aromatic moiety of the phenylacetyl group, the carboxamide group was planned to be substituted. One alternative functionality is represented by the sulfonamide group, which exhibits a lower rotation barrier around the S-N bond because of the missing double bond character,⁴⁻⁵ among other structural differences in comparison to carboxamides. This could be beneficial for the orientation of the respective phenylmethanesulfonyl residue. However, the inhibitory potential of compound **14e** ($k_{\text{inact}}/K_{\text{i}}=362 \text{ M}^{-1}\text{s}^{-1}$) is surprisingly low and indicates that certain structural features of sulfonamides⁵⁻⁷ are not well tolerated in the binding site. Consequently, the dansyl derivative **14f** exhibits also a low reactivity towards hTGase 2 ($k_{\text{inact}}/K_{\text{i}}=95 \text{ M}^{-1}\text{s}^{-1}$). Therefore, the dansyl derivative **13e**, which is discussed in the main text, is 20 times more potent than **14f**.

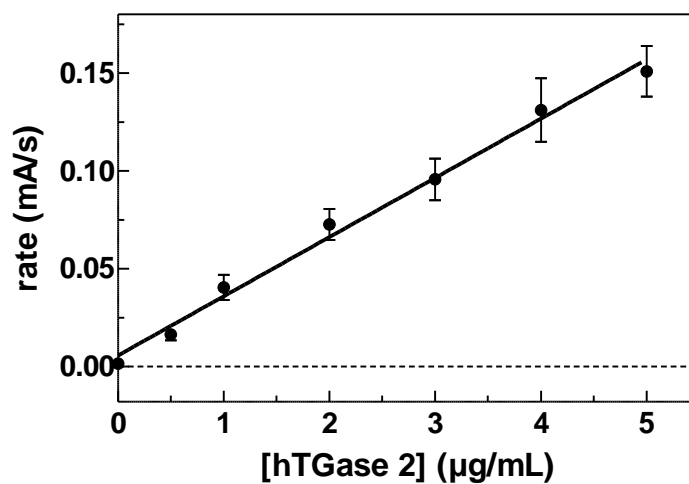
In addition, the carboxamide group was replaced by urea and thiourea functionalities. Again, both modifications lead to a strong reduction of the inactivation constants with carbamoyl residues (in **14g** and **14h** with $k_{\text{inact}}/K_{\text{i}}$ values of 287 and 278 $\text{M}^{-1}\text{s}^{-1}$, respectively) being better tolerated than thiocarbamoyl residues (in **14i** and **14j** with $k_{\text{inact}}/K_{\text{i}}$ values of 79 and 113 $\text{M}^{-1}\text{s}^{-1}$, respectively). The presence of both functional groups leads to a rigidisation, which might impede the orientation of the aromatic rings into the binding site.

In an analogous manner to the piperazine ring, the α -amino group enables ^{18}F -fluorination via incorporation of prosthetic groups containing fluorine-18. In contrast to the 4-fluorobenzoyl and 4-fluorobenzyl groups at the piperazine ring, these residues are badly tolerated at the α -amino group as reflected by the inhibitory potentials of compounds **14k** and **14m**. This is in accordance to the obtained SARs so far as the truncation by the methylene group leads to a limited rotation of the 4-fluorophenyl group as well as a less efficient occupation of the respective pocket. Although the 4-fluorobenzyl group exhibits a higher flexibility than the 4-fluorobenzoyl group, the inactivation constant of compound **14m** is even lower than that of **14k**. Therefore, it can be concluded that positive charge associated with the secondary amine function of **14m** imparts repulsive interactions within the binding site of hTGase 2.

In addition to the labelling with fluorine-18, incorporations of the radioisotopes of iodine can be envisaged. With this regard, indirect labelling with iodine can be achieved using the prosthetic labelling reagent *N*-succinimidyl-3- ^{125}I iodobenzoate.⁸ Kinetic characterisation of the respective

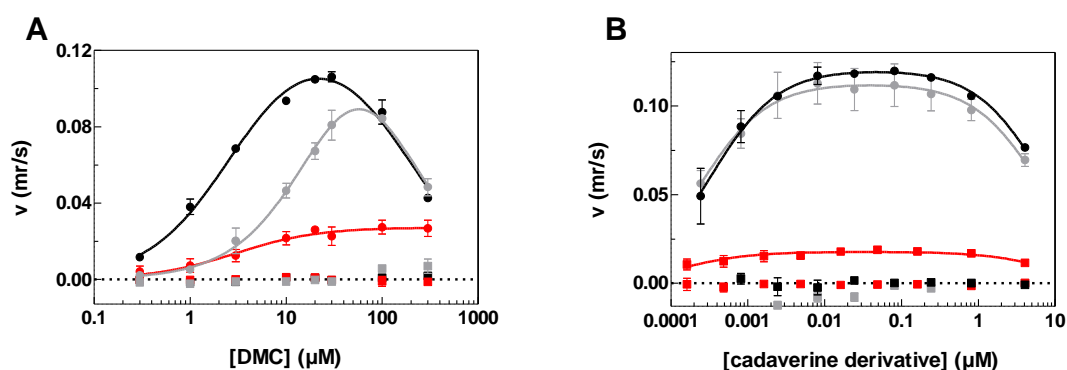
non-radioactive reference compound **14l** revealed a similar reactivity as the 4-fluorobenzoyl derivative **14k**, which was expected based on the observed SARs so far.

Figure S1: Dependence of enzyme activity on hTGase 2 concentration using the fluorescence polarisation assay



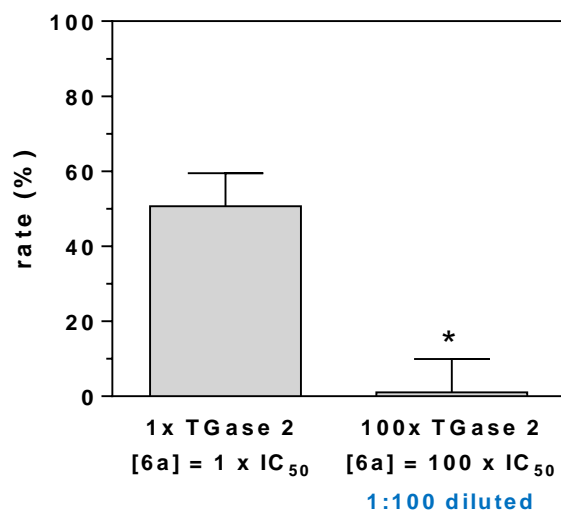
Plot of $\text{rate} = f([\text{hTGase 2}])$ for the reaction of DMC (30 μM) with **R-I-Cad** (0.81 μM) at pH 8.0. Data shown are mean values ($\pm\text{SEM}$) of three separate experiments, each performed in duplicate. Analysis by linear regression gave a slope (mean value \pm SEM) of 0.0303 ± 0.0026 $\text{mA mL s}^{-1} \mu\text{g}^{-1}$.

Figure S2: TGase 2-catalysed incorporation of F-Cad and R-I-Cad in DMC at pH 8.0



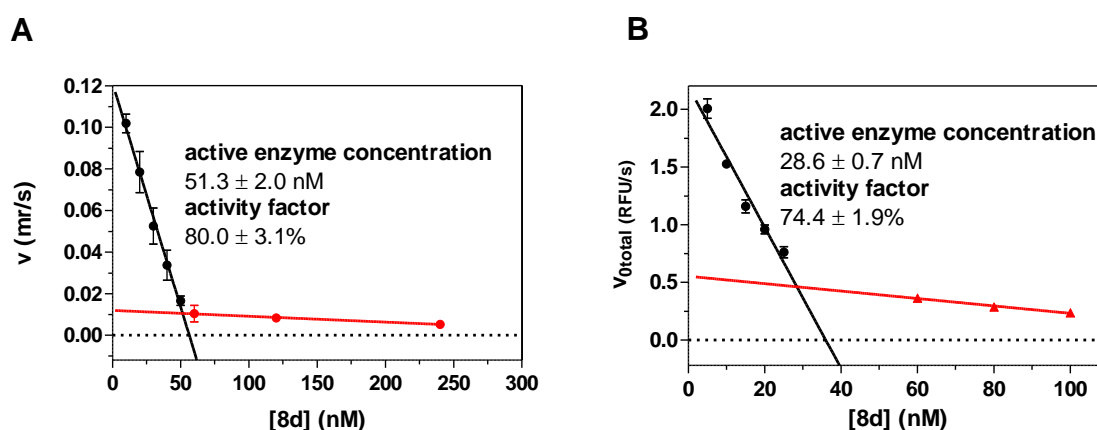
A: Plots of rate versus substrate concentration for the reaction of DMC with **F-Cad** (0.81 μM , red symbols) or **R-I-Cad** (0.81 μM , grey symbols) in the presence (circles) and absence (squares) of gpTGase 2 and for the reaction of DMC with **R-I-Cad** (0.81 μM , black symbols) in the presence (circles) and absence (squares) of hTGase 2. **B:** Plots of rate versus substrate concentration for the reaction of **F-Cad** with DMC (5 μM , red symbols) or **R-I-Cad** with DMC (30 μM , grey symbols) in the presence (circles) and absence (squares) of gpTGase 2 and for the reaction of **R-I-Cad** with DMC (30 μM , black symbols) in the presence (circles) and absence (squares) of hTGase 2. Data shown in **A** and **B** are mean values ($\pm\text{SEM}$) of three (gpTGase 2) or two (hTGase 2) experiments, each performed in duplicate (hTGase 2) or triplicate (gpTGase 2). When not apparent, error bars are smaller than the symbols. Conditions: pH 8.0, 30 $^{\circ}\text{C}$, 5% DMSO, 500 μM DTT (gpTGase 2) or 500 μM TCEP (hTGase 2), 5 $\mu\text{g/mL}$ TGase 2. Plots for gpTGase 2 have already been shown in a previous study⁹.

Figure S3: Confirmation of irreversibility



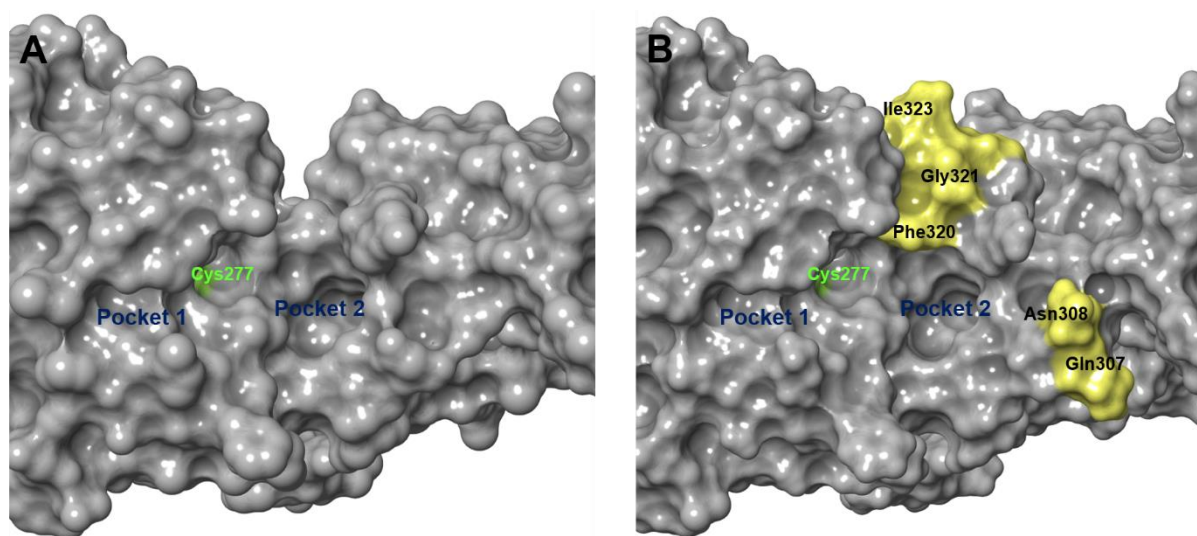
Inhibition of the gpTGase 2-catalysed reaction of DMC (10 μ M) and **F-Cad** (0.81 μ M) by compound **6a**. Prior to the addition of DMC to start the reaction, either TGase 2 (5 μ g/mL=1x TGase 2) was preincubated (30 min) with assay buffer, **F-Cad** and inhibitor (300 nM \approx 1x IC₅₀) or TGase 2 (500 μ g/mL = 100x TGase 2) was preincubated with inhibitor (30 μ M \approx 100x IC₅₀) for 30 min and then diluted (1:100, v/v) into assay buffer and **F-Cad**. Values given (mean values \pm SEM of three separate experiments, each performed in triplicate) are reaction rates in presence of inhibitor relative to the respective rate in absence of inhibitor. * $p \leq 0.05$ unpaired Student's t test

Figure S4: Active site titration using inhibitor 8d



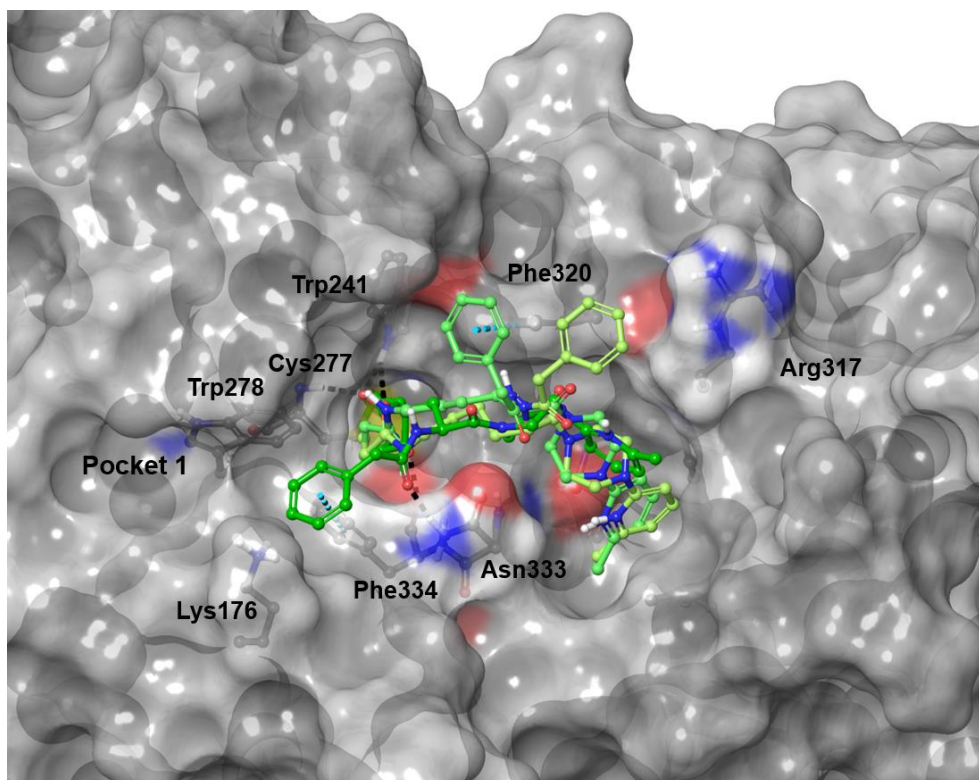
Plots of rate versus concentration of **8d** after preincubation of hTGase 2 with inhibitor for 40 min and determination of residual enzymatic activity by **A**: FA assay, pH=8.0, 30 °C, 5% DMSO, 500 μ M TCEP, 30 μ M DMC, 0.81 μ M **R-I-Cad**, 5 μ g/mL (E_{total} =64.1 nM) hTGase 2 and **B**: fluorimetric assay, pH=6.5, 30 °C, 5% DMSO, 500 μ M TCEP, 30 μ M **Z-Glu(HMC)-Gly-OH**, 3 μ g/mL (E_{total} =38.5 nM) hTGase 2. Linear regressions were separately performed for data below (black) and above (red) the respective enzyme concentrations. The abscissa value of the intersection point of the lines corresponds to the active enzyme concentration, which is given along with the respective activity factor in each diagram. Both assay methods provided activity factors which are not significantly different from each other (unpaired Student's t test, $P \leq 0.05$). Data shown in **A** and **B** are mean values (\pm SEM) of three to four separate experiments, each performed in duplicate.

Figure S5: Modelling of missing residues in the crystal structure of hTGase 2



A) hTGase 2 (PDB ID 2Q3Z, 2.0 Å). **B)** hTGase 2 with modelled residues 307-308 and 319-327. hTGase 2 is shown in gray surface, catalytic Cys277 is highlighted in green and numbered, and modelled residues are highlighted in yellow and numbered. Figure generated in Maestro (Schrödinger).¹⁰

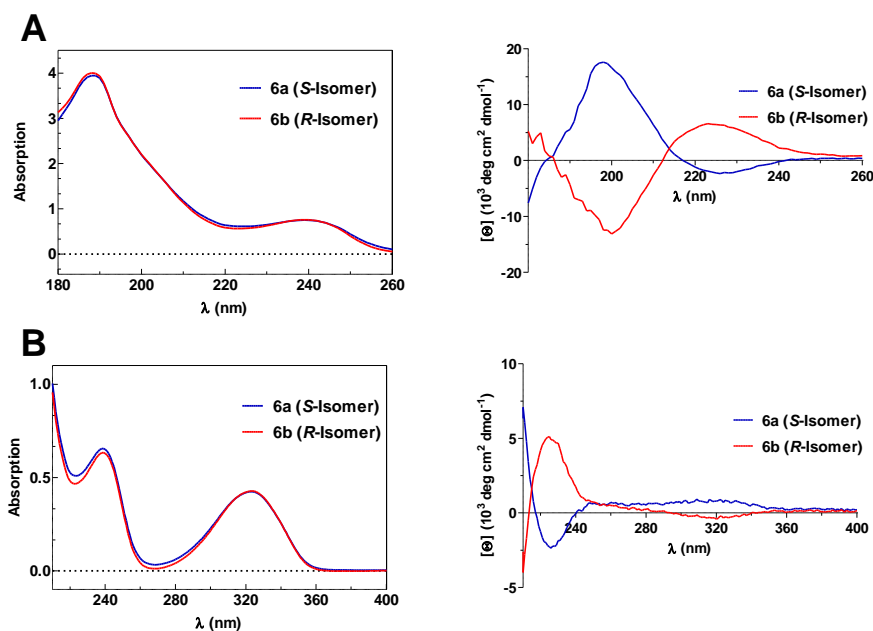
Figure S6: Molecular modelling of the interaction of hTGase 2 with 6a



hTGase 2 is shown in gray surface with relevant residues coloured by atom type and **6a** is shown in sticks and coloured by atom type. Intermolecular H bonds and π - π interactions are depicted by black and cyan dashed lines, respectively. Different binding modes of **6a** are highlighted as gradient of green colour. Figure generated in Maestro (Schrödinger).¹⁰

Figure S7: CD spectroscopy of compounds **6a** and **6b**

Stock solutions of the enantiomers **6a** and **6b** were prepared in a concentration of 0.25 or 0.5 mg/mL in ethanol. The CD spectra were measured in a quartz cuvette with an optical path length of 1 mm (Starna, USA) using a J-810 spectropolarimeter (Jasco, Japan). The conditions of the measurements were as follows: a spectral region of 180–260 nm or 210–400 nm, a scanning speed of 20 nm/min, a response time of 8 s, a resolution of 1 nm, a bandwidth of 1 nm and a sensitivity of 100 mdeg. The final spectrum was obtained as an average of 5 accumulations. The spectra were corrected for a baseline by subtracting the spectra of the corresponding enantiomer-free solution. The ECD measurements were conducted at room temperature.



A) UV absorption and CD spectra between 180 and 260 nm of **6a** and **6b** at a concentration of 0.25 mg/mL. **B)** UV absorption and CD spectra between 210 and 400 nm of **6a** and **6b** at a concentration of 0.5 mg/mL.

Figure S8: HPLC analysis of compounds **6a** and **6b** using a chiral stationary phase

HPLC for determining the enantiomeric composition of compounds **6a** and **6b** was carried out with a system consisting of a Merck Hitachi L7100 gradient pump combined with a Jasco DG2080 four-line degasser with UV detection by a Merck Hitachi L7450 diode array detector. The system was operated with D-700 HSM software and use of a Merck Hitachi D7000 interface. A Chiralpak[®] IA column (250×4.6 mm, 5 μ m) served as stationary phase. Separation of the enantiomers was achieved by an isocratic solvent mixture of 5% hexane/CH₃CN (v/v) at a flow rate of 1 mL/min.

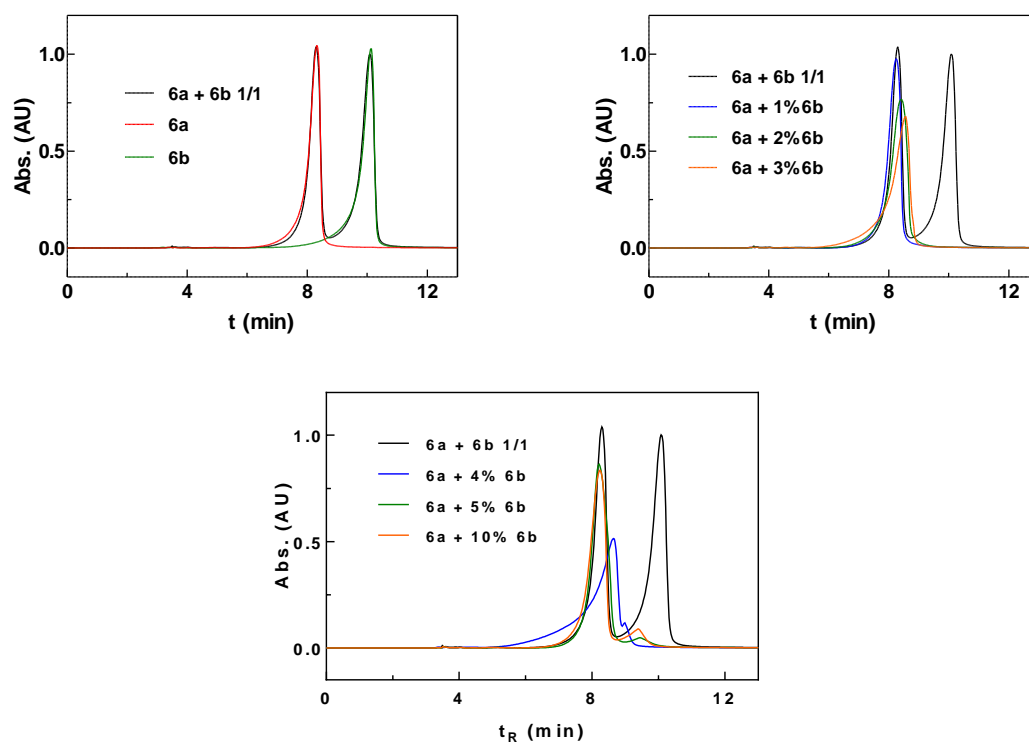
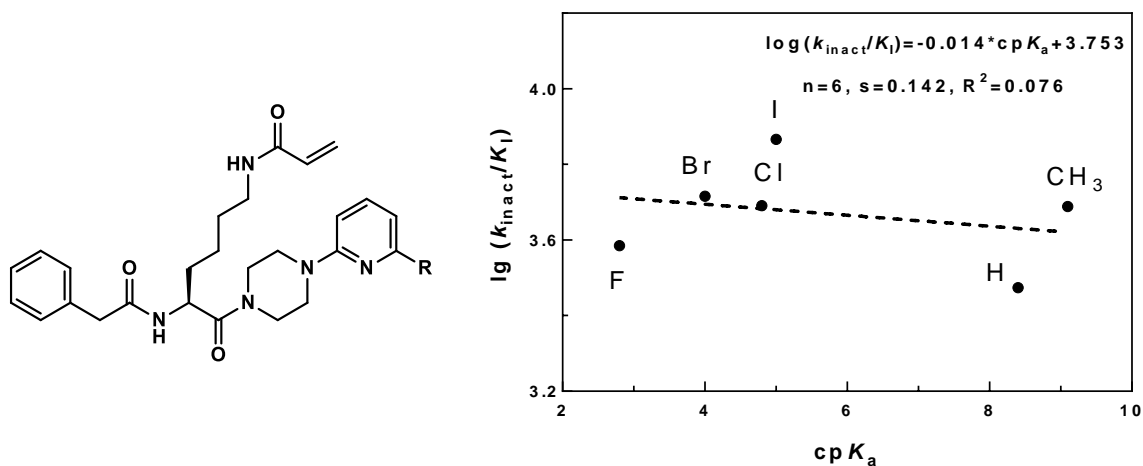
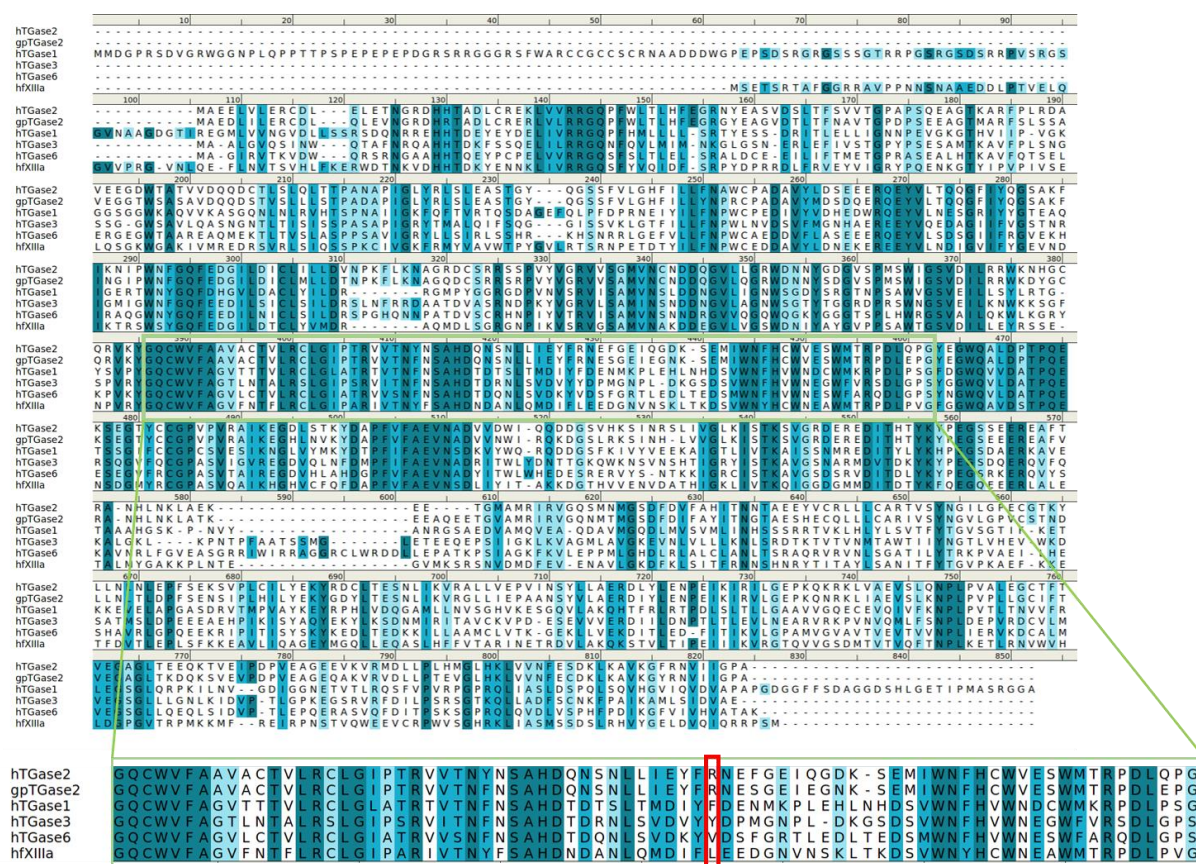


Figure S9: Relationship between the $\text{cp}K_a$ values of the respective pyridinium ions and the inactivation constants of the inhibitors 6a and 7a-e



Plots of $\lg(k_{\text{inact}}/K_I)=f(\text{p}K_a)$ using the mean values of the inactivation constants (Table 4 within the main article) and the following $\text{cp}K_a$ values (Table S1): 8.4 (H), 2.8 (F), 9.1 (CH_3), 4.8 (Cl), 4.0 (Br) and 5.0 (I). The regression analysis was performed by linear regression.

Figure S10: Sequence alignment of TGase family members



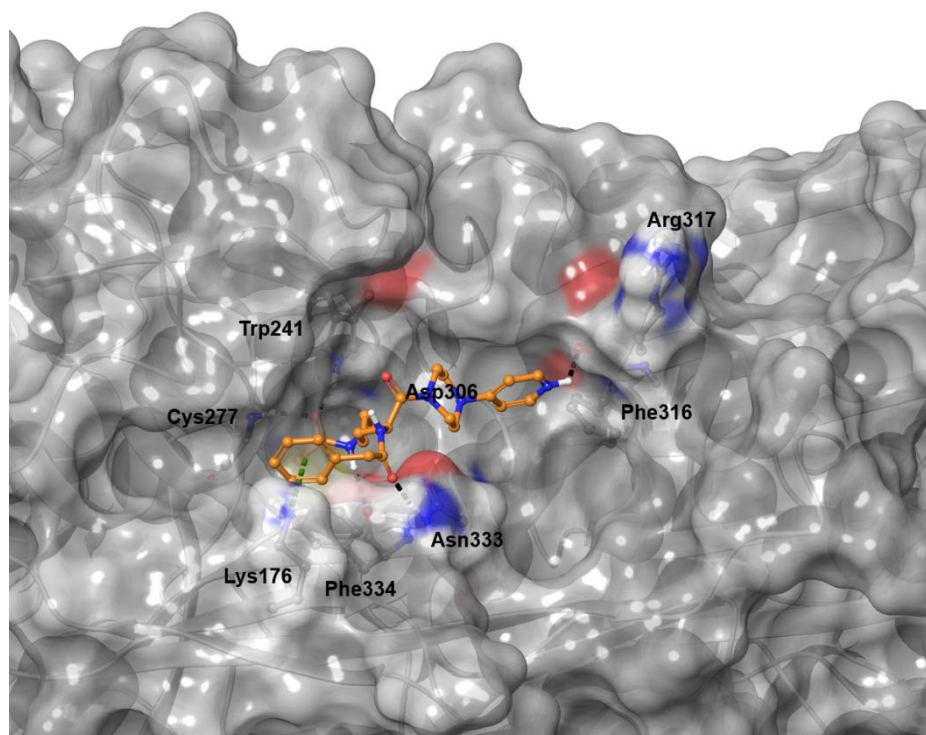
Sequence alignment of htGase 2, gpTGase 2, htGase 1, htGase 3, htGase 6 and hfXIIIa. Arg317 of htGase 2 and the corresponding residues at the same position for the family members are highlighted by the red frame. Figure generated in Discovery Studio (Accelrys).¹¹

Sequence identity and similarity for members of the TGase family.

	htGase 2	gpTGase 2	htGase 1	htGase 3	htGase 6	hfXIIIa
htGase 2		91	52	57	58	51
gpTGase 2	83		52	57	57	50
htGase 1	36	35		44	45	53
htGase 3	38	39	29		66	51
htGase 6	42	40	31	51		50
hfXIIIa	37	36	38	33	34	

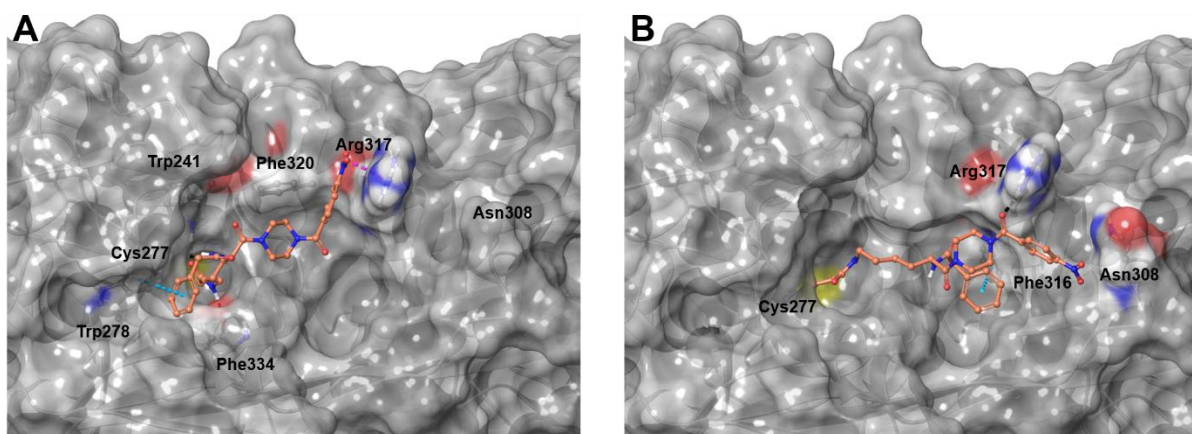
Sequence identity (%) and similarity (%) are shown in yellow and green, respectively.

Figure S11: Alternative binding mode for the interaction of hTGase 2 with 10



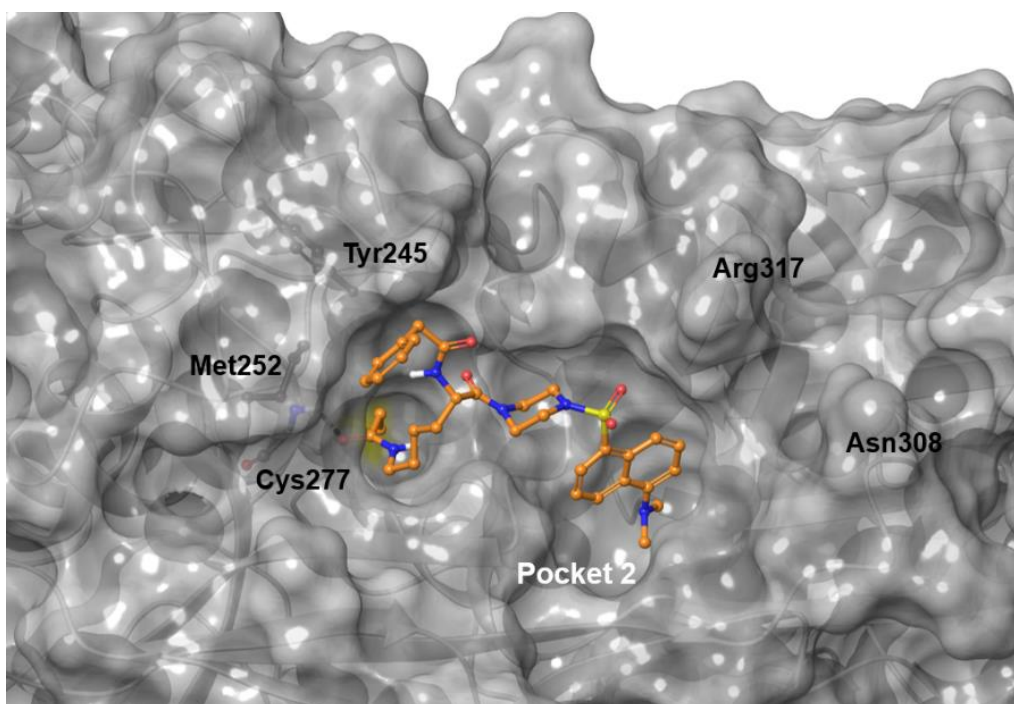
hTGase 2 is shown in gray surface with relevant residues colored by atom type, and inhibitors are shown in sticks and colored by atom type. Intermolecular H bonds and cation- π interactions are depicted by black and green dashed lines, respectively. Figure generated in Maestro (Schrödinger).¹⁰

Figure S12: Binding modes of the interaction for hTGase 2 with 13b



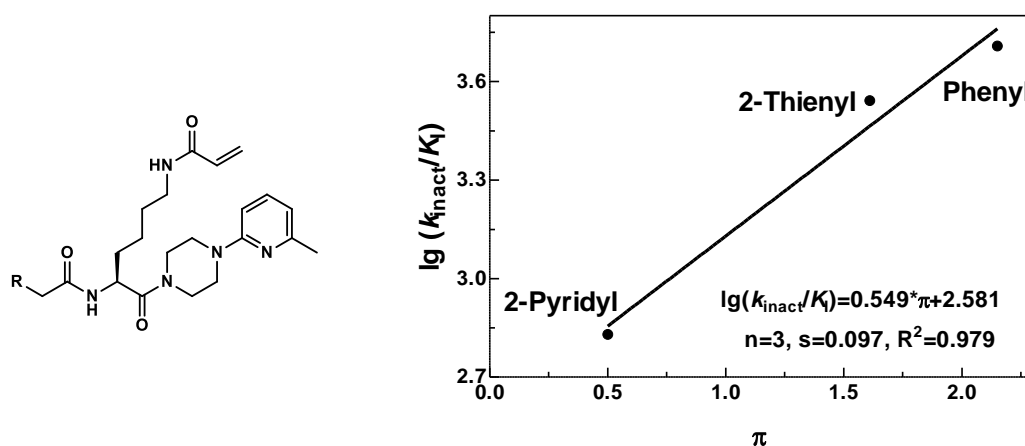
hTGase 2 is shown in gray surface with relevant residues colored by atom type, and inhibitors are shown in sticks and colored by atom type. Intermolecular H bonds, salt bridges and π - π interactions are depicted by black, magenta and cyan dashed lines, respectively. Figure generated in Maestro (Schrödinger).¹⁰

Figure S13: Molecular modelling of the interaction of hTGase 2 with 13e



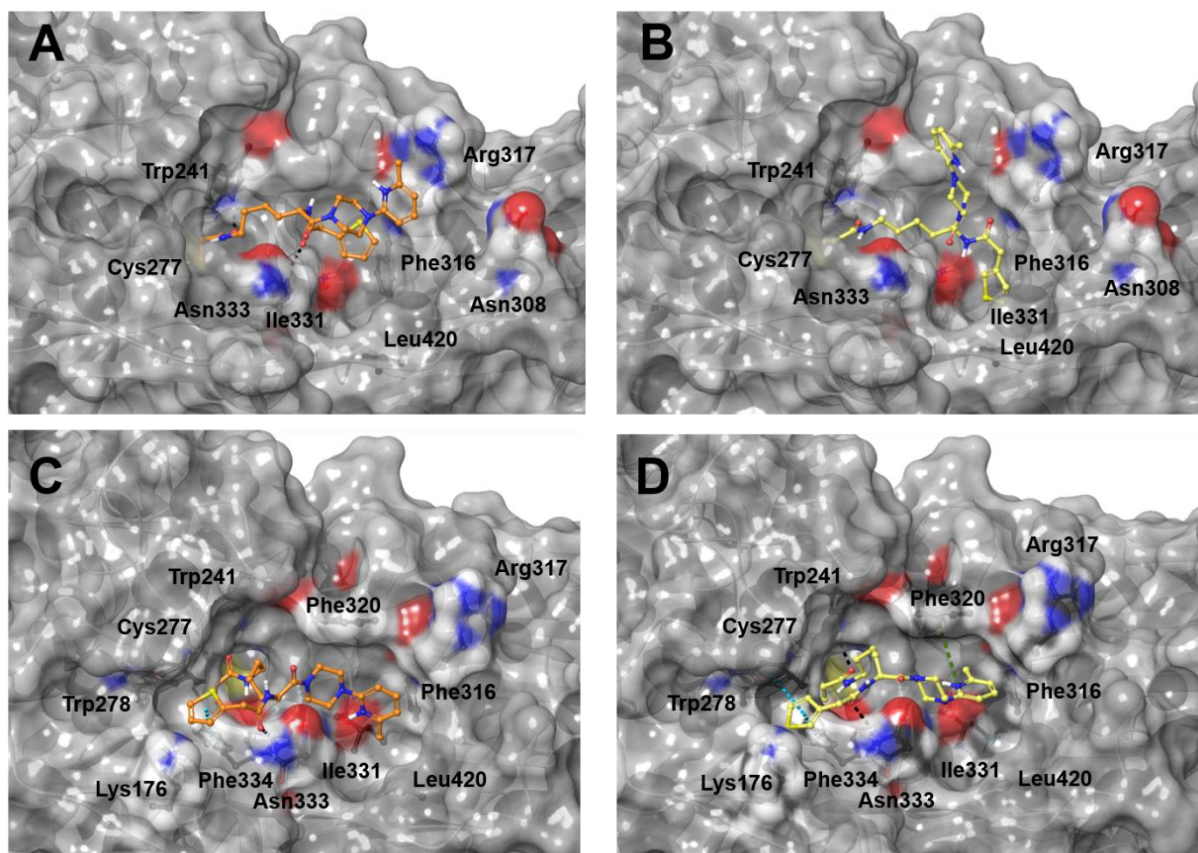
hTGase 2 is shown in gray surface with relevant residues colored by atom type, and inhibitors are shown in sticks and colored by atom type. Intermolecular H bonds are depicted by black dashed lines. Figure generated in Maestro (Schrödinger).¹⁰

Figure S14: Relationship between the hydrophobicity of the bioisosteric substituents phenylacetyl, 2-thienylacetyl and 2-pyridylacetyl and the inactivation constants of the inhibitors 6a and 14a-b



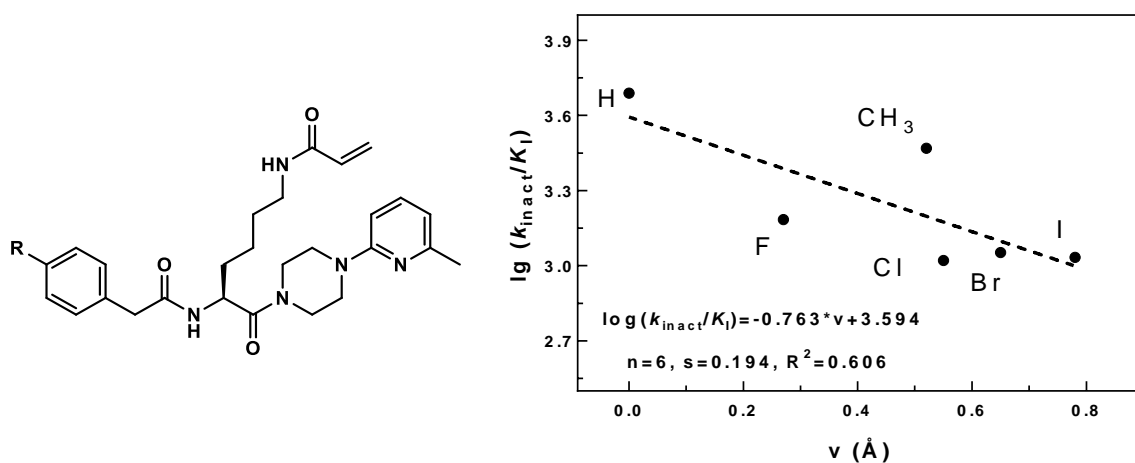
Plots of $\lg(k_{\text{inact}}/K_i)=f(\pi)$ using the mean values of the inactivation constants (Table 3 and Table 8 within the main article) and the following values for π^{12} : 0.5 (2-pyridyl), 1.61 (2-thienyl), 2.15 (phenyl). The regression analysis was performed by linear regression.

Figure S15: Molecular modelling of the interaction of hTGase 2 with 14b (A and C) and 14c (B and D)



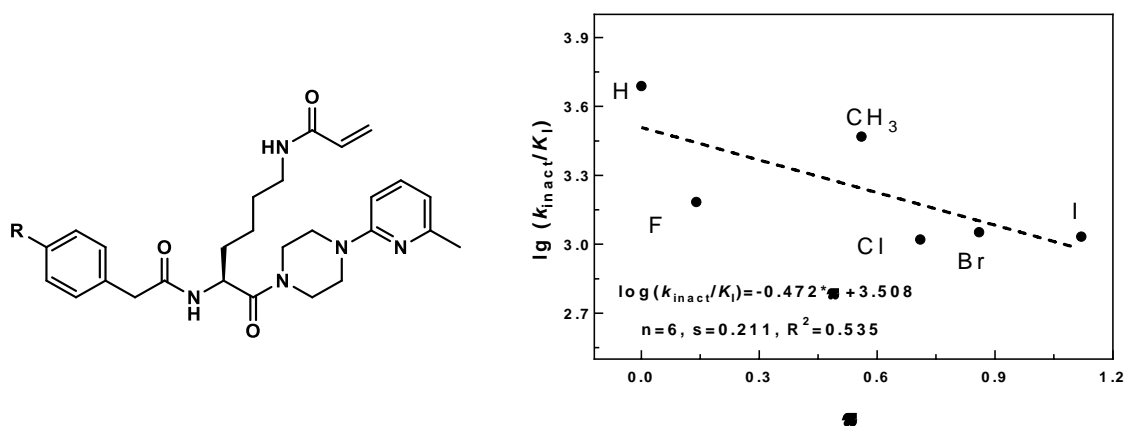
hTGase 2 is shown in gray surface with relevant residues colored by atom type, and inhibitors are shown in sticks and colored by atom type. Intermolecular H bonds, cation- π and π - π interactions are depicted by black, green and cyan dashed lines, respectively. Figure generated in Maestro (Schrödinger).¹⁰

Figure S16: Relationship between the size of the substituent in position 4 of the phenylacetyl moiety and the inactivation constants of the inhibitors 6a and 15a-e



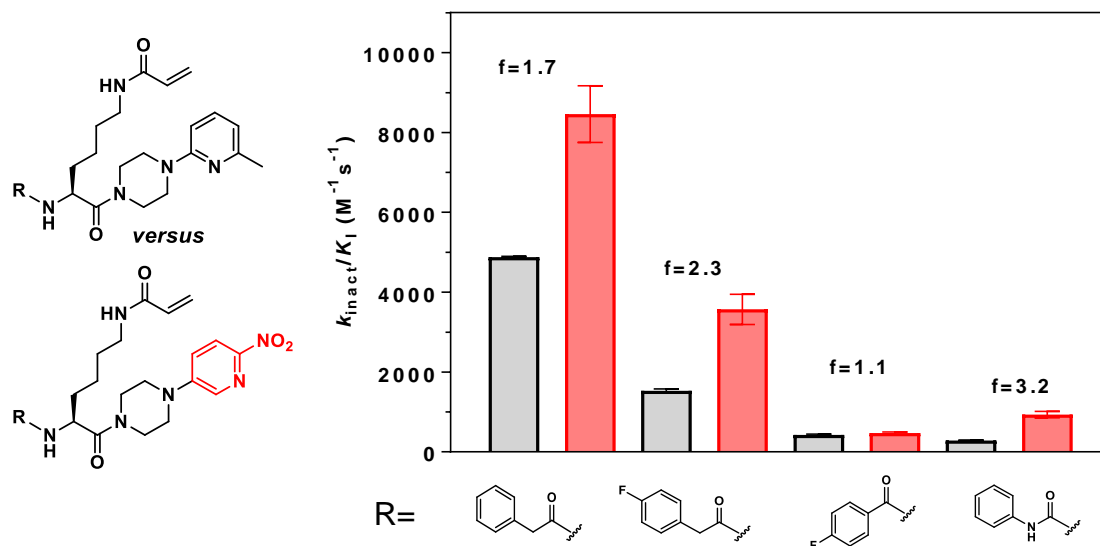
Plots of $\lg(k_{\text{inact}}/K_i)=f(v)$ using the mean values of the inactivation constants (Table 9 within the main article) and the following values for $v(\text{\AA})^{13-15}$: 0.00 (H), 0.27 (F), 0.52 (CH₃), 0.55 (Cl), 0.65 (Br) und 0.78 (I). The regression analysis was performed by linear regression.

Figure S17: Relationship between the hydrophobicity of the substituents in position 4 of the phenylacetyl moiety and the inactivation constants of the inhibitors 6a, 15a-e



Plots of $\lg(k_{\text{inact}}/K_i)=f(\pi)$ using the mean values of the inactivation constants (Table 9 within the main article) and the following values for π^{16} : 0.00 (H), 0.14 (F), 0.55 (CH₃), 0.71 (Cl), 0.86 (Br) und 1.12 (I). The regression analysis was performed by linear regression.

Figure S18: Influence of the 6-nitropyridin-3-yl moiety compared to the 6-methylpyridine-2-yl moiety on the inhibition of hTGase 2



Data shown are mean values (\pm SEM) of two separate experiments, each performed in duplicate. When not apparent, error bars are too small for the representation. For calculation of factors f , mean values of the inactivation constants were used.

Figure S19: Further *N*^ε-acryloyllysines obtained by combination of different pyridylpiperazinyl and *N*^α residues

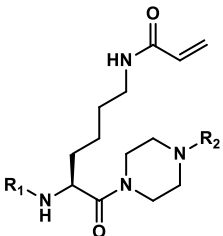
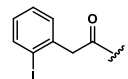
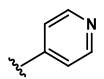
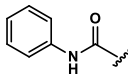
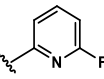
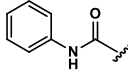
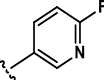
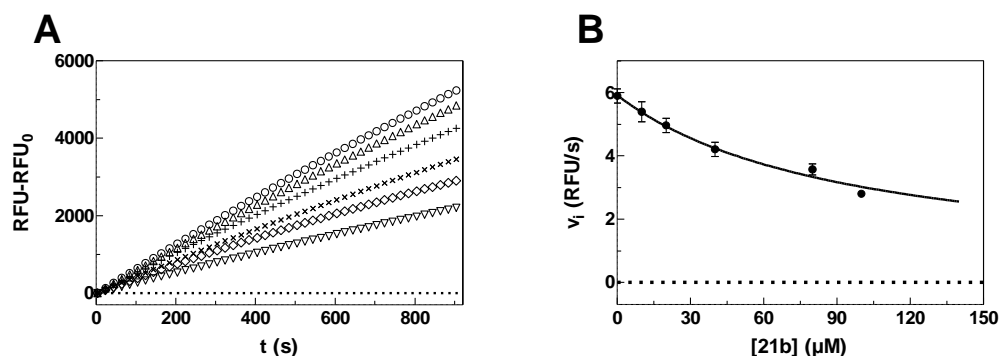
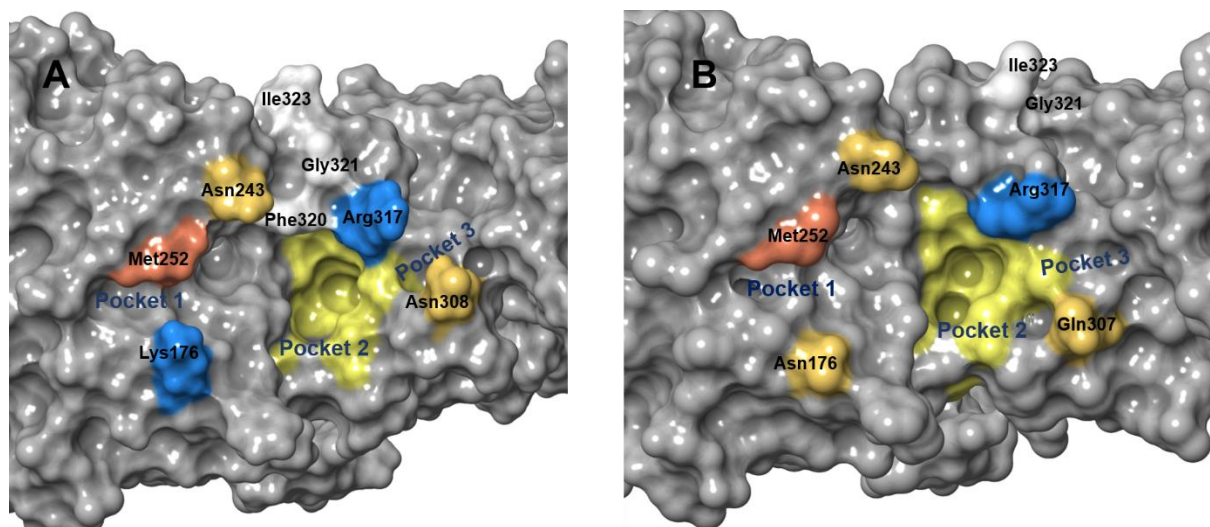
				
compound	R ₁	R ₂	<i>k</i> _{inact} / <i>K</i> _i (M ⁻¹ s ⁻¹)	<i>K</i> _i (μM)
19			6 750 (500)	2.58 (0.38)
20a			385 (3)	-
20b			251 (11)	-
Data shown are mean values (±SEM) of two separate experiments, each performed in duplicate.				

Figure S20: Kinetic characterisation of *N*^ε-propionyllysines **21a and **21b****



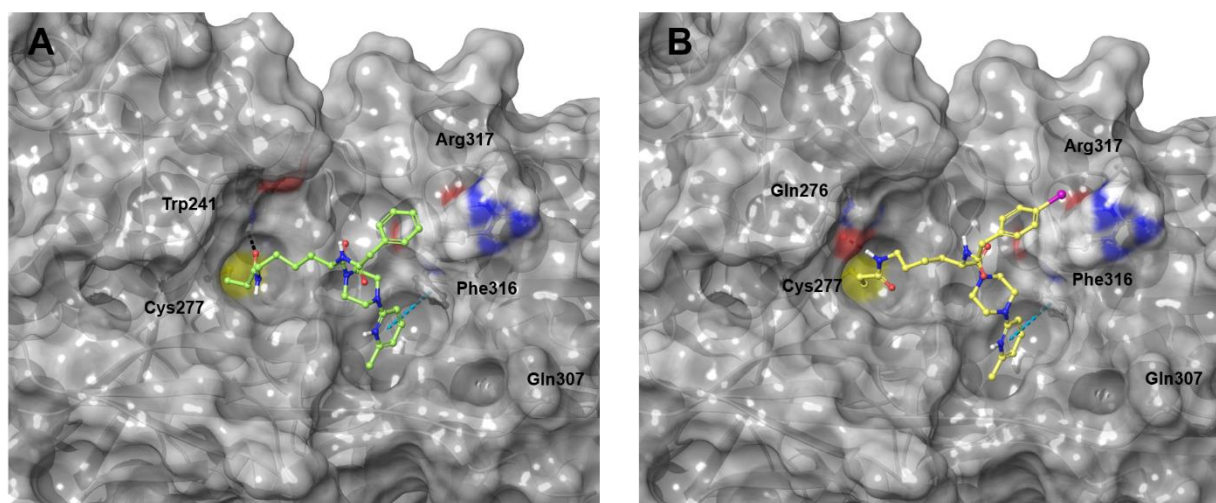
A) Typical time courses of the hTGase 2-catalysed hydrolysis of **Z-Glu(HMC)-Gly-OH** (35 μM, $\approx 5.3 \times K_m$) in the presence of different concentrations of propionylamide **21b** (0 μM (○), 10 μM (△), 20 μM (+), 40 μM (×), 80 μM (◇) and 100 μM (▽)). **B)** Secondary plot of initial rates versus concentration of **21b** with nonlinear regression to the data for determination of K_i^i (assuming competitive inhibition). Data shown in **B** are mean values (\pm SEM) of two separate experiments, each performed in duplicate. Conditions: pH=6.5, 30°C, 5% DMSO, 500 μM TCEP, 3 μg/ml hTGase 2.

Figure S21: Molecular modelling of hTGase 2 (A) and gpTGase 2 (B)



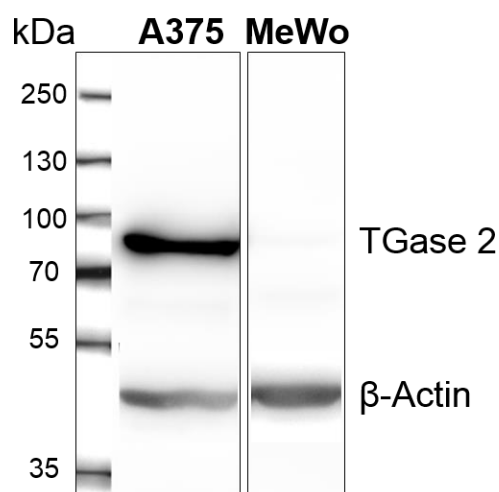
hTGase 2 and gpTGase 2 are shown in gray surface with relevant residues colored and numbered. Pocket two is highlighted in yellow in both. Figure generated in Maestro (Schrödinger).¹⁰

Figure S22: Molecular modelling of the interaction of gpTGase 2 with 6a (A) and 15e (B)



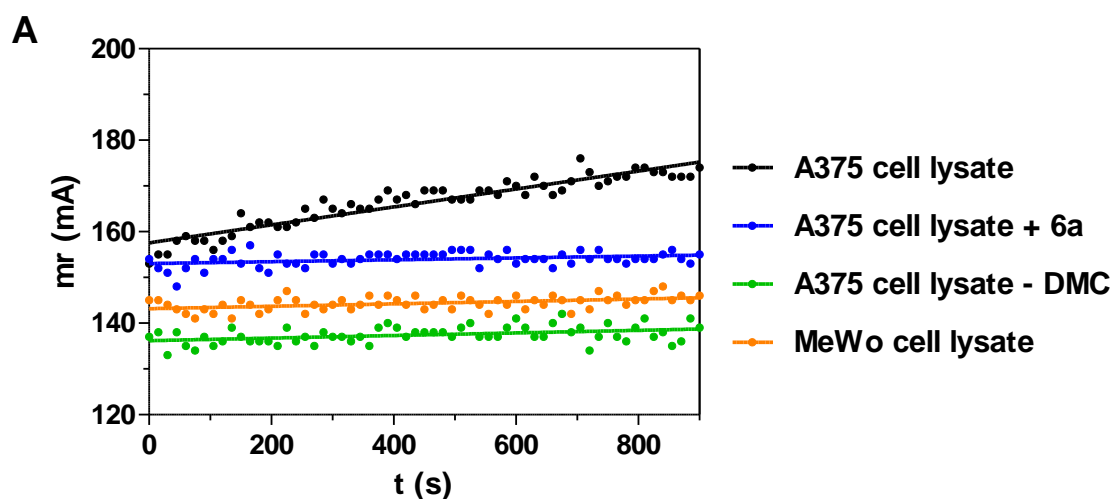
gpTGase 2 is shown in gray surface with relevant residues colored by atom type, and inhibitors are shown in sticks and colored by atom type. Intermolecular H bonds and π - π interactions are depicted by black and cyan dashed lines, respectively. Figure generated in Maestro (Schrödinger).¹⁰

Figure S23: Expression of TGase 2 in A375 and MeWo cells



TGase 2 expression of melanoma cell lines A375 and MeWo determined by Western Blotting. Cell cultivation, cell lysis, SDS-PAGE and Western blotting were performed as described previously¹⁷⁻¹⁸ and the following antibodies were used: primary antibody anti-TGase 2 (monoclonal mouse, ab2386 from Abcam, dilution 1:500) and secondary antibody anti-mouse IgG POD (polyclonal rabbit, A9044 from Sigma-Aldrich, dilution 1:2000).

Figure S24: Determination of hTGase 2-activity in cell lysates

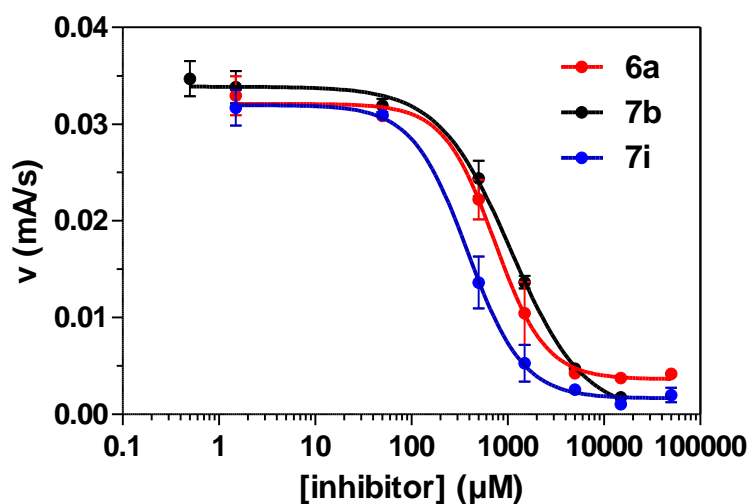


B

	A375	A375 + 6a	A375 - DMC	MeWo	MeWo + 6a	MeWo -DMC
v (mA/s) *10 ³	20.71 (0.44)	1.42 (1.36)	3.31 (0.69)	2.26 (0.64)	1.94 (0.16)	2.26 (0.21)

A) Plots of FA over time for the reaction of **R-I-Cad** (0.81 μ M) with DMC (30 μ M) in the presence of lysates (2 g protein/l) from A375 and MeWo cells. To ensure that the FA increase over time mainly originate from the hTGase 2-catalysed reaction of **R-I-Cad** with DMC, control measurements in the presence of the selective inhibitor **6a** (10 μ M, 10 min precubation time of inhibitor and lysate) and in the absence of DMC were performed. Conditions: pH=8.0, 30 °C, 3 mM CaCl₂, 5% DMSO. **B)** Summary of rates for FA increase under different conditions for lysates from A375 and MeWo cells. Data shown in **B** are mean values (\pm SD) of two separate experiments, each performed in duplicate (or single measurement for –DMC).

Figure S25: Determination of IC₅₀ values of selected inhibitors towards hTGase 2 using A375 cell lysates

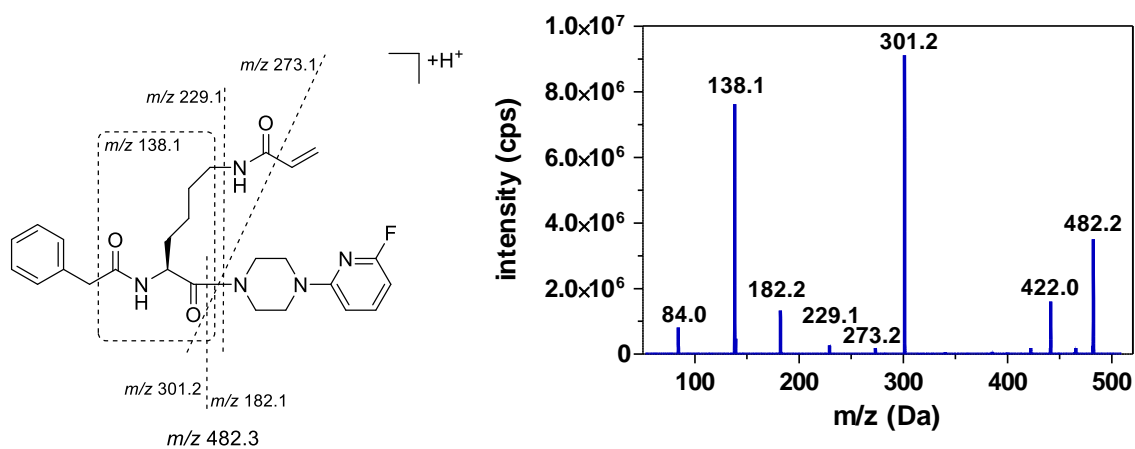


Plots of rate versus inhibitor concentration for the reaction of DMC (30 μM) with **R-I-Cad** (0.81 μM) using lysates from A375 cells (2 g protein/l). The inhibitor concentration, [I], causing 50% inhibition, IC₅₀, and the Hill slope, n_H, were calculated according to the equation

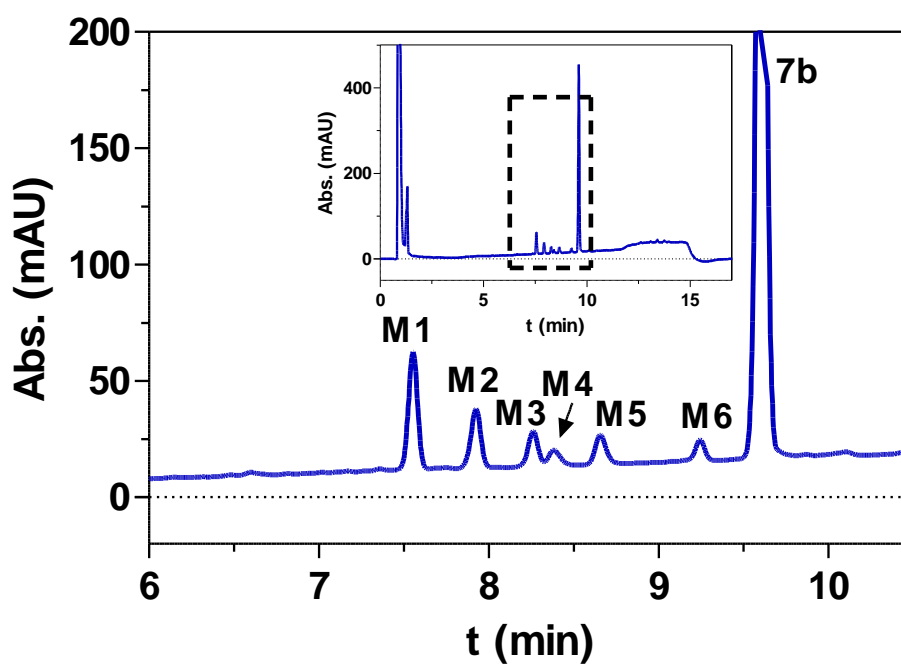
$$\text{rate} = \text{Bottom} + \frac{(\text{Top} - \text{Bottom}) \times [\text{I}]^{n_H}}{[\text{I}]^{n_H} + \text{IC}_{50}^{n_H}}$$

with Bottom and Top representing the lower and upper plateaus of the sigmoid dose–response curve, respectively. Data shown are mean values (±SEM) of two to three separate experiments, each performed in duplicate. Conditions: pH=8.0, 30 °C, 3 mM CaCl₂, 5% DMSO.

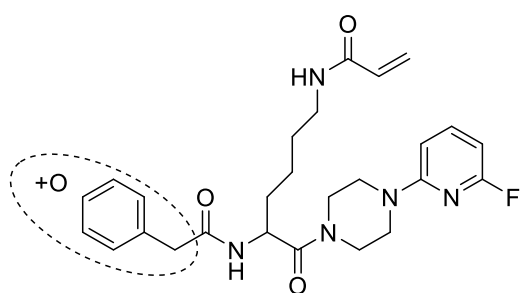
Figure S26: Analysis of potential metabolites of compound 7b



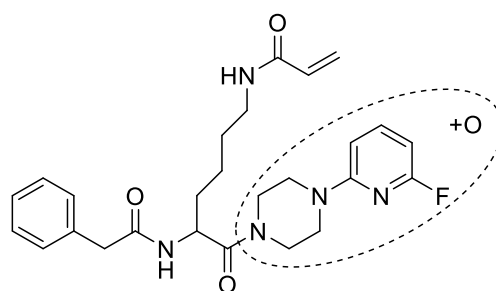
Enhanced-product ion (EPI) mass spectra of original compound **7b**



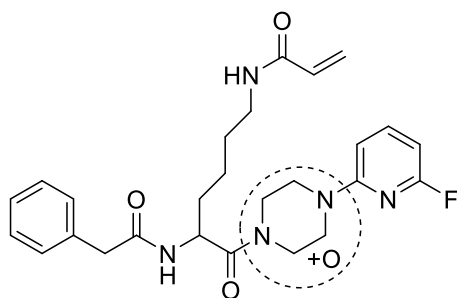
Analytical RP-HPLC chromatogram (@235 nm) of the mixture obtained after incubation of compound **7b** with mouse liver microsomes for 60 min. Potential structures of metabolites (M1-M6, see below) were identified by their EPI mass spectra considering the EPI mass spectra of **7b**.



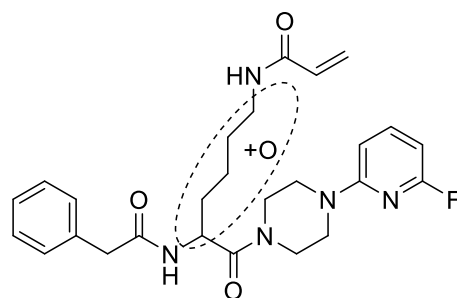
M2



M1, M3



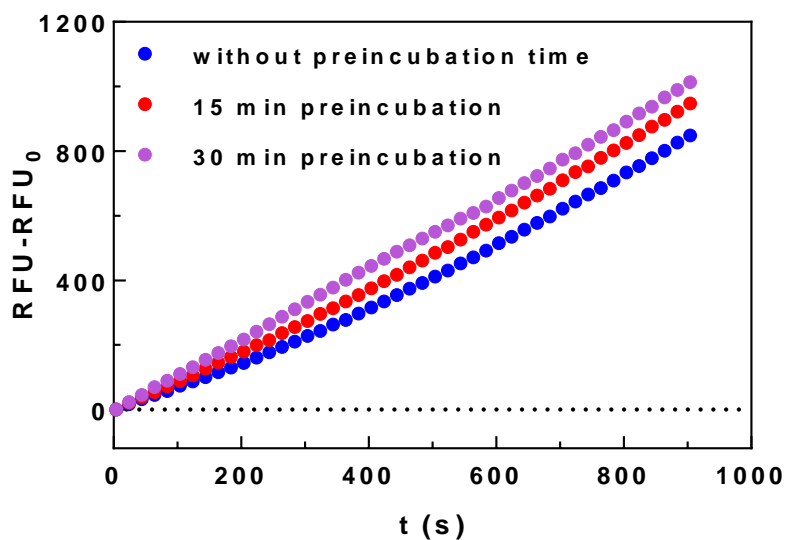
M4*



M5*, M6

Structures of metabolites M1-M6 (m/z 498.3 $[M_{7b}+O+H]^+$) formed by MLM incubation of **7b**,
 *assignment not completely proven.

Figure S27: Influence of preincubation time on the activity of hTGase 3



Plots of $\text{RFU}=f(t)$ for the enzymatic hydrolysis (pH 6.5 and 30 °C in the presence of 5% DMSO and 500 μM TCEP) of **Z-Glu(HMC)-Gly-OH** (80 μM) by hTGase 3 (3 $\mu\text{g/mL}$) after different preincubation times of enzyme at 30 °C. Linear progress curves are obtained after 30 min of preincubation, while shorter times of preincubation result in hysteretic curve progressions (probably because of the increasing activity of hTGase 3 with time).

Table S1: Summary of the determined and calculated physico-chemical parameters of the *N*^E-acryloyllysines

cpd.	cp <i>K</i> _a ^{a,b}	clogP ^a	logD _{7.4} ^c	clogD _{7.4} ^a	P _{e(7.5)} (nm/s) ^d	R _m (%) ^e	CHI IAM _{7.4} ^f
6a	9.1	1.37	-	-0.36	87.7 (3.9)	-1	29.4
6b	9.1	1.37	-	-0.36	101 (7.0)	3	-
7a	8.4	1.15	-	0.05	61.3 (8.2)	2	-
7b	2.8	1.27	2.10	1.27	133 (19)	14	31.8
7c	4.8	1.91	-	1.91	152 (10)	29	-
7d	4.0	2.03	-	2.03	125 (22)	34	-
7e	5.0	2.20	-	2.20	231 (36)	48	-
7f	8.9	2.77	-	1.31	219 (28)	69	39.5
7g	7.6	2.79	-	2.33	219 (57)	64	39.0
7h	6.7	1.62	-	1.54	117 (21)	24	-
7i	0.6	1.02	-	1.02	91.6 (8.1)	10	30.7
8a	7.0	1.17	-	1.13	12.9 (0.9)	-7	-
8b	1.3	1.05	1.66	1.05	35.4 (3.2)	4	26.8
8c	2.3	1.81	2.13	1.81	89.8 (3.1)	11	31.8
8d	-2.5	1.09	-	1.09	17.8 (2.1)	-14	-
8e	6.4 (1.5) ^g	1.18	-	-1.55	3.1 (0.2)	-8	-
8f	3.4	1.22	-	1.22	10.7 (1.3)	2	-
8g	4.3	0.51	-	0.51	3.2 (0.9)	-7	-
9	3.0 ^h	1.87	-	1.87	98.8 (17.5)	-2	-
10	10.7	1.15	-	-0.37	5.1 (0.8)	31	25.4
11	3.2 ^h	2.29	-	2.29	168 (32)	6	-
12	1.5 ^h	1.88	-	1.88	128 (20)	22	-
13a	-	1.18	1.60	1.18	30.5 (5.2)	-3	25.0
13b	-	0.99	-	0.99	28.1 (4.4)	1	-
13c	6.2 ⁱ	1.99	2.65	1.98	103 (13.4)	12	32.0
13d	0.8	1.12	-	1.12	39.9 (23.3)	-15	-
13e	4.1 ⁱ	3.08	-	3.08	76.8 (4.8)	38	37.7
14a	9.1	0.68	-	-1.05	39.7 (11.5)	10	-
14b	9.1	1.41	-	-0.32	99.7 (13.2)	14	-
14c	9.1	1.41	-	-0.32	125 (31)	11	-
14d	9.1	2.44	-	0.71	172 (20)	24	-
14e	9.1	1.40	-	-0.36	150 (20)	25	-
14f	9.1	3.11	-	1.34	156 (18)	66	-
14g	9.1	1.42	-	-0.26	163 (14)	32	-
14h	9.1	1.51	0.47	-0.17	141 (17)	39	34.3
14k	9.1	1.65	0.28	-0.10	127 (27)	16	31.4
14l	9.1	2.11	-	0.36	69.8 (3.2)	51	-
14m	9.1 (7.8) ^k	2.05	-	-0.04	71.9 (8.5)	44	-
15a	9.1	1.87	-	0.14	252 (47)*	5	-
15b	9.1	1.41	0.36	-0.32	114 (7.0)	10	32.4
15c	9.1	2.11	-	0.38	123 (5.0)*	8	-
15d	9.1	2.02	-	0.29	142 (25)*	25	-
15e	9.1	2.26	-	0.53	81.1 (2.3)	34	-
15f	9.1	1.41	-	-0.32	114 (9.0)	21	30.1
15g	9.1	1.41	-	-0.32	125 (32)	24	30.9
16c	7.6	2.27	-	2.22	111 (23)	75	-

cpd.	cpK _a ^{a,b}	clogP ^a	logD _{7.4} ^c	clogD _{7.4} ^a	P _{e(7.5)} (nm/s) ^d	R _m (%) ^e	CHI IAM _{7.4} ^f
17a	-2.5	0.96	-	0.96	11.3 (3.7)	17	-
17b	-2.5	1.04	1.04	1.04	19.7 (3.1)	9	28.3
17c	-2.5	1.17	1.17	1.17	40.8 (5.7)	12	28.5
18	0.6	1.04	-	1.04	87.4 (5.4)	12	30.7
19	10.7	1.79	-	0.27	11.6 (0.8)	21	-
20a	2.8	1.25	-	1.25	172 (15)	56	-
20b	1.3	1.01	-	1.01	63.4 (4.2)	5	-
21a	9.1	1.78	-	0.05	98.4 (33.3)	7	-
21b	-2.5	1.24	-	1.24	16.7 (1.1)	12	-

Fluorinated inhibitors are coloured in blue. ^acpK_a, clogP and clogD_{7.4} values were calculated using Advance Chemistry Development (ACD/Lab) Software V14.0.0 (© 1994-2016 ACD/Labs). clogP values were calculated as „Consensus logP¹⁹ and the cpK_a values were calculated based on the „Classic“ algorithm²⁰. Calculation of the clogD_{7.4} values in turn is based on the obtained clogP and cpK_a values²¹. ^bIf not otherwise stated, the cpK_a value corresponds to the pK_a value of the respective pyridinium ion. ^cData shown are values of one determination. ^dData shown are mean values (±SD) of one experiment which was performed in triplicate or mean values (±SEM) of 2-4 separate experiments, each performed in triplicate. ^eData shown are mean values. ^fData shown are values of one determination. ^gValue in brackets corresponds to the carboxyl group. ^hValue corresponds to the anilinium ion. ⁱValue corresponds to the piperazinium ion. ^jValue corresponds to the dimethylammonio group of the dansyl moiety. ^kValues in brackets corresponds to the α-ammonio group.

Chemistry

General

All commercial reagents and solvents were used without further purification unless otherwise specified. Melting points were determined on a Galen III Boetius apparatus from Cambridge Instruments. Nuclear magnetic resonance spectra were recorded on an Agilent Technologies 400 MR spectrometer (400 MHz for ^1H , 101 MHz for ^{13}C and 376 MHz for ^{19}F). Spectra were processed by using the programme MestreNova (version 6.1.1-6384).²² NMR chemical shifts were referenced to the residual solvent resonances relative to tetramethylsilane (TMS; ^1H and ^{13}C) and trichlorofluoromethane (CFCl_3 ; ^{19}F). Mass spectra (ESI) were obtained on a Waters Xevo TQ-S mass spectrometer driven by the Mass Lynx software.

Chromatography

Thin-layer chromatography (TLC) was performed on Merck silica gel F-254 aluminium plates with visualisation under UV (254 nm) and/or staining with a 0.1% (w/v) ninhydrin solution in ethanol. Preparative column chromatography was carried out on Merck silica gel (mesh size 230–400 ASTM) with solvent mixtures as specified for the particular compounds. For purification of the compounds, analytical and preparative HPLC were performed on a Varian Prepstar system equipped with a UV detector (Prostar, Varian). Two Microsorb C18 60-8 columns (Varian Dynamax 250×4.6 mm and 250×21.4 mm) were used as the stationary phases for analytical and preparative RP-HPLC, respectively. A binary gradient system of 0.1% CF_3COOH /water (solvent A) and 0.1% $\text{CF}_3\text{COOH}/\text{CH}_3\text{CN}$ (solvent B) at a flow rate of 1 mL/min or 10 mL/min served as the eluent. With regards to analytical RP-HPLC, the programme for elution of the compounds was a gradient from low to high percentage of solvent B with a slope of 2% per min. An appropriate range of concentrations were used for each specific compound. With regards to preparative RP-HPLC, similar conditions for the gradient elution of the compounds were applied as for analytical RP-HPLC but with a slope of 1% per min. HPLC for determining the enantiomeric composition of compounds **6a** and **6b** was carried out with a system consisting of a Merck Hitachi L7100 gradient pump combined with a Jasco DG2080 four-line degasser with UV detection by a Merck Hitachi L7450 diode array detector. The system was operated with D-700 HSM software and use of a Merck Hitachi D7000 interface. A Chiralpak[®] IA column (250×4.6 mm, 5 μm) served as stationary phase. Separation of the enantiomers was achieved by an isocratic solvent mixture of 5% hexane/ CH_3CN at a flow rate of 1 mL/min.

General synthetic procedures

GP I: General procedure for Benzoylpiperazines

A solution of the respective benzoyl chloride (1.53 mmol, 0.95 eq.) in the given solvent (3 mL) was added dropwise to a solution of 1-*tert*-butoxycarbonylpiperazine (300 mg, 1.61 mmol, 1 eq.) and TEA (450 μ L, 3.22 mmol, 2 eq.) in the same solvent. The reaction mixture was stirred for 2 h. Subsequently, the solvent was removed *in vacuo* and the residue was dissolved in CH₂Cl₂ (10 mL). The solution was washed with 1 M HCl (2 \times 5 mL), 0.1 M NaOH (2 \times 5 mL) and brine (1 \times 5 mL). The organic phase was dried over Na₂SO₄ and evaporated to obtain the desired products in sufficient purity for further reactions.

GP II: General procedure for Buchwald-Hartwig amination

The procedure is based on the protocol of Yin and Buchwald.²³ To a solution of 1-*tert*-butoxycarbonylpiperazine (500 mg, 2.68 mmol, 1 eq.) in dry THF (10 mL) under Ar atmosphere was added Cs₂CO₃ (2.13 g, 8.04 mmol, 3 eq.). The resulting suspension was stirred for 1 min followed by the addition of the respective halogen-substituted pyridine derivative (2.68 mmol, 1 eq.), Xantphos (93.2 mg, 0.16 mmol, 0.06 eq.) and Pd₂(dba)₃ (49.1 mg, 0.05 mmol, 0.02 eq.) in the given order. The reaction mixture was stirred at 70 °C under Ar atmosphere over night. Afterwards, the solvent was removed *in vacuo* and the residue dissolved in ethyl acetate was washed with 0.03 M sodium diethyldithiocarbamate (5 \times 15 mL) and brine (1 \times 15 mL). The organic phase was filtered through celite, dried over Na₂SO₄ and evaporated. The crude product was purified by column chromatography with the respective solvent mixtures given for each compound.

GP III: General procedure for Boc removal from piperazine derivatives

The Boc-protected piperazine building block was dissolved in CH₂Cl₂ (10 mL). Subsequently, TFA (10 mL) was added slowly under stirring. The reaction mixture was stirred for 3 h. The volatile components were removed in an N₂ stream. The residue was dissolved in water (2 mL) and the pH of the solution was adjusted to 14 with 4 M NaOH. The alkaline solution was extracted with CH₂Cl₂ (5 \times 10 mL). The organic phases were combined, dried over Na₂SO₄ and evaporated to afford the respective free amine.

Due to the possible hydrolysis of the methyl ester group, alkaline extraction for compound **3l** was omitted.

Before alkaline extraction, compound **3o** was purified by preparative RP-HPLC. The product-containing fractions were combined and dried by lyophilisation.

GP IV: General procedure for acylation of N-hydroxysuccinimide

The general procedure is based on the method for the synthesis of *N*-acryloxysuccinimide (**1a**) described by Bergbreiter *et al.*²⁴. To a suspension of *N*-hydroxysuccinimide (5.0 g, 43.0 mmol, 1 eq.) in CHCl_3 (30 mL) was added TEA (6.66 mL, 48.0 mmol, 1.1 eq.). The resulting solution was cooled to 0 °C in an ice bath and subsequently the respective acyl chloride (43.0 mmol, 1 eq.) was added dropwise over 10 min. The reaction mixture was stirred at 0 °C for 10 min and then at room temperature for 1 h. Afterwards, the reaction mixture was washed with water (1×15 mL) and brine (1×15 mL) and the organic phase was dried over Na_2SO_4 . Further specific instructions are given below for the respective *N*-hydroxysuccinimide esters.

GP V: General procedure for N^{F} -acylation

To a solution of N^{B} -Boc-lysine (1.0 g, 4.06 mmol, 1 eq.) and TEA (1.69 mL, 12.18 mmol, 3 eq.) in methanol (20 mL) was added the respective *N*-hydroxysuccinimide ester (687 mg, 4.06 mmol, 1 eq.) in small portions. The mixture was stirred for 2 h followed by removal of the solvent *in vacuo*.

GP VI: General procedure for amide coupling

To a solution of the respective N^{B} -Boc- N^{F} -acyllysine (0.50 mmol, 1 eq.) and DIPEA (174 μL , 1.00 mmol, 2 eq.) in THF (3 mL) was added the respective piperazine building block (0.50 mmol, 1 eq.). Subsequently, PyBOP (312 mg, 0.60 mmol, 1.2 eq.) was added and the reaction mixture was stirred for 3 h. The solvent was removed *in vacuo* and the residue was dissolved in ethyl acetate (10 mL). The organic phase was washed with saturated NaHCO_3 (2×5 mL) and brine (5 mL), followed by drying over Na_2SO_4 and evaporation.

GP VII: General procedure for Boc removal from the lysine piperazides

The N^{B} -Boc- N^{F} -acyllysine piperazide was dissolved in CH_2Cl_2 (5 mL). Subsequently, TFA (5 mL) was added slowly under stirring. The reaction mixture was stirred for 3 h. The volatile components were removed in an N_2 stream. The residue was dissolved in a mixture of water-acetonitrile 3:1 (2 mL) and the solution was lyophilised. The yields were quantitative.

GP VIII: General procedure for coupling of activated carboxylic acid derivatives

To a solution of the respective free amine (0.19 mmol, 1 eq.) and TEA (106 μL , 0.76 mmol, 4 eq.) in CH_2Cl_2 (4 mL) was added the respective activated carboxylic acid derivative (0.19 mmol, 1 eq.). The reaction mixture was stirred for 3 h. Afterwards, CH_2Cl_2 (10 mL) was added and the organic phase was washed with saturated NaHCO_3 (1×5 mL) and brine (1×5 mL), dried over Na_2SO_4 and evaporated. The crude product was purified by preparative

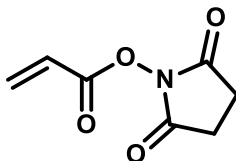
RP-HPLC. The product-containing fractions were combined and lyophilised to afford the respective final inhibitors.

GP IX: General procedure for coupling of carboxylic acids

To a solution of the respective free amine (0.063 mmol, 1 eq.) and DIPEA (33 μ L, 0.188 mmol, 3 eq.) in DMF (2 mL) was added a solution of the respective carboxylic acid (0.063 mmol, 1 eq.) and DIPEA (11 μ L, 0.063 mmol, 1 eq.) in DMF (1 mL). After 1 min of stirring PyBOP (32.5 mg, 0.063 mmol, 1 eq.) was added. The reaction mixture was stirred for 4 h. The solvent was removed *in vacuo* and the residue was dissolved in CH₂Cl₂ (10 mL). The organic phase was washed with saturated NaHCO₃ (6 mL) and brine (6 mL), dried over Na₂SO₄ and evaporated. The crude product was purified by preparative RP-HPLC. The product-containing fractions were combined and lyophilised to afford the respective final inhibitors.

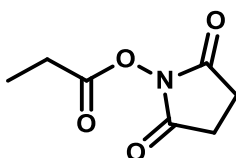
***N*-Acyloxysuccinimide building blocks 1**

***N*-Acryloxysuccinimide (1a)²⁴⁻²⁵**



The synthesis was accomplished according to **GP IV** using acryloyl chloride (43.0 mmol). After drying over Na₂SO₄ the organic phase was concentrated to approx. 20 mL of CHCl₃ *in vacuo*. The solution was cooled to 0 °C in an ice bath, followed by the addition of hexane (10 mL) and ethyl acetate (2 mL). The mixture was stirred at 0 °C for 45 min. The emerging precipitate was filtered off and washed with mixtures of ethyl acetate and hexane (1×10 mL 4:1, 1×10 mL 9:1) and hexane (1×10 mL). To the filtrate was added hexane and the emerging precipitate was filtered off again and washed as described above. The solids were combined and after drying under oil pump vacuum compound **1a** (6.03 g, 83%) was obtained as an off-white solid. *R*_f 0.62 (ethyl acetate-acetic acid 99:1); mp: 67-69 °C (lit.²⁵) 67-69 °C); ¹H-NMR (CDCl₃) δ=6.70 (dd, ³J=17.3 Hz, ²J=0.9 Hz, 1H, C=CHH), 6.33 (dd, ³J=17.3 Hz, ³J=10.7 Hz, 1H, CH=CH₂), 6.17 (dd, ³J=10.7 Hz, ²J=0.9 Hz, 1H, C=CHH), 2.86 (s, 4H, 2×CH₂); ¹³C-NMR (CDCl₃) δ=169.14 (2×CO), 161.18 (COO), 136.31 (CH₂=C), 123.11 (CH₂=C), 25.77 (2×CH₂), ¹H- and ¹³C-NMR data are in agreement with those reported in literature.²⁴⁻²⁵

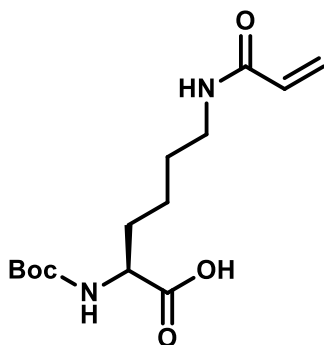
***N*-Propionyloxysuccinimide (1b)²⁶⁻²⁷**



The synthesis was accomplished according to **GP IV** using propionyl chloride (17.4 mmol). After drying over Na₂SO₄ the organic phase was evaporated to afford a colourless oil which solidified during storage in the refrigerator. After drying under oil pump vacuum compound **1b** (1.91 g, 64%) was obtained as a white solid. *R*_f 0.48 (ethyl acetate-petroleum ether 1:1); mp: 43-45 °C (lit.²⁶) 44-46 °C); ¹H-NMR (CDCl₃) δ=2.84 (s, 4H, 2×CH₂ of pyrrolidine), 2.65 (q, ³J=7.5 Hz, 2H, CH₂ of propionyl), 1.28 (t, ³J=7.6 Hz, 3H, CH₃); ¹H-NMR data are in agreement with those reported in literature.²⁷

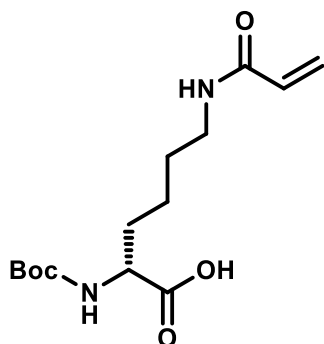
***N*^α-Boc-*N*^ε-acryllysines 2**

***N*^α-Boc-*N*^ε-Acryloyl-L-lysine (2a)²⁸**



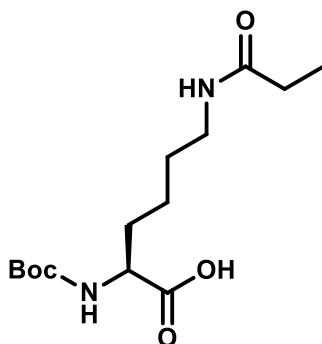
The synthesis was accomplished according to **GP V** using *N*^α-Boc-L-lysine (4.06 mmol) and *N*-acryloxysuccinimide. The crude product was purified *via* column chromatography (gradient from CH₂Cl₂-isopropanol-acetic acid 95:5+2 to 92:8+2). The product-containing fractions were combined and evaporated. Residual acetic acid was removed by repeated addition and evaporation of toluene (3×10 mL, boiling point of the azeotropic mixture acetic acid-toluene (mole fractions 0.375/0.625) at 100.7 °C)²⁹. After drying under oil pump vacuum compound **2a** (609 mg, 50%) was obtained as a colourless oil. *R*_f 0.12 (CH₂Cl₂-isopropanol-acetic acid 95:5+2); ¹H-NMR (CDCl₃) δ=6.29 (d, ³J=16.8 Hz, 1H, CH=CHH), 6.18-6.03 (m, 2H, CH=CH₂, N_εH), 5.65 (d, ³J=10.2 Hz, 1H, CH=CHH), 5.33-5.24 (m, 1H, N_αH), 4.28 (s, 1H, C_αH), 3.39-3.30 (m, 2H, C_εH₂), 1.94-1.80 (m, 1H, C_βHH), 1.80-1.66 (m, 1H, C_βHH), 1.64-1.52 (m, 2H, C_δH₂), 1.50-1.38 (m, 11H, 3×CH₃, C_γH₂); ¹³C-NMR (CDCl₃) δ=175.67 (COOH), 166.38 (CON_ε), 156.11 (CON_α), 130.74 (CH₂=CH), 127.02 (CH₂=CH), 80.40 (quart. C of Boc), 53.25 (C_α), 39.36 (C_ε), 32.05 (C_β), 28.96 (C_δ), 28.48 (3×CH₃), 22.53 (C_γ); MS (ESI⁺): *m/z* calculated for C₁₄H₂₄N₂NaO₅: 323.16 [M+Na]⁺, found: 323.1.

***N*^α-Boc-*N*^ε-Acryloyl-D-lysine (2b)**



The synthesis was accomplished according to **GP V** using *N*^α-Boc-D-lysine (0.81 mmol) and *N*-acryloxysuccinimide. The crude product was directly used for the next step.

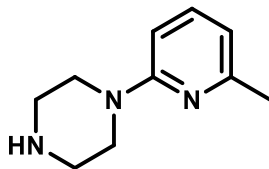
***N*^α-Boc-*N*^ε-Propionyl-L-lysine (**2c**)**³⁰



The synthesis was accomplished according to **GP V** using *N*^ε-Boc-L-lysine (1.46 mmol) and *N*-propionyloxysuccinimide. The crude product was purified *via* column chromatography (CH₂Cl₂-methanol-acetic acid 95:5+2). The product-containing fractions were combined and evaporated. Residual acetic acid was removed by repeated addition and evaporation of toluene (3×10 mL). After drying under oil pump vacuum compound **2c** (418 mg, 95%) was obtained as a reddish oil. *R*_f 0.23 (CH₂Cl₂-methanol-acetic acid 95:5+2); ¹H-NMR (CDCl₃) δ=5.73 (broad s, 1H, N_εH), 5.27 (broad s, 1H, N_αH), 4.28 (broad s, 1H, C_αH), 3.26 (broad s, 2H, C_εH₂), 2.26-2.16 (m, 2H, CH₂-CH₃), 1.87 (broad s, 1H, C_βHH), 1.74 (broad s, 1H, C_βHH), 1.60-1.49 (m, 2H, C_δH₂), 1.45 (s, 11H, 3×CH₃ of Boc, C_γH₂), 1.15 (t, 3H, ³J=7.4 Hz, CH₂-CH₃); ¹³C-NMR (CDCl₃) δ=175.04 (COOH), 174.81 (CON_ε), 156.14 (CON_α), 80.36 (quart. C of Boc), 53.41 (C_α), 39.19 (C_ε), 31.97 (C_β), 29.89 (CH₂-CH₃), 29.16 (C_δ), 28.49 (3×CH₃ of Boc), 22.41 (C_γ), 10.07 (CH₂-CH₃); MS (ESI⁺): *m/z* calculated for C₁₄H₂₆N₂NaO₅: 325.17 [M+Na]⁺, found: 325.1.

Piperazine building blocks 3

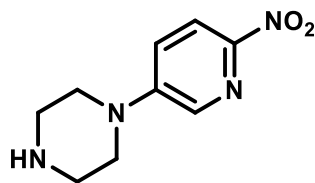
1-(6-Methylpyridine-2-yl)piperazine (**3a**)³¹



The synthesis was accomplished according to Pavia *et al.*³¹ 2-Chloro-6-methylpyridine (2.12 mL, 19.4 mmol, 3 eq.) was added to a solution of piperazine (5.0 g, 58 mmol, 1 eq.) in 1-butanol (20 mL). The mixture was stirred at 130 °C for 5 d. Afterwards, the solvent was removed *in vacuo*. The crude product was purified *via* column chromatography (gradient from CH₂Cl₂-methanol 9:1 to 3:7). The product-containing fractions were combined and evaporated to afford **3a** (2.05 g, 20%) as a red brown oil. *R*_f 0.05 (CH₂Cl₂-methanol 9:1); ¹H-NMR (CDCl₃) δ=7.38 (dd, ³J=8.4, 7.3 Hz, 1H, H-4), 6.52 (d, ³J=7.3 Hz, 1H, H-5), 6.43 (d, ³J=8.4 Hz, 1H, H-3), 3.62-3.56 (m, 4H, H-2,6 of piperazine), 3.09-3.05 (m, 4H, H-3,5 of piperazine), 2.39 (s, 3H, CH₃), signal for NH is not visible; ¹³C-NMR (CDCl₃) δ=159.20, 157.04, 137.96 (C-4), 113.23 (C-5), 103.90 (C-3), 45.65 (C-2,6 of piperazine), 45.41 (C-3,5 of piperazine), 24.70 (CH₃); MS (ESI⁺): *m/z* calculated for C₁₀H₁₆N₃: 178.13 [M+H]⁺, found: 178.2.

As side product 1,4-Bis(6-methylpyridin-2-yl)piperazine was isolated (3.6 mg, buff solid). *R*_f 0.00 (CH₂Cl₂-methanol 9:1); ¹H-NMR (CDCl₃) δ=7.40 (dd, ³J=8.4, 7.3 Hz, 2H, H-4), 6.52 (d, ³J=7.3 Hz, 2H, H-3), 6.48 (d, ³J=8.4 Hz, 2H, H-5), 3.67 (s, 8H, 4×CH₂), 2.42 (s, 6H, 2×CH₃); ¹³C-NMR (CDCl₃) δ=159.24, 156.94, 137.97 (2×C-4), 112.99 (2×C-5), 104.00 (2×C-3), 45.31 (4×CH₂), 24.67 (2×CH₃).

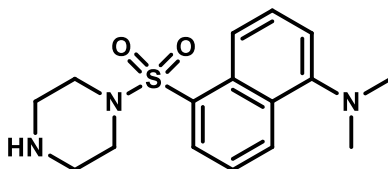
1-(6-Nitropyridin-2-yl)piperazine (**3b**)³²



The synthesis was accomplished according to Swanson *et al.*³² A suspension of 3-bromo-6-nitropyridine (2.0 g, 9.85 mmol, 1 eq.) in acetonitrile (5 mL) was added to a suspension of piperazine (2.29 g, 26.6 mmol, 2.7 eq.) in acetonitrile (15 mL). The mixture was stirred at 95 °C for 6 h. During this time, the suspension cleared off and subsequently a white precipitate was formed. Afterwards, the solvent was removed *in vacuo* and the orange residue was dissolved

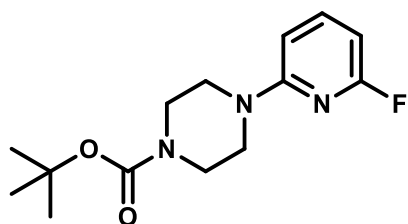
in ethyl acetate (40 mL). The solution was washed with 1 M NaOH (1×60 mL). Then, the organic phase was separated and the aqueous phase was washed with ethyl acetate (4×40 mL). The combined organic layers were dried over Na₂SO₄ and the solvent was removed *in vacuo*. The crude product was purified *via* column chromatography (CH₂Cl₂-methanol-*N,N*-dimethylethylamine 9.5:0.5+0.1). The product-containing fractions were combined and evaporated to afford **3b** (1.79 g, 87%) as a yellow solid. *R*_f 0.30 (CH₂Cl₂-methanol-*N,N*-dimethylethylamine 8:2+0.1); mp: 138-142 °C; ¹H-NMR (CDCl₃) δ=8.16 (d, ³J=9.2 Hz, 1H, H-5), 8.13 (d, ⁴J=3.0 Hz, 1H, H-2), 7.19 (dd, ³J=9.2 Hz, ⁴J=3.1 Hz, 1H, H-4), 3.44–3.39 (m, 4H, H-2,6 of piperazine), 3.08–3.03 (m, 4H, H-3,5 of piperazine), 1.68 (s, 1H, NH), ¹H-NMR data are in agreement with those reported in literature;³² ¹³C-NMR (CDCl₃) δ=150.32, 147.88, 133.89 (C-2), 120.58, 119.86, 47.89 (C-2,6 of piperazine), 45.70 (C-3,5 of piperazine); MS (ESI⁺): *m/z* calculated for C₉H₁₃N₄O₂: 209.10 [M+H]⁺, found: 209.2.

Dansylpiperazine (**3c**)³³⁻³⁴



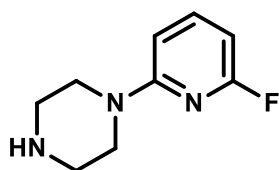
The synthesis was accomplished according to Sashuk *et al.*³³. Dansylchloride (250 mg, 0.93 mmol, 1 eq.) and piperazine (479 mg, 3.71 mmol, 6 eq.) were dissolved in CH₂Cl₂ (30 mL) and the mixture was stirred for 15 min. Afterwards, the reaction mixture was washed with saturated NaHCO₃ (3×20 mL) and the organic phase was separated, dried over Na₂SO₄ and evaporated to obtain compound **3c** (172 mg, 58%) as a light green solid in sufficient purity for further reactions. ¹H-NMR (DMSO-*d*₆) δ=8.56 (d, ³J=8.6 Hz, 1H, H of dansyl), 8.43 (d, ³J=8.8 Hz, 1H, H of dansyl), 8.19 (dd, ³J=7.3 Hz, ⁴J=1.3 Hz, 1H, H of dansyl), 7.56-7.50 (m, 2H, 2×H of dansyl), 7.19-7.17 (m, 1H, H-6 of dansyl), 3.19-3.12 (m, 4H, 2×CH₂), 2.90-2.85 (m, 10H, 2×CH₃, 2×CH₂), 1.61 (s, 1H, NH); ¹³C-NMR (DMSO-*d*₆): δ=151.83 (C-5 of dansyl), 132.77 (quart. C of dansyl), 130.77 (CH of dansyl), 130.75 (CH_{dansyl}), 130.67 (quart. C of dansyl), 130.22 (quart. C of dansyl), 128.08 (CH of dansyl), 123.27 (CH of dansyl), 119.98 (CH of dansyl), 115.35 (C-6 of dansyl), 46.59 (2×CH₂), 45.65 (2×CH₃), 45.58 (2×CH₂), NMR data are in agreement with those reported in literature;³³⁻³⁴ MS (ESI⁺): *m/z* calculated for C₁₆H₂₂N₃O₂S: 320.14 [M+H]⁺, found: 320.1.

4-*tert*-Butoxycarbonyl-1-(6-fluoropyridin-2-yl)piperazine (**Boc-3d**)³⁵



The synthesis was accomplished according to Prante *et al.*³⁵. 2,6 Difluoropyridine (394 μ L, 4.35 mmol, 1 eq.) was added to a solution of 1-*tert*-butoxycarbonylpiperazine (0.81 g, 4.34 mmol, 1 eq.) and TEA (903 μ L, 6.52 mmol, 1.5 eq.) in DMF (3 mL). The mixture was stirred at 150 °C for 24 h. Subsequently, saturated NaHCO₃ (10 mL) was added to the reaction mixture and the aqueous phase was extracted with ethyl acetate (6×20 mL). The organic layer was dried over Na₂SO₄ and the solvent was removed *in vacuo*. The crude product was purified *via* column chromatography (CH₂Cl₂-ethyl acetate 95:5). The product-containing fractions were combined and evaporated to afford **Boc-3d** (550 mg, 45%) as a yellow oil. *R*_f 0.44 (CH₂Cl₂-ethyl acetate 95:5); ¹H-NMR (CDCl₃) δ =7.54 (ps-q, *J*=8.2 Hz, 1H, H-4), 6.41 (dd, ³*J*_{H,H}=8.2 Hz, ⁵*J*_{H,F}=2.5 Hz, 1H, H-3), 6.19 (dd, ³*J*_{H,H}=7.7 Hz, ³*J*_{H,F}=2.9 Hz, 1H, H-5), 3.52 (s, 8H, 4×CH₂), 1.48 (s, 9H, 3×CH₃), ¹H-NMR data are in agreement with those reported in literature;³⁵ ¹³C-NMR (CDCl₃) δ =162.91 (d, ¹*J*_{C,F}=236.3 Hz, C-6), 158.23 (d, ³*J*_{C,F}=16.0 Hz, C-2), 154.90 (C=O of Boc), 142.18 (d, ³*J*_{C,F}=8.3 Hz, C-4), 103.10 (⁴*J*_{C,F}=3.6 Hz, C-3), 96.77 (d, ²*J*_{C,F}=37.2 Hz, C-5), 80.24 (quart. C of Boc), 45.04 (4×CH₂), 28.57 (3×CH₃); ¹⁹F-NMR (CDCl₃) δ =-68.41 (d, ³*J*_{H,F}=8.3 Hz); MS (ESI⁺): *m/z* calculated for C₁₄H₂₀FN₃NaO₂: 304.14 [M+Na]⁺, found: 304.2.

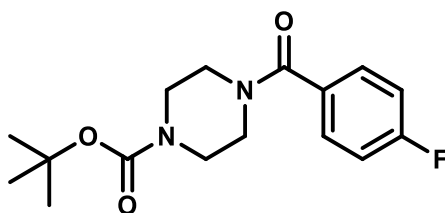
1-(6-Fluoropyridin-2-yl)piperazine (**3d**)³⁵



Compound **3d** (332 mg, orange red, highly fluid oil) was synthesised according to **GP III** using compound **Boc-3d**. ¹H-NMR (CDCl₃) δ =7.52 (ps-q, ³*J*=8.2 Hz, 1H, H-4), 6.40 (dd, ³*J*_{H,H}=8.2 Hz, ⁵*J*_{H,F}=2.6 Hz, 1H, H-3), 6.16 (dd, ³*J*_{H,H}=7.7, ³*J*_{H,F}=2.9 Hz, 1H, H-5), 3.55–3.46 (m, 4H, H-2,6 of piperazine), 3.00–2.92 (m, 4H, H-3,5 of piperazine), signal for NH is not visible, ¹H-NMR data are in agreement with those reported in literature;³⁵ ¹³C-NMR (CDCl₃) δ =162.93 (d, ¹*J*_{C,F}=235.6 Hz, C-6), 158.71 (d, ³*J*_{C,F}=15.8 Hz, C-2), 141.96 (d, ³*J*_{C,F}=8.3 Hz, C-4), 102.77 (d, ⁴*J*_{C,F}=4.0 Hz, C-3), 96.17 (d, ²*J*_{C,F}=37.5 Hz, C-5), 46.08 (C-2,6 of

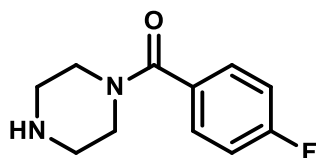
piperazine), 45.81 (C–3,5 of piperazine); $^{19}\text{F-NMR}$ (CDCl_3): δ =-68.54 (broad s); MS (ESI^+): m/z calculated for $\text{C}_9\text{H}_{13}\text{FN}_3$: 182.11 $[\text{M}+\text{H}]^+$, found: 182.2.

4-*tert*-Butoxycarbonyl-1-(4-fluorobenzoyl)piperazine (**Boc-3e**)³⁶



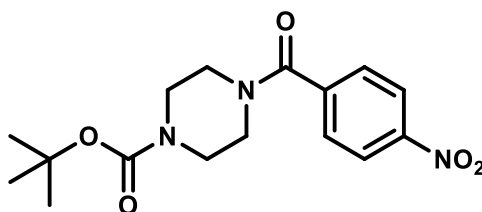
Compound **Boc-3e** (390 mg, 83%) was synthesised according to **GP I** using 4-fluorobenzoyl chloride and CH_2Cl_2 as solvent and was obtained as a white solid. R_f 0.08 (CH_2Cl_2 -ethyl acetate 95:5); $^1\text{H-NMR}$ (CDCl_3) δ =7.41 (dd, $^3J_{\text{H,H}}=8.7$ Hz, $^4J_{\text{H,F}}=5.3$ Hz, 2H, H–2,6), 7.10 (t, $^3J_{\text{H,H}}=^3J_{\text{H,F}}=8.6$ Hz, 2H, H–3,5), 3.85–3.25 (m, 8H, 4 \times CH₂), 1.47 (s, 9H, 3 \times CH₃); $^{13}\text{C-NMR}$ (CDCl_3) δ =169.84 (CO), 163.67 (d, $^1J_{\text{C,F}}=250.4$ Hz, C–4), 154.68 (COO), 131.59 (d, $^4J_{\text{C,F}}=3.5$ Hz, C–1), 129.55 (d, $^3J_{\text{C,F}}=8.5$ Hz, C–2,6), 115.85 (d, $^2J_{\text{C,F}}=21.8$ Hz, C–3,5), 80.57 (quart. C of Boc), 28.52 (3 \times CH₃), signals for 4 \times CH₂ of piperazine are not visible; $^{19}\text{F-NMR}$ (CDCl_3): δ = -109.79– -109.95 (m); MS (ESI^+): m/z calculated for $\text{C}_{16}\text{H}_{21}\text{FN}_2\text{NaO}_3$: 331.14 $[\text{M}+\text{Na}]^+$, found: 330.9.

1-(4-Fluorobenzoyl)piperazine (**3e**)³⁷



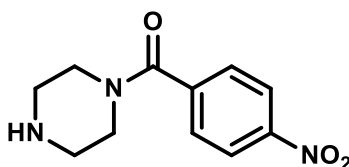
Compound **3e** (244 mg, white solid) was synthesised according to **GP III** using compound **Boc-3e**. $^1\text{H-NMR}$ (CDCl_3) δ =7.44–7.38 (m, 2H, H–2,6), 7.13–7.05 (m, 2H, H–3,5), 3.87–3.28 (m, 4H, 2 \times CH₂), 3.03–2.74 (m, 4H, 2 \times CH₂), 1.77 (s, 1H, NH); $^{13}\text{C-NMR}$ (CDCl_3) δ =169.65 (CO), 163.51 (d, $^1J_{\text{C,F}}=249.6$ Hz, C–4), 132.01 (d, $^4J_{\text{C,F}}=3.5$ Hz, C–1), 129.48 (d, $^3J_{\text{C,F}}=8.6$ Hz, C–2,6), 115.71 (d, $^2J_{\text{C,F}}=21.8$ Hz, C–3,5), signals for 4 \times CH₂ are not visible, ^1H - and ^{13}C -NMR data are in agreement with those reported in literature;³⁷ $^{19}\text{F-NMR}$ (CDCl_3) δ = -110.43– -110.52 (m); MS (ESI^+): m/z calculated for $\text{C}_{11}\text{H}_{14}\text{FN}_2\text{O}$: 209.11 $[\text{M}+\text{H}]^+$, found: 209.2.

4-*tert*-Butoxycarbonyl-1-(4-nitrobenzoyl)piperazine (**Boc-3f**)³⁸



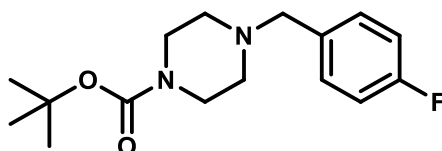
Compound **Boc-3f** (320 mg, 62%) was synthesised according to **GP I** using 4-nitrobenzoyl chloride and THF as solvent and was obtained as a yellow solid. R_f 0.16 (CH₂Cl₂-ethyl acetate 95:5); ¹H-NMR (CDCl₃) δ =8.29 (d, ³J=8.7 Hz, 2H, H-3,5), 7.57 (d, ³J=8.7 Hz, 2H, H-2,6), 3.84–3.25 (m, 8H, 4×CH₂ of piperazine), 1.47 (s, 9H, 3×CH₃ of Boc); ¹³C-NMR (CDCl₃) δ =168.35 (CO), 154.57 (COO), 148.65, 141.67, 128.23 (C-2,6), 124.15 (C-3,5), 80.78 (quart. C of Boc), 47.53 (CH₂), 42.27 (CH₂), 28.49 (3×CH₃), signals for 2×CH₂ of piperazine are not visible; MS (ESI⁺): m/z calculated for C₁₆H₂₁N₃NaO₅: 358.14 [M+H]⁺, found: 358.1.

1-(4-Nitrobenzoyl)piperazine (**3f**)³⁷



Compound **3f** (204 mg, rose solid) was synthesised according to **GP III** using compound **Boc-3f**. ¹H-NMR (CDCl₃) δ =8.31–8.25 (m, 2H, H-3,5), 7.59–7.54 (m, 2H, H-2,6), 3.85–3.70 (m, 2H, CH₂), 3.41–3.27 (m, 2H, CH₂), 3.03–2.90 (m, 2H, CH₂), 2.89–2.77 (m, 2H, CH₂), 1.67 (s, 1H, NH); ¹³C-NMR (CDCl₃) δ =168.16 (CO), 148.50, 142.21, 128.18 (C-2,6), 124.05 (C-3,5), 48.99 (CH₂), 46.63 (CH₂), 46.01 (CH₂), 43.50 (CH₂), ¹H- and ¹³C-NMR data are in agreement with those reported in literature;³⁷ MS (ESI⁺): m/z calculated for C₁₁H₁₄N₃O₃: 236.10 [M+H]⁺, found: 236.2.

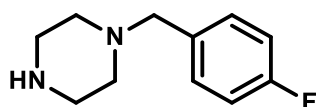
4-*tert*-Butoxycarbonyl-1-(4-fluorobenzyl)piperazine (**Boc-3g**)³⁹



The synthesis was accomplished according to the general procedure for reductive alkylation described by Abdel-Magid and Mehrman.⁴⁰ To a solution of 1-*tert*-butoxycarbonylpiperazine (500 mg, 2.68 mmol, 1 eq.) in THF (10 mL) under N₂ atmosphere was added 4-fluorobenzaldehyde (283 μ L, 2.68 mmol, 1 eq.) and sodium triacetoxymethylborohydride (795 mg,

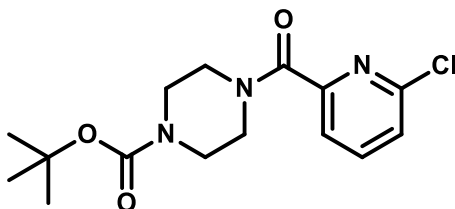
3.75 mmol, 1.4 eq.). The reaction mixture was stirred for 5 h. Subsequently, the solvent was removed, the residue was dissolved in 3 M NaOH (10 mL) and the solution was extracted with ethyl acetate (3×20 mL). The organic phases were combined, dried over Na₂SO₄ and evaporated. The crude product was purified by column chromatography (gradient from CH₂Cl₂–methanol 99.5:0.5 to 97.5:2.5). The product-containing fractions were combined and evaporated to afford **Boc-3g** (334 mg, 42%) as a light yellow liquid. *R*_f 0.11 (CH₂Cl₂–methanol 98:2); ¹H-NMR (CDCl₃) δ=7.30–7.25 (m, 2H, H–2,6), 7.00 (t, ³*J*=8.7 Hz, 2H, H–3,5), 3.47 (s, 2H, CH₂–fluorophenyl), 3.45–3.39 (m, 4H, 2×CH₂ of piperazine), 2.41–2.34 (m, 4H, 2×CH₂ of piperazine), 1.45 (s, 9H, 3×CH₃); ¹³C-NMR (CDCl₃) δ=162.24 (d, ¹*J*_{C,F}=245.1 Hz, C–4), 154.91 (CO), 133.69 (pss, C–1), 130.75 (d, ³*J*_{C,F}=7.8 Hz, C–2,6), 115.25 (d, ²*J*_{C,F}=21.2 Hz, C–3,5), 79.76 (quart. C of Boc), 62.35 (CH₂–Fluorphenyl), 52.93 (CH₂ of piperazine), 28.58 (3×CH₃), signals for 3×CH₂ of piperazine are not visible, ¹H- and ¹³C-NMR data are in agreement with those reported in literature;³⁹ ¹⁹F-NMR (DMSO-*d*₆) δ= -115.50– -116.06 (m); MS (ESI⁺): *m/z* calculated for C₁₆H₂₄FN₂O₂: 295.18 [M+H]⁺, found: 295.2.

1-(4-Fluorobenzyl)piperazine (**3g**)³⁹



Compound **3g** (211 mg, orange oil) was synthesised according to **GP III** using compound **Boc-3g**. ¹H-NMR (CDCl₃) δ=7.30–7.25 (m, 2H, H–2,6), 7.02–6.96 (m, 2H, H–3,5), 3.45 (s, 2H, CH₂–fluorophenyl), 2.92–2.86 (m, 4H, 2×CH₂ of piperazine), 2.47–2.34 (m, 4H, 2×CH₂ of piperazine), 1.83 (s, 1H, NH); ¹³C-NMR (CDCl₃) δ=162.14 (d, ¹*J*_{C,F}=244.8 Hz, C–4), 133.90 (d, ⁴*J*_{C,F}=3.1 Hz, C–1), 130.76 (d, ³*J*_{C,F}=7.9 Hz, C–2,6), 115.12 (d, ²*J*_{C,F}=21.2 Hz, C–3,5), 62.95 (CH₂–fluorophenyl), 54.38 (2×CH₂ of piperazine), 46.13 (2×CH₂ of piperazine), ¹H- and ¹³C-NMR data are in agreement with those reported in literature;³⁹ ¹⁹F-NMR (CDCl₃) δ= -115.99– -116.05 (m); MS (ESI⁺): *m/z* calculated for C₁₁H₁₆FN₂: 195.13 [M+H]⁺, found: 195.2.

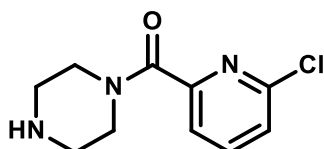
4-*tert*-Butoxycarbonyl-1-(6-chloropyridin-2-yl)piperazine (**Boc-3h**)



Compound **Boc-3h** (135 mg, 19%, brown oil) was synthesised according to **GP II** using 2-chloro-6-trichloromethylpyridine (nitrapyrin). Solvent for column chromatography: gradient

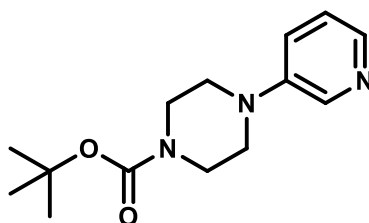
from CH₂Cl₂-ethyl acetate 9:1 to 8:2; *R*_f 0.12 (CH₂Cl₂-ethyl acetate 9:1); **¹H-NMR** (CDCl₃) δ=7.80-7.75 (m, 1H, H-4), 7.62 (d, ³*J*=7.5 Hz, 1H, H-3), 7.40 (dd, ³*J*=8.0 Hz, ⁴*J*=0.9 Hz, 1H, H-5), 3.78-3.72 (m, 2H, CH₂), 3.63-3.46 (m, 8H, 3×CH₂), 1.47 (s, 9H, 3×CH₃); **¹³C-NMR** (CDCl₃) δ=166.04 (CO Amid), 154.73 (CON of Boc), 154.01, 150.16, 139.92 (C-4), 125.69 (C-5), 122.90 (C-3), 80.48 (quart. C of Boc), 47.28 (2×CH₂), 42.62 (2×CH₂), 28.53 (3×CH₃); MS (ESI⁺): *m/z* calculated for C₁₅H₂₀ClN₃O₃: 348.11 [M(³⁵Cl)+Na]⁺, found: 348.1.

1-(6-Chloropicolinoyl)piperazine (3h)



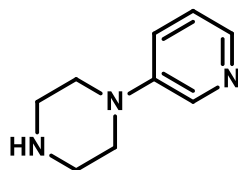
Compound **3h** (70 mg, yellow oil) was synthesised according to **GP III** using compound **Boc-3h**. NMR data were recorded prior to basic extraction (**3h**×2TFA). **¹H-NMR** (DMSO-*d*₆) δ=8.98 (s, 2H, NH₂⁺), 8.03 (t, ³*J*=7.8 Hz, 1H, H-4), 7.69-7.65 (m, 2H, H-3,5), 3.88–3.80 (m, 2H, CH₂), 3.69–3.61 (m, 2H, CH₂), 3.27–3.09 (m, 4H, 2×CH₂); **¹³C-NMR** (DMSO-*d*₆) δ=165.01 (CO), 153.06, 148.95, 141.08 (C-4), 125.68 (CH of pyridine), 122.67 (CH of pyridine), 43.51 (CH₂), 42.78 (CH₂), 42.45 (CH₂), 38.59 (CH₂); **¹⁹F-NMR** (DMSO-*d*₆) δ= -79.79 (s, CF₃ of TFA); MS (ESI⁺): *m/z* calculated for C₁₀H₁₃ClN₃O: 226.07 [M+H]⁺, found: 226.0.

4-*tert*-Butoxycarbonyl-1-pyridin-3-ylpiperazine (Boc-3i)⁴¹



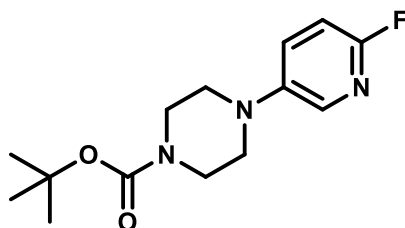
Compound **Boc-3i** (263 mg, 69%, yellow solid) was synthesised according to **GP II** using 3-bromopyridine. Solvent for column chromatography: gradient from CH₂Cl₂-methanol 98:2 to 92:8; *R*_f 0.58 (CH₂Cl₂-methanol 92:8); **¹H-NMR** (CDCl₃) δ=8.32-8.30 (m, 1H, H-2), 8.14-8.11 (dd, ³*J*=3.8 Hz, ⁴*J*=2.2 Hz, 1H, H-6), 7.19-7.16 (m, 2H, H-4,5), 3.61-3.58 (m, 4H, 2×CH₂), 3.18-3.14 (m, 4H, 2×CH₂), 1.48 (s, 9H, 3×CH₃), ¹H-NMR data are in agreement with those reported in literature;⁴¹ **¹³C-NMR** (CDCl₃): δ=154.76 (CON), 147.08 (C-3), 141.31 (C-6), 139.13 (C-2), 123.69 (CH), 123.14 (CH), 80.24 (quart. C of Boc), 48.84 (4×CH₂), 28.56 (3×CH₃); MS (ESI⁺): *m/z* calculated for C₁₄H₂₂N₃O₂: 264.17 [M+H]⁺, found: 264.1.

1-Pyridin-3-ylpiperazine (**3i**)⁴²



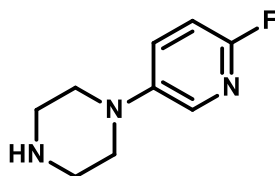
Compound **3i** (97 mg, orange oil) was synthesised according to **GP III** using compound **Boc-3i**. **¹H-NMR** (CDCl₃) δ=8.31 (dd, ⁴J=2.6, 1.0 Hz, 1H, H-2), 8.10 (dd, ³J=4.0 Hz, ⁴J=1.9 Hz, 1H, H-6), 7.20-7.13 (m, 2H, H-4/5), 3.21-3.15 (m, 4H, 2×CH₂), 3.07-3.02 (m, 4H, 2×CH₂), 1.73 (broad s, 1H, NH); **¹³C-NMR** (CDCl₃) δ=147.54 (C-3), 140.89 (C-6), 138.83 (C-2), 123.59 (CH), 122.51 (CH), 49.80 (2×CH₂), 46.09 (2×CH₂), ¹H- and ¹³C-NMR data are in agreement with those reported in literature;⁴² MS (ESI⁺): m/z calculated for C₉H₁₄N₃: 164.12 [M+H]⁺, found: 164.1

4-*tert*-Butoxycarbonyl-1-(6-fluoropyridin-3-yl)piperazine (**Boc-3j**)



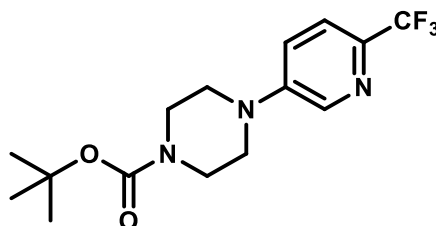
Compound **Boc-3j** (391 mg, 64%, light yellow oil) was synthesised according to **GP II** using 3-bromo-6-fluoropyridine. Solvent for column chromatography: gradient from CH₂Cl₂-ethyl acetate 95:5 to 75:25; *R*_f 0.18 (CH₂Cl₂-ethyl acetate 95:5); **¹H-NMR** (CDCl₃): δ=7.80 (dd, ⁴J_{H,H}=2.9 Hz, ⁵J_{H,H}=1.8 Hz, 1H, H-2), 7.35 (ddd, ³J_{H,H}=8.9 Hz, ⁴J_{H,F}=6.8 Hz, ⁴J_{H,H}=3.2 Hz, 1H, H-4), 6.84 (ddd, ³J_{H,H}=8.8 Hz, ³J_{H,F}=3.6 Hz, ⁵J_{H,H}=0.6 Hz, 1H, H-5), 3.62–3.56 (m, 4H, 2×CH₂), 3.11–3.05 (m, 4H, 2×CH₂), 1.48 (s, 9H, 3×CH₃); **¹³C-NMR** (CDCl₃) δ=158.34 (d, ¹J_{C,F}=233.4 Hz, C-6), 154.71 (CO), 145.56 (d, ⁴J_{C,F}=4.2 Hz, C-3), 135.67 (d, ³J_{C,F}=15.0 Hz, C-2), 130.27 (d, ³J_{C,F}=7.5 Hz, C-4), 109.48 (d, ²J_{C,F}=39.3 Hz, C-5), 80.33 (quart. C of Boc), 50.07 (4×CH₂), 28.56 (3×CH₃); **¹⁹F-NMR** (CDCl₃) δ=-78.30 (s); MS (ESI⁺): m/z calculated for C₁₄H₂₁FN₃O₂: 282.16 [M+H]⁺, found: 282.3.

1-(6-Fluoropyridin-3-yl)piperazine (3j)



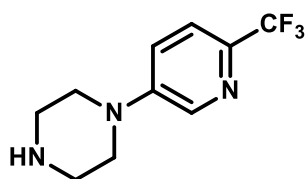
Compound **3j** (213 mg, brown oil) was synthesised according to **GP III** using compound **Boc-3j**. **¹H-NMR** (CDCl₃) δ=7.79 (dd, ⁴J_{H,H}=3.0 Hz, ⁵J_{H,H}=1.8 Hz, 1H, H-2), 7.34 (ddd, ³J_{H,H}=8.9 Hz, ⁴J_{H,F}=6.8 Hz, ⁴J_{H,H}=3.2 Hz, 1H, H-4), 6.82 (dd, ³J_{H,H}=8.8 Hz, ³J_{H,F}=3.4 Hz, 1H, H-5), 3.13–3.02 (m, 8H, 4×CH₂); signal for NH is not visible; **¹³C-NMR** (CDCl₃) δ=158.03 (d, ¹J_{C,F}=232.4 Hz, C-6), 146.04 (d, ⁴J_{C,F}=4.2 Hz, C-3), 135.12 (d, ³J_{C,F}=14.9 Hz, C-2), 129.60 (d, ³J_{C,F}=7.4 Hz, C-4), 109.30 (d, ²J_{C,F}=39.2 Hz, C-5), 50.58 (C-2,6), 45.85 (C-3,5); **¹⁹F-NMR** (CDCl₃) δ=-79.25 (s); MS (ESI⁺): m/z calculated for C₉H₁₃FN₃: 182.11 [M+H]⁺, found: 182.2.

4-*tert*-Butoxycarbonyl-1-(6-trifluoromethylpyridin-3-yl)piperazine (Boc-3k)⁴³



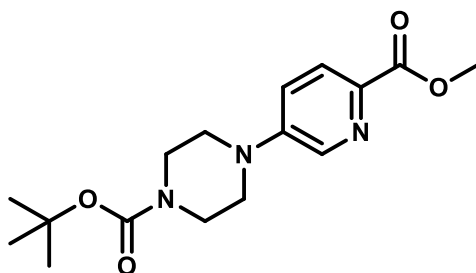
Compound **Boc-3k** (467 mg, 53%, white solid) was synthesised according to **GP II** using 3-bromo-6-trifluoromethylpyridine. Solvent for column chromatography: gradient from CH₂Cl₂-ethyl acetate 100:0 to 66:33; *R*_f 0.19 (CH₂Cl₂-ethyl acetate 95:5); **¹H-NMR** (CDCl₃) δ=8.34 (d, ⁴J=2.9 Hz, 1H, H-2), 7.53 (d, ³J=8.8 Hz, 1H, H-5), 7.20 (dd, ³J=8.7 Hz, ⁴J=2.9 Hz, 1H, H-4), 3.64–3.58 (m, 4H, 2×CH₂), 3.32–3.26 (m, 4H, 2×CH₂), 1.49 (s, 9H, 3×CH₃); ¹H-NMR data are in agreement with those reported in literature;⁴³ **¹³C-NMR** (CDCl₃) δ=154.67 (CO), 148.36 (C-3), 138.39 (q, ²J_{C,F}=35.1 Hz, C-6), 137.81 (C-2), 122.19 (psd, ¹J_{C,F}=272.4 Hz, CF₃), 121.43 (C-4), 121.03 (q, ³J_{C,F}=2.6 Hz, C-5), 80.50 (quart. C of Boc), 47.60 (2×CH₂), 43.17 (2×CH₂), 28.55 (3×CH₃); **¹⁹F-NMR** (CDCl₃): δ= -66.80 (s); MS (ESI⁺): m/z calculated for C₁₅H₂₁F₃N₃O₂: 332.16 [M+H]⁺, found: 332.2.

1-(6-Trifluoromethylpyridin-3-yl)piperazine (**3k**)⁴³



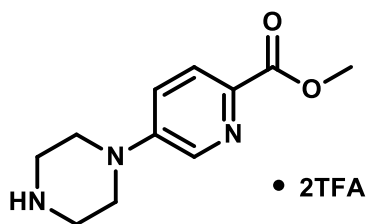
Compound **3k** (275 mg, light yellow solid) was synthesised according to **GP III** using compound **Boc-3k**. **¹H-NMR** (CDCl₃) δ=8.34 (d, ⁴J=2.9 Hz, 1H, H-2), 7.51 (d, ³J=8.8 Hz, 1H, H-5), 7.18 (dd, ³J=8.8 Hz, ⁴J=2.9 Hz, 1H, H-4), 3.31–3.26 (m, 4H, 2×CH₂), 3.08–3.02 (m, 4H, 2×CH₂), 1.73 (s, NH); **¹H-NMR** data are in agreement with those reported in literature;⁴³ **¹³C-NMR** (CDCl₃): δ=148.80 (C-3), 137.84 (q, ²J_{C,F}=35.0 Hz, C-6), 137.51 (C-2), 122.28 (q, ¹J_{C,F}=273.9 Hz, CF₃), 120.96 (q, ³J_{C,F}=2.8 Hz), 120.90 (C-4), 48.51 (2×CH₂), 45.78 (2×CH₂); **¹⁹F-NMR** (CDCl₃): δ= -66.74 (s); MS (ESI⁺): m/z calculated for C₁₀H₁₃F₃N₃: 232.11 [M+H]⁺, found: 232.2.

4-*tert*-Butoxycarbonyl-1-(6-methoxycarbonylpyridin-3-yl)piperazine (**Boc-3l**)



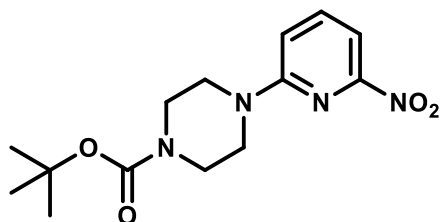
Compound **Boc-3l** (347 mg, 40%, light yellow solid) was synthesised according to **GP II** using methyl-5-bromopicolinate. Solvent for column chromatography: gradient from CH₂Cl₂-ethyl acetate 100:0 to 66:33; *R*_f 0.07 (CH₂Cl₂-ethyl acetate 95:5); **¹H-NMR** (CDCl₃) δ=8.34 (d, ⁴J=2.9 Hz, 1H, H-2), 8.01 (d, ³J=8.8 Hz, 1H, H-5), 7.15 (dd, ³J=8.8 Hz, ⁴J=2.9 Hz, 1H, H-4), 3.96 (s, 3H, CH₃O), 3.64–3.57 (m, 4H, 2×CH₂), 3.38–3.31 (m, 4H, 2×CH₂), 1.48 (s, 9H, 3×CH₃); **¹³C-NMR** (CDCl₃) δ=165.83 (COOCH₃), 154.65 (NCOO), 148.60 (C-3), 137.78 (C-6), 137.06 (C-2), 126.25 (C-5), 120.46 (C-4), 80.49 (quart. C of Boc), 52.62 (CH₃O), 47.13 (2×CH₂), 43.04 (2×CH₂), 28.54 (3×CH₃); MS (ESI⁺): m/z calculated for C₁₆H₂₄N₃O₄: 322.18 [M+H]⁺, found: 322.2.

1-(6-Methoxycarbonylpyridin-3-yl)piperazine×2TFA (3l)



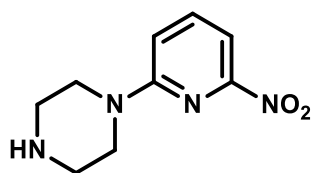
Compound **3l** (475 mg, yellow solid) was synthesised according to **GP III** using compound **Boc-3l**. **¹H-NMR** (DMSO-*d*₆): δ=8.87 (broad s, 2H, NH₂⁺), 8.44 (d, ⁴*J*=2.9 Hz, 1H, H-2), 7.93 (d, ³*J*=8.8 Hz, 1H, H-5), 7.44 (dd, ³*J*=8.9 Hz, ⁴*J*=3.0 Hz, 1H, H-4), 3.82 (s, 3H, CH₃), 3.63–3.56 (m, 4H, 2×CH₂), 3.29–3.22 (m, 4H, 2×CH₂); **¹³C-NMR** (DMSO-*d*₆): δ=164.97 (CO), 158.27 (q, ²*J*_{C,F}=36.0 Hz, CO of TFA), 147.46 (C-3), 136.87 (C-6), 136.77 (C-2), 125.74 (C-5), 120.53 (C-4), 51.92 (CH₃), 43.57 (2×CH₂), 42.32 (2×CH₂); **¹⁹F-NMR** (DMSO-*d*₆): δ= -74.73 (s, CF₃ of TFA); MS (ESI⁺): *m/z* calculated for C₁₁H₁₆N₃O₂: 222.12 [M+H]⁺, found: 222.2.

4-*tert*-Butoxycarbonyl-1-(6-nitropyridin-2-yl)piperazine (Boc-3m)



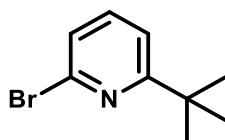
Compound **Boc-3m** (329 mg, 40%, yellow solid) was synthesised according to **GP II** using 2-chloro-6-nitropyridine. Solvent for column chromatography: gradient from CH₂Cl₂-ethyl acetate 100:0 to 66:33; *R*_f 0.10 (CH₂Cl₂); **¹H-NMR** (CDCl₃) δ=7.72 (dd, ³*J*=8.4, 7.6 Hz, 1H, H-4), 7.47 (d, ³*J*=7.5 Hz, 1H, H-5), 6.91 (d, ³*J*=8.5 Hz, 1H, H-3), 3.69–3.61 (m, 4H, 2×CH₂), 3.60–3.51 (m, 4H, 2×CH₂), 1.49 (s, 9H, 3×CH₃); **¹³C-NMR** (CDCl₃) δ=157.79, 155.96, 154.83, 140.49 (C-4), 111.94 (C-5), 106.00 (C-3), 80.41 (quart. C of Boc), 44.75 (CH₂), 28.55 (3×CH₃), signals for 3×CH₂ of piperazine are not visible; MS (ESI⁺): *m/z* calculated for C₁₆H₂₀N₄NaO₄: 331.14 [M+Na]⁺, found: 331.2.

1-(6-Nitropyridin-2-yl)piperazine (3m)



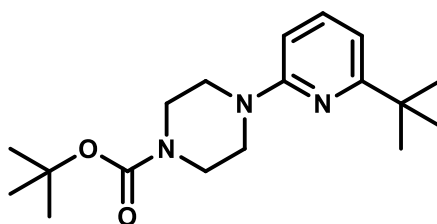
Compound **3m** (167 mg, orange solid) was synthesised according to **GP III** using compound **Boc-3m**. **¹H-NMR** (CDCl₃) δ=7.69 (dd, ³J=8.5, 7.6 Hz, 1H, H-4), 7.43 (d, ³J=7.5 Hz, 1H, H-5), 6.89 (d, ³J=8.5 Hz, 1H, H-3), 3.65–3.60 (m, 4H, 2×CH₂), 3.02–2.95 (m, 4H, 2×CH₂), 1.63 (s, 1H, NH); **¹³C-NMR** (CDCl₃): δ=158.16, 156.06, 140.22 (C-4), 111.75 (C-5), 105.51 (C-3), 46.10–45.72 (4×CH₂); MS (ESI⁺): m/z calculated for C₉H₁₃N₄O₂: 209.10 [M+H]⁺, found: 209.2.

2-Bromo-6-*tert*-butylpyridine (Br-3n)⁴⁴



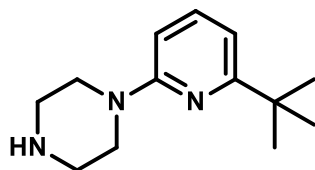
The synthesis was accomplished according to Hintermann *et al.*⁴⁵ and Henrion *et al.*⁴⁶. A mixture of 2,6-dibromopyridine (311 mg, 1.31 mmol, 1 eq.) and CuI (10 mg, 0.05 mmol, 0.04 eq.) in dry THF (4 mL) was cooled to 0 °C in an ice bath under Ar atmosphere. *tert*-Butylmagnesium chloride (1 M in THF, 1.97 mL, 1.97 mmol, 1.5 eq.) was added dropwise over 30 min *via* a syringe through a septum. Afterwards, the ice bath was removed and the reaction mixture was allowed to warm up to room temperature. The reaction was stopped after an overall time of 3 h. After removal of the solvent *in vacuo*, the residue was suspended in saturated NaHCO₃ (30 mL) and extracted with CH₂Cl₂ (5×5 mL). The combined organic phases were washed with brine, dried over Na₂SO₄ and evaporated. The crude product was purified *via* column chromatography (gradient from petroleum ether-ethyl acetate 100:0 to 95:5). The product-containing fractions were combined and evaporated to afford **Br-3n** (181 mg, 64%) as a yellow liquid. *R*_f 0.80 (petroleum ether–ethyl acetate 95:5); **¹H-NMR** (CDCl₃) δ=7.44 (t, ³J=7.8 Hz, 1H, H-4), 7.28–7.23 (m, 2H, H-3,5), 1.34 (s, 9H, 3×CH₃); **¹³C-NMR** (CDCl₃) δ=171.38 (C-6), 141.33 (C-2), 138.60 (C-4), 125.09 (C-3), 117.93 (C-5), 37.76 (quart. C of *tert*-butyl), 30.13 (3×CH₃); NMR data are in agreement with those reported in literature;⁴⁴ MS (ESI⁺): m/z calculated for C₁₀H₁₃BrN: 214.02 [M(⁷⁹Br)+H]⁺, found: 214.0.

4-*tert*-Butoxycarbonyl-1-(6-*tert*-butylpyridin-2-yl)piperazine (**Boc-3n**)



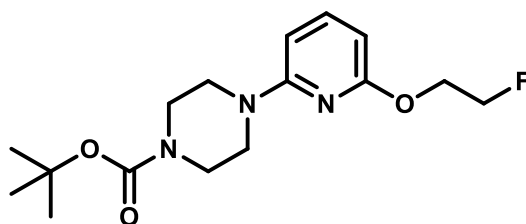
Compound **Boc-3n** (115 mg, 70%, orange oil) was synthesised according to **GP II** using 2-bromo-6-*tert*-butylpyridine (**Br-3n**). Solvent for column chromatography: gradient from CH₂Cl₂-methanol 100:0 to 98.5:1.5; *R*_f 0.52 (CH₂Cl₂-methanol 99:1); ¹H-NMR (CDCl₃): δ=7.43 (dd, ³J=8.3, 7.6 Hz, 1H, H-4), 6.68 (d, ³J=7.5 Hz, 1H, H-5), 6.45 (d, ³J=8.2 Hz, 1H, H-3), 3.54 (s, 8H, 4×CH₂), 1.48 (s, 9H, 3×CH₃ of Boc), 1.30 (s, 9H, 3×CH₃ of *tert*-butyl); ¹³C-NMR (CDCl₃): δ=167.83 (C-6), 158.25 (C-2), 155.03 (C, CON), 137.94 (C-4), 108.88 (C-5), 104.08 (C-3), 79.94 (quart. C of Boc), 45.39 (4×CH₂), 37.60 (quart. C of *tert*-butyl), 30.22 (3×CH₃ of *tert*-butyl), 28.61 (3×CH₃ of Boc).

1-(6-*tert*-Butylpyridin-2-yl)piperazine (**3n**)³¹



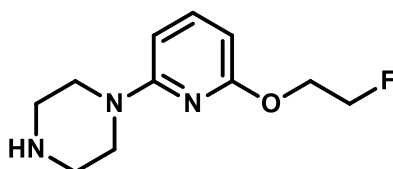
Compound **3n** (70 mg, colourless oil) was synthesised according to **GP III** using compound **Boc-3n**. ¹H-NMR (CDCl₃) δ=7.42 (dd, ³J=8.3, 7.6 Hz, 1H, H-4), 6.66 (d, ³J=7.5 Hz, 1H, H-5), 6.43 (d, ³J=8.3 Hz, 1H, H-3), 3.56-3.47 (m, 4H, 2×CH₂), 3.05-2.93 (m, 4H, 2×CH₂), 1.71 (broad s, 1H, NH), 1.31 (s, 9H, 3×CH₃); ¹³C-NMR (CDCl₃) δ=167.56 (C-6), 158.58 (C-2), 137.53 (C-4), 108.28 (C-5), 103.47 (C-3), 46.34 (C-2,6 of piperazine), 45.93 (C-3,5 of piperazine), 37.42 (quart. C of *tert*-butyl), 30.06 (3×CH₃); MS (ESI⁺): *m/z* calculated for C₁₃H₂N₃: 220.18 [M+H]⁺, found: 220.2.

4-*tert*-Butoxycarbonyl-1-(6-(2-fluoroethoxy)pyridin-2-yl)piperazine (**Boc-3o**)



The synthesis was accomplished according to the general procedure for the preparation of fluoropyridyl ethers described by Debien *et al.*⁴⁷. Sodium hydride (107 mg, 4.44 mmol, 5 eq.) and 2-fluoroethanol (259 μ L, 4.44 mmol, 5 eq.) were dissolved in DMSO (4 mL) under Ar atmosphere. After 20 min of stirring, 4-*tert*-butoxycarbonyl-1-(6-fluoropyridin-2-yl)piperazine (**Boc-3d**, 250 mg, 0.89 mmol, 1 eq.) was added and the reaction mixture was stirred at 100 °C for 2 d. Afterwards, water (25 mL) and CH₂Cl₂ (15 mL) were added to the reaction mixture, the organic phase was separated and the aqueous phase was repeatedly extracted with CH₂Cl₂ (5×5 mL). The combined organic phases were washed with brine (1×10 mL), dried over Na₂SO₄ and evaporated. Due to similar retention factors and retention times in TLC and RP-HPLC analyses, the product was purified after removal of the Boc group (see compound **3o**). The crude product (265 mg) contained compounds **Boc-3o** and **Boc-3d** in a ratio of 1:0.75 based on NMR integration. ¹H-NMR (CDCl₃) δ =7.55 (dd, ³J_{H,F}=16.6 Hz, ³J_{H,H}=8.1 Hz, 0.75H, H-5 pyridine_{Boc-3d}), 7.43 (t, ³J=8.0 Hz, 1H, H-4 pyridine_{Boc-3o}), 6.42 (dd, ³J_{H,H}=8.2 Hz, ⁴J_{H,F}=2.5 Hz, 0.75H, H-4 pyridine_{Boc-3d}), 6.23-6.12 (m, 2 + 0.75H, H-3/5 pyridine_{Boc-3o}, H-3 pyridine_{Boc-3d}), 4.81-4.65 (dm, ²J_{H,F}=48.0 Hz, 2H, CH₂-CH₂-F), 4.58-4.45 (dm, 2H, ³J_{H,F}=28.0 Hz, CH₂-CH₂-F), 3.58-3.45 (s, 8+6H, 4×CH₂ piperazine_{Boc-3o/Boc-3d}), 1.49 (s, 9+6.75H, 3×CH₃ Boc_{Boc-3o/Boc-3d}); ¹⁹F-NMR (CDCl₃) δ = -68.37- -68.45 (m, F_{Boc-3d/Boc-3o}); MS (ESI⁺): m/z calculated for C₁₆H₂₅FN₃O₂: 326.19 [M+H]⁺, found: 326.1.

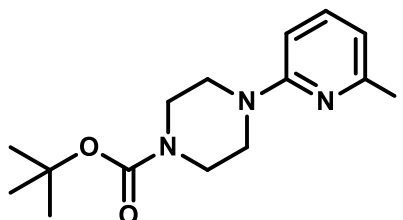
1-(6-(2-Fluoroethoxy)pyridin-2-yl)piperazine (**3o**)



Compound **3o** (52 mg, 37% starting from compound **Boc-3d**, yellow oil) was synthesised according to **GP III** using compound **Boc-3o**. ¹H-NMR (DMSO-*d*₆) δ =7.45 (t, ³J=8.0 Hz, 1H, H-4), 6.30 (d, ³J=8.1 Hz, 1H, H-3), 6.05 (d, ³J=7.7 Hz, 1H, H-5), 4.80-4.62 (dm, ²J_{H,F}=48.0 Hz, 2H, CH₂-CH₂-F), 4.49-4.36 (dm, ³J_{H,F}=32.0 Hz, 2H, CH₂-CH₂-F), 3.39-3.34 (m, 4H, 2×CH₂ of piperazine), 2.86-2.71 (m, 4H, 2×CH₂ of piperazine); ¹³C-NMR (DMSO-*d*₆): δ =161.43 (C-6),

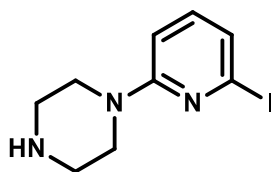
157.99 (C-2), 140.50 (C-4), 98.49 (C-3), 97.43 (C-5), 82.18 (d, $^1J_{C,F}=165.8$ Hz, CH₂-CH₂-F), 64.09 (d, $^2J_{C,F}=19.0$ Hz, CH₂-CH₂-F), 45.53 (2×CH₂ of piperazine), 45.20 (2×CH₂ of piperazine); MS (ESI⁺): m/z calculated for C₁₁H₁₇FN₃O: 226.14 [M+H]⁺, found: 226.1.

4-*tert*-Butoxycarbonyl-1-(6-iodopyridin-2-yl)piperazine (**Boc-3p**)



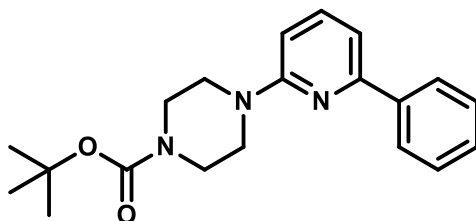
The synthesis was accomplished according to the general procedure for an aromatic Finkelstein reaction described by Klapars and Buchwald⁴⁸. Under Ar atmosphere, TMEDA (17.2 μ L, 0.11 mmol, 0.2 eq.) was added to a suspension of 4-*tert*-butoxycarbonyl-1-(6-bromopyridin-2-yl)piperazine (200 mg, 0.53 mmol, 1 eq.), CuI (12 mg, 0.06 mmol, 0.1 eq.) and NaI (351 mg, 2.34 mmol, 4 eq.) in 1,4-dioxane (1 mL). The reaction mixture was stirred at 100 °C for 44 h. Afterwards, water (5 mL) was added and the mixture was extracted with ethyl acetate (3×10 mL). The organic phases were combined and dried over Na₂SO₄. Evaporation afforded **Boc-3p** (237 mg, >100%, contains residual ethyl acetate) as a brown waxy solid. *R*_f 0.51 (petroleum ether–ethyl acetate 8:2); mp: 108–113 °C; ¹H-NMR (CDCl₃) δ =7.08–7.00 (m, 2H, H-4,5), 6.52 (d, $^3J=7.8$ Hz, 1H, H-3), 3.55–3.48 (m, 8H, 4×CH₂), 1.48 (s, 9H, 3×CH₃); ¹³C-NMR (CDCl₃) δ =159.06 (C-2), 154.90 (CO), 138.84 (C-4), 123.86 (C-5), 116.37 (C-6), 105.54 (C-3), 80.20 (quart. C of Boc), 44.87 (4×CH₂), 28.57 (3×CH₃); MS (ESI⁺): m/z calculated for C₁₄H₂₁IN₃O₂: 390.07 [M+H]⁺, found: 389.9.

1-(6-Iodopyridin-2-yl)piperazine (**3p**)⁴⁹



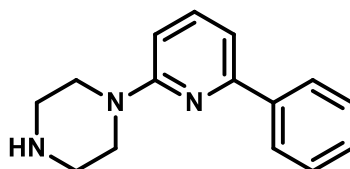
Compound **3p** (81 mg, dark yellow, waxy solid) was synthesised according to **GP III** using compound **Boc-3p**. ¹H-NMR (CDCl₃) δ =7.06–6.97 (m, 2H, H-4,5), 6.51 (dd, $^3J=8.1$ Hz, $^4J=0.8$ Hz, 1H, H-3), 3.50–3.45 (m, 4H, H-2,6 of piperazine), 2.97–2.92 (m, 4H, H-3,5 of piperazine); signal for NH is not visible; ¹³C-NMR (CDCl₃) δ =159.49 (C-2), 138.70 (C-4), 123.41 (C-5), 116.46 (C-6), 105.31 (C-3), 46.12 (2×CH₂), 45.95 (2×CH₂), ¹H- and ¹³C-NMR data are in agreement with those reported in literature⁴⁹; MS (ESI⁺): m/z calculated for C₉H₁₃IN₃: 290.01 [M+H]⁺, found: 290.0.

4-*tert*-Butoxycarbonyl-1-(6-phenylpyridin-2-yl)piperazine (**Boc-3q**)



The synthesis was accomplished according to the procedure for Suzuki coupling reactions with β -chloroacroleins in aqueous media described by Hesse and Kirsch.⁵⁰ A suspension of 4-*tert*-butoxycarbonyl-1-(6-bromopyridin-2-yl)piperazine (250 mg, 0.73 mmol, 1 eq.), phenylboronic acid (98 mg, 0.80 mmol, 1.1 eq.), Pd(OAc)₂ (3.3 mg, 0.015 mmol, 0.02 eq.), tetra-*n*-butylammonium chloride (235 mg, 0.73 mmol, 1 eq.) and K₂CO₃ (252 mg, 1.80 mmol, 2.3 eq.) in water (5 mL) was stirred at 100 °C for 6 h. The solvent was removed *in vacuo* and the residue was dissolved in ethyl acetate (10 mL), followed by washing with saturated NaHCO₃ (2×5 mL) and brine (5 mL). The organic phase was dried over Na₂SO₄ and the solvent was removed *in vacuo*. The crude product was purified by column chromatography (gradient from petroleum ether-ethyl acetate 95:5 to 80:20). The product-containing fractions were combined and evaporated to afford **Boc-3q** (147 mg, 59%) as a light yellow solid. *R*_f 0.40 (petroleum ether–ethyl acetate 90:10); ¹H-NMR (CDCl₃) δ =8.05-7.98 (m, 2H, H-2/6 of phenyl), 7.57 (dd, ³J=8.4 Hz, ³J=7.5 Hz, 1H, H-4 of pyridine), 7.46-7.41 (m, 2H, H-3/5 of phenyl), 7.40-7.35 (m, 1H, H-4 of phenyl), 7.13 (d, ³J=7.5 Hz, 1H, H-5 of pyridine), 6.61 (d, ³J=8.4 Hz, 1H, H-3 of pyridine), 3.69-3.54 (m, 8H, 4×CH₂), 1.50 (s, 9H, 3×CH₃); ¹³C-NMR (CDCl₃) δ =159.02, 155.40, 155.02 (C-2, C-6 of pyridine, CON), 139.86 (C-1 of phenyl), 138.45 (C-4 of pyridine), 128.80 (C-4 of phenyl), 128.63 (C-3/5 of phenyl), 126.89 (C-2/6 of phenyl), 110.20 (C-5 of pyridine), 105.78 (C-3 of pyridine), 80.04 (quart. C of Boc), 45.25 (4×CH₂), 28.61 (3×CH₃); MS (ESI⁺): *m/z* calculated for C₂₀H₂₆N₃O₂: 340.20 [M+H]⁺, found: 340.2.

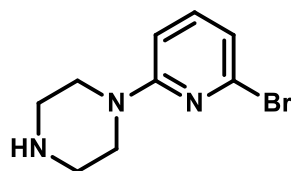
1-(6-Phenylpyridin-2-yl)piperazine (**3q**)



Compound **3q** (81 mg, yellow oil) was synthesised according to **GP III** using compound **Boc-3q**. ¹H-NMR (DMSO-*d*₆) δ =8.07-8.00 (m, 2H, H-2,6 of phenyl), 7.66-7.57 (m, 1H, H-4 of pyridine), 7.49-7.42 (m, 2H, H-3,5 of phenyl), 7.41-7.36 (m, 1H, H-4 of phenyl), 7.24-7.19 (m, 1H, H-5 of pyridine), 6.84-6.74 (m, 1H, H-3 of pyridine), 3.57-3.49 (m, 4H, 2×CH₂), 2.91- 2.80

(m, 4H, 2×CH₂), signal for NH is not visible; ¹³C-NMR (DMSO-*d*₆) δ=158.78 (C-2 of pyridine), 153.69 (C-6 of pyridine), 139.19 (C-1 of phenyl), 138.45 (C-4 of pyridine), 128.59 (C-4 of phenyl), 128.50 (C-3,5 of phenyl), 126.25 (C-2,6 of phenyl), 108.97 (C-5 of pyridine), 105.81 (C-3 of pyridine), 45.22 (2×CH₂), 45.10 (2×CH₂); MS (ESI⁺): *m/z* calculated for C₁₅H₁₈N₃: 240.15 [M+H]⁺, found: 240.1.

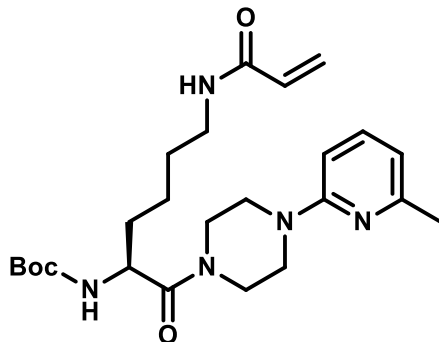
1-(6-Bromopyridin-2-yl)piperazine (3r)^{49,35}



Compound **3r** (98 mg, yellow oil) was synthesised according to **GP III** using 4-*tert*-Butoxycarbonyl-1-(6-bromopyridin-2-yl)piperazine. ¹H-NMR (CDCl₃) δ=7.27 (dd, ³*J*=8.4, 7.5 Hz, 1H, H-4), 6.73 (d, ³*J*=7.3 Hz, 1H, H-5), 6.50 (d, ³*J*=8.3 Hz, 1H, H-3), 3.52–3.48 (m, 4H, H-2,6), 2.98–2.93 (m, 4H, H-3,5); ¹³C-NMR (CDCl₃) δ=159.57 (C-2), 140.37 (C-6), 139.56 (C-4), 116.07 (C-5), 104.85 (C-3), 46.16 (2×CH₂), 45.94 (2×CH₂), ¹H- and ¹³C-NMR data are in agreement with those reported in literature;^{49,35} MS (ESI⁺): *m/z* calculated for C₉H₁₃BrN₃: 242.03 [M(⁷⁹Br)+H]⁺, found: 242.1.

***N*^α-Boc-*N*^ε-acryllysine piperazides 4**

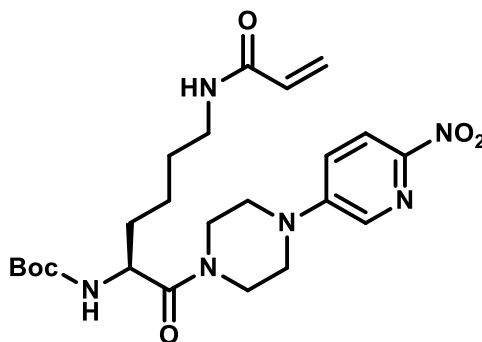
***N*^α-Boc-*N*^ε-Acryloyl-L-lysine-4-(6-methylpyridin-2-yl)piperazide (4a)**



Compound **4a** (118 mg, 46%, colourless oil) was synthesised according to **GP VI** using compounds **2a** and **3a** (0.56 mmol). Solvent for column chromatography: gradient from ethyl acetate-methanol 100:0 to 85:15; *R*_f 0.35 (ethyl acetate); **¹H-NMR** (CDCl₃) δ=7.40 (dd, ³*J*=8.3, 7.4 Hz, 1H, H-4), 6.55 (d, ³*J*=7.3 Hz, 1H, H-5), 6.45 (d, ³*J*=8.4 Hz, 1H, H-3), 6.27 (dd, ³*J*=17.0 Hz, ²*J*=1.5 Hz, 1H, C=CHH), 6.09 (dd, ³*J*=17.0, 10.2 Hz, 1H, CH=CH₂), 5.85 (broad s, 1H, N_εH), 5.61 (dd, ³*J*=10.2 Hz, ²*J*=1.6 Hz, 1H, C=CHH), 5.52 (d, ³*J*=8.5 Hz, 1H, N_αH), 4.66–4.59 (m, 1H, C_αH), 3.83–3.47 (m, 8H, 4×CH₂ of piperazine), 3.42–3.25 (m, 2H, C_εH₂), 2.40 (s, 3H, CH₃ of pyridine), 1.79–1.53 (m, 4H, C_βH₂, C_δH₂), 1.49–1.41 (m, 11H, 3×CH₃ of Boc, C_γH₂); **¹³C-NMR** (CDCl₃) δ=170.81 (CON), 165.74 (CON_ε), 158.75, 157.14, 155.90, 138.11 (C-4), 131.03 (CH₂=C), 126.36 (CH₂=C), 113.62 (C-5), 104.09 (C-3), 79.93 (quart. C of Boc), 49.82 (C_α), 45.58 (CH₂ of piperazine), 45.44 (CH₂ of piperazine), 45.40 (CH₂ of piperazine), 42.01 (CH₂ of piperazine), 39.37 (C_ε), 33.50 (C_β), 28.96 (C_δ), 28.54 (3×CH₃ of Boc), 24.67 (CH₃ of pyridine), 22.60 (C_γ); MS (ESI⁺): *m/z* calculated for C₂₄H₃₈N₅O₄: 460.29 [M+H]⁺, found: 460.3.

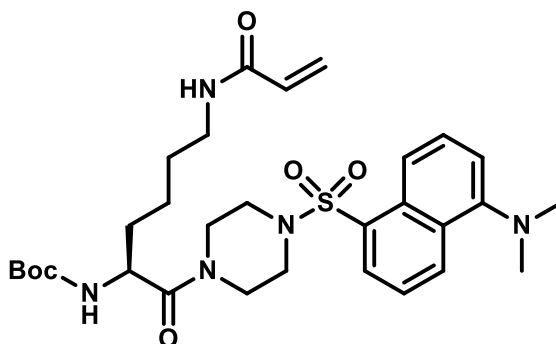
Product contains significant amounts of tris(pyrrolidinophosphine) oxide which was not removed by column chromatography. **¹H-NMR** (CDCl₃) δ=3.19-3.14 (m, 6×CH₂N), 1.84-1.79 (m, 6×CH₂); **¹³C-NMR** (CDCl₃) δ=46.45 (d, ²*J*_{C,P}=4.5 Hz, 6×CH₂N), 26.58 (d, ³*J*_{C,P}=8.0 Hz, 6×CH₂).

***N*^α-Boc-*N*^ε-Acryloyl-L-lysine-4-(6-nitropyridin-3-yl)piperazide (**4b**)**



Compound **4b** (161 mg, 27%, yellow oil) was synthesised according to **GP VI** using compounds **2a** and **3b** (1.22 mmol). Solvent for column chromatography: gradient from ethyl acetate-methanol 100:0 to 85:15; *R*_f 0.06 (ethyl acetate); ¹H-NMR (CDCl₃) δ=8.20 (d, ³J=9.1 Hz, 1H, H-5), 8.15 (d, ⁴J=3.0 Hz, 1H, H-2), 7.24 (dd, ³J=9.2 Hz, ⁴J=3.0 Hz, 1H, H-4), 6.24 (dd, ³J=17.0 Hz, ²J=1.5 Hz, 1H, C=CHH), 6.08 (dd, ³J=17.0, 10.2 Hz, 1H, CH=CH₂), 5.75 (broad s, 1H, N_εH), 5.62 (dd, ³J=10.2 Hz, ²J=1.5 Hz, 1H, C=CHH), 5.38 (d, ³J=8.6 Hz, 1H, N_αH), 4.64–4.56 (m, 1H, C_αH), 3.97–3.44 (m, 8H, 4×CH₂ of piperazine), 3.44–3.25 (m, 2H, C_εH₂), 1.79–1.55 (m, 4H, C_βH₂, C_δH₂), 1.47–1.38 (m, 11H, 3×CH₃ of Boc, C_γH₂); ¹³C-NMR (CDCl₃) δ=171.19 (CON), 165.75 (CON_ε), 155.82 (COON_α), 149.61, 148.57, 134.23, 130.97 (CH₂=C), 126.54 (CH₂=C), 121.39, 119.84, 80.17 (quart. C of Boc), 49.85 (C_α), 47.01 (CH₂ of piperazine), 46.65 (CH₂ of piperazine), 44.71 (CH₂ of piperazine), 41.41 (CH₂ of piperazine), 39.04 (C_ε), 33.02 (C_β), 29.15 (C_δ), 28.50 (3×CH₃ of Boc), 22.49 (C_γ); MS (ESI⁺): *m/z* calculated for C₁₈H₂₇N₆O₄: 391.21 [M-Boc+H]⁺, found: 391.3.

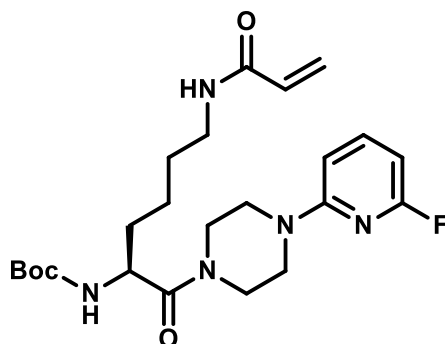
***N*^α-Boc-*N*^ε-Acryloyl-L-lysine-4-dansylpiperazide (**4c**)**



Compound **4c** (42 mg, 27%, yellow-green solid) was synthesised according to **GP VI** using compounds **2a** and **3c** (0.26 mmol). The crude product was purified by preparative RP-HPLC; ¹H-NMR (CDCl₃) δ=8.64 (d, ³J=8.6 Hz, 1H, H of dansyl), 8.55 (d, ³J=8.8 Hz, 1H, H of dansyl), 8.26 (d, ³J=7.3 Hz, 1H, H of dansyl), 7.67–7.59 (m, 2H, 2×H of dansyl), 7.38 (d, ³J=7.7 Hz, 1H,

H-6 of dansyl), 6.26 (dd, $^3J=16.9$ Hz, $^2J=0.8$ Hz, 1H, C=CH₂), 6.09 (dd, $^3J=17.0$, 10.3 Hz, 1H, CH=CH₂), 6.00 (s, 1H, N_εH), 5.66 (dd, $^3J=10.3$ Hz, $^2J=1.1$ Hz, 1H, C=CH₂), 5.38 (d, $^3J=8.7$ Hz, 1H, N_αH), 4.51-4.42 (m, 1H, C_αH), 3.83 (broad s, 1H, H of piperazine), 3.63 (broad s, 1H, H of piperazine), 3.50 (s, 2H, 2×H of piperazine), 3.39-3.04 (m, 12H, C_εH₂, 2×CH₂ of piperazine, 2×CH₃ of dansyl), 1.62-1.24 (m, 15H, C_βH₂, C_γH₂, C_δH₂, 3×CH₃ of Boc); $^{13}\text{C-NMR}$ (CDCl₃) δ =171.00 (CCON), 166.49 (CON_ε), 155.86 (CON_α), 132.96 (quart. C of dansyl), 131.37 (CH of dansyl), 130.49 (CH₂=C), 130.46 (quart. C of dansyl), 130.04 (CH of dansyl), 128.17 (CH of dansyl), 127.23 (CH₂=C), 124.61 (CH of dansyl), 122.13 (CH of dansyl), 116.55 (C-6 of dansyl), 80.33 (quart. C of Boc), 49.75 (C_α), 46.02 (2×CH₃ of dansyl), 45.79 (CH₂ of piperazine), 45.45 (CH₂ of piperazine), 45.36 (CH₂ of piperazine), 41.91 (CH₂ of piperazine), 39.40 (C_ε), 32.99 (C_β), 28.76 (C_δ), 28.43 (3×CH₃ of Boc), 22.47 (C_γ), signals for C-5 and 1×C_{quart.} of dansyl are not visible; MS (ESI⁺): *m/z* calculated for C₃₀H₄₄N₅O₆S: 602.30 [M+H]⁺, found: 602.3.

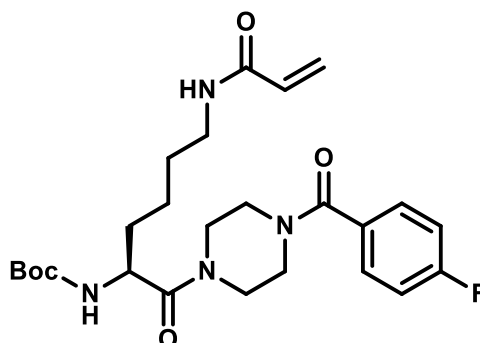
N^α-Boc-N^ε-Acryloyl-L-lysine-4-(6-fluoropyridin-2-yl)piperazide (4d)



Compound **4d** (205 mg, 35%, brown oil) was synthesised according to **GP VI** using compounds **2a** and **3d** (1.22 mmol). Solvent for column chromatography: gradient from ethyl acetate-methanol 100:0 to 85:15; *R_f* 0.19 (ethyl acetate); $^1\text{H-NMR}$ (CDCl₃) δ =7.57 (ps-q, $J=8.2$ Hz, 1H, H-4), 6.43 (dd, $^3J_{\text{H,H}}=8.2$ Hz, $^5J_{\text{H,F}}=2.4$ Hz, 1H, H-3), 6.26 (dd, $^3J=17.0$ Hz, $^2J=1.5$ Hz, 1H, C=CHH), 6.23 (dd, $^3J_{\text{H,H}}=7.9$ Hz, $^3J_{\text{H,F}}=2.7$ Hz, 1H, H-5), 6.09 (dd, $^3J=17.0$, 10.2 Hz, 1H, CH=CH₂), 5.80 (broad s, 1H, N_εH), 5.61 (dd, $^3J=10.2$ Hz, $^2J=1.6$ Hz, 1H, C=CHH), 5.46 (d, $^3J=8.5$ Hz, 1H, N_αH), 4.68-4.53 (m, 1H, C_αH), 3.84-3.47 (m, 8H, 4×CH₂ of piperazine), 3.44-3.25 (m, 2H, C_εH), 1.76-1.52 (m, 4H, C_βH₂, C_δH₂), 1.47-1.39 (m, 11H, 3×CH₃ of Boc, C_γH₂); $^{13}\text{C-NMR}$ (CDCl₃) δ =170.94 (CON), 165.74 (CON_ε), 162.87 (d, $^1J_{\text{C,F}}=236.9$ Hz, C-6), 157.95 (d, $^3J_{\text{C,F}}=15.5$ Hz, C-2), 155.86 (COON_α), 142.32 (d, $^3J_{\text{C,F}}=8.4$ Hz, C-4), 131.00 (CH₂=C), 126.42 (CH₂=C), 103.04 (d, $^4J_{\text{C,F}}=4.1$ Hz, C-3), 97.19 (d, $^2J_{\text{C,F}}=37.2$ Hz, C-5), 80.00 (quart. C of Boc), 49.84 (C_α), 45.14 (2×CH₂ of piperazine), 44.93 (CH₂ of piperazine), 41.75 (CH₂ of piperazine), 39.28 (C_ε), 33.36 (C_β), 29.02 (C_δ), 28.52 (3×CH₃

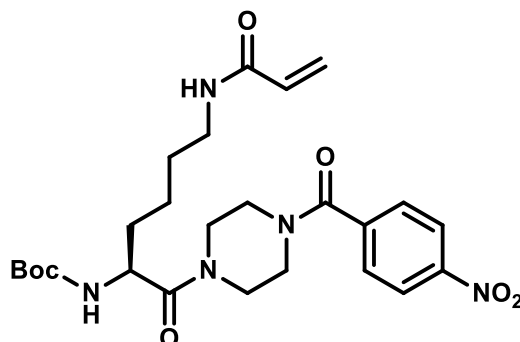
of Boc), 22.55 (C_γ); ^{19}F -NMR (CDCl_3) δ = -68.27 (d, $^3J_{\text{HF}}$ =8.6 Hz); MS (ESI⁺): m/z calculated for $\text{C}_{23}\text{H}_{35}\text{FN}_5\text{O}_4$: 464.27 $[\text{M}+\text{H}]^+$, found: 464.3.

***N*^α-Boc-*N*^ε-Acryloyl-L-lysine-4-(4-fluorobenzoyl)piperazide (4e)**



Compound **4e** (31 mg, 13%, white solid) was synthesised according to **GP VI** using compounds **2a** and **3e** (0.50 mmol). Solvent for column chromatography: gradient from ethyl acetate-methanol 100:0 to 90:10; R_f 0.07 (ethyl acetate); ^1H -NMR (CDCl_3) δ =7.48–7.40 (m, 2H, H-2,6), 7.16–7.09 (m, 2H, H-3,5), 6.26 (dd, 3J =17.0 Hz, 2J =1.2 Hz, 1H, C=CHH), 6.08 (dd, 3J =17.0, 10.2 Hz, 1H, CH=CH₂), 5.77–5.69 (m, 1H, N_εH), 5.63 (dd, 3J =10.2 Hz, 2J =1.5 Hz, 1H, C=CHH), 5.39 (d, 3J =8.5 Hz, 1H, N_αH), 4.63–4.51 (m, 1H, C_αH), 3.87–3.44 (m, 8H, 4×CH₂ of piperazine), 3.43–3.25 (m, 2H, C_εH₂), 1.75–1.50 (m, 4H, C_βH₂, C_δH₂), 1.47–1.36 (m, 11H, C_γH₂, 3×CH₃ of Boc); ^{13}C -NMR (CDCl_3) δ =171.11, 169.86, 165.72, 163.82 (d, $^1J_{\text{C,F}}$ =250.8 Hz, C-4), 155.81 (COO), 131.15 (d, $^4J_{\text{C,F}}$ =3.5 Hz, C-1), 130.96 (CH₂=C), 129.68 (d, $^3J_{\text{C,F}}$ =8.6 Hz, C-2,6), 126.53 (CH₂=C), 115.97 (d, $^2J_{\text{C,F}}$ =21.9 Hz, C-3,5), 80.11 (quart. C of Boc), 49.84 (C_α), 45.67 (2×CH₂ of piperazine), 42.29 (2×CH₂ of piperazine), 39.15 (C_ε), 33.15 (C_β), 29.11 (C_δ), 28.51 (3×CH₃ of Boc), 22.51 (C_γ); ^{19}F -NMR (CDCl_3) δ =-109.32– -109.44 (m); MS (ESI⁺): m/z calculated for $\text{C}_{25}\text{H}_{35}\text{FN}_4\text{NaO}_5$: 513.25 $[\text{M}+\text{Na}]^+$, found: 513.3.

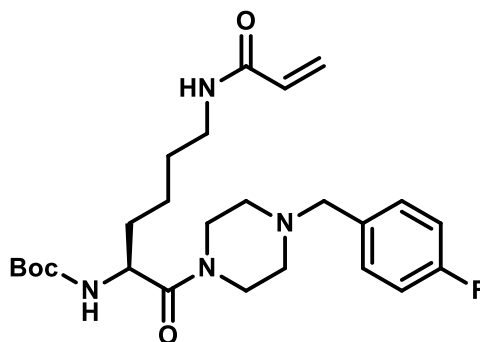
***N*^α-Boc-*N*^ε-Acryloyl-L-lysine-4-(4-nitrobenzoyl)piperazide (4f)**



Compound **4f** (60 mg, 23%, white solid) was synthesised according to **GP VI** using compounds **2a** and **3f** (0.50 mmol). Solvent for column chromatography: gradient from ethyl acetate-

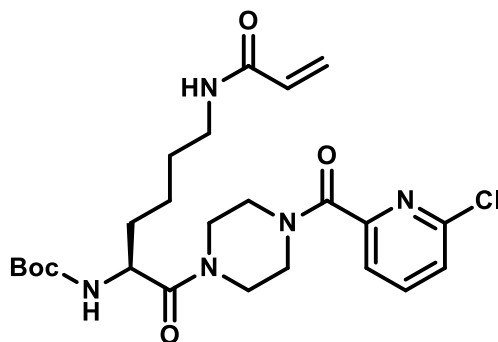
methanol 100:0 to 90:10; R_f 0.24 (ethyl acetate-methanol 95:5); $^1\text{H-NMR}$ (CDCl_3) δ =8.31 (d, 3J =8.8 Hz, 1H, H-3,5), 7.61 (d, 3J =8.6 Hz, 1H, H-2,6), 6.31–6.18 (m, 1H, C=CHH), 6.07 (dd, 3J =16.8, 10.2 Hz, 1H, CH=CH₂), 5.71 (broad s, 1H, N_HH), 5.65–5.60 (m, 1H, C=CHH), 5.36 (d, 3J =8.4 Hz, 1H, N_HH), 4.57 (s, 1H, C_HH), 4.03–3.24 (m, 10H, 4×CH₂ of piperazine, C_HH₂), 1.76–1.51 (m, 4H, C_HH₂, C_HH₂), 1.49–1.35 (m, 11H, 3×CH₃ of Boc, C_HH₂), diffuse signals due to the amide bonds on both sides of the piperazine ring; $^{13}\text{C-NMR}$ (CDCl_3) δ =171.20, 168.39, 165.74, 155.79, 148.81, 141.26, 130.94 (CH₂=C), 128.35 (C-2,6), 126.58 (CH₂=C), 124.22 (C-3,5), 80.17 (quart. C of Boc), 49.85 (C_H), 39.06 (C_H), 33.01 (C_H), 29.16 (C_H), 28.50 (3×CH₃ of Boc), 22.45 (C_H), signals for 4×CH₂ of piperazine are not visible; MS (ESI⁺): m/z calculated for C₂₅H₃₅N₅NaO₇: 540.24 [M+Na]⁺, found: 540.2.

N^α-Boc-N^ε-Acryloyl-L-lysine-4-(4-fluorobenzyl)piperazide (4g)



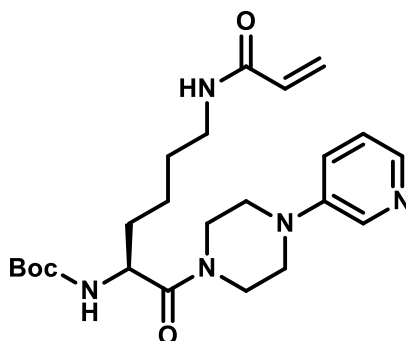
Compound **4g** (53 mg, 22%, colourless, waxy solid) was synthesised according to **GP VI** using compounds **2a** and **3g** (0.50 mmol). Solvent for column chromatography: gradient from ethyl acetate-methanol 100:0 to 90:10; R_f 0.21 (ethyl acetate-methanol 96:4); $^1\text{H-NMR}$ (CDCl_3) δ =7.31–7.24 (m, 2H, H-2,6), 7.01 (t, 3J =8.7 Hz, 2H, H-3,5), 6.27 (dd, 3J =17.0 Hz, 2J =1.5 Hz, 1H, C=CHH), 6.09 (dd, 3J =17.0, 10.2 Hz, 1H, CH=CH₂), 5.90–5.82 (m, 1H, N_HH), 5.62 (dd, 3J =10.2 Hz, 2J =1.5 Hz, 1H, C=CHH), 5.51 (d, 3J =8.3 Hz, 1H, N_HH), 4.62–4.50 (m, 1H, C_HH), 3.73–3.42 (m, 6H, 2×CH₂ of piperazine, CH₂-fluorophenyl), 3.42–3.22 (m, 2H, C_HH₂), 2.53–2.36 (m, 4H, 2×CH₂ of piperazine), 1.72–1.48 (m, 4H, C_HH₂, C_HH₂), 1.48–1.34 (m, 11H, 3×CH₃ of Boc, C_HH₂); $^{13}\text{C-NMR}$ (CDCl_3) δ =170.53, 165.75, 162.31 (d, $^1J_{\text{C,F}}$ =245.4 Hz, C-4), 155.90 (COO), 131.03 (CH₂=C), 130.75 (d, $^3J_{\text{C,F}}$ =6.0 Hz, C-2,6), 126.38 (CH₂=C), 115.37 (d, $^2J_{\text{C,F}}$ =21.5 Hz, C-3,5), 79.87 (quart. C of Boc), 62.04 (CH₂-fluorophenyl), 53.04 (CH₂ of piperazine), 52.66 (CH₂ of piperazine), 49.68 (C_H), 45.59 (CH₂ of piperazine), 42.17 (CH₂ of piperazine), 39.38 (C_H), 33.48 (C_H), 28.89 (C_H), 28.52 (3×CH₃ of Boc), 22.54 (C_H), signal for C-1 is not visible; $^{19}\text{F-NMR}$ (CDCl_3) δ = -115.18– -115.64 (m); MS (ESI⁺): m/z calculated for C₂₅H₃₈FN₄O₄: 477.29 [M+H]⁺, found: 477.2.

N^α-Boc-N^ε-Acryloyl-L-lysine-4-(6-chloropyridinoyl)piperazide (4h)



Compound **4h** (28 mg, 18%, yellow oil) was synthesised according to **GP VI** using compounds **2a** and **3h** (0.30 mmol). Solvent for column chromatography: CH₂Cl₂-methanol 95:5; *R*_f 0.28 (CH₂Cl₂-methanol 95:5); ¹H-NMR (CDCl₃) δ=7.80 (t, ³J=7.8 Hz, 1H, H-4), 7.67 (pst, ³J=8.1 Hz, 1H, H-3), 7.42 (d, ³J=8.0 Hz, 1H, H-5), 6.34-6.19 (m, 1H, CH=CHH), 6.15-6.02 (m, 1H, CH=CH₂), 5.77 (broad s, 1H, N_εH), 5.69-5.58 (m, 1H, CH=CHH), 5.41 (d, ³J=8.4 Hz, 1H, N_αH), 4.56 (m, 1H, C_αH), 4.01-3.52 (m, 8H, 4×CH₂ of piperazine), 3.43-3.24 (m, 2H, C_εH₂), 1.78-1.49 (m, 4H, C_βH₂, C_δH₂), 1.42 (s, 11H, 3×CH₃ of Boc, C_γH₂), diffuse signals (partly in duplicate) due to the amide bonds on both sides of the piperazine ring; ¹³C-NMR (CDCl₃) δ=165.72, 155.82, 153.57, 140.04 (C-4), 130.98 (CH₂=CH), 126.49 (CH₂=CH), 125.95 (C-5), 123.24/123.10 (C-3), 80.09 (quart. C of Boc), 49.84 (C_α), 47.44/47.13 (CH₂ of piperazine), 45.87/45.32 (CH₂ of piperazine), 42.86/42.61 (CH₂ of piperazine), 42.50/41.95 (CH₂ of piperazine), 39.24 (C_ε), 33.22 (C_β), 29.07 (C_δ), 28.52 (3×CH₃ of Boc), 22.56 (C_γ), signals for 3×C_{quart.} are not visible; MS (ESI⁺): m/z calculated for C₂₄H₃₅ClN₅O₅: 508.23 [M(³⁵Cl)+H]⁺, found: 508.1.

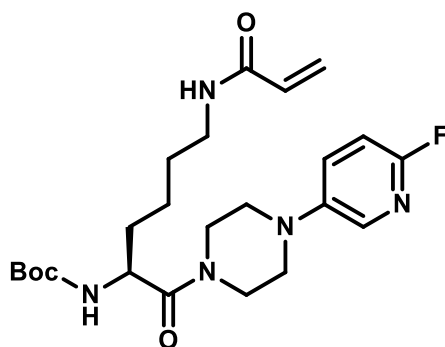
N^α-Boc-N^ε-Acryloyl-L-lysine-4-(pyridin-3-yl)piperazide (4i)



Compound **4i** (109 mg, 41%, brown oil) was synthesised according to **GP VI** using compounds **2a** and **3i** (0.59 mmol). Solvent for column chromatography: gradient from CH₂Cl₂-methanol 95:5 to 91:9; *R*_f 0.59 (CH₂Cl₂-methanol 91:9); ¹H-NMR (CDCl₃) δ=8.31 (s, 1H, H-2), 8.18-8.08

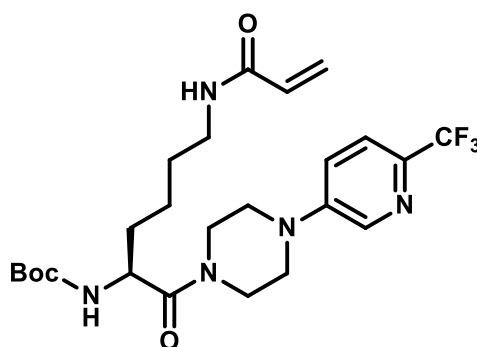
(m, 1H, H-6), 7.25-7.22 (m, 2H, H-4,5), 6.25 (dd, $^3J=17.0$ Hz, $^2J=1.6$ Hz, 1H, CH=CH₂), 6.10 (dd, $^3J=17.0$, $^3J=10.2$ Hz, 1H, CH=CH₂), 5.87 (broad s, 1H, N_εH), 5.61 (dd, $^3J=10.2$ Hz, $^2J=1.6$ Hz, 1H, CH=CH₂), 5.45 (d, $^3J=8.5$ Hz, 1H, N_αH), 4.66-4.57 (m, 1H, C_αH), 3.93-3.62 (m, 4H, 2×CH₂ of piperazine), 3.44-3.09 (m, 6H, 2×CH₂ of piperazine, C_εH₂), 1.76-1.66 (m, 1H, C_βHH), 1.65-1.53 (m, 3H, C_βHH, C_δH₂), 1.53-1.37 (s, 11H, 3×CH₃ of Boc, C_γH₂); ¹³C-NMR (CDCl₃) δ=170.86 (CON), 165.81 (CON_ε), 155.86 (CON_α), 146.82 (C-3), 140.86 (C-6), 138.39 (C-2), 131.03 (CH₂=CH), 126.42 (CH₂=CH), 124.05 (CH of pyridine), 123.70 (CH of pyridine), 80.01 (quart. C of Boc), 49.80 (C_α), 48.99 (CH₂ of piperazine), 48.63 (CH₂ of piperazine), 45.32 (CH₂ of piperazine), 41.89 (CH₂ of piperazine), 39.27 (C_ε), 33.34 (C_β), 29.00 (C_δ), 28.52 (3×CH₃ of Boc), 22.56 (C_γ); MS (ESI⁺): m/z calculated for C₂₃H₃₆N₅O₄: 446.28 [M+H]⁺, found: 446.2.

N^α-Boc-N^ε-Acryloyl-L-lysine-4-(6-fluoropyridin-3-yl)piperazide (4j)



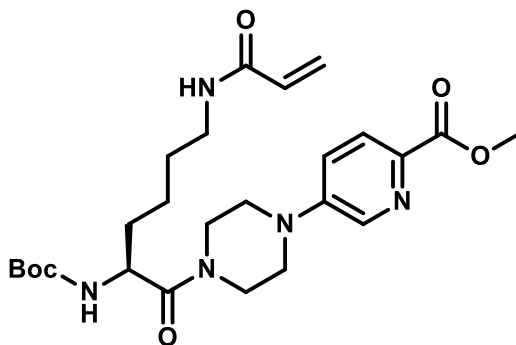
Compound **4j** (189 mg, 34%, yellow oil) was synthesised according to **GP VI** using compounds **2a** and **3j** (1.22 mmol). Solvent for column chromatography: gradient from ethyl acetate-methanol 100:0 to 85:15; *R_f* 0.13 (ethyl acetate); ¹H-NMR (CDCl₃) δ=7.82 (dd, $^4J_{H,H}=2.9$ Hz, $^5J_{H,H}=1.7$ Hz, 1H, H-2), 7.37 (ddd, $^3J_{H,H}=9.0$ Hz, $^4J_{H,F}=6.7$ Hz, $^4J_{H,H}=3.1$ Hz, 1H, H-4), 6.86 (dd, $^3J_{H,H}=8.9$ Hz, $^3J_{H,F}=3.4$ Hz, 1H, H-5), 6.26 (dd, $^3J=17.0$ Hz, $^2J=1.5$ Hz, 1H, C=CHH), 6.08 (dd, $^3J=17.0$, 10.2 Hz, 1H, CH=CH₂), 5.77 (broad s, 1H, N_εH), 5.62 (dd, $^3J=10.2$ Hz, $^2J=1.5$ Hz, 1H, C=CHH), 5.44 (d, $^3J=8.5$ Hz, 1H, N_αH), 4.65–4.57 (m, 1H, C_αH), 3.91–3.60 (m, 4H, 2×CH₂ of piperazine), 3.43–3.24 (m, 2H, C_εH₂), 3.20–3.06 (m, 4H, 2×CH₂ of piperazine), 1.77–1.53 (m, 4H, C_βH₂, C_δH₂), 1.48–1.39 (m, 11H, 3×CH₃ of Boc, C_γH₂); ¹³C-NMR (CDCl₃) δ=170.80 (CON), 165.71 (CON_ε), 158.48 (d, $^1J_{C,F}=233.7$ Hz, C-6), 155.85 (COON_α), 145.24 (d, $^4J_{C,F}=4.3$ Hz, C-3), 135.85 (d, $^3J_{C,F}=14.9$ Hz, C-2), 131.01 (CH₂=C), 130.29 (d, $^3J_{C,F}=7.6$ Hz, C-4), 126.45 (CH₂=C), 109.57 (d, $^2J_{C,F}=39.4$ Hz, C-5), 80.03 (quart. C of Boc), 50.31 (C_α), 49.97 (CH₂ of piperazine), 49.77 (CH₂ of piperazine), 45.45 (CH₂ of piperazine), 41.98 (CH₂ of piperazine), 39.24 (C_ε), 33.34 (C_β), 29.07 (C_δ), 28.53 (3×CH₃ of Boc), 22.55 (C_γ); ¹⁹F-NMR (CDCl₃) δ= -77.65 (s); MS (ESI⁺): m/z calculated for C₂₃H₃₅FN₅O₄: 464.27 [M+H]⁺, found: 464.1.

***N*^α-Boc-*N*^ε-Acryloyl-L-lysine-4-(6-trifluoromethylpyridin-3-yl)piperazide (4k)**



Compound **4k** (61 mg, 24%, colourless oil) was synthesised according to **GP VI** using compounds **2a** and **3k** (0.50 mmol). Solvent for column chromatography: gradient from ethyl acetate-methanol 100:0 to 90:10; *R*_f 0.13 (ethyl acetate); ¹H-NMR (CDCl₃) δ=8.35 (d, ⁴*J*=2.8 Hz, 1H, H-2), 7.55 (d, ³*J*=8.7 Hz, 1H, H-5), 7.22 (dd, ³*J*=8.7 Hz, ⁴*J*=2.9 Hz, 1H, H-4), 6.25 (dd, ³*J*=17.0 Hz, ²*J*=1.5 Hz, 1H, C=CHH), 6.08 (dd, ³*J*=17.0, 10.2 Hz, 1H, CH=CH₂), 5.75 (broad s, 1H, N_εH), 5.62 (dd, ³*J*=10.2 Hz, ²*J*=1.5 Hz, 1H, C=CHH), 5.40 (d, ³*J*=8.6 Hz, 1H, N_αH), 4.66–4.57 (m, 1H, C_αH), 3.96–3.64 (m, 4H, 2×CH₂ of piperazine), 3.44–3.25 (m, 6H, 2×CH₂ of piperazine, C_εH₂), 1.79–1.53 (m, 4H, C_βH₂, C_δH₂), 1.49–1.39 (m, 11H, 3×CH₃ of Boc, C_γH₂); ¹³C-NMR (CDCl₃) δ=170.97, 165.74, 155.84 (COO), 148.01 (C-3), 138.88 (q, ²*J*_{C,F}=35.3 Hz, C-6), 137.93 (C-2), 130.98 (CH₂=C), 126.51 (CH₂=C), 122.11 (q, ¹*J*_{C,F}=272.7 Hz, CF₃), 121.68 (C-4), 121.08 (q, ³*J*_{C,F}=2.7 Hz, C-5), 80.11 (quart. C of Boc), 49.80 (C_α), 47.94 (CH₂ of piperazine), 47.58 (CH₂ of piperazine), 45.04 (CH₂ of piperazine), 41.64 (CH₂ of piperazine), 39.16 (C_ε), 33.20 (C_β), 29.11 (C_δ), 28.52 (3×CH₃ of Boc), 22.53 (C_γ); ¹⁹F-NMR (CDCl₃) δ= -66.88 (s); MS (ESI⁺): *m/z* calculated for C₂₄H₃₅F₃N₅O₄: 514.26 [M+H]⁺, found: 514.3.

***N*^α-Boc-*N*^ε-Acryloyl-L-lysine-4-(6-methoxycarbonylpyridin-3-yl)piperazide (4l)**

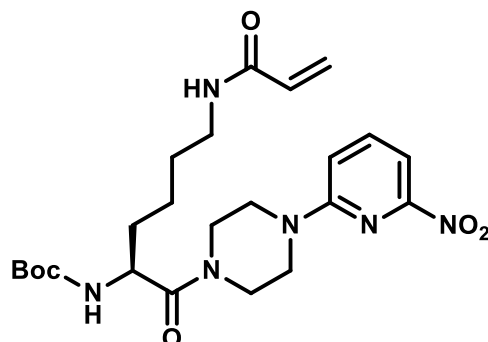


Compound **4l** (159 mg, colourless oil) was synthesised according to **GP VI** using compounds **2a** and **3l** (0.70 mmol). Solvent for column chromatography: gradient from ethyl acetate-methanol 100:0 to 90:10; *R*_f 0.20 (ethyl acetate-methanol 90:10); ¹H-NMR (CDCl₃) δ=8.35 (d,

$^4J=2.9$ Hz, 1H, H-2), 8.03 (d, $^3J=8.8$ Hz, 1H, H-5), 7.18 (dd, $^3J=8.8$ Hz, $^4J=3.0$ Hz, 1H, H-4), 6.25 (dd, $^3J=17.0$ Hz, $^2J=1.6$ Hz, 1H, C=CHH), 6.09 (dd, $^3J=17.0$, 10.2 Hz, 1H, CH=CH₂), 5.86 (broad s, 1H, N_εH), 5.61 (dd, $^3J=10.2$ Hz, $^2J=1.6$ Hz, 1H, C=CHH), 5.41 (d, $^3J=8.5$ Hz, 1H, N_αH), 4.64–4.56 (m, 1H, C_αH), 3.99–3.65 (m, 7H, CH₃O, 2×CH₂ of piperazine), 3.50–3.25 (m, 6H, 2×CH₂ of piperazine, C_εH₂), 1.76–1.53 (m, 4H, C_βH₂, C_δH₂), 1.48–1.37 (m, 11H, 3×CH₃ of Boc, C_γH₂); **¹³C-NMR** (CDCl₃) δ=170.99, 165.77, 165.74, 155.83 (NCOO), 148.26 (C-3), 138.29 (C-6), 137.20 (C-2), 130.98 (CH₂=C), 126.47 (CH₂=C), 126.26 (C-5), 120.71 (C-4), 80.09 (quart. C of Boc), 52.68 (CH₃O), 49.80 (C_α), 47.46 (CH₂ of piperazine), 47.08 (CH₂ of piperazine), 44.97 (CH₂ of piperazine), 41.60 (CH₂ of piperazine), 39.14 (C_ε), 33.19 (C_β), 29.08 (C_δ), 28.50 (3×CH₃ of Boc), 22.53 (C_γ); MS (ESI⁺): m/z calculated for C₂₅H₃₈N₅O₆: 504.28 [M+H]⁺, found: 504.2.

Product contains significant amounts of tris(pyrrolidinophosphine) oxide which was not removed by column chromatography. **¹H-NMR** (CDCl₃) δ=3.20-3.11 (m, 6×CH₂N), 1.87-1.77 (m, 6×CH₂); **¹³C-NMR** (CDCl₃) δ=46.44 (d, $^2J_{C,P}=4.5$ Hz, 6×CH₂N), 26.57 (d, $^3J_{C,P}=8.0$ Hz, 6×CH₂).

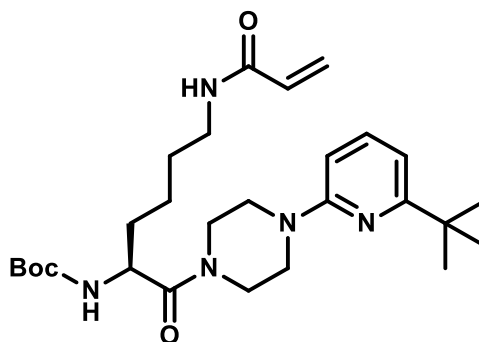
N^α-Boc-N^ε-Acryloyl-L-lysine-4-(6-nitropyridin-2-yl)piperazide (4m)



Compound **4m** (146 mg, 72%, yellow solid) was synthesised according to **GP VI** using compounds **2a** and **3m** (0.41 mmol). Solvent for column chromatography: gradient from CH₂Cl₂-methanol 95:5 to 92:8; *R_f* 0.27 (CH₂Cl₂-methanol 95:5); **¹H-NMR** (CDCl₃) δ=7.76 (dd, $^3J=8.3$, 7.7 Hz, 1H, H-4), 7.51 (d, $^3J=7.6$ Hz, 1H, H-5), 6.94 (d, $^3J=8.4$ Hz, 1H, H-3), 6.26 (dd, $^3J=17.0$ Hz, $^2J=1.5$ Hz, 1H, C=CHH), 6.09 (dd, $^3J=17.0$, 10.2 Hz, 1H, CH=CH₂), 5.80 (broad s, 1H, N_εH), 5.62 (dd, $^3J=10.2$ Hz, $^2J=1.5$ Hz, 1H, C=CHH), 5.44 (d, $^3J=8.4$ Hz, 1H, N_αH), 4.66–4.57 (m, 1H, C_αH), 3.88–3.59 (m, 8H, 4×CH₂ of piperazine), 3.43–3.25 (m, 2H, C_εH₂), 1.78–1.52 (m, 4H, C_βH₂, C_δH₂), 1.49–1.39 (m, 11H, 3×CH₃ of Boc, C_γH₂); **¹³C-NMR** (CDCl₃) δ=171.08 (CON), 165.75 (CON_ε), 157.54, 155.92, 155.85, 140.72 (C-4), 130.98 (CH₂=C), 126.49 (CH₂=C), 112.01 (C-3), 106.50 (C-5), 80.06 (quart. C of Boc), 49.88 (C_α), 45.06 (CH₂ of

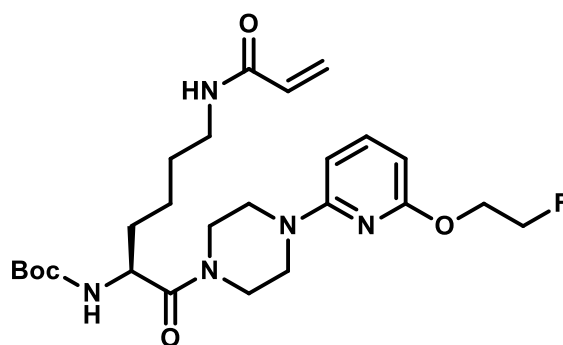
piperazine), 44.88 (CH₂ of piperazine), 44.76 (CH₂ of piperazine), 41.69 (CH₂ of piperazine), 39.22 (C_ε), 33.29 (C_β), 29.07 (C_δ), 28.52 (3×CH₃ of Boc), 22.56 (C_γ); MS (ESI⁺): m/z calculated for C₂₃H₃₄N₆NaO₆: 513.24 [M+Na]⁺, found: 513.3.

N^α-Boc-N^ε-Acryloyl-L-lysine-4-(6-*tert*-butylpyridin-2-yl)piperazide (4n)



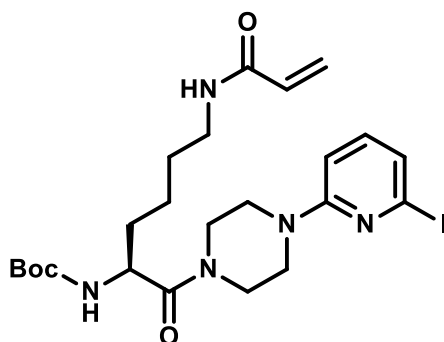
Compound **4n** (45 mg, 28%, brown oil) was synthesised according to **GP VI** using compounds **2a** and **3n** (0.32 mmol). Solvent for column chromatography: gradient from ethyl acetate-petroleum ether 77:33 to 100:0; *R_f* 0.33 (ethyl acetate); ¹H-NMR (CDCl₃) δ=7.45 (dd, ³*J*=8.2, 7.6 Hz, 1H, H-4), 6.72 (d, ³*J*=7.4 Hz, 1H, H-5), 6.47 (d, ³*J*=8.3 Hz, 1H, H-3), 6.27 (dd, ³*J*=17.0 Hz, ²*J*=1.6 Hz, 1H, CH=CHH), 6.09 (dd, ³*J*=17.0, 10.2 Hz, 1H, CH=CH₂), 5.84 (broad s, 1H, N_εH), 5.61 (dd, ³*J*=10.2, ²*J*=1.6 Hz, 1H, CH=CHH), 5.50 (d, ³*J*=8.5 Hz, 1H, N_αH), 4.69-4.57 (m, 1H, C_αH), 3.89-3.21 (m, 10H, 4×CH₂ of piperazine, C₆H₂), 1.75-1.65 (m, 1H, C_βHH), 1.64-1.52 (m, 3H; C_βHH, C_δH₂), 1.50-1.40 (m, 11H, 3×CH₃ of Boc, C_γH₂), 1.31 (s, 9H, 3×CH₃ of *tert*-butyl); ¹³C-NMR (CDCl₃) δ=170.78 (CCON), 167.95, 165.73 (CON_ε), 157.88, 155.90 (CON_α), 138.06 (C-4), 131.05 (CH₂=CH), 126.35 (CH₂=CH), 109.30 (C-5), 104.13 (C-3), 79.92 (quart. C of Boc), 49.81 (C_α), 45.56 (CH₂ of piperazine), 45.39 (2×CH₂ of piperazine), 41.95 (CH₂ of piperazine), 39.39 (C_ε), 37.62 (quart. C of *tert*-butyl), 33.51 (C_β), 30.22 (3×CH₃ of *tert*-butyl), 28.96 (C_δ), 28.54 (3×CH₃ of Boc), 22.62 (C_γ); MS (ESI⁺): m/z calculated for C₂₇H₄₄N₅O₄: 502.34 [M+H]⁺, found: 502.2.

***N*^α-Boc-*N*^ε-Acryloyl-L-lysine-4-(6-(2-fluoroethoxy)pyridin-2-yl)piperazide (4o)**



Compound **4o** (26 mg, 22%, colourless oil) was synthesised according to **GP VI** using compounds **2a** and **3o** (0.23 mmol). Solvent for column chromatography: gradient from ethyl acetate-petroleum ether 77:33 to 100:0; *R*_f 0.36 (ethyl acetate); ¹H-NMR (CDCl₃) δ=7.45 (t, ³J=8.0 Hz, 1H, H-4), 6.26 (dd, ³J=17.0 Hz, ²J=1.5 Hz, 1H, CH=CHH), 6.21-6.17 (m, 2H, H-3,5), 6.09 (dd, ³J=17.0 Hz, ³J=10.2 Hz, 1H, CH=CH₂), 5.82 (broad s, 1H, N_εH) 5.62 (dd, ³J=10.2 Hz, ²J=1.5 Hz, 1H, CH=CHH), 5.48 (d, ³J=8.5 Hz, 1H, N_αH), 4.74 (dm, ²J_{H,F}=47.5 Hz, 2H, CH₂-CH₂-F), 4.66-4.58 (m, 1H, C_αH), 4.52 (dm, ³J_{H,F}=28.5 Hz, 2H, CH₂-CH₂-F), 3.84-3.25 (m, 10H, 4×CH₂ of piperazine, C_εH₂), 1.89-1.50 (m, 4H, C_βH₂, C_δH₂), 1.50-1.37 (m, 11H, 3×CH₃ of Boc, C_γH₂); ¹³C-NMR (CDCl₃) δ=170.86 (C=O), 165.75 (CON_ε), 162.26 (C-6), 157.62 (C-2), 155.89 (CON_α), 140.72 (CH, C-4), 131.01 (CH₂=CH), 126.42 (CH₂=CH), 99.95 (CH of pyridine), 98.94 (CH of pyridine), 82.23 (d, ³J_{C,F}=169.4 Hz, CH₂-CH₂-F), 79.99 (quart. C of Boc), 64.50 (d, ³J_{C,F}=20.4 Hz, CH₂-CH₂-F), 49.82 (C_α), 45.51 (CH₂ of piperazine), 45.29 (CH₂ of piperazine), 45.24 (CH₂ of piperazine), 41.86 (CH₂ of piperazine), 39.34 (C_ε), 33.42 (C_β), 29.01 (C_δ), 28.53 (3×CH₃ of Boc), 22.60 (C_γ); ¹⁹F-NMR (CDCl₃) δ= -75.76– -75.82 (m); MS (ESI⁺): *m/z* calculated for C₂₅H₃₉FN₅O₅: 508.29 [M+H]⁺, found: 508.2.

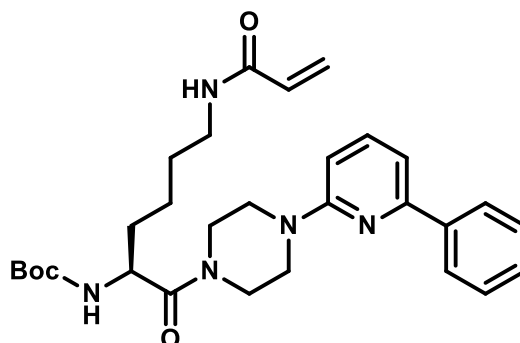
***N*^α-Boc-*N*^ε-Acryloyl-L-lysine-4-(6-iodopyridin-2-yl)piperazide (4p)**



Compound **4p** (28 mg, 11%, light yellow oil) was synthesised according to **GP VI** using compounds **2a** and **3p** (0.26 mmol). Solvent for column chromatography: gradient from ethyl

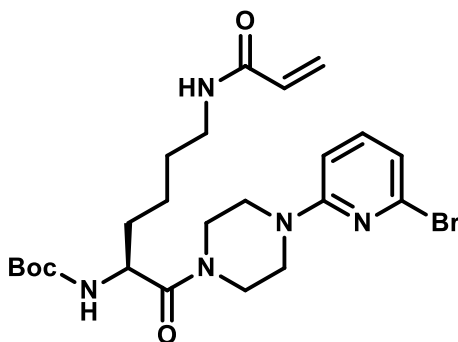
acetate-methanol 100:0 to 85:15; R_f 0.31 (ethyl acetate); $^1\text{H-NMR}$ (CDCl_3) δ =8.04 (t, 3J =5.6 Hz, 1H, N_H), 7.22 (dd, 3J =7.42, 8.32 Hz, 1H, H-4), 7.06 (d, 3J =7.3 Hz, 1H, H-5), 6.94 (d, 3J =8.2 Hz, 1H, N_H), 6.83 (d, 3J =8.4 Hz, 1H, H-3), 6.18 (dd, 3J =17.1, 10.1 Hz, 1H, $\text{CH}=\text{CH}_2$), 6.04 (dd, 3J =17.1 Hz, 2J =2.3 Hz, 1H, $\text{C}=\text{CHH}$), 5.54 (dd, 3J =10.1 Hz, 2J =2.3 Hz, 1H, $\text{C}=\text{CHH}$), 4.41–4.32 (m, 1H, C_αH), 3.69–3.37 (m, 8H, $4\times\text{CH}_2$ of piperazine), 3.16–3.05 (m, 2H, C_H), 1.61–1.21 (m, 15H, $3\times\text{CH}_3$ of Boc, C_βH_2 , $\text{C}_\gamma\text{H}_2$, $\text{C}_\delta\text{H}_2$); $^{13}\text{C-NMR}$ (CDCl_3) δ =170.48 (CON), 164.39 (CON_H), 158.63, 155.28, 139.47 (C-4), 131.85 ($\text{CH}_2=\text{C}$), 124.74 ($\text{CH}_2=\text{C}$), 123.04 (C-5), 116.21 (C-6), 106.06 (C-3), 77.98 (quart. C of Boc), 50.03 (C_α), 44.52 (CH_2 of piperazine), 44.22 (CH_2 of piperazine), 44.14 (CH_2 of piperazine), 41.08 (CH_2 of piperazine), 38.25 (C_H), 31.03 (C_β), 28.81 (C_δ), 28.19 ($3\times\text{CH}_3$ of Boc), 22.73 (C_γ); MS (ESI $^+$): m/z calculated for $\text{C}_{23}\text{H}_{35}\text{N}_5\text{O}_4$: 572.17 $[\text{M}+\text{H}]^+$, found: 572.1.

***N*^B-Boc-*N*^F-Acryloyl-L-lysine-4-(6-phenylpyridin-2-yl)piperazide (4q)**



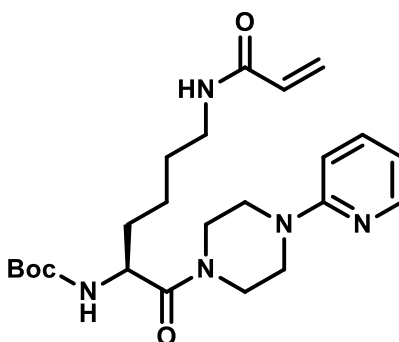
Compound **4q** (54 mg, 32%, yellow oil) was synthesised according to **GP VI** using compounds **2a** and **3q** (0.32 mmol). Solvent for column chromatography: ethyl acetate; R_f 0.30 (ethyl acetate); $^1\text{H-NMR}$ (CDCl_3) δ =8.02–7.97 (m, 2H, H-2,6), 7.59 (dd, 3J =8.4, 7.5 Hz, 1H, H-4 of pyridine), 7.48–7.36 (m, 3H, H-3,4,5 of phenyl), 7.17 (d, 3J =7.4 Hz, 1H, H-5 of pyridine), 6.62 (d, 3J =8.3 Hz, 1H, H-3 of pyridine), 6.27 (dd, 3J =17.0 Hz, 2J =1.6 Hz, 1H, $\text{CH}=\text{CHH}$), 6.09 (dd, 3J =17.0, 10.2 Hz 1H, $\text{CH}=\text{CH}_2$), 5.84 (broad s, 1H, N_H), 5.61 (dd, 3J =10.2 Hz, 2J =1.6 Hz, 1H, $\text{CH}=\text{CHH}$), 5.51 (d, 3J =8.3 Hz, 1H, N_H), 4.68–4.60 (m, 1H, C_αH), 3.88–3.57 (m, 8H, $4\times\text{CH}_2$ of piperazine), 3.43–3.26 (m, 2H, C_H), 1.76–1.52 (m, 4H, C_βH_2 , $\text{C}_\delta\text{H}_2$), 1.45 (s, 11H, $3\times\text{CH}_3$ of Boc, $\text{C}_\gamma\text{H}_2$); $^{13}\text{C-NMR}$ (CDCl_3) δ =171.30 ($\text{C}_\alpha\text{CON}$), 165.73 (CON_H), 158.65, 155.90 155.48, 139.69 (C-1 of phenyl), 138.61 (C-4 of pyridine), 131.02 ($\text{CH}=\text{CH}_2$), 128.91 (C-4 of phenyl), 128.68 (C-3,5 of phenyl), 126.88 (C-2,6 of phenyl), 126.40 ($\text{CH}=\text{CH}_2$), 110.65 (C-5 of pyridine), 105.85 (C-3 of pyridine), 79.95 (quart. C of Boc), 49.83 (C_α), 45.42 ($2\times\text{CH}_2$ of piperazine), 45.30 (CH_2 of piperazine), 42.00 (CH_2 of piperazine), 39.37 (C_H), 33.50(C_β), 28.98 (C_δ), 28.54 ($3\times\text{CH}_3$ of Boc), 22.61 (C_γ); MS (ESI $^+$): m/z calculated for $\text{C}_{29}\text{H}_{40}\text{N}_5\text{O}_4$: 522.31 $[\text{M}+\text{H}]^+$, found: 522.2.

***N*^α-Boc-*N*^ε-Acryloyl-L-lysine-4-(6-bromopyridin-2-yl)piperazide (4r)**



Compound **4r** (62 mg, 31%, colourless solid) was synthesised according to **GP VI** using compounds **2a** and **3r** (0.38 mmol). Solvent for column chromatography: ethyl acetate; *R*_f 0.28 (ethyl acetate); ¹H-NMR (CDCl₃) δ=7.33 (dd, ³*J*=7.6, 8.3 Hz, 1H, H-4), 6.81 (d, ³*J*=7.5 Hz, 1H, H-5), 6.53 (d, ³*J*=8.3 Hz, 1H, H-3), 6.26 (dd, ³*J*=17.0 Hz, ²*J*=1.5 Hz, 1H, C=CHH), 6.09 (dd, ³*J*=17.0, 10.2 Hz, 1H, CH=CH₂), 5.80 (broad s, 1H, N_εH), 5.62 (dd, ³*J*=10.2 Hz, ²*J*=1.6 Hz, 1H, C=CHH), 5.46 (d, ³*J*=8.4 Hz, 1H, N_αH), 4.65–4.58 (m, 1H, C_αH), 3.85–3.46 (m, 8H, 4×CH₂ of piperazine), 3.43–3.24 (m, 2H, C_εH₂), 1.76–1.65 (m, 4H, C_βH₂, C_δH₂), 1.48–1.38 (m, 11H, 3×CH₃ of Boc, C_γH₂); ¹³C-NMR (CDCl₃) δ=170.94 (CON), 165.74 (CON_ε), 158.81, 155.86, 140.39, 139.86, 131.00 (CH₂=C), 126.44 (CH₂=C), 117.09 (C-5), 105.18 (C-3), 80.00 (quart. C of Boc), 49.83 (C_α), 45.16 (CH₂ of piperazine), 45.09 (CH₂ of piperazine), 44.91 (CH₂ of piperazine), 41.77 (CH₂ of piperazine), 39.29 (C_ε), 33.39 (C_β), 29.02 (C_δ), 28.53 (3×CH₃ of Boc), 22.57 (C_γ); MS (ESI⁺): *m/z* calculated for C₂₃H₃₅BrN₅O₄: 524.19 [M(⁷⁹Br)+H]⁺, found: 524.1.

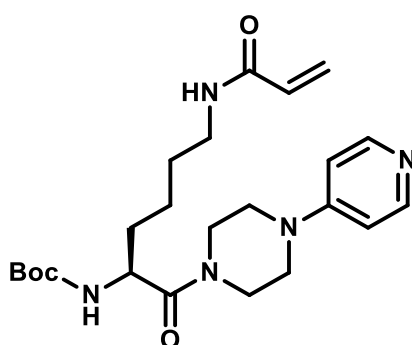
***N*^α-Boc-*N*^ε-Acryloyl-L-lysine-4-(pyridin-2-yl)piperazide (4s)**



Compound **4s** (44 mg, 20%, light yellow oil) was synthesised according to **GP VI** using compounds **2a** and commercially available 1-(pyridin-2-yl)piperazine (0.50 mmol). Solvent for column chromatography: gradient from ethyl acetate-methanol 100:0 to 85:15; *R*_f 0.20 (ethyl acetate); ¹H-NMR (CDCl₃) δ=8.22–8.18 (m, 1H, H-6), 7.54–7.48 (m, 1H, H-4), 6.70–6.64

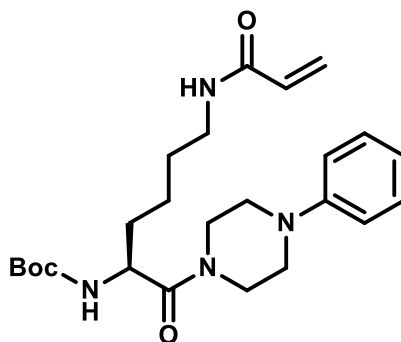
(m, 2H, H-3,5), 6.26 (dd, $^3J=17.0$ Hz, $^2J=1.5$ Hz, 1H, C=CHH), 6.09 (dd, $^3J=17.0$, 10.2 Hz, 1H, CH=CH₂), 5.84 (broad s, 1H, N_εH), 5.61 (dd, $^3J=10.2$ Hz, $^2J=1.5$ Hz, 1H, C=CHH), 5.49 (d, $^3J=7.9$ Hz, N_αH), 4.66–4.58 (m, 1H, C_αH), 3.83–3.48 (m, 8H, 4×CH₂ of piperazine), 3.42–3.26 (m, 2H, C_εH₂), 1.77–1.52 (m, 4H, C_βH₂, C_δH₂), 1.48–1.37 (m, 11H, 3×CH₃ of Boc, C_γH₂); **¹³C-NMR** (CDCl₃) δ=170.85 (CON), 165.73 (CON_ε), 159.06, 155.88, 148.14 (C-6), 137.88 (C-4), 131.03 (CH₂=C), 126.38 (CH₂=C), 114.24 (C-5), 107.46 (C-3), 79.95 (quart. C of Boc), 49.82 (C_α), 45.49 (CH₂ of piperazine), 45.35 (CH₂ of piperazine), 45.29 (CH₂ of piperazine), 41.94 (CH₂ of piperazine), 39.33 (C_ε), 33.45 (C_β), 28.99 (C_δ), 28.53 (3×CH₃ of Boc), 22.57 (C_γ); MS (ESI⁺): m/z calculated for C₂₃H₃₆N₅O₄: 446.28 [M+H]⁺, found: 446.2.

N^α-Boc-N^ε-Acryloyl-L-lysine-4-(pyridin-4-yl)piperazide (4t)



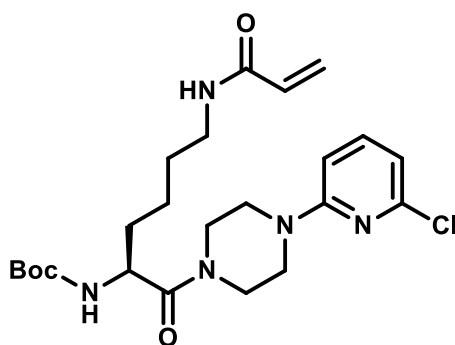
Compound **4t** (62 mg, 28%, brown oil) was synthesised according to **GP VI** using compounds **2a** and commercially available 1-(pyridin-4-yl)piperazine (0.50 mmol). Solvent for column chromatography: gradient from CH₂Cl₂-methanol 85:15 to 75:25; *R*_f 0.13 (CH₂Cl₂-methanol 87:13); **¹H-NMR** (CDCl₃) δ=8.31 (dd, $^3J=5.1$ Hz, $^4J=1.5$ Hz, 2H, H-2,6), 6.68 (dd, $^3J=5.1$ Hz, $^4J=1.6$ Hz, 2H, H-3,5), 6.25 (dd, $^3J=17.0$ Hz, $^2J=1.6$ Hz, 1H, CH=CHH), 6.08 (dd, $^3J=17.0$, $^3J=10.2$ Hz, 1H, CH=CH₂), 5.83 (broad s, 1H, N_εH), 5.61 (dd, $^3J=10.2$ Hz, $^2J=1.6$ Hz, 1H, CH=CHH), 5.41 (d, $^3J=8.6$ Hz, 1H, N_αH), 4.60 (td, $^3J=8.5$ Hz, $^3J=4.7$ Hz, 1H, C_αH), 3.90-3.60 (m, 4H, 2×CH₂ of piperazine), 3.49-3.23 (m, 6H, 2×CH₂ of piperazine, C_εH₂), 1.75-1.65 (m, 1H, C_βHH), 1.64-1.52 (m, 3H, C_βHH, C_δH₂), 1.43 (s, 11H, 3×CH₃ of Boc, C_γH₂); **¹³C-NMR** (CDCl₃) δ=171.05 (CCON), 165.73 (CON_ε), 155.83 (CON_α), 154.91 (C-4), 149.57 (C-2,6), 130.99 (CH₂=CH), 126.46 (CH₂=CH), 108.60 (C-3,5), 80.08 (quart. C of Boc), 49.83 (C_α), 46.20 (CH₂ of piperazine), 45.81 (CH₂ of piperazine), 44.81 (CH₂ of piperazine), 41.51 (CH₂ of piperazine), 39.14 (C_ε), 33.16 (C_β), 29.10 (C_δ), 28.51 (3×CH₃ of Boc), 22.52 (C_γ); MS (ESI⁺): m/z calculated for C₂₃H₃₆N₅O₄: 446.28 [M+H]⁺, found: 446.2.

***N*^α-Boc-*N*^ε-Acryloyl-L-lysine-4-phenylpiperazide (4u)**



Compound **4u** (90 mg, 40%, yellowish solid) was synthesised according to **GP VI** using compounds **2a** and commercially available 1-phenylpiperazine (0.50 mmol). Solvent for column chromatography: gradient from CH₂Cl₂-methanol 97:3 to 95:5; *R*_f 0.58 (CH₂Cl₂-methanol 95:5); ¹H-NMR (CDCl₃) δ=7.31-7.24 (m, 2H, H-2,6), 6.96-6.91 (m, 3H, H-3,4,5), 6.27 (dd, ³J=17.0 Hz, ²J=1.6 Hz, 1H, CH=CHH), 6.09 (dd, ³J=17.0, 10.2 Hz, 1H, CH=CH₂), 5.85 (broad s, 1H, N_εH), 5.61 (dd, ³J=10.2 Hz, ²J=1.6 Hz, 1H, CH=CHH), 5.49 (d, ³J=8.5 Hz, 1H, N_αH), 4.62 (td, ³J=8.5, 4.3 Hz, 1H, C_αH), 3.89-3.49 (m, 4H, 2×CH₂ of piperazine), 3.43-3.10 (m, 6H, 2×CH₂ of piperazine, C_βH₂), 1.76-1.52 (m, 4H, C_βH₂, C_δH₂), 1.44 (s, 11H, 3×CH₃ of Boc, C_γH₂); ¹³C-NMR (CDCl₃) δ=170.68 (C=O), 165.73 (CON_ε), 155.88 (CON_α), 150.90 (C-1), 131.03 (CH₂=CH), 129.35 (C-2,6), 126.38 (CH₂=CH), 120.86 (C-4), 116.87 (C-3,5), 79.94 (quart. C of Boc), 49.92, 49.76, 49.55, 45.63 (CH₂ of piperazine), 42.20 (CH₂ of piperazine), 39.34 (C_ε), 33.46 (C_β), 28.98 (C_δ), 28.53 (3×CH₃ of Boc), 22.59 (C_γ); MS (ESI⁺): *m/z* calculated for C₂₄H₃₇N₄O₄: 445.28 [M+H]⁺, found: 445.2.

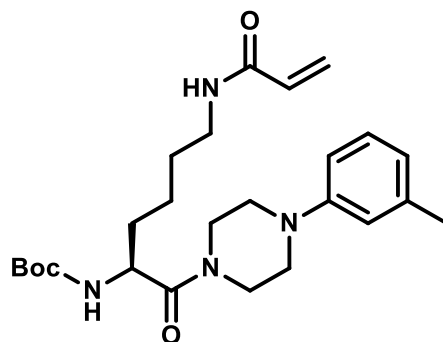
***N*^α-Boc-*N*^ε-Acryloyl-L-lysine-4-(6-chloropyridin-2-yl)piperazide (4v)**



Compound **4v** (71 mg, 20%, yellowish oil) was synthesised according to **GP VI** using compounds **2a** and commercially available 1-(6-chloropyridin-2-yl)piperazine (0.76 mmol). Solvent for column chromatography: gradient from ethyl acetate-methanol 100:0 to 85:15; *R*_f 0.33 (ethyl acetate); ¹H-NMR (CDCl₃) δ=7.44 (dd, ³J=8.3, 7.4 Hz, 1H, H-4), 6.66 (d, ³J=7.4 Hz,

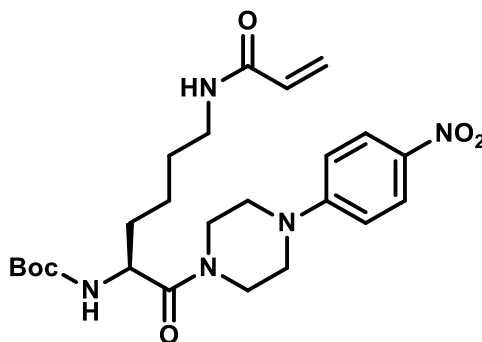
1H, H-5), 6.50 (d, $^3J=8.3$ Hz, 1H, H-3), 6.26 (dd, $^3J=17.0$ Hz, $^2J=1.6$ Hz, 1H, C=CHH), 6.09 (dd, $^3J=17.0$, 10.2 Hz, 1H, CH=CH₂), 5.80 (broad s, 1H, N_εH), 5.62 (dd, $^3J=10.2$ Hz, $^2J=1.5$ Hz, 1H, C=CHH), 5.46 (d, $^3J=8.5$ Hz, 1H, N_αH), 4.65–4.58 (m, 1H, C_αH), 3.82–3.49 (m, 8H, 4×CH₂ of piperazine), 3.42–3.26 (m, 2H, C_εH₂), 1.75–1.53 (m, 4H, C_βH₂, C_δH₂), 1.48–1.38 (m, 11H, 3×CH₃ of Boc, C_γH₂); ¹³C-NMR (CDCl₃) δ=170.93 (CON), 165.72 (CON_ε), 158.74, 155.86, 149.75 (C-6), 140.12 (C-4), 131.01 (CH₂=C), 126.42 (CH₂=C), 113.22 (C-5), 104.88 (C-3), 80.00 (quart. C of Boc), 49.84 (C_α), 45.17 (CH₂ of piperazine), 45.11 (CH₂ of piperazine), 44.93 (CH₂ of piperazine), 41.78 (CH₂ of piperazine), 39.29 (C_ε), 33.40 (C_β), 29.02 (C_δ), 28.53 (3×CH₃ of Boc), 22.57 (C_γ); MS (ESI⁺): m/z calculated for C₂₃H₃₅ClN₅O₄: 480.24 [M(³⁵Cl)+H]⁺, found: 480.1.

N^α-Boc-N^ε-Acryloyl-L-lysine-4-(3-methylphenyl)piperazide (4w)



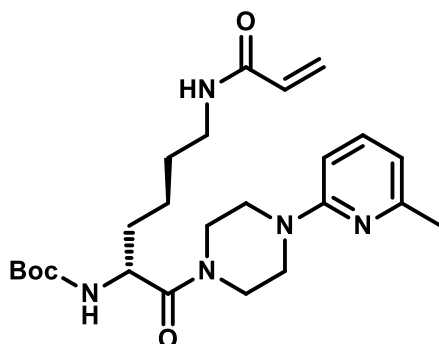
Compound **4w** (45 mg, 25%, white solid) was synthesised according to **GP VI** using compounds **2a** and 1-(3-methylphenyl)piperazine (0.40 mmol). Solvent for column chromatography: gradient from ethyl acetate-methanol 100:0 to 90:10; *R_f* 0.37 (ethyl acetate-methanol 95:5); ¹H-NMR (CDCl₃) δ=7.18 (t, $^3J=7.8$ Hz, 1H, H-5), 6.80–6.71 (m, 3H, H-2,4,6), 6.27 (dd, $^3J=17.0$ Hz, $^2J=1.5$ Hz, 1H, C=CHH), 6.09 (dd, $^3J=17.0$ Hz, 10.2 Hz, 1H, CH=CH₂), 5.85 (broad s, 1H, N_εH), 5.62 (dd, $^3J=10.2$ Hz, $^2J=1.5$ Hz, 1H, C=CHH), 5.50 (d, $^3J=8.5$ Hz, 1H, N_αH), 4.66–4.58 (m, 1H, C_αH), 3.88–3.59 (m, 4H, 2×CH₂ of piperazine), 3.42–3.25 (m, 2H, C_εH₂), 3.24–3.11 (m, 4H, 2×CH₂ of piperazine), 2.33 (s, CH₃), 1.75–1.52 (m, 4H, C_βH₂, C_δH₂), 1.49–1.39 (m, 11H, 3×CH₃ of Boc, C_γH₂); ¹³C-NMR (CDCl₃) δ=165.74, 155.90, 131.01 (CH₂=C), 129.29 (C-5), 126.42 (CH₂=C), 79.96 (quart. C of Boc), 49.74 (C_α, 2×CH₂ of piperazine), 45.59 (CH₂ of piperazine), 42.11 (CH₂ of piperazine), 39.35 (C_ε), 33.47 (C_β), 28.97 (C_δ), 28.53 (3×CH₃ of Boc), 22.59 (C_γ), 21.87 (CH₃), signals for C-1,2,3,4,6 and 1×CO are not visible; MS (ESI⁺): m/z calculated for C₂₅H₃₉N₄O₄: 459.30 [M+H]⁺, found: 459.3.

***N*^α-Boc-*N*^ε-Acryloyl-L-lysine-4-(4-nitrophenyl)piperazide (4x)**



Compound **4x** (66 mg, 27%, yellow oil) was synthesised according to **GP VI** using compounds **2a** and 1-(4-nitrophenyl)piperazine (0.50 mmol). Solvent for column chromatography: gradient from ethyl acetate-methanol 100:0 to 90:10; *R*_f 0.20 (ethyl acetate); ¹H-NMR (CDCl₃) δ=8.19–8.13 (m, 2H, H–3,5), 6.87–6.81 (m, 2H, H–2,6), 6.25 (dd, ³*J*=17.0 Hz, ²*J*=1.5 Hz, 1H, C=CHH), 6.08 (dd, ³*J*=17.0, 10.2 Hz, 1H, CH=CH₂), 5.75 (broad s, 1H, N_εH), 5.62 (dd, ³*J*=10.2 Hz, ²*J*=1.5 Hz, 1H, C=CHH), 5.40 (d, ³*J*=8.6 Hz, 1H, N_αH), 4.65–4.57 (m, 1H, C_αH), 3.93–3.65 (m, 4H, 2×CH₂ of piperazine), 3.57–3.25 (m, 6H, 2×CH₂ of piperazine, C_εH₂), 1.78–1.68 (m, 1H, C_βHH), 1.66–1.53 (m, 3H, C_βHH, C_δH₂), 1.48–1.38 (m, 11H, 3×CH₃ of Boc, C_γH₂); ¹³C-NMR (CDCl₃) δ=171.09, 165.72, 155.84, 154.47, 139.43, 130.98 (CH₂=C), 126.50 (CH₂=C), 126.10 (C–3,5), 113.27 (C–2,6), 80.11 (quart. C of Boc), 49.85 (C_α), 47.35 (CH₂ of piperazine), 46.98 (CH₂ of piperazine), 44.88 (CH₂ of piperazine), 41.61 (CH₂ of piperazine), 39.13 (C_ε), 33.16 (C_β), 29.12 (C_δ), 28.52 (3×CH₃ of Boc), 22.52 (C_γ); MS (ESI⁺): *m/z* calculated for C₂₄H₃₆N₅O₆: 490.27 [M+H]⁺, found: 490.2.

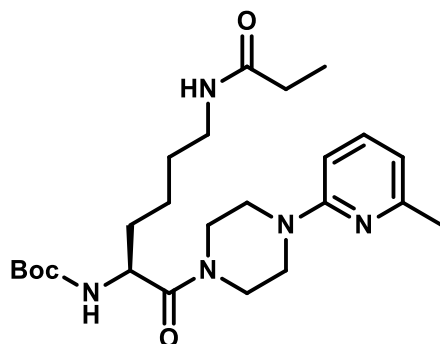
***N*^α-Boc-*N*^ε-Acryloyl-D-lysine-4-(6-methylpyridin-2-yl)piperazide (4y)**



Compound **4y** (127 mg, 34%, brown oil) was synthesised according to **GP VI** using compounds **2b** and **3a** (0.81 mmol). Solvent for column chromatography: gradient from ethyl acetate-methanol 100:0 to 85:15; *R*_f 0.35 (ethyl acetate); ¹H-NMR (CDCl₃) δ=7.40 (dd, ³*J*=8.3, 7.4 Hz, 1H, H–4), 6.55 (d, ³*J*=7.3 Hz, 1H, H–5), 6.45 (d, ³*J*=8.4 Hz, 1H, H–3), 6.27 (dd,

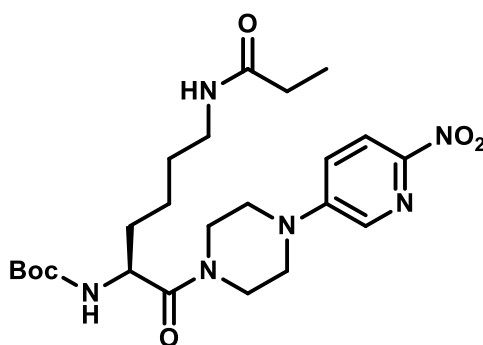
$^3J=17.0$ Hz, $^2J=1.6$ Hz, 1H, C=CHH), 6.09 (dd, $^3J=17.0$, 10.2 Hz, 1H, CH=CH₂), 5.84 (broad s, 1H, N_εH), 5.61 (dd, $^3J=10.2$ Hz, $^2J=1.6$ Hz, 1H, C=CHH), 5.50 (d, $^3J=8.5$ Hz, 1H, N_αH), 4.66–4.59 (m, 1H, C_αH), 3.86–3.45 (m, 8H, 4×CH₂ of piperazine), 3.43–3.23 (m, 2H, C_εH₂), 2.40 (s, 3H, CH₃ of pyridine), 1.76–1.53 (m, 4H, C_βH₂, C_δH₂), 1.48–1.39 (m, 11H, 3×CH₃ of Boc, C_γH₂); $^{13}\text{C-NMR}$ (CDCl₃) δ =170.79 (CON), 165.72 (CON_ε), 158.75, 157.14, 155.89, 138.10 (C–4), 131.04 (CH₂=C), 126.35 (CH₂=C), 113.62 (C–5), 104.09 (C–3), 79.93 (quart. C of Boc), 49.81 (C_α), 45.58 (CH₂ of piperazine), 45.43 (CH₂ of piperazine), 45.40 (CH₂ of piperazine), 42.01 (CH₂ of piperazine), 39.38 (C_ε), 33.52 (C_β), 28.97 (C_δ), 28.54 (3×CH₃ of Boc), 24.67 (CH₃ of pyridine), 22.60 (C_γ); MS (ESI⁺): m/z calculated for C₂₄H₃₈N₅O₄: 460.29 [M+H]⁺, found: 460.3.

N^α-Boc-N^ε-Propionyl-L-lysine-4-(6-methylpyridin-2-yl)piperazide (4z)



Compound **4z** (77 mg, 50%, yellow oil) was synthesised according to **GP VI** using compounds **2c** and **3a** (0.33 mmol). Solvent for column chromatography: gradient from CH₂Cl₂-methanol 97:3 to 95:5; *R_f* 0.47 (CH₂Cl₂-methanol 95:5); $^1\text{H-NMR}$ (CDCl₃) δ =7.41 (t, $^3J=7.8$ Hz, 1H, H-4), 6.55 (d, $^3J=7.3$ Hz, 1H, H-5), 6.45 (d, $^3J=8.5$ Hz, 1H, H-3), 5.60 (broad s, 1H, N_εH), 5.48 (d, $^3J=8.3$ Hz, 1H, N_αH), 4.68–4.57 (m, 1H, C_αH), 3.83–3.47 (m, 8H, 4×CH₂ of piperazine), 3.33–3.19 (m, 2H, C_εH₂), 2.40 (s, 3H, CH₃ of pyridine), 2.19 (q, $^3J=7.6$ Hz, 2H, -CH₂-CH₃), 1.75–1.65 (m, 1H, C_βHH), 1.63–1.48 (m, 3H, C_βHH, C_δH₂), 1.48–1.34 (m, 11H, 3×CH₃ of Boc, C_γH₂), 1.15 (t, $^3J=7.6$ Hz, 3H, -CH₂-CH₃); $^{13}\text{C-NMR}$ (CDCl₃) δ =173.92 (CON_ε), 170.82 (CCON), 158.74, 157.14, 155.85 (CON_α), 138.10 (C-4), 113.63 (C-5), 104.09 (C-3), 79.88 (quart. C of Boc), 49.86 (C_α), 45.60 (CH₂ of piperazine), 45.43 (2×CH₂ of piperazine), 41.99 (CH₂ of piperazine), 39.31 (C_ε), 33.51 (C_β), 29.89 (-CH₂-CH₃), 29.20 (C_δ), 28.53 (3×CH₃ of Boc), 24.68 (-CH₃), 22.61 (C_γ), 10.09 (-CH₂-CH₃); MS (ESI⁺): m/z calculated for C₂₄H₄₀N₅O₄: 462.31 [M+H]⁺, found: 462.2.

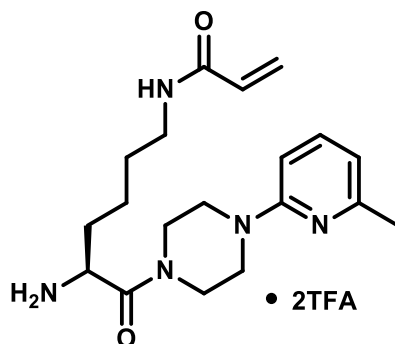
***N*^α-Boc-*N*^ε-Propionyl-L-lysine-4-(6-nitropyridin-3-yl)piperazide (4aa)**



Compound **4aa** (141 mg, 87%, yellow oil) was synthesised according to **GP VI** using compounds **2c** and **3b** (0.33 mmol). Solvent for column chromatography: gradient from ethyl acetate-methanol 95:5 to 91:9; *R*_f 0.43 (ethyl acetate-methanol 91:9); ¹H-NMR (CDCl₃) δ=8.20 (d, ³*J*=9.1 Hz, 1H, H-5), 8.15 (d, ⁴*J*=2.9 Hz, 1H, H-2), 7.26-7.22 (m, 1H, H-4), 5.54 (broad s, 1H, N_εH), 5.36 (d, ³*J*=8.7 Hz, 1H, N_αH), 4.67-4.51 (m, 1H, C_αH), 4.01-3.66 (m, 4H, 2×CH₂ of piperazine), 3.63-3.38 (m, 4H, 2×CH₂ of piperazine), 3.36-3.12 (m, 2H, C_εH₂), 2.18 (q, ³*J*=7.6 Hz, 2H, -CH₂-CH₃), 1.72 (m, 1H, C_βHH), 1.65-1.47 (m, 3H, C_βHH, C_δH₂), 1.43 (s, 11H, 3×CH₃ of Boc, C_γH₂), 1.14 (t, ³*J*=7.6 Hz, 3H, -CH₂-CH₃); ¹³C-NMR (CDCl₃) δ=173.98 (CON_ε), 171.22 (CCON), 155.81 (CON_α), 149.62, 148.58, 134.24 (C-2), 121.39 (C-4), 119.84 (C-5 Pyridin), 80.13 (quart. C of Boc), 49.88(C_α), 47.04 (CH₂ of piperazine), 46.66(CH₂ of piperazine), 44.70 (CH₂ of piperazine), 41.41 (CH₂ of piperazine), 38.96 (C_ε), 33.01 (C_β), 29.89 (-CH₂-CH₃), 29.34 (C_δ), 28.50 (3×CH₃ of Boc), 22.49 (C_γ), 10.08 (-CH₂-CH₃); MS (ESI⁺): *m/z* calculated for C₂₃H₃₇N₆O₆: 493.28 [M+H]⁺, found: 493.2.

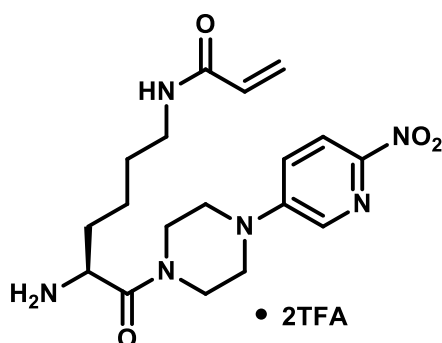
N^ε-Acyllysine piperazides (5)

N^ε-Acryloyl-L-lysine-4-(6-methylpyridin-2-yl)piperazide×2TFA (5a)



Compound **5a** (149 mg, amber oil) was synthesised according to **GP VII** using compound **4a**. **¹H-NMR** (DMSO-*d*₆) δ=8.12 (d, ³*J*=3.8 Hz, 3H, NH₃⁺), 8.07 (t, ³*J*=5.6 Hz, 1H, NH), 7.64 (ps-t, ³*J*=8.3 Hz, 1H, H-4), 6.85 (d, ³*J*=7.9 Hz, 1H, H-3), 6.67 (d, ³*J*=7.2 Hz, 1H, H-5), 6.18 (dd, ³*J*=17.1, 10.1 Hz, 1H, CH=CH₂), 6.02 (dd, ³*J*=17.1 Hz, ²*J*=2.3 Hz, 1H, C=CHH), 5.53 (dd, ³*J*=10.1 Hz, ²*J*=2.3 Hz, 1H, C=CHH), 4.48–4.38 (m, 1H, C_αH), 3.76–3.40 (m, 8H, 4×CH₂ of piperazine), 3.26–2.99 (m, 2H, C_εH₂), 2.38 (s, 3H, CH₃), 1.75–1.65 (m, 2H, C_βH₂), 1.53–1.18 (m, 4H, C_γH₂, C_δH₂); **¹³C-NMR** (DMSO-*d*₆) δ=167.38 (CON), 164.51 (CON_ε), 158.17 (q, ²*J*_{C,F}=35.8 Hz, CO TFA), 131.78 (CH₂=C), 124.88 (CH₂=C), 115.79 (psd, ¹*J*_{C,F}=292.6 Hz, CF₃ TFA), 112.84 (C-5), 49.48 (C_α), 45.20 (CH₂ of piperazine), 44.73 (CH₂ of piperazine), 44.15 (CH₂ of piperazine), 41.26 (CH₂ of piperazine), 37.97 (C_ε), 30.02 (C_β), 28.70 (C_δ), 21.24 (C_γ), signals for C-2,3,4,6 and CH₃ are not visible; **¹⁹F-NMR** (DMSO-*d*₆): δ= -74.69 (s, TFA); MS (ESI⁺): *m/z* calculated for C₁₉H₃₀N₅O₂: 360.24 [M+H]⁺, found: 360.2.

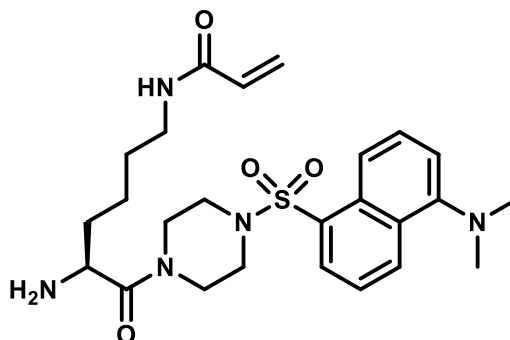
N^ε-Acryloyl-L-lysine-4-(6-nitropyridin-3-yl)piperazide×2TFA (5b)



Compound **5b** (165 mg, yellow oil) was synthesised according to **GP VII** using compound **4b**. **¹H-NMR** (DMSO-*d*₆) δ=8.29 (d, ⁴*J*=3.0 Hz, 1H, H-2), 8.20 (d, ³*J*=9.2 Hz, 1H, H-5), 8.11 (d, ³*J*=3.7 Hz, 3H, NH₃⁺), 8.06 (t, ³*J*=5.7 Hz, 1H, NH), 7.52 (dd, ³*J*=9.3 Hz, ⁴*J*=3.1 Hz, 1H, H-4), 6.17 (dd, ³*J*=17.1, 10.1 Hz, 1H, CH=CH₂), 6.01 (dd, ³*J*=17.1 Hz, ²*J*=2.3 Hz, 1H, C=CHH), 5.53

(dd, $^3J=10.1$ Hz, $^2J=2.3$ Hz, 1H, C=CHH), 4.49–4.39 (m, 1H, C $_{\alpha}$ H), 3.77–3.45 (m, 8H, 4 \times CH $_2$ of piperazine), 3.22–3.05 (m, 2H, C $_{\epsilon}$ H $_2$), 1.76–1.63 (m, 1H, C $_{\beta}$ H $_2$), 1.52–1.28 (m, 4H, C $_{\gamma}$ H $_2$, C $_{\delta}$ H $_2$); $^{19}\text{F-NMR}$ (DMSO- d_6): $\delta = -74.28$ (s, TFA); MS (ESI $^+$): m/z calculated for C $_{18}$ H $_{27}$ N $_6$ O $_4$: 391.21 [M+H] $^+$, found: 391.3.

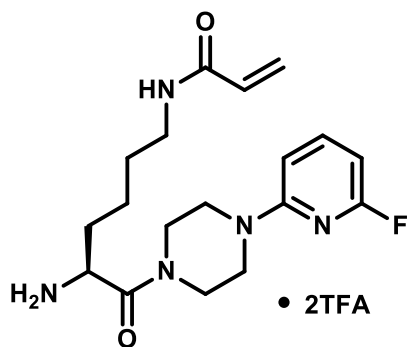
N $^{\epsilon}$ -Acryloyl-L-lysine-4-dansylpiperazide \times 2TFA (5c)



• 2TFA

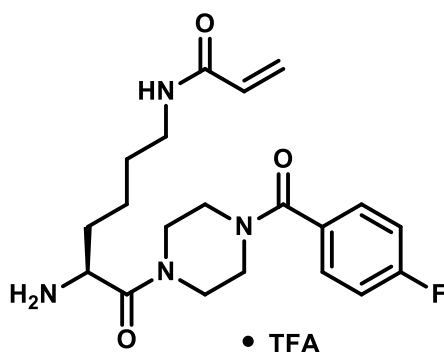
Compound **5c** (35 mg, yellow oil) was synthesised according to **GP VII** using compound **4c**. $^1\text{H-NMR}$ (DMSO- d_6) $\delta=8.55$ (d, $^3J=8.5$ Hz, 1H, H of dansyl), 8.30 (d, $^3J=8.7$ Hz, 1H, H of dansyl), 8.16 (dd, $^3J=7.4$ Hz, $^2J=1.2$ Hz, 1H, H of dansyl), 8.03 (t, $^3J=5.7$ Hz, 1H, N $_2$ H), 7.97 (broad d, $^3J=4.8$ Hz, 3H, NH $_3^+$), 7.69 (dd, $^3J=8.5$ Hz, $^2J=7.4$ Hz, 1H, H of dansyl), 7.63 (dd, $^3J=8.7$, 7.6 Hz, 1H, H of dansyl), 7.28 (d, $^3J=7.0$ Hz, 1H, H of dansyl), 6.16 (dd, $^3J=17.1$, 10.2 Hz, 1H, CH=CH $_2$), 6.03 (dd, $^3J=17.1$ Hz, $^2J=2.2$ Hz, 1H, CH=CHH), 5.54 (dd, $^3J=10.2$ Hz, $^2J=2.2$ Hz, 1H, CH=CHH), 4.32–4.22 (m, 1H, C $_{\alpha}$ H), 3.83–3.75 (m, 1H, CH of piperazine), 3.67–3.56 (m, 1H, CH of piperazine), 3.49–3.25 (m, 4H, 2 \times CH $_2$ of piperazine), 3.10–3.01 (m, 2H, C $_{\epsilon}$ H $_2$), 2.95–2.87 (m, 2H, CH $_2$ of piperazine), 2.83 (s, 6H, 2 \times CH $_3$), 1.63–1.53 (m, 2H, C $_{\beta}$ H $_2$), 1.43–1.31 (m, 2H, C $_{\delta}$ H $_2$), 1.31–1.15 (m, 2H, C $_{\gamma}$ H $_2$); $^{13}\text{C-NMR}$ (DMSO- d_6) $\delta=167.37$, 164.47, 157.97 (d, $^2J_{\text{C,F}}=34.0$ Hz, CO of TFA), 151.45 (quart. C of dansyl), 132.23, 131.78 (CH=CH $_2$), 130.57 (CH of dansyl), 130.31 (CH of dansyl), 129.60 (quart. C of dansyl), 129.19 (quart. C of dansyl), 128.38 (CH of dansyl), 124.88 (CH=CH $_2$), 123.74 (CH of dansyl), 118.80 (CH of dansyl), 115.39 (CH of dansyl), 49.41 (C $_{\alpha}$), 45.41 (CH $_2$ of piperazine), 45.16 (CH $_2$ of piperazine), 45.05 (2 \times CH $_3$), 44.52 (CH $_2$ of piperazine), 41.29 (CH $_2$ of piperazine), 37.90 (C $_{\epsilon}$ H $_2$), 29.85 (C $_{\beta}$ H $_2$), 28.60 (C $_{\delta}$ H $_2$), 21.22 (C $_{\gamma}$ H $_2$), signal for 1 \times C $_{\text{quart.}}$ of dansyl is not visible; $^{19}\text{F-NMR}$ (DMSO- d_6) $\delta = -74.24$ (s, TFA); MS (ESI $^+$): m/z calculated for C $_{25}$ H $_{36}$ N $_5$ O $_4$ S: 502.25 [M+H] $^+$, found: 501.9.

N^ε-Acryloyl-L-lysine-4-(6-fluoropyridin-2-yl)piperazide×2TFA (5d)



Compound **5d** (257 mg, yellow oil) was synthesised according to **GP VII** using compound **4d**. **¹H-NMR** (DMSO-*d*₆) δ=8.11 (d, ³*J*=3.9 Hz, 3H, NH₃⁺), 8.06 (t, ³*J*=5.6 Hz, 1H, NH), 7.72 (ps-q, ³*J*=8.3 Hz, 1H, H-4), 6.73 (dd, ³*J*_{H,H}=8.3 Hz, ⁵*J*_{H,F}=2.6 Hz, 1H, H-3), 6.33 (dd, ³*J*_{H,H}=7.7 Hz, ³*J*_{H,F}=2.7 Hz, 1H, H-5), 6.17 (dd, ³*J*=17.1, 10.1 Hz, 1H, CH=CH₂), 6.02 (dd, ³*J*=17.1 Hz, ²*J*=2.3 Hz, 1H, C=CHH), 5.52 (dd, ³*J*=10.1 Hz, ²*J*=2.3 Hz, 1H, C=CHH), 4.47–4.38 (m, 1H, C_αH), 3.74–3.39 (m, 8H, 4×CH₂ of piperazine), 3.20–3.04 (m, 2H, C_εH₂), 1.74–1.63 (m, 2H, C_βH₂), 1.51–1.20 (m, 4H, C_γH₂, C_δH₂); **¹³C-NMR** (DMSO-*d*₆) δ=167.34 (CON), 164.49 (CON_ε), 161.96 (d, ¹*J*_{C,F}=233.3 Hz, C-6), 158.18 (q, ²*J*_{C,F}=35.8 Hz, CO of TFA), 157.56 (d, ³*J*_{C,F}=16.0 Hz, C-2), 142.81 (d, ³*J*_{C,F}=8.1 Hz, C-4), 131.77 (CH₂=C), 124.85 (CH₂=C), 115.81 (psd, ¹*J*_{C,F}=293.1 Hz, CF₃ of TFA), 103.72 (d, ⁴*J*_{C,F}=3.8 Hz, C-3), 95.87 (d, ²*J*_{C,F}=36.9 Hz, C-5), 49.49 (C_α), 44.48 (CH₂ of piperazine), 44.21 (CH₂ of piperazine), 44.02 (CH₂ of piperazine), 41.24 (CH₂ of piperazine), 37.96 (C_ε), 30.03 (C_β), 28.67 (C_δ), 21.23 (C_γ); **¹⁹F-NMR** (DMSO-*d*₆) δ= -68.81– -68.87 (m, F-6), -74.68 (s, TFA); MS (ESI⁺): *m/z* calculated for C₁₈H₂₇FN₅O₂: 364.21 [M+H]⁺, found: 364.3.

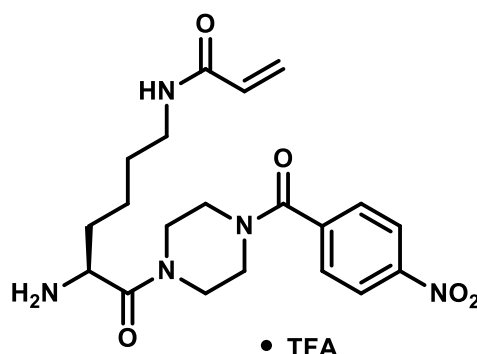
N^ε-Acryloyl-L-lysine-4-(4-fluorobenzoyl)piperazide×TFA (5e)



Compound **5e** (32 mg, brown solid) was synthesised according to **GP VII** using compound **4e**. **¹H-NMR** (DMSO-*d*₆) δ=8.15–8.02 (m, 4H, NH₃⁺, N_εH), 7.52 (dd, ³*J*_{H,H}=8.7 Hz, ⁴*J*_{H,F}=5.5 Hz, 2H, H-2,6), 7.31 (t, ³*J*_{H,H}=³*J*_{H,F}=8.9 Hz, 2H, H-3,5), 6.19 (dd, ³*J*=17.1, 10.1 Hz, 1H, CH=CH₂), 6.05

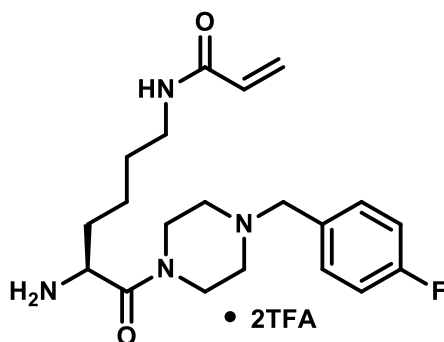
(dd, $^3J=17.1$ Hz, $^2J=2.0$ Hz, 1H, C=CHH), 5.57 (dd, $^3J=10.1$ Hz, $^2J=2.3$ Hz, 1H, C=CHH), 4.44–4.29 (m, 1H, C $_{\alpha}$ H), 3.95–3.30 (m, 8H, 4 \times CH $_2$ of piperazine), 3.20–3.03 (m, 2H, C $_{\epsilon}$ H $_2$), 1.73–1.61 (m, 2H, C $_{\beta}$ H $_2$), 1.49–1.20 (m, 4H, C $_{\gamma}$ H $_2$, C $_{\delta}$ H $_2$); $^{13}\text{C-NMR}$ (DMSO- d_6) δ =168.32, 167.36, 164.51, 131.78 (CH $_2$ =C), 129.67 (d, $^3J_{\text{C,F}}=8.6$ Hz, C–2,6), 124.88 (CH $_2$ =C), 115.44 (d, $^2J_{\text{C,F}}=21.8$ Hz, C–3,5), 49.51 (C $_{\alpha}$), 37.92 (C $_{\epsilon}$), 29.96 (C $_{\beta}$), 28.64 (C $_{\delta}$), 21.21 (C $_{\gamma}$), signals for 4 \times CH $_2$ of piperazine and C-1,4 are not visible; $^{19}\text{F-NMR}$ (DMSO- d_6) δ = -73.81(s, TFA), -110.76– -110.88 (m, F-4); MS (ESI $^+$): m/z calculated for C $_{20}$ H $_{28}$ FN $_4$ O $_3$: 391.21 [M+H] $^+$, found: 391.3.

N $^{\epsilon}$ -Acryloyl-L-lysine-4-(4-nitrobenzoyl)piperazide \times TFA (5f)



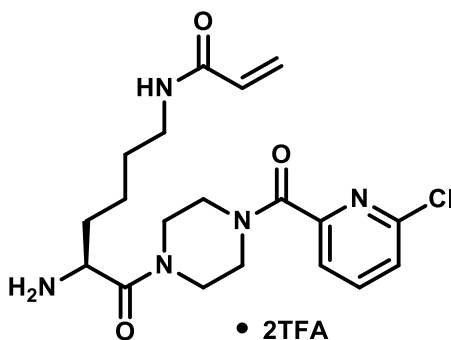
Compound **5f** (66 mg, light brown solid) was synthesised according to **GP VII** using compound **4f**. $^1\text{H-NMR}$ (DMSO- d_6) δ =8.32 (d, $^3J=8.8$ Hz, 2H, H–3,5), 8.16–8.03 (m, 4H, N $_{\epsilon}$ H, NH $_3^+$), 7.72 (d, $^3J=8.2$ Hz, 2H, H–2,6), 6.25–6.13 (m, 1H, CH=CH $_2$), 6.11–5.98 (m, 1H, C=CHH), 5.61–5.51 (m, 1H, C=CHH), 4.48–4.27 (m, 1H, C $_{\alpha}$ H), 3.80–3.41 (m, 6H, 3 \times CH $_2$ of piperazine), 3.39–3.22 (m, 2H, CH $_2$ of Piperazine), 3.20–3.03 (m, 2H, C $_{\epsilon}$ H $_2$), 1.75–1.59 (m, 2H, C $_{\beta}$ H $_2$), 1.51–1.20 (m, 4H, C $_{\gamma}$ H $_2$, C $_{\delta}$ H $_2$), diffuse signals (partly in duplicate) due to the amide bonds on both sides of the piperazine ring; $^{13}\text{C-NMR}$ (DMSO- d_6) δ =167.41, 167.31, 164.53, 158.11 (q, $^2J_{\text{C,F}}=35.3$ Hz, CO of TFA), 147.93, 141.78, 131.80 (CH $_2$ =C), 128.40 (C–2,6), 124.90 (CH $_2$ =C), 123.81 (C–3,5), 49.50 (C $_{\alpha}$), 37.94 (C $_{\epsilon}$), 29.97 (C $_{\beta}$), 28.66 (C $_{\delta}$), 21.22 (C $_{\gamma}$), signals for 4 \times CH $_2$ of piperazine are not visible; $^{19}\text{F-NMR}$ (DMSO- d_6) δ = -74.58 (s, TFA); MS (ESI $^+$): m/z calculated for C $_{20}$ H $_{28}$ N $_5$ O $_5$: 418.21 [M+H] $^+$, found: 418.3.

N^ε-Acryloyl-L-lysine-4-(4-fluorobenzyl)piperazide×2TFA (5g)



Compound **5g** (66 mg, yellow oil) was synthesised according to **GP VII** using compound **4g**. **¹H-NMR** (DMSO-*d*₆) δ=8.19–8.06 (m, 4H, NH₃⁺, N_εH), 7.58–7.49 (m, 2H, H–2,6), 7.33 (t, ³J=8.5 Hz, 2H, H–3,5), 6.20 (dd, ³J=17.1, 10.1 Hz, 1H, CH=CH₂), 6.06 (dd, ³J=17.1 Hz, ²J=2.3 Hz, 1H, C=CHH), 5.58 (dd, ³J=10.0 Hz, ²J=2.2 Hz, 1H, C=CHH), 4.41–4.25 (m, 1H, C_αH), 3.18–3.07 (m, 2H, C_εH₂), 1.74–1.59 (m, 2H, C_βH₂), 1.50–1.20 (m, 4H, C_γH₂, C_δH₂), signals for 4×CH₂ of piperazine and CH₂-fluorobenzyl are not visible; **¹³C-NMR** (DMSO-*d*₆) δ=164.61, 158.08 (d, ²J_{C,F}=32.8 Hz, CO of TFA), 133.43 (pss, C–2,6), 131.82 (CH₂=C), 124.98 (CH₂=C), 115.80 (d, ²J_{C,F}=20.9 Hz, C–3,5), 49.44 (C_α), 37.90 (C_ε), 28.71 (C_δ), 21.29 (C_γ), signals for 4×CH₂ of piperazine, CH₂-fluorobenzyl, C-1,2,4,6, C_β, 1×CO are not visible; **¹⁹F-NMR** (DMSO-*d*₆) δ= -74.04 (s, TFA), -111.91– -112.04 (m, F-4); MS (ESI⁺): m/z calculated for C₂₀H₃₀FN₄O₂: 377.23 [M+H]⁺, found: 377.2.

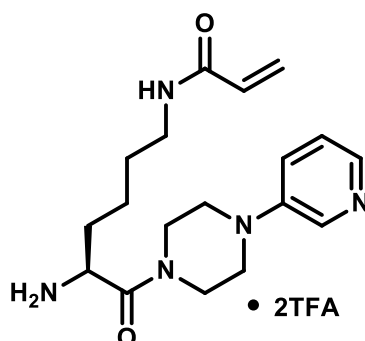
N^ε-Acryloyl-L-lysine-4-(6-chloropyridinoyl)piperazide×2TFA (5h)



Compound **5h** (35 mg, yellow oil) was synthesised according to **GP VII** using compound **4h**. **¹H-NMR** (DMSO-*d*₆) δ=8.14–7.99 (m, 5H, NH₃⁺, N_εH, H-4 of pyridine), 7.69–7.61 (m, 2H, H-3,5 of pyridine), 6.23–6.14 (m, 1H, CH=CH₂), 6.10–6.01 (m, 1H, CH=CHH), 5.60–5.53 (m, 1H, CH=CHH), 4.46–4.29 (m, 1H, C_αH), 3.81–3.27 (m, 8H, 4×CH₂ of piperazine), 3.20–3.05 (m, 2H, C_εH₂), 1.73–1.61 (m, 2H, C_βH₂), 1.55–1.17 (m, 4H, C_γH₂, C_δH₂), diffuse signals (partly in duplicate) due to the amide bonds on both sides of the piperazine ring; **¹⁹F-NMR** (DMSO-*d*₆)

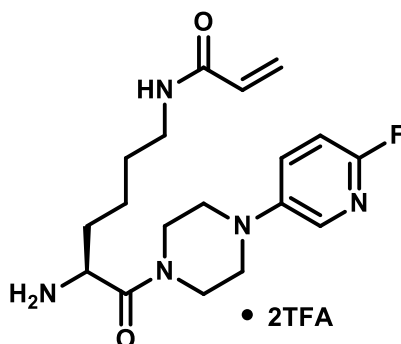
$\delta = -73.68$ (s, TFA); MS (ESI⁺): m/z calculated for C₁₉H₂₇ClN₅O₃: 408.18 [M(³⁵Cl)+H]⁺, found: 408.0.

N^F-Acryloyl-L-lysine-4-(pyridin-3-yl)piperazide×2TFA (5i)



Compound **5i** (144 mg, yellow oil) was synthesised according to **GP VII** using compound **4i**. **¹H-NMR** (DMSO-*d*₆) δ =8.47 (d, ⁴*J*=2.7 Hz, 1H, H-2), 8.23 (d, ³*J*=5.1 Hz, 1H, H-6), 8.20-8.03 (m, 4H, NH₃⁺/N_εH), 7.99 (d, ³*J*=8.8 Hz, ⁴*J*=2.3 Hz, 1H, H-4), 7.78 (dd, ³*J*=8.8, 5.2 Hz, 1H, H-5), 6.17 (dd, ³*J*=17.1, 10.1 Hz, 1H, CH=CH₂), 6.00 (dd, ³*J*=17.1 Hz, ²*J*=2.2 Hz, 1H, CH=CHH), 5.53 (dd, ³*J*=10.1 Hz, ²*J*=2.3 Hz, 1H, CH=CHH), 4.50-4.40 (m, 1H, C_αH), 3.81-3.54 (m, 4H, 2×CH₂ of piperazine), 3.54-3.28 (m, 4H, 2×CH₂ of piperazine), 3.23-3.07 (m, 2H, C_εH₂), 1.78-1.62 (m, 2H, C_βH₂), 1.52-1.29 (m, 4H, C_γH₂, C_δH₂); **¹³C-NMR** (DMSO-*d*₆) δ =167.38 (C_αCON), 164.50 (CON_ε), 158.10 (q, ²*J*_{C,F}=34.6 Hz, CO of TFA), 147.61 (C-3), 131.78 (CH=CH₂), 124.87 (CH=CH₂), 49.41 (C_α), 46.63 (CH₂ of piperazine), 46.17 (CH₂ of piperazine), 43.92 (CH₂ of piperazine), 40.96 (CH₂ of piperazine), 37.95 (C_ε), 30.04 (C_β), 28.70 (C_δ), 21.20 (C_γ), signals for C-2,4,5,6 of are not visible; MS (ESI⁺): m/z calculated for C₁₈H₂₈N₅O₂: 346.22 [M+H]⁺, found: 346.2.

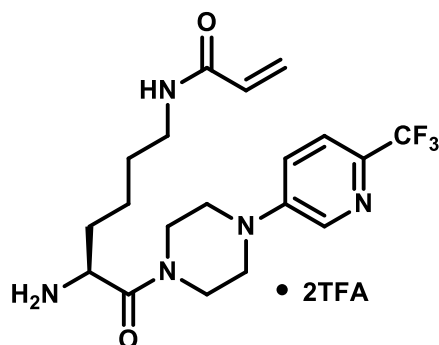
N^F-Acryloyl-L-lysine-4-(6-fluoropyridin-3-yl)piperazide×2TFA (5j)



Compound **5j** (270 mg, yellow oil) was synthesised according to **GP VII** using compound **4j**. **¹H-NMR** (DMSO-*d*₆) δ =8.12 (broad s, 3H, NH₃⁺), 8.06 (t, ³*J*=5.5 Hz, 1H, NH), 7.87 (broad s, 1H, H-2), 7.65 (ddd, ³*J*_{H,H}=10.0 Hz, ⁴*J*_{H,F}=7.1 Hz, ⁴*J*_{H,H}=3.1 Hz, 1H, H-4), 7.07 (dd,

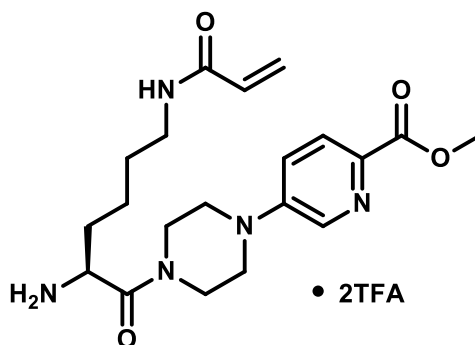
$^3J_{H,H}=8.9$ Hz, $^3J_{H,F}=3.4$ Hz, 1H, H-5), 6.17 (dd, $^3J=17.1$, 10.1 Hz, 1H, $CH=CH_2$), 6.02 (dd, $^3J=17.1$ Hz, $^2J=2.2$ Hz, 1H, $C=CHH$), 5.53 (dd, $^3J=10.1$ Hz, $^2J=2.3$ Hz, 1H, $C=CHH$), 4.49–4.37 (m, 1H, $C_\alpha H$), 3.78–3.53 (m, 4H, $2\times CH_2$ of piperazine), 3.28–3.03 (m, 6H, $2\times CH_2$ of piperazine, $C_\epsilon H_2$), 1.75–1.62 (m, 2H, $C_\beta H_2$), 1.52–1.20 (m, 4H, $C_\gamma H_2$, $C_\delta H_2$); ^{13}C -NMR (DMSO- d_6) δ =167.19 (CON), 164.50 (CON $_\epsilon$), 158.16 (q, $^2J_{C,F}=35.9$ Hz, CO of TFA), 157.03 (d, $^1J_{C,F}=228.9$ Hz, C-6), 145.15 (d, $^4J_{C,F}=3.9$ Hz, C-3), 134.15 (d, $^3J_{C,F}=15.3$ Hz, C-2), 131.79 ($CH_2=C$), 129.82 (d, $^3J_{C,F}=7.3$ Hz, C-4), 124.86 ($CH_2=C$), 109.14 (d, $^2J_{C,F}=39.6$ Hz, C-5 Pyridin), 49.40 (C_α), 48.74 (CH_2 of piperazine), 48.27 (CH_2 of piperazine), 44.48 (CH_2 of piperazine), 41.32 (CH_2 of piperazine), 37.98 (C_ϵ), 30.10 (C_β), 28.70 (C_δ), 21.25 (C_γ); ^{19}F -NMR (DMSO- d_6) δ = -74.69 (s, TFA), -79.89 (broad s, F-6); MS (ESI $^+$): m/z calculated for $C_{18}H_{27}FN_5O_2$: 364.21 $[M+H]^+$, found: 364.1.

N $^\epsilon$ -Acryloyl-L-lysine-4-(6-trifluoromethylpyridin-3-yl)piperazide \times 2TFA (5k)



Compound **5k** (76 mg, yellow oil) was synthesised according to **GP VII** using compound **4k**. 1H -NMR (DMSO- d_6) δ =8.47 (d, $^4J=2.8$ Hz, 1H, H-2), 8.11 (d, $^3J=4.0$ Hz, 3H, NH_3^+), 8.06 (t, $^3J=5.7$ Hz, 1H, $N_\epsilon H$), 7.69 (d, $^3J=8.8$ Hz, 1H, H-5), 7.48 (dd, $^3J=8.8$ Hz, $^4J=2.8$ Hz, 1H, H-4), 6.17 (dd, $^3J=17.1$, 10.1 Hz, 1H, $CH=CH_2$), 6.01 (dd, $^3J=17.1$ Hz, $^2J=2.3$ Hz, 1H, $C=CHH$), 5.52 (dd, $^3J=10.1$ Hz, $^2J=2.3$ Hz, 1H, $C=CHH$), 4.49–4.40 (m, 1H, $C_\alpha H$), 3.79–3.56 (m, 4H, $2\times CH_2$ of piperazine), 3.53–3.30 (m, 4H, $2\times CH_2$ of piperazine), 3.21–3.04 (m, 2H, $C_\epsilon H_2$), 1.75–1.64 (m, 2H, $C_\beta H_2$), 1.51–1.21 (m, 4H, $C_\gamma H_2$, $C_\delta H_2$); ^{13}C -NMR (DMSO- d_6) δ =167.32, 164.48, 158.06 (q, $^2J_{C,F}=35.2$ Hz, CO of TFA), 147.86 (C-3), 137.03 (C-2), 135.53 (q, $^2J_{C,F}=34.3$ Hz, C-6), 131.77 ($CH_2=C$), 124.85 ($CH_2=C$), 121.05–120.91 (C-4,5), 49.42 (C_α), 46.56 (CH_2 of piperazine), 46.06 (CH_2 of piperazine), 44.06 (CH_2 of piperazine), 41.08 (CH_2 of piperazine), 37.96 (C_ϵ), 30.05 (C_β), 28.69 (C_δ), 21.24 (C_γ), signal for CF_3 at pyridine is not visible; ^{19}F -NMR (DMSO- d_6) δ = -64.92 (s, CF_3 of pyridine), -74.54 (s, TFA); MS (ESI $^+$): m/z calculated for $C_{19}H_{27}F_3N_5O_2$: 414.21 $[M+H]^+$, found: 414.2.

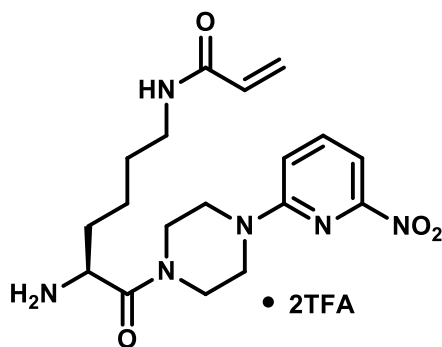
N^ε-Acryloyl-L-lysine-4-(6-methoxycarbonylpyridin-3-yl)piperazide×2TFA (5I)



Compound **5I** (228 mg, brown oil) was synthesised according to **GP VII** using compound **4I**. **¹H-NMR** (DMSO-*d*₆) δ=8.41 (d, ⁴*J*=2.9 Hz, 1H, H-2), 8.11 (d, ³*J*=4.0 Hz, 3H, NH₃⁺), 8.05 (t, ³*J*=5.7 Hz, 1H, N_εH), 7.91 (d, ³*J*=8.8 Hz, 1H, H-5), 7.39 (dd, ³*J*=8.9 Hz, ⁴*J*=3.0 Hz, 1H, H-4), 6.17 (dd, ³*J*=17.1, 10.1 Hz, 1H, CH=CH₂), 6.01 (dd, ³*J*=17.1 Hz, ²*J*=2.3 Hz, 1H, C=CHH), 5.52 (dd, ³*J*=10.1 Hz, ²*J*=2.3 Hz, 1H, C=CHH), 4.49–4.39 (m, 1H, C_αH), 3.81 (s, 3H, CH₃), 3.77–3.33 (m, 8H, 4×CH₂ of piperazine), 1.49–1.20 (m, 4H, C_γH₂, C_δH₂), signals for C_βH₂ and C_εH₂ interfere with the signals from tris(pyrrolidinophosphine) oxide and pyrrolidine; **¹³C-NMR** (DMSO-*d*₆) δ=167.35, 165.00, 164.49, 158.12 (q, ²*J*_{C,F}=35.5 Hz, CO of TFA), 147.81 (C-3), 136.32, 136.19, 131.77 (CH₂=C), 125.73, 124.87, 119.91 (C-4), 51.79 (CH₃), 49.43 (C_α), 46.25 (CH₂ of piperazine), 45.73 (CH₂ of piperazine), 44.06 (CH₂ of piperazine), 41.13 (CH₂ of piperazine), 37.96 (C_ε), 30.04 (C_β), 28.69 (C_δ), 21.25 (C_γ); **¹⁹F-NMR** (DMSO-*d*₆) δ= -74.60 (s, TFA); MS (ESI⁺): *m/z* calculated for C₂₀H₃₀N₅O₄: 404.23 [M+H]⁺, found: 404.3.

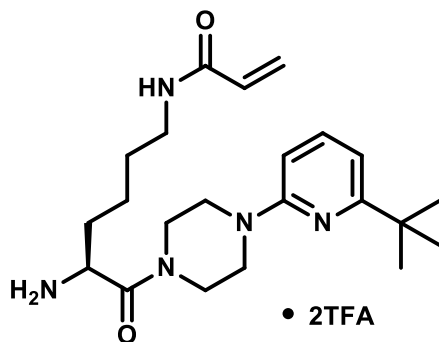
Product contains significant amounts of tris(pyrrolidinophosphine) oxide: **¹H-NMR** (CDCl₃) δ=3.05-2.95 (m, 6×CH₂N), 1.79-1.65 (m, 6×CH₂); **¹³C-NMR** (CDCl₃) δ=45.85 (d, ²*J*_{C,P}=4.1 Hz, 6×CH₂N), 25.88 (d, ³*J*_{C,P}=7.7 Hz, 6×CH₂) and pyrrolidine: **¹H-NMR** (CDCl₃) δ=3.18–3.06 (m, 2×CH₂N), 1.86–1.81 (m, 2×CH₂); **¹³C-NMR** (CDCl₃) δ=44.89 (2×CH₂N), 23.61 (2×CH₂).

***N*^ε-Acryloyl-L-lysine-4-(6-nitropyridin-2-yl)piperazide×2TFA (5m)**



Compound **5m** (108 mg, yellow oil) was synthesised according to **GP VII** using compound **4m**. **¹H-NMR** (DMSO-*d*₆) δ=8.12 (d, ³*J*=4.0 Hz, 3H, NH₃⁺), 8.07 (t, ³*J*=5.6 Hz, 1H, N_εH), 7.94 (dd, ³*J*=8.5, 7.6 Hz, 1H, H-4), 7.52 (d, ³*J*=7.5 Hz, 1H, H-5), 7.34 (d, ³*J*=8.5 Hz, 1H, H-3), 6.17 (dd, ³*J*=17.1, 10.1 Hz, 1H, CH=CH₂), 6.01 (dd, ³*J*=17.1 Hz, ²*J*=2.3 Hz, 1H, C=CHH), 5.52 (dd, ³*J*=10.1 Hz, ²*J*=2.3 Hz, 1H, C=CHH), 4.47–4.38 (m, 1H, C_αH), 3.79–3.52 (m, 8H, 4×CH₂ of piperazine), 3.20–3.04 (m, 2H, C_εH₂), 1.75–1.64 (m, 2H, C_βH₂), 1.51–1.20 (m, 4H, C_γH₂, C_δH₂); **¹³C-NMR** (DMSO-*d*₆) δ=167.40, 164.50, 158.09 (q, ²*J*_{C,F}=35.1 Hz, CO of TFA), 157.19, 155.22, 141.15 (C-4), 131.77 (CH₂=C), 124.85 (CH₂=C), 113.27 (C-3), 105.83 (C-5), 49.51 (C_α), 44.31 (CH₂ of piperazine), 44.16 (CH₂ of piperazine), 43.90 (CH₂ of piperazine), 41.23 (CH₂ of piperazine), 37.96 (C_ε), 30.03 (C_β), 28.68 (C_δ), 21.25 (C_γ); **¹⁹F-NMR** (DMSO-*d*₆) δ= -74.56 (s, TFA); MS (ESI⁺): *m/z* calculated for C₁₈H₂₇N₆O₄: 391.21 [M+H]⁺, found: 391.3.

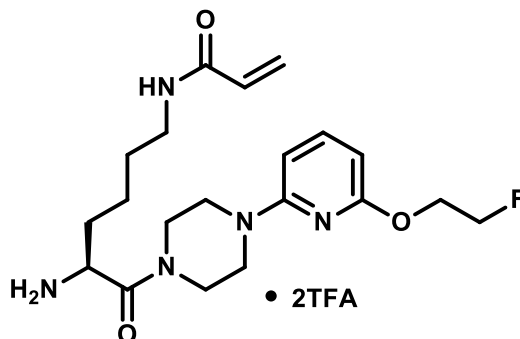
***N*^ε-Acryloyl-L-lysine-4-(6-*tert*-butylpyridin-2-yl)piperazide×2TFA (5n)**



Compound **5n** (61 mg, orange oil) was synthesised according to **GP VII** using compound **4n**. **¹H-NMR** (DMSO-*d*₆) δ=8.13–8.00 (m, 4H, NH₃⁺, N_εH), 7.51 (dd, ³*J*=8.3, 7.6 Hz, 1H, H-4), 6.72 (d, ³*J*=7.5 Hz, 1H), 6.67 (d, ³*J*=8.4 Hz, 1H), 6.17 (dd, ³*J*=17.1, 10.1 Hz, 1H, CH=CH₂), 6.02 (dd, ³*J*=17.1 Hz, ²*J*=2.3 Hz, 1H, CH=CHH), 5.52 (dd, ³*J*=10.1 Hz, ²*J*=2.3 Hz, 1H, CH=CHH), 4.47–4.38 (m, 1H, C_αH), 3.75–3.39 (m, 8H, 4×CH₂ of piperazine), 3.19–3.05 (m, 2H, C_εH₂), 1.74–1.63

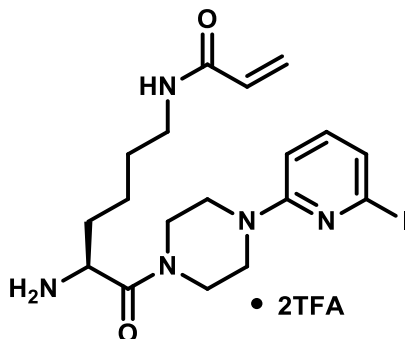
(m, 2H, C_βH₂), 1.50-1.14 (m, 4H, C_δH₂, C_γH₂), 1.26 (s, 9H, 3×CH₃ *tert*-butyl); ¹⁹F-NMR (DMSO-*d*₆) δ = -73.76 (s, TFA); MS (ESI⁺): *m/z* calculated for C₂₂H₃₆N₅O₂: 402.29 [M+H]⁺, found: 402.2.

N^ε-Acryloyl-L-lysine-4-(6-(2-fluoroethoxy)pyridin-2-yl)piperazide×2TFA (5o)



Compound **5o** (16 mg, colourless solid) was synthesised according to **GP VII** using compound **4o**. ¹H-NMR (DMSO-*d*₆) δ = 8.18-8.09 (m, 3H, NH₃⁺), 8.07 (t, ³*J* = 5.4 Hz, 1H, N_εH), 7.51 (t, ³*J* = 8.0 Hz, 1H, H-4), 6.39 (d, ³*J* = 8.1 Hz, 1H, H of pyridine), 6.24-6.10 (m, 2H, CH=CH₂, H of pyridine), 6.02 (dd, ³*J* = 17.1 Hz, ²*J* = 2.2 Hz, 1H, CH=CHH), 5.52 (dd, ³*J* = 10.1 Hz, ²*J* = 2.2 Hz, 1H, CH=CHH), 4.72 (dm, ²*J*_{H,F} = 48.0 Hz, 2H, CH₂-CH₂-F), 4.45 (dm, ³*J*_{H,F} = 28.0 Hz, 2H, CH₂-CH₂-F), 4.45-4.41 (m, 1H, C_αH), 3.81-3.36 (m, 8H, 4×CH₂ of piperazine), 3.24-3.02 (m, 2H, C_εH₂), 1.84-1.60 (m, 2H, C_βH₂), 1.58-1.16 (m, 4H, C_δH₂, C_γH₂); ¹³C-NMR (DMSO-*d*₆) δ = 167.29 (C_αCON), 164.51 (CON_ε), 161.53 (C-6), 157.25 (C-2), 140.81 (C-4), 131.79 (CH=CH₂), 124.83 (CH=CH₂), 98.99 (CH of pyridine), 98.25 (CH of pyridine), 82.15 (d, ²*J*_{C,F} = 165.8 Hz, CH₂-CH₂-F), 64.24 (d, ³*J*_{C,F} = 19.1 Hz, CH₂-CH₂-F), 49.49 (C_α), 44.72 (CH₂ of piperazine), 44.34 (CH₂ of piperazine), 44.28 (CH₂ of piperazine), 41.32 (CH₂ of piperazine), 37.98 (C_ε), 30.05 (C_β), 28.67 (C_δ), 21.26 (C_γ); ¹⁹F-NMR (DMSO-*d*₆) δ = -74.51 (s, TFA); MS (ESI⁺): *m/z* calculated for C₂₀H₃₁FN₅O₃: 408.24 [M+H]⁺, found: 408.0.

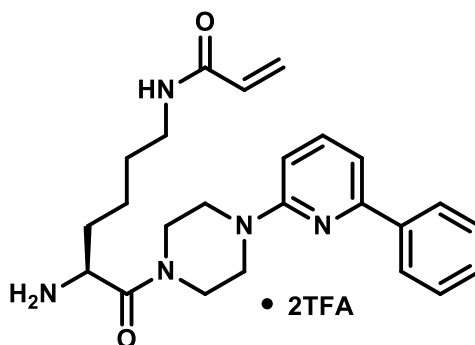
N^ε-Acryloyl-L-lysine-4-(6-iodopyridin-2-yl)piperazide×2TFA (5p)



Compound **5p** (49 mg, yellow, waxy solid) was synthesised according to **GP VII** using compound **4p**. ¹H-NMR (DMSO-*d*₆) δ = 8.11 (s, 3H, NH₃⁺), 8.06 (t, ³*J* = 5.4 Hz, 1H, NH), 7.24 (dd,

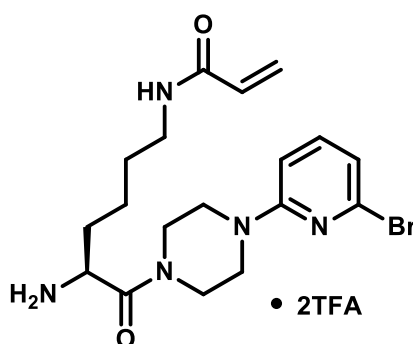
$^3J=8.4$, 7.4 Hz, 1H, H-4), 7.08 (d, $^3J=7.2$ Hz, H-5), 6.86 (d, $^3J=8.4$ Hz, 1H, H-3), 6.17 (dd, $^3J=17.1$, 10.1 Hz, 1H, CH=CH₂), 6.02 (dd, $^3J=17.1$, $^2J=2.3$ Hz, 1H, C=CHH), 5.53 (dd, $^3J=10.1$ Hz, $^2J=2.3$ Hz, 1H, C=CHH), 4.42 (broad s, 1H, C_αH), 3.95–3.37 (m, 8H, 4×CH₂ of piperazine), 3.20–3.05 (m, 2H, C_εH₂), 1.74–1.65 (m, 2H, C_βH₂), 1.50–1.19 (m, 4H, C_γH₂, C_δH₂); **¹³C-NMR** (DMSO-*d*₆) δ=167.31 (CON), 164.50 (CON_ε), 158.53 (C-2), 157.97 (psd, $^2J_{C,F}=34.4$ Hz, CO of TFA), 139.54 (C-4), 131.77 (CH₂=C), 124.88 (CH₂=C), 123.27 (C-5), 116.20 (C-6), 106.19 (C-3), 49.50 (C_α), 44.39 (CH₂ of piperazine), 44.23 (CH₂ of piperazine), 43.95 (CH₂ of piperazine), 41.27 (CH₂ of piperazine), 37.97 (C_ε), 30.03 (C_β), 28.67 (C_δ), 21.25 (C_γ); **¹⁹F-NMR** (DMSO-*d*₆) δ= -74.29 (s, TFA); MS (ESI⁺): *m/z* calculated for C₁₈H₂₇IN₅O₂: 472.12 [M+H]⁺, found: 472.0.

N^ε-Acryloyl-L-lysine-4-(6-phenylpyridin-2-yl)piperazide×2TFA (5q)



Compound **5q** (70 mg, yellow oil) was synthesised according to **GP VII** using compound **4q**. Analytical data (NMR, MS) of this compound were not recorded.

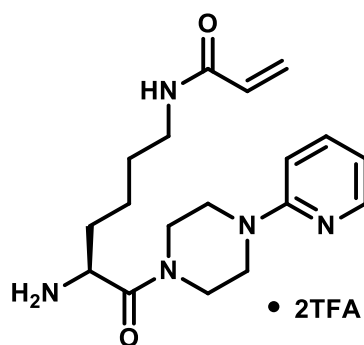
N^ε-Acryloyl-L-lysine-4-(6-bromopyridin-2-yl)piperazide×2TFA (5r)



Compound **5r** (41 mg, yellow oil) was synthesised according to **GP VII** using compound **4r**. **¹H-NMR** (DMSO-*d*₆) δ=8.15–8.08 (m, 3H, NH₃⁺), 8.05 (t, $^3J=5.58$ Hz, N_εH), 7.49 (dd, $^3J=8.4$, 7.5 Hz, 1H, H-4), 6.86 (d, $^3J=8.4$ Hz, 1H, H-3), 6.85 (d, $^3J=7.4$ Hz, 1H, H-5), 6.17 (dd, $^3J=17.1$, 10.1 Hz, 1H, CH=CH₂), 6.02 (dd, $^3J=17.1$ Hz, $^2J=2.3$ Hz, 1H, C=CHH), 5.53 (dd, $^3J=10.1$ Hz, $^2J=2.3$ Hz, 1H, C=CHH), 4.50–4.14 (m, 1H, C_αH), 3.71–3.40 (m, 8H, 4×CH₂ of

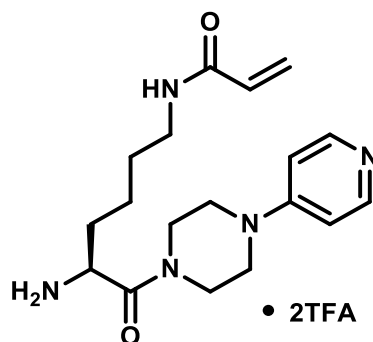
piperazine), 3.19–3.05 (m, 2H, C_εH₂), 1.74–1.66 (m, 2H, C_βH₂), 1.50–1.22 (m, 4H, C_γH₂, C_δH₂); ¹³C-NMR (DMSO-*d*₆) δ=167.32 (CON), 164.50 (CON_ε), 158.53 (C-2), 158.09 (q, ²J_{C,F}=35.7 Hz, CO of TFA), 140.54 (C-4), 139.11 (C-6), 131.77 (CH₂=C), 124.87 (CH₂=C), 115.92 (C-5), 105.91 (C-3), 49.50 (C_α), 44.43 (CH₂ of piperazine), 44.22 (CH₂ of piperazine), 43.97 (CH₂ of piperazine), 41.26 (CH₂ of piperazine), 37.96 (C_ε), 30.03 (C_β), 28.67 (C_δ), 21.24 (C_γ); ¹⁹F-NMR (DMSO-*d*₆) δ= -74.64 (s, TFA); MS (ESI⁺): m/z calculated for C₁₈H₂₇BrN₅O₂: 424.13 [M(⁷⁹Br)+H]⁺, found: 424.0.

N^ε-Acryloyl-L-lysine-4-(pyridin-2-yl)piperazide×2TFA (5s)



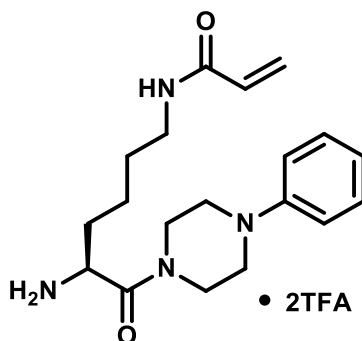
Compound **5s** (89 mg, light brown oil) was synthesised according to **GP VII** using compound **4s**. ¹H-NMR (DMSO-*d*₆) δ=8.18–8.09 (m, 4H, NH₃⁺, H-6), 8.06 (t, ³J=5.6 Hz, 1H, N_εH), 7.74–7.67 (m, 1H, H-4), 7.02 (d, ³J=7.9 Hz, 1H, H-3), 6.78 (dd, ³J=5.6, 6.7 Hz, 1H, H-5), 6.17 (dd, ³J=17.1, 10.1 Hz, 1H, CH=CH₂), 6.02 (dd, ³J=17.1 Hz, ²J=2.3 Hz, 1H, C=CHH), 5.53 (dd, ³J=10.1 Hz, ²J=2.3 Hz, 1H, C=CHH), 4.46–4.41 (m, 1H, C_αH), 3.75–3.46 (m, 8H, 4×CH₂ of piperazine), 3.19–3.05 (m, 2H, C_εH₂), 1.74–1.65 (m, 2H, C_βH₂), 1.49–1.21 (m, 4H, C_γH₂, C_δH₂); ¹³C-NMR (DMSO-*d*₆) δ=167.38 (CON), 164.51 (CON_ε), 158.08 (q, ²J_{C,F}=34.9 Hz, CO of TFA), 144.79 (C-6), 139.29 (C-4), 131.77 (CH₂=C), 124.88 (CH₂=C), 116.05 (psd, ¹J_{C,F}=293.0 Hz, CF₃ of TFA), 113.40 (C-5), 108.71 (C-3), 49.48 (C_α), 44.91 (CH₂ Piperazin), 44.43 (CH₂ of piperazine), 44.12 (CH₂ of piperazine), 41.23 (CH₂ of piperazine), 37.96 (C_ε), 30.01 (C_β), 28.69 (C_δ), 21.23 (C_γ), signal for C-2 is not visible; ¹⁹F-NMR (DMSO-*d*₆) δ= -74.49 (s, TFA); MS (ESI⁺): m/z calculated for C₁₈H₂₈N₅O₂: 346.22 [M+H]⁺, found: 346.2.

N^ε-Acryloyl-L-lysine-4-(pyridin-4-yl)piperazide×2TFA (5t)



Compound **5t** (60 mg, brown oil) was synthesised according to **GP VII** using compound **4t**. **¹H-NMR** (DMSO-*d*₆) δ=8.31 (d, ³*J*=7.4 Hz, 2H, H-2,6), 8.24-8.12 (m, 3H, NH₃⁺), 8.09 (t, ³*J*=5.6 Hz, 1H, N_εH), 7.21 (d, ³*J*=7.7 Hz, 2H, H-3,5), 6.26-6.13 (m, 1H, CH=CH₂), 6.10-5.94 (m, 1H, CH=CHH), 5.62-5.48 (m, 1H, CH=CHH), 4.50-4.35 (m, 1H, C_αH), 3.95- 3.55 (m, 8H, 4×CH₂ of piperazine), 3.22-2.91 (m, 2H, C_εH₂), 1.84-1.56 (m, 2H, C_βH₂), 1.50-1.17 (m, 4H, C_γH₂, C_δH₂); **¹³C-NMR** (DMSO-*d*₆) δ=168.15 (C_αCON), 164.96 (CON_ε), 158.47 (q, ²*J*_{C,F}=33.6 Hz, CO of TFA), 157.10 (C-1), 140.35 (C-3,5), 132.22 (CH=CH₂), 125.34 (CH=CH₂), 108.02 (C-2,6), 49.89 (C_α), 45.85 (CH₂ of piperazine), 45.28 (CH₂ of piperazine), 43.82 (CH₂ of piperazine), 41.39 (CH₂ of piperazine), 38.35 (C_ε), 30.36 (C_β), 29.14 (C_δ), 21.66 (C_γ); **¹⁹F-NMR** (DMSO-*d*₆) δ= -74.22 (s, TFA); MS (ESI⁺): *m/z* calculated for C₁₈H₂₈N₅O₂: 346.22 [M+H]⁺, found: 346.2.

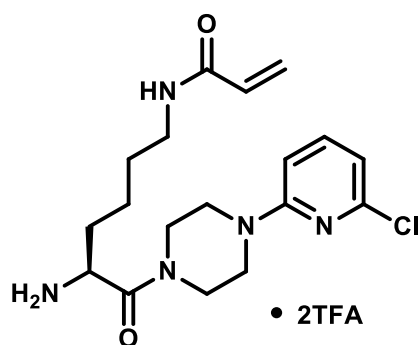
N^ε-Acryloyl-L-lysine-4-phenylpiperazide×2TFA (5u)



Compound **5u** (60 mg, orange crystals) was synthesised according to **GP VII** using compound **4u**. **¹H-NMR** (DMSO-*d*₆) δ=8.14 (d, ³*J*=3.6 Hz, 3H, NH₃⁺), 8.08 (t, ³*J*=5.6 Hz, 1H, N_εH), 7.30-7.17 (m, 2H, H-3,5), 7.04-6.95 (m, 2H, H-2,6), 6.86-6.80 (m, 1H, H-4), 6.18 (dd, ³*J*=17.1, 10.1 Hz, 1H, CH=CH₂), 6.03 (dd, ³*J*=17.1 Hz, ²*J*=2.3 Hz, 1H, CH=CHH), 5.53 (dd, ³*J*=10.1 Hz, ²*J*=2.3 Hz, 1H, CH=CHH), 4.49-4.36 (m, 1H, C_αH), 3.80-3.53 (m, 4H, 2×CH₂ of piperazine), 3.31-2.98 (m, 6H, 2×CH₂ of piperazine, C_εH₂), 1.82-1.61 (m, 2H, C_βH₂), 1.52-1.10 (m, 4H, C_γH₂, C_δH₂); **¹³C-NMR** (DMSO-*d*₆) δ=167.21 (C_αCON), 164.58 (CON_ε), 158.46 (q, ²*J*_{C,F}=36.6 Hz, CO

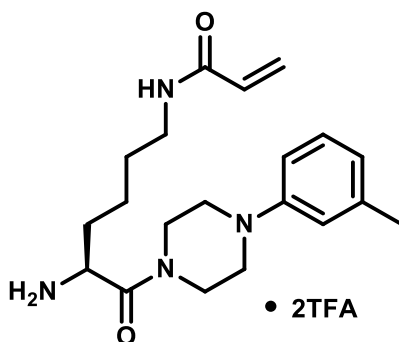
of TFA), 150.49 (C-1), 131.85 (CH=CH₂), 129.07 (C-3,5), 124.88 (CH=CH₂), 119.74 (C-4), 116.09 (C-2,6), 115.69 (q, ¹J_{C,F}=292.4 Hz, CF₃ of TFA), 49.49 (C_α), 48.82 (CH₂ of piperazine), 48.36 (CH₂ of piperazine), 44.71 (CH₂ of piperazine), 41.58 (CH₂ of piperazine), 38.05 (C_ε), 30.14 (C_β), 28.73 (C_δ), 21.32 (C_γ); ¹⁹F-NMR (DMSO-*d*₆) δ= -74.95 (s, TFA); MS (ESI⁺): m/z calculated for C₁₉H₂₉N₄O₂: 345.23 [M+H]⁺, found: 345.2.

N^ε-Acryloyl-L-lysine-4-(6-chloropyridin-2-yl)piperazide×2TFA (5v)



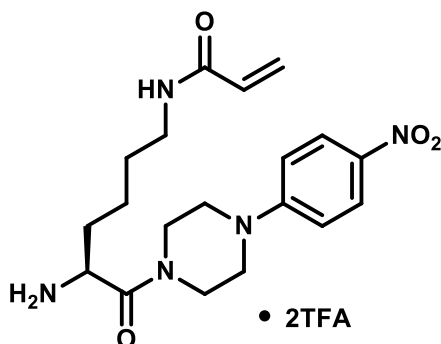
Compound **5v** (107 mg, yellow oil) was synthesised according to **GP VII** using compound **4v**. ¹H-NMR (DMSO-*d*₆) δ=8.17–8.08 (m, 3H, NH₃⁺), 8.06 (t, ³J=5.6 Hz, 1H, N_εH), 7.60 (dd, ³J=8.4, 7.5 Hz, 1H, H–4), 6.83 (d, ³J=8.4 Hz, 1H, H–3), 6.72 (d, ³J=7.4 Hz, 1H, H–5), 6.17 (dd, ³J=17.1, 10.1 Hz, 1H, CH=CH₂), 6.02 (dd, ³J=17.1 Hz, ²J=2.3 Hz, 1H, C=CHH), 5.53 (dd, ³J=10.1 Hz, ²J=2.3 Hz, 1H, C=CHH), 4.47–4.37 (m, 1H, C_αH), 3.73–3.41 (m, 8H, 4×CH₂ of piperazine), 3.20–3.04 (m, 2H, C_εH₂), 1.74–1.65 (m, 2H, C_βH₂), 1.51–1.22 (m, 4H, C_γH₂, C_δH₂); ¹³C-NMR (DMSO-*d*₆) δ=167.33 (CON), 164.50 (CON_ε), 158.43 (C–2), 158.15 (q, ²J_{C,F}=36.3 Hz, CO of TFA), 148.10 (C–6), 140.75 (C–4), 131.77 (CH₂=C), 124.87 (CH₂=C), 115.68 (psd, ¹J_{C,F}=293.0 Hz, CF₃ of TFA), 112.06 (C–5), 105.66 (C–3), 49.50 (C_α), 44.45 (CH₂ of piperazine), 44.23 (CH₂ of piperazine), 43.99 (CH₂ of piperazine), 41.27 (CH₂ of piperazine), 37.97 (C_ε), 30.03 (C_β), 28.67 (C_δ), 21.24 (C_γ); ¹⁹F-NMR (DMSO-*d*₆) δ= -74.77 (s, TFA); MS (ESI⁺): m/z calculated for C₁₈H₂₇ClN₅O₂: 380.18 [M(³⁵Cl)+H]⁺, found: 380.1.

N^ε-Acryloyl-L-lysine-4-(3-methylphenyl)piperazide×2TFA (5w)



Compound **5w** (54 mg, yellow oil) was synthesised according to **GP VII** using compound **4w**. **¹H-NMR** (DMSO-*d*₆) δ=8.15–8.02 (m, 4H, NH₃⁺, N_εH), 7.12 (t, ³*J*=7.8 Hz, 1H, H-5), 6.82–6.73 (m, 2H, 2×H of phenyl), 6.65 (d, ³*J*=7.3 Hz, 1H, H of phenyl), 6.18 (dd, ³*J*=17.1, 10.1 Hz, 1H, CH=CH₂), 6.03 (dd, ³*J*=17.1 Hz, ²*J*=2.3 Hz, 1H, C=CHH), 5.54 (dd, ³*J*=10.0 Hz, ²*J*=2.3 Hz, 1H, C=CHH), 4.48–4.37 (m, 1H, C_αH), 3.76–3.47 (m, 4H, 2×CH₂ of piperazine), 3.25–3.00 (m, 6H, 2×CH₂ of piperazine, C_εH₂), 2.26 (s, 3H, CH₃), 1.75–1.61 (m, 2H, C_βH₂), 1.52–1.21 (m, 4H, C_γH₂, C_δH₂); **¹³C-NMR** (DMSO-*d*₆) δ=167.11, 164.50, 158.03 (q, ²*J*_{C,F}=35.0 Hz, CO of TFA), 150.57, 138.10, 131.78 (CH₂=C), 128.83 (C-5), 124.87 (CH₂=C), 120.39 (C of phenyl), 116.63 (C of phenyl), 113.18 (C of phenyl), 49.44 (C_α), 48.74 (CH₂ of piperazine), 48.31 (CH₂ of piperazine), 44.69 (CH₂ of piperazine), 41.58 (CH₂ of piperazine), 38.00 (C_ε), 30.07 (C_β), 28.68 (C_δ), 21.36 (CH₃), 21.26 (C_γ); **¹⁹F-NMR** (DMSO-*d*₆) δ= -74.46 (s, TFA); MS (ESI⁺): *m/z* calculated for C₂₀H₃₁N₄O₂: 359.24 [M+H]⁺, found: 359.3.

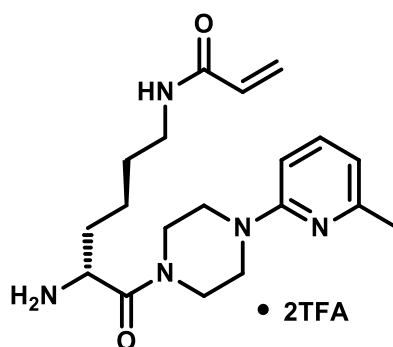
N^ε-Acryloyl-L-lysine-4-(4-nitrophenyl)piperazide×2TFA (5x)



Compound **5x** (73 mg, brown oil) was synthesised according to **GP VII** using compound **4x**. **¹H-NMR** (DMSO-*d*₆) δ=8.15–8.03 (m, 6H, H-3,5, NH₃⁺, N_εH), 7.09–7.03 (m, 2H, H-2,6), 6.17 (dd, ³*J*=17.1, 10.1 Hz, 1H, CH=CH₂), 6.02 (dd, ³*J*=17.1 Hz, ²*J*=2.3 Hz, 1H, C=CHH), 5.53 (dd, ³*J*=10.1 Hz, ²*J*=2.3 Hz, 1H, C=CHH), 4.47–4.40 (m, 1H, C_αH), 3.77–3.42 (m, 8H, 4×CH₂ of piperazine), 3.19–3.04 (m, 2H, C_εH₂), 1.74–1.65 (m, 2H, C_βH₂), 1.50–1.21 (m, 4H, C_γH₂, C_δH₂);

¹³C-NMR (DMSO-*d*₆) δ=167.45, 164.50, 158.03 (q, ²J_{C,F}=34.5 Hz, CO of TFA), 154.27, 137.25, 131.76 (CH₂=C), 125.69 (C-3,5), 124.89 (CH₂=C), 112.76 (C-2,6), 49.46 (C_α), 46.20 (CH₂ of piperazine), 45.64 (CH₂ of piperazine), 43.92 (CH₂ of piperazine), 41.20 (CH₂ of piperazine), 37.95 (C_ε), 29.99 (C_β), 28.69 (C_δ), 21.25 (C_γ); **¹⁹F-NMR** (DMSO-*d*₆) δ= -74.43 (s, TFA); MS (ESI⁺): m/z calculated for C₁₉H₂₈N₅O₄: 390.21 [M+H]⁺, found: 390.2.

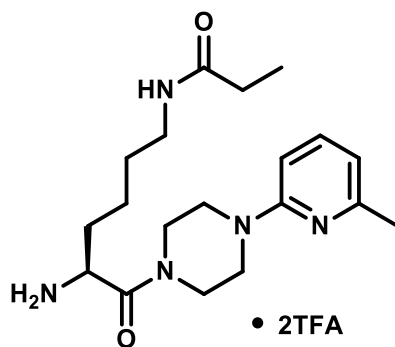
N^ε-Acryloyl-D-lysine-4-(6-methylpyridin-2-yl)piperazide×2TFA (5y)



Compound **5y** (196 mg, yellow oil) was synthesised according to **GP VII** using compound **4y**.

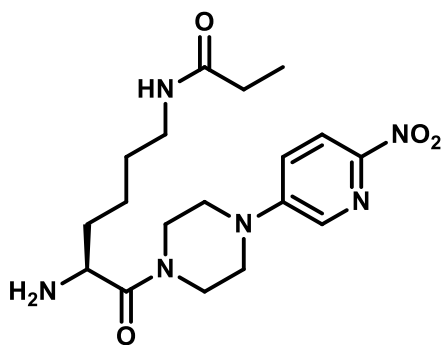
¹H-NMR (DMSO-*d*₆) δ=8.13 (d, ³J=4.5 Hz, 3H, NH₃⁺), 8.07 (t, ³J=5.6 Hz, 1H, NH), 7.66 (ps-t, ³J=7.6 Hz, 1H, H-4), 6.87 (d, ³J=8.6 Hz, 1H, H-3), 6.68 (d, ³J=7.2 Hz, 1H, H-5), 6.18 (dd, ³J=17.1, 10.1 Hz, 1H, CH=CH₂), 6.02 (dd, ³J=17.1 Hz, ²J=2.3 Hz, 1H, C=CHH), 5.53 (dd, ³J=10.1 Hz, ²J=2.3 Hz, 1H, C=CHH), 4.49–4.38 (m, 1H, C_αH), 3.77–3.41 (m, 8H, 4×CH₂ of piperazine), 3.22–3.01 (m, 2H, C_εH₂), 2.40 (s, 3H, CH₃), 1.75–1.64 (m, 2H, C_βH₂), 1.54–1.19 (m, 4H, C_γH₂, C_δH₂); **¹³C-NMR** (DMSO-*d*₆) δ=167.40 (CON), 164.52 (CON_ε), 158.18 (q, ²J_{C,F}=35.9 Hz, CO TFA), 131.79 (CH₂=C), 124.88 (CH₂=C), 115.77 (psd, ¹J_{C,F}=291.8 Hz, CF₃ of TFA), 112.86 (C-5), 49.48 (C_α), 45.27 (CH₂ of piperazine), 44.79 (CH₂ of piperazine), 44.13 (CH₂ of piperazine), 41.24 (CH₂ of piperazine), 37.97 (C_ε), 30.02 (C_β), 28.70 (C_δ), 21.24 (C_γ), signals for C-2,3,4,6 and CH₃ are not visible; **¹⁹F-NMR** (DMSO-*d*₆): δ= -74.72 (s, TFA); MS (ESI⁺): m/z calculated for C₁₉H₃₀N₅O₂: 360.24 [M+H]⁺, found: 360.2.

N^ε-Propionyl-L-lysine-4-(6-methylpyridin-2-yl)piperazide×2TFA (5z)



Compound **5z** (103 mg, colourless oil) was synthesised according to **GP VII** using compound **4z**. **¹H-NMR** (DMSO-*d*₆) δ=8.11 (d, ³*J*=3.7 Hz, 3H, NH₃⁺), 7.70 (t, ³*J*=5.6 Hz, 1H, N₆H), 7.55 (t, ³*J*=7.8 Hz, 1H, H-4), 6.75 (d, ³*J*=8.0 Hz, 1H), 6.62 (d, ³*J*=7.2 Hz, 1H), 4.46-4.37 (m, 1H, C_αH), 3.78-3.40 (m, 8H, 4×CH₂ of piperazine), 3.12-2.96 (m, 2H, C_εH₂), 2.35 (s, 3H, CH₃), 2.03 (q, ³*J*=7.6 Hz, 2H, -CH₂-CH₃), 1.78-1.63 (m, 2H, C_βH₂), 1.46-1.19 (m, 4H, C_δH₂, C_γH₂), 0.96 (t, ³*J*=7.6 Hz, 3H, CH₂-CH₃); **¹³C-NMR** (DMSO-*d*₆) δ=172.69 (CON_ε), 167.30 (C_αCON), 158.01 (q, ³*J*_{C,F}=34.3 Hz, CO of TFA), 112.73 (CH of pyridine), 49.52 (C_α), 44.96 (CH₂ of piperazine), 44.52 (CH₂ of piperazine), 44.31 (CH₂ of piperazine), 41.35 (CH₂ of piperazine), 37.85 (C_ε), 30.03 (C_β), 28.81 (C_δ), 28.49 (-CH₂-CH₃), 23.59 (-CH₃), 21.20 (C_γ), 9.94 (-CH₂-CH₃), signals for 4×C of pyridine are not visible; **¹⁹F-NMR** (DMSO-*d*₆): δ= -74.35 (s, TFA); MS (ESI⁺): *m/z* calculated for C₁₉H₃₂N₅O₂: 362.26 [M+H]⁺, found: 362.1.

N^ε-Propionyl-L-lysine-4-(6-nitropyridin-3-yl)piperazide (5aa)

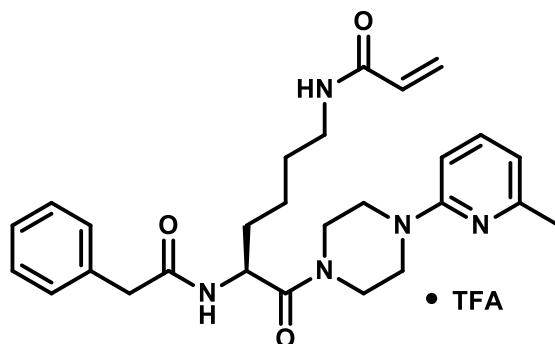


Compound **5aa** (yellow oil) was synthesised according to **GP VII** using compound **4aa**. After removal of volatile components in a N₂ stream the residue was dissolved in CH₂Cl₂ (20 mL) and the organic phase was washed with NaHCO₃ (2×10 mL). Then, the solvent was removed *in vacuo* and the residue was dissolved in a mixture of water-acetonitrile 3:1 (2 mL) and the solution was lyophilised. **¹H-NMR** (DMSO-*d*₆) δ=8.26 (d, ⁴*J*=3.0 Hz, 1H, H-2), 8.18 (d, ³*J*=9.2 Hz, 1H, H-5), 7.71 (t, ³*J*=5.2 Hz, 1H, N₆H), 7.49 (dd, ³*J*=9.3 Hz, ⁴*J*=3.1 Hz, 1H, H-4),

3.79-3.46 (m, 9H, C_αH, 4×CH₂ of piperazine), 3.08-2.92 (m, 2H, C_εH₂), 2.03 (q, ³J=7.6 Hz, 2H, -CH₂-CH₃), 1.57-1.47 (m, 1H, C_βHH), 1.45-1.19 (m, 5H, C_βHH, C_γH₂, C_δH₂), 0.96 (t, ³J=7.6 Hz, 3H, -CH₂-CH₃), signal for N_αH₂ is not visible; ¹³C-NMR (DMSO-*d*₆) δ=173.27, 172.59 (C_αCON, CON_ε), 157.75 (q, ²J_{C,F}=30.5 Hz, CO of TFA), 149.48 (C-6), 146.84 (C-3), 133.51 (C-2), 120.62 (C-4), 119.80 (C-5), 117.36 (q, ¹J_{C,F}=301.1 Hz, CF₃ of TFA), 49.95 (C_α), 46.07 (CH₂ of piperazine), 45.63 (CH₂ of piperazine), 43.63 (CH₂ of piperazine), 40.66 (CH₂ of piperazine), 38.24 (C_ε), 34.27 (C_β), 29.14 (C_δ), 28.49 (-CH₂-CH₃), 22.52 (C_γ), 9.99 (-CH₂-CH₃); MS (ESI⁺): m/z calculated for C₁₈H₂₉N₆O₄: 393.22 [M+H]⁺, found: 393.1.

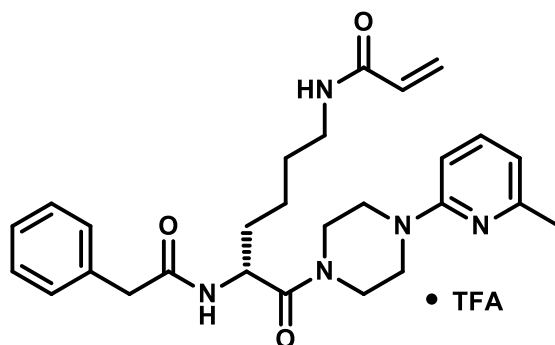
Final inhibitors 6-21

N^α-Phenylacetyl-*N*^ε-acryloyl-L-lysine-4-(6-methylpyridin-2-yl)piperazide×TFA (**6a**)²⁸



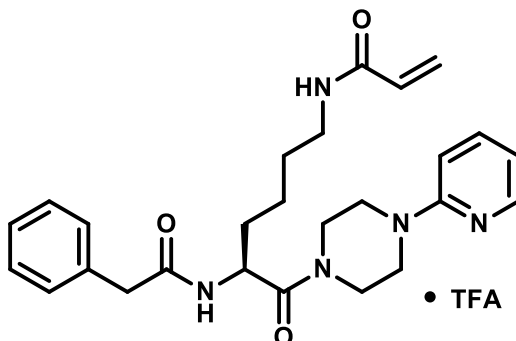
Compound **6a** (26 mg, 23%, white solid) was synthesised according to **GP VIII** using compound **5a** (0.17 mmol) and phenylacetyl chloride. **¹H-NMR** (DMSO-*d*₆) δ=8.40 (d, ³*J*=8.2 Hz, 1H, N_αH), 8.04 (t, ³*J*=5.4 Hz, 1H, N_εH), 7.70 (broad s, 1H, H-4 of pyridine), 7.32–7.22 (m, 4H, 4×H of phenyl), 7.21–7.13 (m, 1H, H of phenyl), 6.89 (broad s, 1H, H-3 of pyridine), 6.70 (d, ³*J*=6.9 Hz, 1H, H-5 of pyridine), 6.19 (dd, ³*J*=17.1, 10.1 Hz, 1H, CH=CH₂), 6.04 (dd, ³*J*=17.1 Hz, ²*J*=2.3 Hz, 1H, C=CHH), 5.54 (dd, ³*J*=10.1 Hz, ²*J*=2.3 Hz, 1H, C=CHH), 4.74–4.66 (m, 1H, C_αH), 3.76–3.38 (m, 10H, 4×CH₂ of piperazine, CH₂-phenyl), 3.14–3.02 (m, 2H, C_εH₂), 2.41 (s, 3H, CH₃), 1.71–1.60 (m, 1H, C_βHH), 1.59–1.47 (m, 1H, C_βHH), 1.46–1.35 (m, 2H, C_δH₂), 1.31–1.17 (m, 2H, C_γH₂); **¹³C-NMR** (DMSO-*d*₆) δ=170.16, 169.79, 164.42 (CON_ε), 136.35 (C-1 of phenyl), 131.85 (CH₂=C), 128.96 (2×C of phenyl), 128.13 (2×C of phenyl), 126.29 (C-4 of phenyl), 124.76 (CH₂=C), 112.72 (C-5 of phenyl), 48.16 (C_α), 45.45 (CH₂ of piperazine), 45.06 (CH₂ of piperazine), 44.05 (CH₂ of piperazine), 41.93 (CH₂-phenyl), 40.90 (CH₂ of piperazine), 38.27 (C_ε), 31.28 (C_β), 28.82 (C_δ), 22.56 (C_γ), signals for C-2,3,4,6 of pyridine and CH₃ are not visible; **¹⁹F-NMR** (DMSO-*d*₆) δ= -74.57 (s, TFA); MS (ESI⁺): *m/z* calculated for C₂₇H₃₆N₅O₃: 478.28 [M+H]⁺, found: 478.1.

***N*^α-Phenylacetyl-*N*^ε-acryloyl-D-lysine-4-(6-methylpyridin-2-yl)piperazide×TFA (6b)**



Compound **6b** (109 mg, 70%, yellow oil) was synthesised according to **GP VIII** using compound **5y** (0.28 mmol) and phenylacetyl chloride. **¹H-NMR** (DMSO-*d*₆) δ=8.40 (d, ³*J*=8.1 Hz, 1H, N_δH), 8.05 (t, ³*J*=5.6 Hz, 1H, N_εH), 7.79 (ps-t, ³*J*=7.7 Hz, 1H, H-4 of pyridine), 7.31–7.23 (m, 4H, 4×H of phenyl), 7.22–7.15 (m, 1H, H of phenyl), 6.98 (d, ³*J*=8.4 Hz, 1H, H-3 of pyridine), 6.75 (d, ³*J*=7.2 Hz, 1H, H-5 of pyridine), 6.19 (dd, ³*J*=17.1, 10.1 Hz, 1H, CH=CH₂), 6.04 (dd, ³*J*=17.1 Hz, ²*J*=2.3 Hz, 1H, C=CHH), 5.54 (dd, ³*J*=10.1 Hz, ²*J*=2.3 Hz, 1H, C=CHH), 4.74–4.66 (m, 1H, C_αH), 3.76–3.40 (m, 10H, 4×CH₂ of piperazine, CH₂-Phenyl), 3.13–3.02 (m, 2H, C_εH₂), 2.45 (s, 3H, CH₃), 1.70–1.60 (m, 1H, C_βHH), 1.59–1.47 (m, 1H, C_βHH), 1.47–1.34 (m, 2H, C_δH₂), 1.33–1.17 (m, 2H, C_γH₂); **¹³C-NMR** (DMSO-*d*₆) δ=170.25, 169.83, 164.43 (CON_ε), 158.34, 158.00, 136.35 (C-1 of phenyl), 131.85 (CH₂=C), 128.97 (2×C of phenyl), 128.14 (2×C of phenyl), 126.30 (C-4 of phenyl), 124.78 (CH₂=C), 112.83 (C-5 of pyridine), 48.18 (C_α), 45.68 (CH₂ of piperazine), 45.29 (CH₂ of piperazine), 43.90 (CH₂ of piperazine), 41.93 (CH₂-phenyl), 40.78 (CH₂ of piperazine), 38.27 (C_ε), 31.25 (C_β), 28.84 (C_δ), 22.56 (C_γ), signals for C-3,4 of pyridine and CH₃ are not visible; **¹⁹F-NMR** (DMSO-*d*₆) δ= -74.86 (s, TFA); MS (ESI⁺): *m/z* calculated for C₂₇H₃₆N₅O₃: 478.28 [M+H]⁺, found: 478.1.

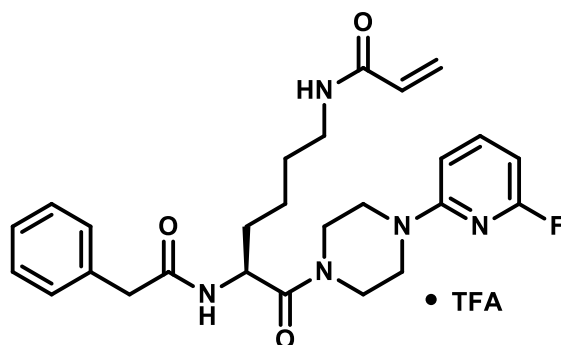
***N*^α-Phenylacetyl-*N*^ε-acryloyl-L-lysine-4-(pyridin-2-yl)piperazide×TFA (7a)**



Compound **7a** (22 mg, 83%, colourless oil) was synthesised according to **GP VIII** using compound **5s** (0.05 mmol) and phenylacetyl chloride. **¹H-NMR** (DMSO-*d*₆) δ=8.39 (d,

$^3J=8.1$ Hz, 1H, $N_\alpha H$), 8.08 (dd, $^3J=5.6$ Hz, $^2J=1.4$ Hz, 1H, H-6 of pyridine), 8.04 (t, $^3J=5.6$ Hz, 1H, $N_\epsilon H$), 7.86–7.79 (m, 1H, H-4 of pyridine), 7.30–7.09 (m, 6H, 5×H of phenyl, H-3 of pyridine), 6.87–6.82 (m, 1H, H-5 of pyridine), 6.18 (dd, $^3J=17.1$, 10.1 Hz, 1H, $CH=CH_2$), 6.03 (dd, $^3J=17.1$ Hz, $^2J=2.3$ Hz, 1H, $C=CHH$), 5.54 (dd, $^3J=10.1$ Hz, $^2J=2.3$ Hz, 1H, $C=CHH$), 4.74–4.67 (m, 1 H, $C_\alpha H$), 3.76–3.37 (m, 10H, 4× CH_2 of piperazine, CH_2 -phenyl), 3.11–3.04 (m, 2H, $C_\epsilon H_2$), 1.73–1.59 (m, 1H, $C_\beta HH$), 1.58–1.47 (m, 1H, $C_\beta HH$), 1.46–1.34 (m, 2H, $C_\delta H_2$), 1.34–1.14 (m, 2H, $C_\gamma H_2$); ^{13}C -NMR (DMSO- d_6) δ =170.23, 169.81, 164.42 (CON_ϵ), 136.34 (C-1 of phenyl), 131.85 ($CH_2=C$), 128.96 (2×C of phenyl), 128.13 (2×C of phenyl), 126.29 (C-4 of phenyl), 124.77 ($CH_2=C$), 113.08 (C-5 of pyridine), 48.17 (C_α), 45.15 (CH_2 of piperazine), 44.72 (CH_2 of piperazine), 43.85 (CH_2 of piperazine), 41.92 (CH_2 -phenyl), 40.74 (CH_2 of piperazine), 38.26 (C_ϵ), 31.26 (C_β), 28.83 (C_δ), 22.55 (C_γ), signals for C-2,3,4,6 of pyridine are not visible; ^{19}F -NMR (DMSO- d_6) δ = -74.65 (s, TFA); MS (ESI $^+$): m/z calculated for $C_{26}H_{34}N_5O_3$: 464.27 [M+H] $^+$, found: 464.2.

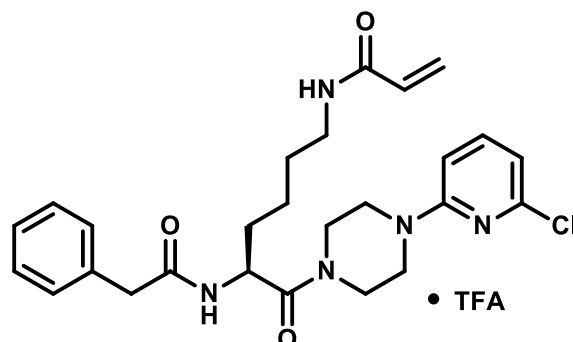
***N* $^\alpha$ -Phenylacetyl-*N* $^\epsilon$ -acryloyl-L-lysine-4-(6-fluoropyridin-2-yl)piperazide×TFA (7b)**



Compound **7b** (57 mg, 45%, yellow solid) was synthesised according to **GP VIII** using compound **5d** (0.21 mmol) and phenylacetyl chloride. 1H -NMR (DMSO- d_6) δ =8.38 (d, $^3J=8.3$ Hz, 1H, $N_\alpha H$), 8.03 (t, $^3J=5.3$ Hz, 1H, $N_\epsilon H$), 7.69 (ps-q, $J=8.3$ Hz, 1H, H-4 of pyridine), 7.32–7.22 (m, 4H, 4×H of phenyl), 7.22–7.13 (m, 1H, H of phenyl), 6.66 (dd, $^3J_{H,H}=8.2$ Hz, $^5J_{H,F}=2.5$ Hz, 1H, H-3 of pyridine), 6.30 (dd, $^3J_{H,H}=7.7$ Hz, $^3J_{H,F}=2.7$ Hz, 1H, H-5 of pyridine), 6.18 (dd, $^3J=17.1$, 10.1 Hz, 1H, $CH=CH_2$), 6.03 (dd, $^3J=17.1$ Hz, $^2J=2.3$ Hz, 1H, $C=CHH$), 5.53 (dd, $^3J=10.1$ Hz, $^2J=2.3$ Hz, 1H, $C=CHH$), 4.75–4.65 (m, 1H, $C_\alpha H$), 3.68–3.24 (m, 10H, 4× CH_2 of piperazine, CH_2 -phenyl), 3.13–3.01 (m, 2H, $C_\epsilon H_2$), 1.70–1.59 (m, 1H, $C_\beta HH$), 1.59–1.47 (m, 1H, $C_\beta HH$), 1.47–1.34 (m, 2H, $C_\delta H_2$), 1.31–1.19 (m, 2H, $C_\gamma H_2$); ^{13}C -NMR (DMSO- d_6) δ =170.00, 169.74, 164.40 (CON_ϵ), 161.94 (d, $^1J_{C,F}=233.2$ Hz, C-6 of pyridine), 157.64 (d, $^3J_{C,F}=15.7$ Hz, C-2 of pyridine), 142.68 (d, $^3J_{C,F}=8.2$ Hz, C-4 of pyridine), 136.36 (C-1 of phenyl), 131.85 ($CH_2=C$), 128.95 (2×C of phenyl), 128.12 (2×C of phenyl), 126.28 (C-4 of phenyl), 124.73 ($CH_2=C$), 103.59 (d, $^4J_{C,F}=3.9$ Hz, C-3 of pyridine), 95.64 (d, $^2J_{C,F}=37.0$ Hz,

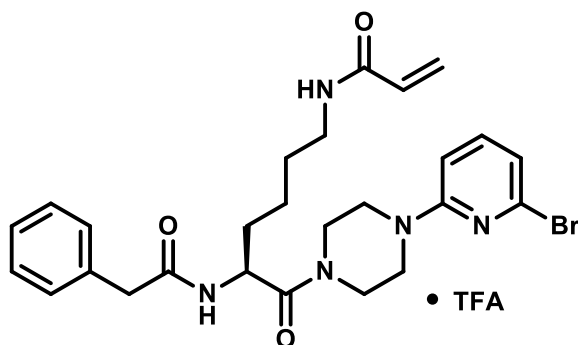
C–5 of pyridine), 48.12 (C_α), 44.56 (CH_2 of piperazine), 44.25 (CH_2 of piperazine), 44.10 (CH_2 of piperazine), 41.95 (CH_2 -phenyl), 41.01 (CH_2 of piperazine), 38.27 (C_ϵ), 31.35 (C_β), 28.80 (C_δ), 22.56 (C_γ); ^{19}F -NMR (DMSO- d_6) δ = -68.80– -68.88 (m, F-6), -74.70 (s, TFA); MS (ESI $^+$): m/z calculated for $\text{C}_{26}\text{H}_{33}\text{FN}_5\text{O}_3$: 482.26 $[\text{M}+\text{H}]^+$, found: 482.1.

***N* $^\alpha$ -Phenylacetyl-*N* $^\epsilon$ -acryloyl-L-lysine-4-(6-chloropyridin-2-yl)piperazide \times TFA (**7c**)**



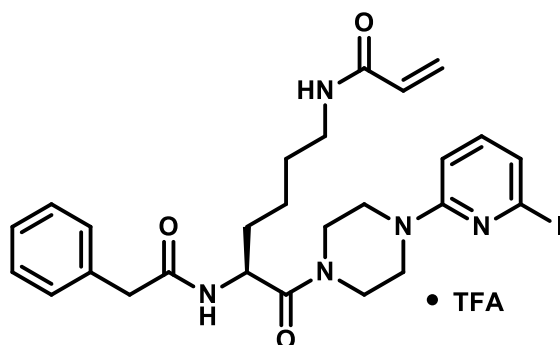
Compound **7c** (57 mg, 50%, light yellow oil) was synthesised according to **GP VIII** using compound **5v** (0.19 mmol) and phenylacetyl chloride. ^1H -NMR (DMSO- d_6) δ =8.38 (d, 3J =8.3 Hz, 1H, $N_\alpha\text{H}$), 8.03 (t, 3J =5.6 Hz, 1H, $N_\epsilon\text{H}$), 7.57 (dd, 3J =7.51, 8.38 Hz, 1H, H–4 of pyridine), 7.30–7.24 (m, 4H, 4 \times H of phenyl), 7.21–7.15 (m, 1H, H–4 of phenyl), 6.76 (d, 3J =8.4 Hz, 1H, H–3 of pyridine), 6.69 (d, 3J =7.4 Hz, 1H, H–5 of pyridine), 6.18 (dd, 3J =17.1, 10.1 Hz, 1H, $\text{CH}=\text{CH}_2$), 6.03 (dd, 3J =17.1 Hz, 2J =2.3 Hz, 1H, $\text{C}=\text{CHH}$), 5.53 (dd, 3J =10.1 Hz, 2J =2.3 Hz, 1H, $\text{C}=\text{CHH}$), 4.74–4.67 (m, 1H, $C_\alpha\text{H}$), 3.66–3.44 (m, 8H, 3 \times CH_2 of piperazine, CH_2 -phenyl), 3.43–3.28 (m, 2H, CH_2 of piperazine), 3.11–3.04 (m, 2H, $\text{C}_\epsilon\text{H}_2$), 1.70–1.59 (m, 1H, C_βHH), 1.59–1.47 (m, 1H, C_βHH), 1.46–1.34 (m, 2H, $\text{C}_\delta\text{H}_2$), 1.30–1.19 (m, 2H, $\text{C}_\gamma\text{H}_2$); ^{13}C -NMR (DMSO- d_6) δ =169.99, 169.74, 164.40 (CON_ϵ), 158.49 (C–2 of pyridine), 148.06 (C–6 of pyridine), 140.64 (C–4 of pyridine), 136.36 (C–1 of phenyl), 131.85 ($\text{CH}_2=\text{C}$), 128.95 (2 \times C of phenyl), 128.12 (2 \times C of phenyl), 126.29 (C–4 of phenyl), 124.74 ($\text{CH}_2=\text{C}$), 111.83 (C–5 of pyridine), 105.51 (C–3 of pyridine), 48.13 (C_α), 44.51 (CH_2 of piperazine), 44.26 (CH_2 of piperazine), 44.06 (CH_2 of piperazine), 41.95 (CH_2 -Phenyl), 41.03 (CH_2 of piperazine), 38.27 (C_ϵ), 31.35 (C_β), 28.80 (C_δ), 22.57 (C_γ); ^{19}F -NMR (DMSO- d_6) δ = -74.82 (s, TFA); MS (ESI $^+$): m/z calculated for $\text{C}_{26}\text{H}_{33}\text{ClN}_5\text{O}_3$: 498.23 $[\text{M}(^{35}\text{Cl})+\text{H}]^+$, found: 498.0.

***N*^α-Phenylacetyl-*N*^ε-acryloyl-L-lysine-4-(6-bromopyridin-2-yl)piperazide×TFA (7d)**



Compound **7d** (16 mg, 28%, colourless solid) was synthesised according to **GP VIII** using compound **5r** (0.09 mmol) and phenylacetyl chloride. **¹H-NMR** (DMSO-*d*₆) δ=8.38 (d, ³*J*=8.2 Hz, 1H, N_αH), 8.03 (t, ³*J*=5.4 Hz, 1H, N_εH), 7.46 (dd, ³*J*=8.1, 7.7 Hz, 1H, H-4 of pyridine), 7.31-7.22 (m, 4H, H-2,3,5,6 of phenyl), 7.21-7.13 (m, 1H, H-4 of phenyl), 6.82 (d, ³*J*=7.4 Hz, 1H, H of pyridine), 6.79 (d, ³*J*=8.4 Hz, 1H, H of pyridine), 6.18 (dd, ³*J*=17.1, 10.0 Hz, 1H, CH=CH₂), 6.03 (dd, ³*J*=17.1 Hz, ²*J*=2.3 Hz, 1H, CH=CHH), 5.53 (dd, ³*J*=10.1 Hz, ²*J*=2.3 Hz, 1H, CH=CHH), 4.74-4.66 (m, 1H, C_αH), 3.67-3.25 (m, 10H, 4×CH₂ of piperazine, CH₂-phenyl), 3.13-3.03 (m, 2H, C_εH₂), 1.71-1.58 (m, 1H, C_βHH), 1.58-1.46 (m, 1H, C_βHH), 1.46-1.34 (m, 2H, C_δH₂), 1.33-1.19 (m, 2H, C_γH₂); **¹³C-NMR** (DMSO-*d*₆) δ=169.98, 169.73, 164.39 (C_αCON, CON_α, CON_ε), 158.59 (C-2 of pyridine), 140.43 (C-4 of pyridine), 139.08 (C-6 of pyridine), 136.35 (C-1 phenyl), 131.84 (CH₂=C), 128.94 (2×CH of phenyl), 128.12 (2CH of phenyl), 126.28 (C-4 of phenyl), 124.73 (CH₂=C), 115.69 (CH of pyridine), 105.76 (CH of pyridine), 48.12 (C_α), 44.49 (CH₂ of piperazine), 44.25 (CH₂ of piperazine), 44.06 (CH₂ of piperazine), 41.94 (CH₂-phenyl), 41.02 (CH₂ of piperazine), 38.27 (C_ε), 31.35 (C_β), 28.79 (C_δ), 22.57 (C_γ); MS (ESI⁺): *m/z* calculated for C₂₆H₃₃BrN₅O₃: 542.18 [M(⁷⁹Br)+H]⁺, found: 542.2.

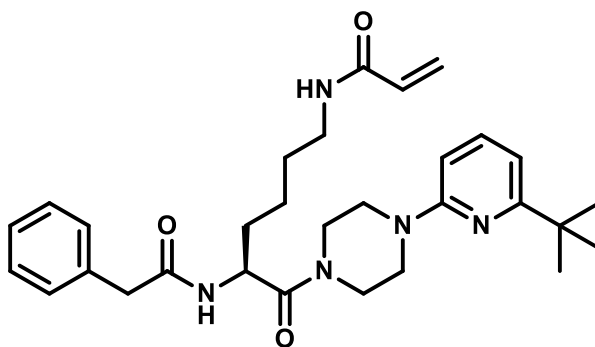
***N*^α-Phenylacetyl-*N*^ε-acryloyl-L-lysine-4-(6-iodopyridin-2-yl)piperazide×TFA (7e)**



Compound **7e** (15 mg, 50%, yellow solid) was synthesised according to **GP VIII** using compound **5p** (0.04 mmol) and phenylacetyl chloride. **¹H-NMR** (DMSO-*d*₆) δ=8.37 (d,

$^3J=8.3$ Hz, 1H, $N_\alpha H$), 8.03 (t, $^3J=5.6$ Hz, 1H, $N_\epsilon H$), 7.32–7.14 (m, 6H, 5×H of phenyl, H–4 of pyridine), 7.05 (d, $^3J=7.3$ Hz, 1H, H–5 of pyridine), 6.79 (d, $^3J=8.4$ Hz, 1H, H–3 of pyridine), 6.18 (dd, $^3J=17.1$, 10.1 Hz, 1H, $CH=CH_2$), 6.04 (dd, $^3J=17.1$ Hz, $^2J=2.3$ Hz, 1H, $C=CHH$), 5.54 (dd, $^3J=10.1$ Hz, $^2J=2.3$ Hz, 1H, $C=CHH$), 4.74–4.65 (m, 1H, $C_\alpha H$), 3.64–3.24 (m, 10H, 4× CH_2 of piperazine, CH_2 -phenyl), 3.13–3.03 (m, 2H, $C_\epsilon H_2$), 1.69–1.59 (m, 1H, $C_\beta HH$), 1.58–1.46 (m, 1H, $C_\beta HH$), 1.46–1.35 (m, 2H, $C_\delta H_2$), 1.32–1.20 (m, 2H, $C_\gamma H_2$); ^{13}C -NMR (DMSO- d_6) δ =169.96, 169.74, 164.40 (CON_ϵ), 158.59 (C–2 of pyridine), 139.45 (C–4 of pyridine), 136.36 (C–1 of phenyl), 131.85 ($CH_2=C$), 128.95 (2×C of phenyl), 128.13 (2×C of phenyl), 126.29 (C–4 of phenyl), 124.75 ($CH_2=C$), 123.05 (C–5 of pyridine), 116.19 (C–6 of pyridine), 106.04 (C–3 of pyridine), 48.13 (C_α), 44.46 (CH_2 of piperazine), 44.26 (CH_2 of piperazine), 44.04 (CH_2 of piperazine), 41.96 (CH_2 -phenyl), 41.04 (CH_2 of piperazine), 38.28 (C_ϵ), 31.36 (C_β), 28.80 (C_δ), 22.58 (C_γ); MS (ESI $^+$): m/z calculated for $C_{26}H_{33}N_5O_3$: 590.16 $[M+H]^+$, found: 590.0.

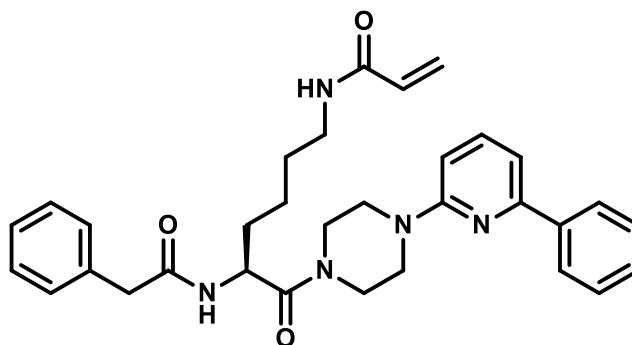
***N*^ϵ-Phenylacetyl-*N*^ϵ-acryloyl-L-lysine-4-(6-*tert*-butylpyridin-2-yl)piperazide (7f)**



Compound **7f** (16 mg, 27%, colourless solid) was synthesised according to **GP VIII** using compound **5n** (0.09 mmol) and phenylacetyl chloride. To separate compound **7f** from its *N*^ϵ-trifluoroacetyl analogue, which could not be separated by RP-HPLC, the product was finally purified by column chromatography (ethyl acetate). 1H -NMR ($CDCl_3$) δ =7.60 (dd, $^3J=8.3$, 7.8 Hz, 1H, H-4 of pyridine), 7.38-7.22 (m, 5H, H-2,3,4,5,6 of phenyl), 6.80 (d, $^3J=7.5$ Hz, 1H, H of pyridine), 6.69 (d, $^3J=7.8$ Hz, 1H, $N_\alpha H$), 6.60 (d, $^3J=8.5$ Hz, 1H, H of pyridine), 6.33-6.26 (m, 1H, $N_\epsilon H$), 6.26 (dd, $^3J=17.0$ Hz, $^2J=1.3$ Hz, 1H, $CH=CHH$), 6.08 (dd, $^3J=17.0$, 10.3 Hz, 1H, $CH=CH_2$), 5.62 (dd, $^3J=10.3$ Hz, $^2J=1.3$ Hz, 1H, $CH=CHH$), 4.93 (td, $^3J=8.4$, 4.4 Hz, 1H, $C_\alpha H$), 3.89-3.43 (m, 8H, 4× CH_2 of piperazine), 3.60 (s, 2H, CH_2 -phenyl), 3.35-3.22 (m, 2H, $C_\epsilon H_2$), 1.75-1.50 (m, 4H $C_\beta H_2$, $C_\delta H_2$), 1.36 (s, 9H, 3× CH_3 of *tert*-butyl), 1.35-1.21 (m, 2H, $C_\gamma H_2$); ^{13}C -NMR ($CDCl_3$) δ =171.82, 170.41, 166.57, 166.19, 156.93, 140.37 (C-4 of pyridine), 134.37, 130.68 ($CH_2=CH$), 129.45 (2×CH of phenyl), 129.16 (2×CH of phenyl), 127.67 (C-4 of phenyl), 126.84 ($CH_2=CH$), 110.14 (CH of pyridine), 106.39 (CH of pyridine), 48.65 (C_α), 46.59 (CH_2 of piperazine), 46.21 (CH_2 of piperazine), 45.14 (CH_2 of piperazine), 43.64 (CH_2 -phenyl), 41.76

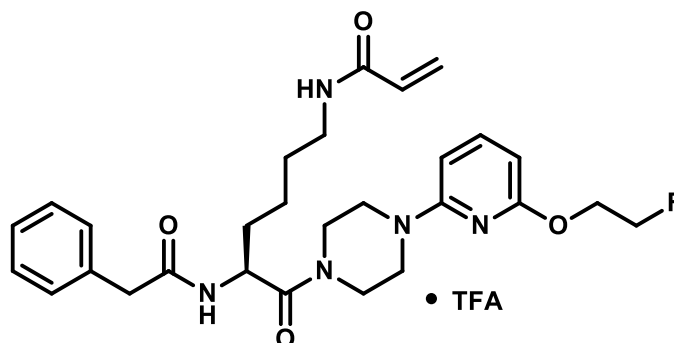
(CH₂ of piperazine), 39.36 (C_ε), 37.32 (quart. C of *tert*-butyl), 32.79 (C_β), 29.85 (3×CH₃ *tert*-butyl), 28.32 (C_δ), 22.34 (C_γ); MS (ESI⁺): *m/z* calculated for C₃₀H₄₂N₅O₃: 520.33 [M+H]⁺, found: 520.4.

***N*⁶-Phenylacetyl-*N*⁷-acryloyl-L-lysine-4-(6-phenylpyridin-2-yl)piperazide (7g)**



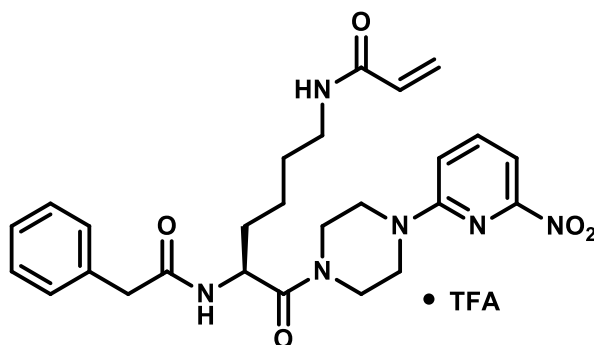
Compound **7g** (23 mg, 34%, white solid) was synthesised according to **GP VIII** using compound **5q** (0.10 mmol) and phenylacetyl chloride. To separate compound **7g** from its *N*⁶-trifluoroacetyl analogue **16c**, which could not be separated by RP-HPLC, the product was finally purified by column chromatography (ethyl acetate). **¹H-NMR** (CDCl₃) δ=7.92 (dd, ³*J*=8.0 Hz, ⁴*J*=1.4 Hz, 2H, H-2,6 of phenyl), 7.67 (dd, ³*J*=8.3, 7.7 Hz, 1H, H-4 of pyridine), 7.49-7.38 (m, 3H, H-3,4,5 of phenyl), 7.38-7.32 (m, 2H, H-2,6 of benzyl), 7.31-7.24 (m, 3H, H-3,4,5 of benzyl), 7.15 (d, ³*J*=7.5 Hz, 1H, H-5 of pyridine), 6.76 (d, ³*J*=7.8 Hz, 1H, N_H), 6.68 (d, ³*J*=8.5 Hz, 1H, H-3 of pyridine), 6.26 (dd, ³*J*=17.0 Hz, ²*J*=1.2 Hz, 2H, CH=CHH, N_H), 6.06 (dd, ³*J*=17.0, 10.3 Hz, 1H, CH=CH₂), 5.62 (dd, ³*J*=10.3 Hz, ²*J*=1.2 Hz, 1H, CH=CHH), 4.96 (td, ³*J*=8.4 Hz, ⁴*J*=4.2 Hz, 1H, C_αH), 3.89-3.62 (m, 8H, 4×CH₂ of piperazine), 3.61 (s, 2H, CH₂-benzyl), 3.36-3.21 (m, 2H, C_εH₂), 1.75-1.45 (m, 4H, C_βH₂, C_δH₂), 1.39-1.28 (m, 2H, C_γH₂); **¹³C-NMR** (CDCl₃) δ=171.88, 170.40, 166.59, 157.66, 154.81, 139.86 (C-4 of pyridine), 137.96, 134.35, 130.61 (CH=CH₂), 129.54 (C-4 phenyl), 129.44 (2×C of benzyl), 129.16 (2×C of benzyl), 128.78 (C-3,5 of phenyl), 127.67 (C-4 of benzyl), 127.20 (C-2,6 of phenyl), 126.92 (CH=CH₂), 111.38 (C-5 of pyridine), 106.81 (C-3 of pyridine), 48.66 (C_α), 45.87 (CH₂ of piperazine), 45.68 (CH₂ of piperazine), 45.25 (CH₂ of piperazine), 43.63 (CH₂-phenyl), 41.95 (CH₂ of piperazine), 39.36 (C_ε), 32.80 (C_β), 28.32 (C_δ), 22.32 (C_γ); MS (ESI⁺): *m/z* calculated for C₃₂H₃₈N₅O₃: 540.30 [M+H]⁺, found: 540.3.

***N*^α-Phenylacetyl-*N*^ε-acryloyl-L-lysine-4-(6-(2-fluoroethoxy)pyridin-2-yl)piperazide×TFA
(7h)**



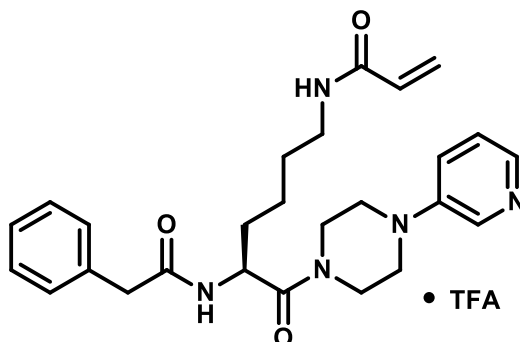
Compound **7h** (7 mg, 42%, white solid) was synthesised according to **GP VIII** using compound **5o** (0.025 mmol) and phenylacetyl chloride. **¹H-NMR** (CDCl₃) δ=7.45 (t, ³J=8.0 Hz, 1H, H-4 of pyridine), 7.38-7.24 (m, 5H, H-2,3,4,5,6 of phenyl), 6.81 (d, ³J=7.9 Hz, N_aH), 6.27 (dd, ³J=17.0 Hz, ²J=1.2 Hz, 1H, CH=CHH), 6.26-6.17 (m, 3H, H-3,5 of pyridine, N_εH), 6.07 (dd, ³J=17.0, 10.4 Hz, 1H, CH=CH₂), 5.66 (dd, ³J=10.4 Hz, ²J=1.2 Hz, 1H, CH=CHH), 4.96 (td, ³J=8.7, 4.1 Hz, 1H, C_αH), 4.73 (dm, ²J_{H,F}=48.0 Hz, 2H, CH₂-CH₂-F), 4.51 (dm, ³J_{H,F}=28.0 Hz, 2H, CH₂-CH₂-F), 3.81-3.40 (m, 8H, 4×CH₂ of piperazine), 3.62 (s, 2H, CH₂-phenyl), 3.37-3.20 (m, 2H, C_εH₂), 1.79-1.43 (m, 4H, C_βH₂, C_δH₂), 1.39-1.22 (m, 2H, C_γH₂); **¹³C-NMR** (CDCl₃) δ=172.32, 170.27, 166.90, 162.26, 157.40, 140.82 (C-4 of pyridine), 134.07, 130.36 (CH₂=C), 129.45 (2×CH of phenyl), 129.23 (2×CH of phenyl), 127.81 (C-4 of phenyl), 127.37 (CH₂=C), 100.16 (CH of pyridine), 99.06 (CH of pyridine), 82.18 (d, ¹J_{C,F}=169.4 Hz, CH₂-CH₂-F), 64.58 (d, ¹J_{C,F}=20.5 Hz, CH₂-CH₂-F), 48.69 (C_α), 45.43 (CH₂ of piperazine), 54.37 (CH₂ of piperazine), 45.19 (CH₂ of piperazine), 43.57 (CH₂-phenyl), 42.08 (CH₂ of piperazine), 39.51 (C_ε), 32.86 (C_β), 28.25 (C_δ), 22.35 (C_γ); **¹⁹F-NMR** (CDCl₃) δ= -75.90 (s); MS (ESI⁺): m/z calculated for C₂₈H₃₇FN₅O₄: 526.28 [M+H]⁺, found: 526.3.

***N*^α-Phenylacetyl-*N*^ε-acryloyl-L-lysine-4-(6-nitropyridin-2-yl)piperazide×TFA (7i)**



Compound **7i** (18 mg, 59%, yellow solid) was synthesised according to **GP VIII** using compound **5m** (0.05 mmol) and phenylacetyl chloride. **¹H-NMR** (DMSO-*d*₆) δ=8.39 (d, ³*J*=8.2 Hz, 1H, N_δH), 8.03 (t, ³*J*=5.5 Hz, 1H, N_εH), 7.91 (dd, ³*J*=8.5, 7.6 Hz, 1H, H-4 of pyridine), 7.49 (d, ³*J*=7.5 Hz, 1H, H-5 of pyridine), 7.30–7.23 (m, 5H, 4×H of phenyl, H-3 of pyridine), 7.20–7.14 (m, 1H, H of phenyl), 6.18 (dd, ³*J*=17.1, 10.1 Hz, 1H, CH=CH₂), 6.03 (dd, ³*J*=17.1 Hz, ²*J*=2.3 Hz, 1H, C=CHH), 5.53 (dd, ³*J*=10.1 Hz, ²*J*=2.3 Hz, 1H, C=CHH), 4.75–4.67 (m, 1H, C_αH), 3.69–3.40 (m, 10H, 4×CH₂ of piperazine, CH₂-phenyl), 3.12–3.04 (m, 2H, C_εH₂), 1.72–1.60 (m, 1H, C_βHH), 1.59–1.48 (m, 1H, C_βHH), 1.47–1.34 (m, 2H, C_δH₂), 1.32–1.20 (m, 2H, C_γH₂); **¹³C-NMR** (DMSO-*d*₆) δ=170.08, 169.76, 164.39, 157.22, 155.22, 141.02 (C-4 of pyridine), 136.36, 131.85 (CH₂=C), 128.95 (2×C of phenyl), 128.12 (2×C of phenyl), 126.28 (C-4 of phenyl), 124.74 (CH₂=C), 113.12 (C-3 of pyridine), 105.61 (C-5 of pyridine), 48.16 (C_α), 44.38 (CH₂ of piperazine), 44.20 (CH₂ of piperazine), 43.97 (CH₂ of piperazine), 41.95 (CH₂-phenyl), 40.99 (CH₂ of piperazine), 38.28 (C_ε), 31.34 (C_β), 28.81 (C_δ), 22.58 (C_γ); **¹⁹F-NMR** (DMSO-*d*₆) δ= -75.72 (s, TFA); MS (ESI⁺): *m/z* calculated for C₂₆H₃₃N₆O₅: 509.25 [M+H]⁺, found: 509.3.

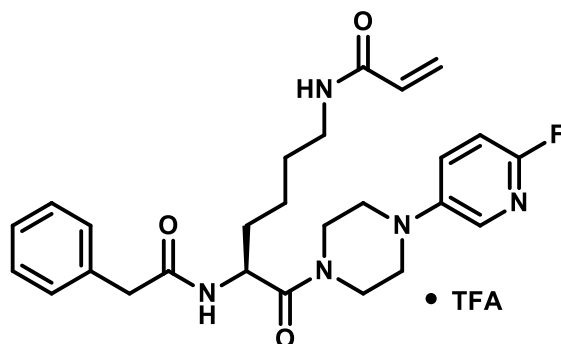
***N*^α-Phenylacetyl-*N*^ε-acryloyl-L-lysine-4-(pyridin-3-yl)piperazide×TFA (8a)**



Compound **8a** (49 mg, 42%, colourless solid) was synthesised according to **GP VIII** using compound **5i** (0.20 mmol) and phenylacetyl chloride. **¹H-NMR** (DMSO-*d*₆) δ=8.43-8.39 (m, 2H,

N_α H, H-2 of pyridine), 8.22 (d, $^3J=5.2$ Hz, 1H, H-6 of pyridine), 8.08-7.94 (m, 2H, N_ϵ H, H of pyridine), 7.88-7.76 (m, 1H, H of pyridine), 7.29-7.22 (m, 4H, H-2,3,5,6 of phenyl), 7.20-7.11 (m, 1H, H-4 of phenyl), 6.18 (dd, $^3J=17.1$, 10.1 Hz, 1H, $CH=CH_2$), 6.03 (dd, $^3J=17.1$ Hz, $^2J=2.3$ Hz, 1H, $CH=CHH$), 5.54 (dd, $^3J=10.1$ Hz, $^2J=2.3$ Hz, 1H, $CH=CHH$), 4.75-4.64 (m, 1H, C_α H), 3.81-3.15 (m, 10H, $4\times CH_2$ of piperazine, CH_2 -phenyl), 3.11-3.05 (m, 2H, $C_\epsilon H_2$), 1.74-1.60 (m, 1H, $C_\beta HH$), 1.60-1.48 (m, 1H, $C_\beta HH$), 1.46-1.34 (m, 2H, $C_\delta H_2$), 1.34-1.13 (m, 2H, $C_\gamma H_2$); ^{13}C -NMR (DMSO- d_6) δ =170.07 (C_α CON), 169.78 (CON_α), 164.41 (CON_ϵ), 158.15 (q, $^2J_{C,F}=35.6$ Hz, CO of TFA), 147.87 (C-3 of pyridine), 136.36 (C-1 of phenyl), 131.85 ($CH=CH_2$), 130.70 (C-6 of pyridine), 128.95 ($2\times CH$ of phenyl), 128.74 (CH of pyridine), 128.13 ($2\times CH$ of phenyl), 128.05 (C-2 of pyridine), 126.83 (CH of pyridine), 126.28 (C-4 of phenyl), 124.75 ($CH=CH_2$), 48.06 (C_α), 46.48 (CH_2 of piperazine), 46.09 (CH_2 of piperazine), 43.93 (CH_2 of piperazine), 41.95 (CH_2 -phenyl), 40.68 (CH_2 of piperazine), 38.26 (C_ϵ), 31.27 (C_β), 28.84 (C_δ), 22.57 (C_γ); MS (ESI $^+$): m/z calculated for $C_{26}H_{34}N_5O_3$: 464.27 $[M+H]^+$, found: 464.4.

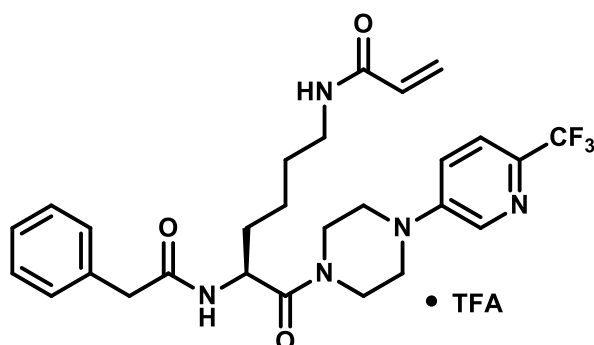
***N* $^\epsilon$ -Phenylacetyl-*N* $^\epsilon$ -acryloyl-L-lysine-4-(6-fluoropyridin-3-yl)piperazide \times TFA (**8b**)**



Compound **8b** (61 mg, 51%, brownish oil) was synthesised according to **GP VIII** using compound **5j** (0.20 mmol) and phenylacetyl chloride. 1H -NMR (DMSO- d_6) δ =8.39 (d, $^3J=8.4$ Hz, 1H, N_α H), 8.03 (t, $^3J=5.6$ Hz, 1H, N_ϵ H), 7.80 (dd, $^4J_{H,H}=2.9$ Hz, $^5J_{H,H}=1.7$ Hz, 1H, H-2 of pyridine), 7.57 (ddd, $^3J_{H,H}=9.1$ Hz, $^4J_{H,F}=7.1$ Hz, $^4J_{H,H}=3.2$ Hz, 1H, H-4 of pyridine), 7.30-7.23 (m, 4H, $4\times H$ of phenyl), 7.20-7.12 (m, 1H, H of phenyl), 7.04 (dd, $^3J_{H,H}=9.0$ Hz, $^3J_{H,F}=3.5$ Hz, 1H, H-5 of pyridine), 6.18 (dd, $^3J=17.1$, 10.1 Hz, 1H, $CH=CH_2$), 6.03 (dd, $^3J=17.1$ Hz, $^2J=2.3$ Hz, 1H, $C=CHH$), 5.54 (dd, $^3J=10.0$ Hz, $^2J=2.3$ Hz, 1H, $C=CHH$), 4.75-4.66 (m, 1H, C_α H), 3.72-3.40 (m, 6H, $2\times CH_2$ of piperazine, CH_2 -phenyl), 3.18-2.84 (m, 6H, $2\times CH_2$ of piperazine, $C_\epsilon H_2$), 1.71-1.59 (m, 1H, $C_\beta HH$), 1.58-1.46 (m, 1H, $C_\beta HH$), 1.46-1.33 (m, 2H, $C_\delta H_2$), 1.33-1.17 (m, 2H, $C_\gamma H_2$); ^{13}C -NMR (DMSO- d_6) δ =169.75, 169.71, 164.39 (CON_ϵ), 156.92 (d, $^1J_{C,F}=228.5$ Hz, C-6 of pyridine), 145.26 (d, $^4J_{C,F}=3.9$ Hz, C-3 of pyridine), 136.35 (C-1 of phenyl), 134.02 (d, $^3J_{C,F}=15.3$ Hz, C-2 of pyridine), 131.85 ($CH_2=C$), 129.63 (d, $^3J_{C,F}=7.2$ Hz, C-4 of pyridine), 128.94 ($2\times C$ of phenyl), 128.12 ($2\times C$ of phenyl), 126.28 (C-4

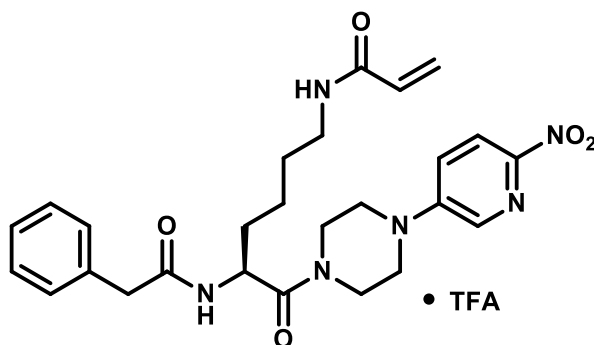
of phenyl), 124.74 (CH₂=C), 109.04 (d, ²J_{C,F}=39.6 Hz, C-5 of pyridine), 48.77 (CH₂ of piperazine), 48.37 (CH₂ of piperazine), 47.98 (C_α), 44.50 (CH₂ of piperazine), 41.97 (CH₂-phenyl), 41.10 (CH₂ of piperazine), 38.29 (C_ε), 31.37 (C_β), 28.81 (C_δ), 22.59 (C_γ); ¹⁹F-NMR (DMSO-*d*₆) δ= -80.13 (s, F-6), -74.58 (s, TFA); MS (ESI⁺): *m/z* calculated for C₂₆H₃₃FN₅O₃: 482.26 [M+H]⁺, found: 482.1.

***N*^α-Phenylacetyl-*N*^ε-acryloyl-L-lysine-4-(6-trifluoromethylpyridin-3-yl)piperazide•TFA (8c)**



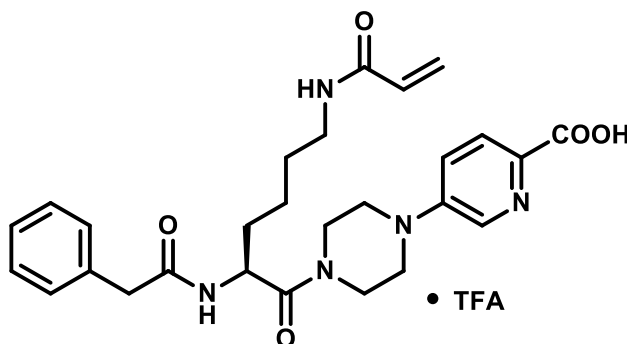
Compound **8c** (58 mg, 80%, yellow solid) was synthesised according to **GP VIII** using compound **5k** (0.11 mmol) and phenylacetyl chloride. ¹H-NMR (DMSO-*d*₆) δ=8.44–8.36 (m, 2H, N_H, H-2 of pyridine), 8.03 (t, ³J=5.6 Hz, 1H, N_H), 7.66 (d, ³J=8.8 Hz, 1H, H-5 of pyridine), 7.40 (dd, ³J=8.8 Hz, ⁴J=2.8 Hz, 1H, H-4 of pyridine), 7.29–7.21 (m, 4H, 4×H of phenyl), 7.20–7.11 (m, 1H, H-4 of phenyl), 6.18 (dd, ³J=17.1, 10.1 Hz, 1H, CH=CH₂), 6.03 (dd, ³J=17.1 Hz, ²J=2.3 Hz, 1H, C=CHH), 5.53 (dd, ³J=10.1 Hz, ²J=2.3 Hz, 1H, C=CHH), 4.75–4.66 (m, 1H, C_αH), 3.74–3.31 (m, 8H, 3×CH₂ of piperazine, CH₂-phenyl), 3.29–3.12 (m, 2H, CH₂ of piperazine), 3.12–3.03 (m, 2H, C_εH₂), 1.73–1.60 (m, 1H, C_βHH), 1.60–1.46 (m, 1H, C_βHH), 1.46–1.33 (m, 2H, C_δH₂), 1.32–1.18 (m, 2H, C_γH₂); ¹³C-NMR (DMSO-*d*₆) δ=169.92, 169.74, 164.39, 158.21 (q, ²J_{C,F}=37.5 Hz, CO of TFA), 147.94 (C-3 of pyridine), 136.91 (C-2 of pyridine), 136.35 (C-1 of phenyl), 131.85 (CH₂=C), 128.94 (2×C of phenyl), 128.12 (2×C of phenyl), 126.28 (C-4 of phenyl), 124.74 (CH₂=C), 122.36 (q, ¹J_{C,F}=272.2 Hz, CF₃ of pyridine), 120.91 (d, ³J_{C,F}=2.2 Hz, C-5 of pyridine), 120.77 (C-4 of pyridine), 48.04 (C_α), 46.54 (CH₂ of piperazine), 46.17 (CH₂ of piperazine), 44.12 (CH₂ of piperazine), 41.96 (CH₂-phenyl), 40.85 (CH₂ of piperazine), 38.28 (C_ε), 31.33 (C_β), 28.82 (C_δ), 22.59 (C_γ); ¹⁹F-NMR (DMSO-*d*₆) δ= -64.89 (s, CF₃ of pyridine), -74.99 (s, TFA); MS (ESI⁺): *m/z* calculated for C₂₇H₃₃F₃N₅O₃: 532.25 [M+H]⁺, found: 532.2.

***N*^α-Phenylacetyl-*N*^ε-acryloyl-L-lysine-4-(6-nitropyridin-3-yl)piperazide×TFA (8d)**



Compound **8d** (59 mg, 70%, orange solid) was synthesised according to **GP VIII** using compound **5b** (0.16 mmol) and phenylacetyl chloride. ¹H-NMR (DMSO-*d*₆) δ=8.41 (d, ³*J*=8.3 Hz, 1H, N_δH), 8.22 (d, ⁴*J*=3.0 Hz, 1H, H-2 of pyridine), 8.17 (d, ³*J*=9.2 Hz, 1H, H-5 of pyridine), 8.03 (t, ³*J*=5.6 Hz, 1H, N_εH), 7.44 (dd, ³*J*=9.3 Hz, ²*J*=3.1 Hz, 1H, H-4 of pyridine), 7.30–7.24 (m, 4H, 4×H of phenyl), 7.22–7.12 (m, 1H, H of phenyl), 6.18 (dd, ³*J*=17.1, 10.1 Hz, 1H, CH=CH₂), 6.03 (dd, ³*J*=17.1 Hz, ²*J*=2.3 Hz, 1H, C=CHH), 5.54 (dd, ³*J*=10.1 Hz, ²*J*=2.3 Hz, 1H, C=CHH), 4.74–4.66 (m, 1H, C_αH), 3.78–3.26 (m, 10H, 4×CH₂ of piperazine, CH₂ of phenyl), 3.12–3.01 (m, 2H, C_εH₂), 1.73–1.59 (m, 1H, C_βHH), 1.59–1.47 (m, 1H, C_βHH), 1.47–1.33 (m, 2H, C_δH₂), 1.33–1.18 (m, 2H, C_γH₂); ¹³C-NMR (DMSO-*d*₆) δ=170.10, 169.78, 164.40 (CON_ε), 149.43, 146.86, 136.34 (C-1 of phenyl), 133.52 (C-2 of pyridine), 131.85 (CH₂=C), 128.95 (2×C of phenyl), 128.13 (2×C of phenyl), 126.30 (C-4 of phenyl), 124.76 (CH₂=C), 120.63 (C-4 of pyridine), 119.77 (C-5 of pyridine), 48.09 (C_α), 45.94 (CH₂ of piperazine), 45.58 (CH₂ of piperazine), 43.88 (CH₂ of piperazine), 41.95 (CH₂ of phenyl), 40.76 (CH₂ of piperazine), 38.28 (C_ε), 31.28 (C_β), 28.83 (C_δ), 22.59 (C_γ); ¹⁹F-NMR (DMSO-*d*₆) δ= -74.86 (s, TFA); MS (ESI⁺): *m/z* calculated for C₂₆H₃₃N₆O₅: 509.25 [M+H]⁺, found: 509.1.

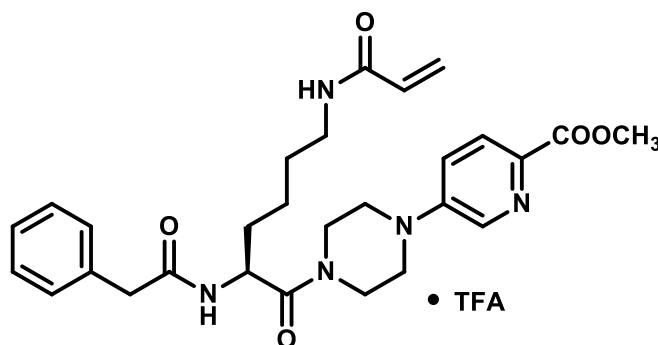
***N*^α-Phenylacetyl-*N*^ε-acryloyl-L-lysine-4-(6-carboxypyridin-3-yl)piperazide×TFA (8e)**



Compound **8f** (54 mg, 0.085 mmol, 1 eq.) was dissolved in a mixture of THF-methanol (4 mL, 3:1). To this solution 1 M NaOH (0.21 mL, 0.21 mmol, 2.5 eq.) was added and the reaction

mixture was stirred for 20 h. Subsequently, 1 M NaOH (0.043 mL, 0.043 mmol, 0.5 eq.) was added again and the reaction mixture was stirred for another 24 h. Finally, 1 M HCl (0.255 mL, 0.255 mmol, 3 eq.) was added and the solvent was removed *in vacuo*. The crude product was purified by preparative RP-HPLC. The product-containing fractions were combined and lyophilised to afford compound **8e** (37 mg, 70%) as a light yellow solid. **¹H-NMR** (DMSO-*d*₆) δ =8.40 (d, ³*J*=8.2 Hz, 1H, N_aH), 8.32 (d, ⁴*J*=2.9 Hz, 1H, H-2 of pyridine), 8.04 (t, ³*J*=5.5 Hz, 1H, N_εH), 7.94 (d, ³*J*=8.9 Hz, 1H, H-5 of pyridine), 7.44 (dd, ³*J*=9.0 Hz, ⁴*J*=2.9 Hz, 1H, H-4 of pyridine), 7.30–7.22 (m, 4H, 4×H of phenyl), 7.21–7.12 (m, 1H, H-4 of phenyl), 6.18 (dd, ³*J*=17.1, 10.1 Hz, 1H, CH=CH₂), 6.03 (dd, ³*J*=17.1 Hz, ²*J*=2.3 Hz, 1H, C=CHH), 5.53 (dd, ³*J*=10.1 Hz, ²*J*=2.3 Hz, 1H, C=CHH), 4.76–4.65 (m, 1H, C_αH), 3.75–3.17 (m, 10H, 4×CH₂ of piperazine, CH₂-phenyl), 3.13–3.03 (m, 2H, C_εH₂), 1.72–1.60 (m, 1H, C_βHH), 1.59–1.47 (m, 1H, C_βHH), 1.46–1.35 (m, 2H, C_δH₂), 1.31–1.19 (m, 2H, C_γH₂); **¹³C-NMR** (DMSO-*d*₆) δ =170.00, 169.76, 165.02, 164.40, 158.19 (q, ²*J*_{C,F}=37.4 Hz, CO of TFA), 148.12 (C-3 of pyridine), 136.35 (C-1 phenyl), 134.53 (C-2 of pyridine), 131.85 (CH₂=C), 128.95 (2×C of phenyl), 128.13 (2×C of phenyl), 126.30 (C-4 of phenyl), 125.91 (C-5 of pyridine), 124.76 (CH₂=C), 121.19 (C-4 of pyridine), 48.06 (C_α), 46.29 (CH₂ of piperazine), 45.93 (CH₂ of piperazine), 44.05 (CH₂ of piperazine), 41.95 (CH₂-phenyl), 40.84 (CH₂ of piperazine), 38.28 (C_ε), 31.31 (C_β), 28.83 (C_δ), 22.59 (C_γ); **¹⁹F-NMR** (DMSO-*d*₆) δ = -74.96 (s, TFA); MS (ESI⁺): *m/z* calculated for C₂₇H₃₄N₅O₅: 508.26 [M+H]⁺, found: 508.3.

***N*^a-Phenylacetyl-*N*^ε-acryloyl-L-lysine-4-(6-methoxycarbonylpyridin-3-yl)piperazide×TFA (**8f**)**



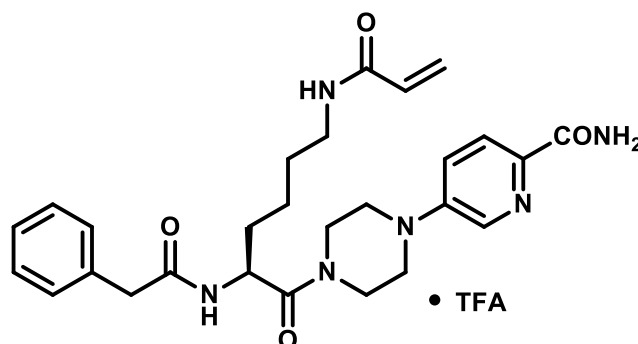
Compound **8f** (63 mg, 47%, yellow oil) was synthesised according to **GP VIII** using compound **5l** (0.21 mmol) and phenylacetyl chloride. **¹H-NMR** (DMSO-*d*₆) δ =8.40 (d, ³*J*=8.3 Hz, 1H, N_aH), 8.34 (d, ⁴*J*=2.9 Hz, 1H, H-2 of pyridine), 8.03 (t, ³*J*=5.4 Hz, 1H, N_εH), 7.90 (d, ³*J*=8.9 Hz, 1H, H-5 of pyridine), 7.33 (dd, ³*J*=8.9 Hz, ⁴*J*=3.0 Hz, 1H, H-4 of pyridine), 7.28–7.23 (m, 4H, 4×H of phenyl), 7.19–7.13 (m, 1H, H-4 of phenyl), 6.18 (dd, ³*J*=17.1, 10.1 Hz, 1H, CH=CH₂), 6.03 (dd, ³*J*=17.1 Hz, ²*J*=2.3 Hz, 1H, C=CHH), 5.53 (dd, ³*J*=10.1 Hz, ²*J*=2.3 Hz, 1H, C=CHH), 4.75–

4.66 (m, 1H, C_αH), 3.81 (s, CH₃), 3.72–3.15 (m, 10H, 4×CH₂ of piperazine, CH₂-phenyl), 3.12–3.03 (m, 2H, C_εH₂), 1.72–1.60 (m, 1H, C_βHH), 1.58–1.46 (m, 1H, C_βHH), 1.46–1.34 (m, 2H, C_δH₂), 1.30–1.18 (m, 2H, C_γH₂); ¹³C-NMR (DMSO-*d*₆) δ=169.96, 169.75, 164.90, 164.39, 158.18 (q, ²J_{C,F}=36.9 Hz, CO of TFA), 147.93 (C–3 of pyridine), 136.35, 136.00, 135.70, 131.85 (CH₂=C), 128.94 (2×C of phenyl), 128.20 (2×C of phenyl), 126.29 (C–4 of phenyl), 125.76 (C–5 of pyridine), 124.75 (CH₂=C), 119.87 (C–4 of pyridine), 51.80 (CH₃), 48.05 (C_α), 46.22 (CH₂ of piperazine), 45.84 (CH₂ of piperazine), 44.09 (CH₂ of piperazine), 41.95 (CH₂-phenyl), 40.87 (CH₂ of piperazine), 38.28 (C_ε), 31.32 (C_β), 28.82 (C_δ), 22.59 (C_γ); ¹⁹F-NMR (DMSO-*d*₆) δ= -74.92 (s, TFA); MS (ESI⁺): m/z calculated for C₂₈H₃₆N₅O₅: 522.27 [M+H]⁺, found: 522.3.

N-Phenylacetylpyrrolidine (2.3 mg, white solid) was isolated as side product.

¹H-NMR (DMSO-*d*₆) δ=7.32–7.18 (m, 5H, 5×H of phenyl), 3.61 (s, 2H, CH₂CO), 3.45 (t, ³J=6.8 Hz, 2H, CH₂N), 3.28 (t, ³J=6.8 Hz, 2H, CH₂N), 1.91–1.81 (m, 2H, CH₂), 1.80–1.70 (m, 2H, CH₂); ¹³C-NMR (DMSO-*d*₆) δ=168.46 (CO), 135.72 (C–1 of phenyl), 129.21 (2×C of phenyl), 128.14 (2×C of phenyl), 126.22 (C–4 of phenyl), 46.23 (CH₂N), 45.44 (CH₂N), 41.00 (CH₂CO), 25.62 (CH₂), 23.92 (CH₂); MS (ESI⁺): m/z calculated for C₁₂H₁₆NO: 190.12 [M+H]⁺, found: 190.1.

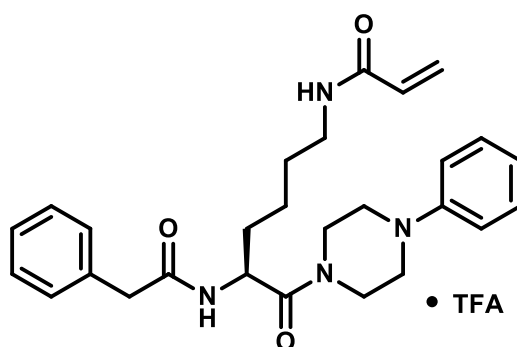
N^α-Phenylacetyl-N^ε-acryloyl-L-lysine-4-(6-carbamoylpyridin-3-yl)piperazide×TFA (8g)



A solution of compound **8e** (20 mg, 0.03 mmol, 1 eq.) and NMM (8.9 μL, 0.08 mmol, 2.5 eq.) in THF (2 mL) was cooled to -30 °C by a mixture of isopropanol and liquid nitrogen. Subsequently, isobutyl chloroformate (4.2 μL, 0.03 mmol, 1 eq.) and aqueous NH₃ (ω=25%, 12.1 μL, 0.16 mmol, 5 eq.) was added. Cooling was stopped and the reaction mixture was stirred until the temperature reached 4 °C (approx. 2 h). To completely convert the acyl isobutyl carbonate to the desired amide, aqueous NH₃ (ω=25%, 12.1 μL, 0.16 mmol, 5 eq.) was added again and the reaction mixture was heated to 66 °C for 30 min. The solvent was removed *in vacuo* and the residue was dissolved in CH₂Cl₂. The organic phase was washed with NaHCO₃ (3×6 mL) and brine (1×6 mL), dried over Na₂SO₄ and the solvent was removed *in vacuo*. The

crude product was purified by preparative RP-HPLC. The product-containing fractions were combined and lyophilised to afford compound **8g** (5.4 mg, 27%) as a light yellow solid. **¹H-NMR** (DMSO-*d*₆) δ=8.40 (d, ³*J*=8.3 Hz, 1H, N_aH), 8.25 (d, ⁴*J*=2.6 Hz, 1H, H-2 of pyridine), 8.03 (t, ³*J*=5.7 Hz, 1H, N_εH), 7.88 (d, ³*J*=8.8 Hz, 1H, H-5 of pyridine), 7.84, (s, 1H, NHH), 7.40 (dd, ³*J*=8.9 Hz, ⁴*J*=2.7 Hz, 1H, H-4 of pyridine), 7.37 (s, 1H, NHH), 7.29–7.22 (m, 4H, 4×H of phenyl), 7.20–7.12 (m, 1H, H-4 of phenyl), 6.18 (dd, ³*J*=17.1, 10.1 Hz, 1H, CH=CH₂), 6.03 (dd, ³*J*=17.1 Hz, ²*J*=2.3 Hz, 1H, C=CHH), 5.53 (dd, ³*J*=10.1 Hz, ²*J*=2.3 Hz, 1H, C=CHH), 4.76–4.66 (m, 1H, C_αH), 3.74–3.03 (m, 12H, 4×CH₂ of piperazine, CH₂-phenyl, C_εH₂), 1.71–1.60 (m, 1H, C_βHH), 1.59–1.47 (m, 1H, C_βHH), 1.46–1.34 (m, 2H, C_δH₂), 1.31–1.18 (m, 2H, C_γH₂); **¹³C-NMR** (DMSO-*d*₆) δ=169.90, 169.74, 165.88, 164.39, 147.78 (C-3 of pyridine), 136.35 (C-1 phenyl), 134.93 (C-2 of pyridine), 131.85 (CH₂=C), 128.94 (2×C of phenyl), 128.12 (2×C of phenyl), 126.29 (C-4 of phenyl), 124.75 (CH₂=C), 122.53 (C-5 of pyridine), 121.37 (C-4 of pyridine), 48.03 (C_α), 46.79 (CH₂ of piperazine), 46.41 (CH₂ of piperazine), 44.19 (CH₂ of piperazine), 41.95 (CH₂-phenyl), 40.92 (CH₂ of piperazine), 38.28 (C_ε), 31.34 (C_β), 28.82 (C_δ), 22.59 (C_γ); **¹⁹F-NMR** (DMSO-*d*₆) δ= -74.75 (s, TFA); MS (ESI⁺): *m/z* calculated for C₂₇H₃₅N₆O₄: 507.27 [M+H]⁺, found: 507.3.

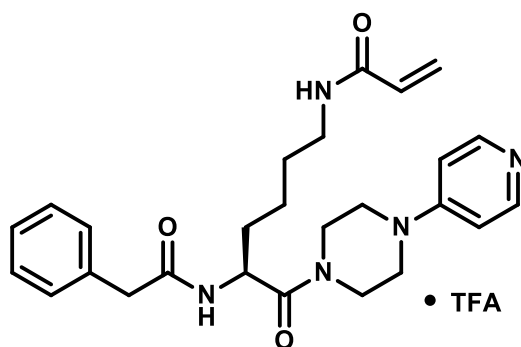
N^ε-Phenylacetyl-N^α-acryloyl-L-lysine-4-phenylpiperazide×TFA (9)



Compound **9** (63 mg, 47%, yellow oil) was synthesised according to **GP VIII** using compound **5u** (0.21 mmol) and phenylacetyl chloride. **¹H-NMR** (DMSO-*d*₆) δ=8.40 (d, ³*J*=8.3 Hz, 1H, N_aH), 8.34 (d, ⁴*J*=2.9 Hz, 1H, H-2 of pyridine), 8.03 (t, ³*J*=5.4 Hz, 1H, N_εH), 7.90 (d, ³*J*=8.9 Hz, 1H, H-5 of pyridine), 7.33 (dd, ³*J*=8.9 Hz, ⁴*J*=3.0 Hz, 1H, H-4 of pyridine), 7.28–7.23 (m, 4H, 4×H of phenyl), 7.19–7.13 (m, 1H, H-4 of phenyl), 6.18 (dd, ³*J*=17.1, 10.1 Hz, 1H, CH=CH₂), 6.03 (dd, ³*J*=17.1 Hz, ²*J*=2.3 Hz, 1H, C=CHH), 5.53 (dd, ³*J*=10.1 Hz, ²*J*=2.3 Hz, 1H, C=CHH), 4.75–4.66 (m, 1H, C_αH), 3.81 (s, CH₃), 3.72–3.15 (m, 10H, 4×CH₂ of piperazine, CH₂-phenyl), 3.12–3.03 (m, 2H, C_εH₂), 1.72–1.60 (m, 1H, C_βHH), 1.58–1.46 (m, 1H, C_βHH), 1.46–1.34 (m, 2H, C_δH₂), 1.30–1.18 (m, 2H, C_γH₂); **¹³C-NMR** (DMSO-*d*₆) δ=169.96, 169.75, 164.90, 164.39, 158.18 (q, ²*J*_{C,F}=36.9 Hz, CO of TFA), 147.93 (C-3 of pyridine), 136.35, 136.00, 135.70, 131.85

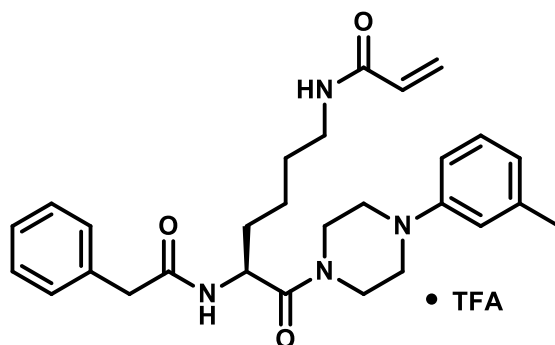
(CH₂=C), 128.94 (2×C of phenyl), 128.20 (2×C of phenyl), 126.29 (C-4 of phenyl), 125.76 (C-5 of pyridine), 124.75 (CH₂=C), 119.87 (C-4 of pyridine), 51.80 (CH₃), 48.05 (C_α), 46.22 (CH₂ of piperazine), 45.84 (CH₂ of piperazine), 44.09 (CH₂ of piperazine), 41.95 (CH₂-phenyl), 40.87 (CH₂ of piperazine), 38.28 (C_ε), 31.32 (C_β), 28.82 (C_δ), 22.59 (C_γ); ¹⁹F-NMR (DMSO-*d*₆) δ = -74.92 (s, TFA); MS (ESI⁺): *m/z* calculated for C₂₈H₃₆N₅O₅: 522.27 [M+H]⁺, found: 522.3.

N^α-Phenylacetyl-N^ε-acryloyl-L-lysine-4-(pyridin-4-yl)piperazide×TFA (10)



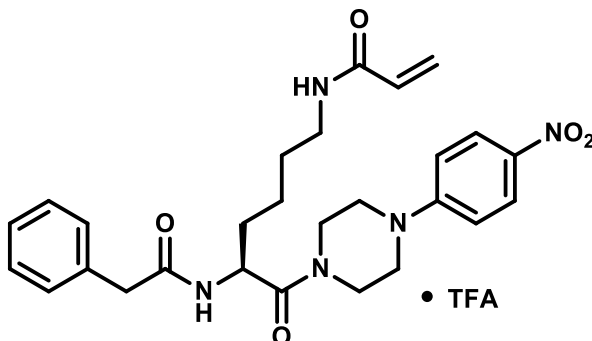
Compound **10** (10 mg, 16%, colourless solid) was synthesised according to **GP VIII** using compound **5t** (0.10 mmol) and phenylacetyl chloride. ¹H-NMR (DMSO-*d*₆) δ=8.42 (d, ³*J*=8.2 Hz, 1H, N_αH), 8.28 (d, ³*J*=6.3 Hz, 2H, H-2,6 of pyridine), 8.04 (t, ³*J*=5.6 Hz, 1H, N_εH), 7.31-7.23 (m, 4H, H-2,3,5,6 of phenyl), 7.21-7.17 (m, 1H, H-4 of phenyl), 7.15 (d, ³*J*=7.7 Hz, 2H, H-3,5 of pyridine), 6.18 (dd, ³*J*=17.1, 10.1 Hz, 1H, CH=CH₂), 6.04 (dd, ³*J*=17.1 Hz, ²*J*=2.3 Hz, 1H, CH=CHH), 5.54 (dd, ³*J*=10.1 Hz, ²*J*=2.3 Hz, 1H, CH=CHH), 4.71-4.65 (m, 1H, C_αH), 3.80-3.52 (m, 8H, 4×CH₂ of piperazine), 3.51-3.40 (m, 2H, CH₂-phenyl), 3.15-3.02 (m, 2H, C_εH₂), 1.72-1.60 (m, 1H, C_βHH), 1.59-1.49 (m, 1H, C_βHH), 1.47-1.33 (m, 2H, C_δH₂), 1.33-1.19 (m, 2H, C_γH₂); ¹³C-NMR (DMSO-*d*₆) δ=170.42, 169.85, 164.41 (C_αCON, CON_α, CON_ε), 156.59 (C-4 of pyridine), 139.77 (C-3,5 of pyridine), 136.32 (C-1 of phenyl), 131.84 (CH=CH₂), 128.95 (2×CH of phenyl), 128.13 (2×CH of phenyl), 126.31 (C-4 of phenyl), 124.78 (CH=CH₂), 107.44 (C-2,6 of pyridine), 48.20 (C_α), 41.90 (CH₂-phenyl), 38.24 (C_ε), 31.13 (C_β), 28.82 (C_δ), 22.55 (C_γ), signals for 4×CH₂ of piperazine are not visible; ¹⁹F-NMR (DMSO-*d*₆) δ = -74.36 (s, TFA); MS (ESI⁺): *m/z* calculated for C₂₆H₃₄N₅O₃: 464.27 [M+H]⁺, found: 464.2.

***N*^α-Phenylacetyl-*N*^ε-acryloyl-L-lysine-4-(3-methylphenyl)piperazide×TFA (11)**



Compound **11** (31 mg, 74%, light yellow solid) was synthesised according to **GP VIII** using compound **5w** (0.09 mmol) and phenylacetyl chloride. **¹H-NMR** (DMSO-*d*₆) δ=8.38 (d, ³*J*=8.3 Hz, 1H, N_αH), 8.03 (t, ³*J*=5.5 Hz, 1H, N_εH), 7.31–7.23 (m, 4H, 4×H of phenyl), 7.23–7.15 (m, 1H, H-4 of phenyl), 7.10 (t, ³*J*=7.8 Hz, 1H, H-5 of methylphenyl), 6.77–6.69 (m, 2H, 2×H of methylphenyl), 6.64 (d, ³*J*=7.4 Hz, 1H, H of methylphenyl), 6.18 (dd, ³*J*=17.1, 10.1 Hz, 1H, CH=CH₂), 6.04 (dd, ³*J*=17.1 Hz, ²*J*=2.3 Hz, 1H, C=CHH), 5.54 (dd, ³*J*=10.0 Hz, ²*J*=2.3 Hz, 1H, C=CHH), 4.74–4.66 (m, 1H, C_αH), 3.72–3.40 (m, 6H, 2×CH₂ of piperazine, CH₂-phenyl), 3.18–2.89 (m, 6H, 2×CH₂ of piperazine, C_εH₂), 2.25 (s, 3H, CH₃), 1.71–1.59 (m, 1H, C_βHH), 1.58–1.46 (m, 1H, C_βHH), 1.46–1.34 (m, 2H, C_δH₂), 1.32–1.19 (m, 2H, C_γH₂); **¹³C-NMR** (DMSO-*d*₆) δ=169.72, 169.70, 164.40, 150.55, 138.04, 136.36, 131.85 (CH₂=C), 128.94 (2×C of phenyl), 128.77 (C-5 of methylphenyl), 128.12 (2×C of phenyl), 126.29 (C-4 of phenyl), 124.74 (CH₂=C), 120.35, 116.62, 113.18, 48.80 (CH₂ of piperazine), 48.57 (CH₂ of piperazine), 48.02 (C_α), 44.67 (CH₂ of piperazine), 41.95 (CH₂-phenyl), 41.32 (CH₂ of piperazine), 38.29 (C_ε), 31.40 (C_β), 28.79 (C_δ), 22.59 (C_γ), 21.35 (CH₃); MS (ESI⁺): *m/z* calculated for C₂₈H₃₇N₄O₃: 477.29 [M+H]⁺, found: 477.3.

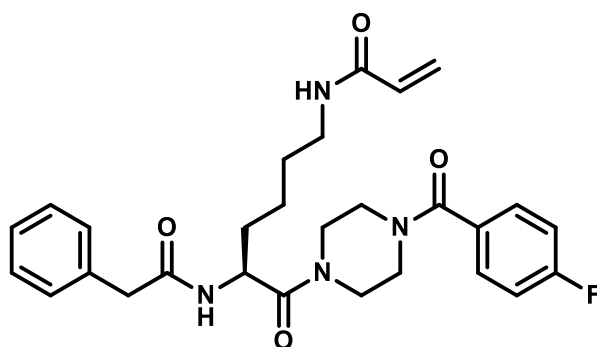
***N*^α-Phenylacetyl-*N*^ε-acryloyl-L-lysine-4-(4-nitrophenyl)piperazide×TFA (12)**



Compound **12** (20 mg, 57%, yellow solid) was synthesised according to **GP VIII** using compound **5x** (0.07 mmol) and phenylacetyl chloride. **¹H-NMR** (DMSO-*d*₆) δ=8.40 (d,

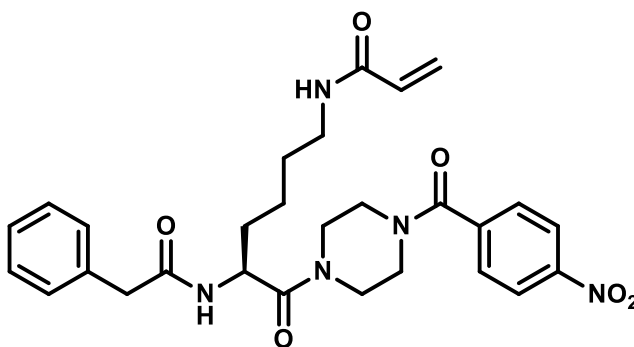
$^3J=8.3$ Hz, 1H, $N_\alpha H$), 8.10–8.05 (m, 2H, H–3,5 of nitrophenyl), 8.03 (t, $^3J=5.5$ Hz, 1H, $N_\epsilon H$), 7.31–7.23 (m, 4H, 4×H of phenyl), 7.22–7.14 (m, 1H, H–4 of phenyl), 7.02–6.95 (m, 2H, H–2,6 of nitrophenyl), 6.18 (dd, $^3J=17.1$, 10.1 Hz, 1H, $CH=CH_2$), 6.03 (dd, $^3J=17.1$ Hz, $^2J=2.3$ Hz, 1H, $C=CHH$), 5.54 (dd, $^3J=10.1$ Hz, $^2J=2.3$ Hz, 1H, $C=CHH$), 4.74–4.66 (m, 1H, $C_\alpha H$), 3.74–3.26 (m, 10H, 4× CH_2 of piperazine, CH_2 -phenyl), 3.12–3.03 (m, 2H, $C_\epsilon H_2$), 1.72–1.60 (m, 1H, $C_\beta HH$), 1.59–1.47 (m, 1H, $C_\beta HH$), 1.46–1.35 (m, 2H, $C_\delta H_2$), 1.31–1.19 (m, 2H, $C_\gamma H_2$); ^{13}C -NMR (DMSO- d_6) δ =170.09, 169.77, 164.39, 154.33, 137.05, 136.34, 131.84 ($CH_2=C$), 128.94 (2×C of phenyl), 128.13 (2×C of phenyl), 126.31 (C–4 of phenyl), 125.66 (C–3,5 of nitrophenyl), 124.76 ($CH_2=C$), 112.59 (C–2,6 of nitrophenyl), 48.12 (C_α), 46.17 (CH_2 of piperazine), 45.78 (CH_2 of piperazine), 43.97 (CH_2 of piperazine), 41.94 (CH_2 -phenyl), 40.92 (CH_2 of piperazine), 38.27 (C_ϵ), 31.29 (C_β), 28.82 (C_δ), 22.58 (C_γ); ^{19}F -NMR (DMSO- d_6) δ = -73.45 (s, TFA); MS (ESI $^+$): m/z calculated for $C_{27}H_{34}N_5O_5$: 508.26 [M+H] $^+$, found: 530.2.

***N* $^\alpha$ -Phenylacetyl-*N* $^\epsilon$ -acryloyl-L-lysine-4-(4-fluorobenzoyl)piperazide×TFA (13a)**



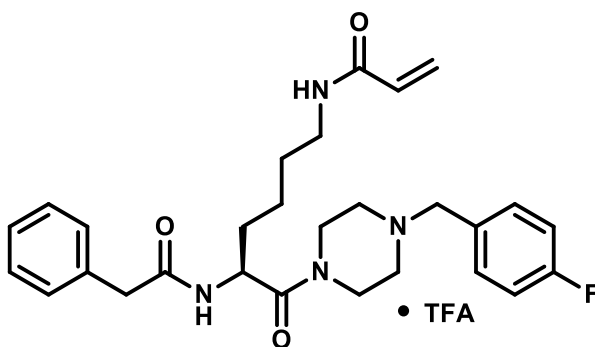
Compound **13a** (16 mg, 53%, yellow oil) was synthesised according to **GP VIII** using compound **5e** (0.06 mmol) and phenylacetyl chloride. 1H -NMR (DMSO- d_6) δ =8.37 (d, $^3J=8.2$ Hz, 1H, $N_\alpha H$), 8.03 (t, $^3J=5.4$ Hz, 1H, $N_\epsilon H$), 7.48 (dd, $^3J_{H,H}=8.6$ Hz, $^4J_{H,F}=5.6$ Hz, 2H, H–2,6 of fluorobenzoyl), 7.32–7.13 (m, 7H, 5×H of phenyl, H–3,5 of fluorobenzoyl), 6.19 (dd, $^3J=17.1$, 10.1 Hz, 1H, $CH=CH_2$), 6.04 (dd, $^3J=17.0$ Hz, $^2J=2.1$ Hz, 1H, $C=CHH$), 5.55 (dd, $^3J=10.0$ Hz, $^2J=2.3$ Hz, 1H, $C=CHH$), 4.65 (m, 1H, $C_\alpha H$), 3.50–3.38 (m, 2H, CH_2 -phenyl), 3.12–3.03 (m, 2H, $C_\epsilon H_2$), 1.69–1.57 (m, 1H, $C_\beta HH$), 1.57–1.45 (m, 1H, $C_\beta HH$), 1.45–1.33 (m, 2H, $C_\delta H_2$), 1.31–1.16 (m, 2H, $C_\gamma H_2$); ^{13}C -NMR (DMSO- d_6) δ =170.07, 169.74, 168.25, 164.40, 136.34 (C–1 of phenyl), 131.97 (d, $^4J_{C,F}=3.4$ Hz, C–1 of fluorobenzoyl), 131.85 ($CH_2=C$), 129.62 (d, $^3J=8.7$ Hz, C–2,6 of fluorobenzoyl), 128.95 (2×C of phenyl), 128.12 (2×C of phenyl), 126.31 (C–4 of phenyl), 124.75 ($CH_2=C$), 115.39 (d, $^2J_{C,F}=21.5$ Hz, C–3,5 of fluorobenzoyl), 48.16 (C_α), 41.93 (CH_2 -phenyl), 38.25 (C_ϵ), 31.28 (C_β), 28.79 (C_δ), 22.54 (C_γ), signals for 4× CH_2 of piperazine are not visible; MS (ESI $^+$): m/z calculated for $C_{28}H_{34}FN_4O_4$: 509.26 [M+H] $^+$, found: 509.3.

***N*^α-Phenylacetyl-*N*^ε-acryloyl-L-lysine-4-(4-nitrobenzoyl)piperazide·TFA (13b)**



Compound **13b** (22 mg, 73%, white solid) was synthesised according to **GP VIII** using compound **5f** (0.06 mmol) and phenylacetyl chloride. **¹H-NMR** (DMSO-*d*₆) δ=8.43–8.35 (m, 1H, N_αH), 8.30 (d, ³J=8.8 Hz, 2H, H–3,5 of nitrobenzoyl), 8.04 (s, 1H, N_εH), 7.73–7.64 (m, 2H, H–2,6 of nitrobenzoyl), 7.32–7.16 (m, 5H, 5×H of phenyl), 6.25–6.12 (m, 1H, CH=CH₂), 6.10–5.99 (m, 1H, C=CHH), 5.60–5.51 (m, 1H, C=CHH), 4.76–4.56 (m, 1H, C_αH), 3.74–3.13 (m, 8H, 4×CH₂ of piperazine), 3.12–3.00 (m, 2H, C_εH₂), 1.69–1.57 (m, 1H, C_βHH), 1.57–1.45 (m, 1H, C_βHH), 1.45–1.32 (m, 2H, C_δH₂), 1.32–1.14 (m, 2H, C_γH₂), diffuse signals (partly in duplicate) due to the amide bonds on both sides of the piperazine ring; **¹³C-NMR** (DMSO-*d*₆) δ=170.11, 169.77, 167.24, 164.42, 147.85, 141.93, 136.34, 131.85 (CH₂=C), 128.97 (2×C_{Phenyl}), 128.35 (C–2,6 of nitrobenzoyl), 128.14 (2×C of phenyl), 126.33 (C–4 of phenyl), 124.79 (CH₂=C), 123.78 (C–3,5 of nitrobenzoyl), 48.16 (C_α), 41.94 (CH₂-phenyl), 38.26 (C_ε), 31.27 (C_β), 28.80 (C_δ), 22.56 (C_γ), signals for 4×CH₂ of piperazine are not visible; MS (ESI⁺): *m/z* calculated for C₂₈H₃₄N₅O₆: 536.25 [M+H]⁺, found: 536.3.

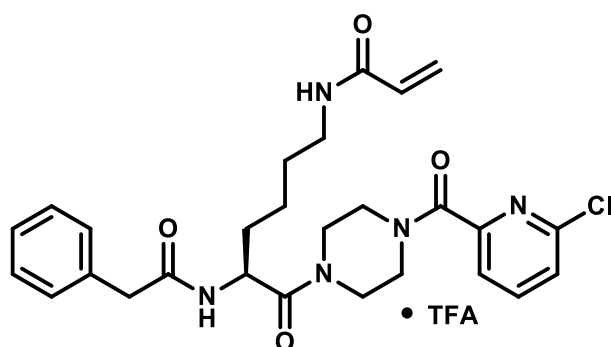
***N*^α-Phenylacetyl-*N*^ε-acryloyl-L-lysine-4-(4-fluorobenzyl)piperazide·TFA (13c)**



Compound **13c** (12 mg, 42%, white solid) was synthesised according to **GP VIII** using compound **5g** (0.05 mmol) and phenylacetyl chloride. **¹H-NMR** (DMSO-*d*₆) δ=8.39 (d, ³J=7.7 Hz, 1H, N_αH), 8.12–7.99 (m, 1H, N_εH), 7.59–7.48 (m, 2H, H–2,6 of fluorophenyl), 7.42–7.09 (m, 7H, 5×H of phenyl, H–3,5 of fluorophenyl), 6.20 (dd, ³J=17.1, 9.9 Hz, 1H, CH=CH₂),

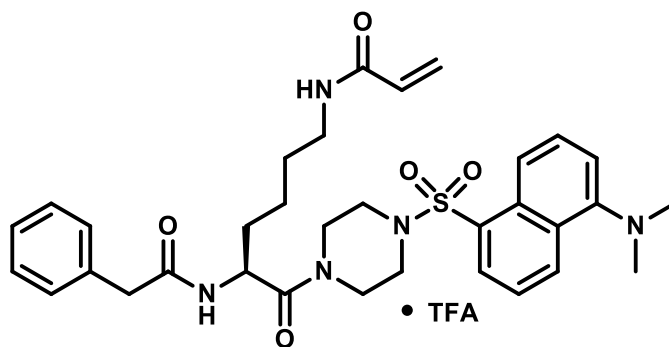
6.06 (dd, $^3J=17.1$ Hz, $^2J=2.1$ Hz, 1H, C=CHH), 5.60–5.54 (m, 1H, C=CHH), 4.70–4.58 (m, 1H, C $_{\alpha}$ H), 4.50–4.10 (m, 2H, CH₂), 3.53–3.19 (m, 8H, CH₂-phenyl, 3×CH₂), 3.17–2.73 (m, 4H, C $_{\epsilon}$ H₂, CH₂), 1.69–1.46 (m, 2H, C $_{\beta}$ H₂), 1.46–1.34 (m, 2H, C $_{\delta}$ H₂), 1.34–1.12 (m, 2H, C $_{\gamma}$ H₂); $^{13}\text{C-NMR}$ (DMSO-*d*₆) δ =170.27, 169.93, 164.48, 136.28 (C–1 of phenyl), 133.61 (d, $^3J_{\text{C,F}}=6.6$ Hz, C–2,6 of fluorophenyl), 131.86 (CH₂=C), 128.96 (2×C of phenyl), 128.16 (2×C of phenyl), 126.34 (C–4 of phenyl), 124.81 (CH₂=C), 115.79 (d, $^2J_{\text{C,F}}=22.1$ Hz, C–3,5 fluorophenyl), 58.11 (CH₂), 50.40 (CH₂), 48.10 (C $_{\alpha}$), 41.85 (CH₂-phenyl), 38.19 (C $_{\epsilon}$), 31.11 (C $_{\beta}$), 28.80 (C $_{\delta}$), 22.49 (C $_{\gamma}$), signals for C-1,4 fluorophenyl and 3×CH₂ are not visible; $^{19}\text{F-NMR}$ (DMSO-*d*₆) δ = -73.92 (s, TFA), -111.46– -111.63 (m, F-4); MS (ESI⁺): *m/z* calculated for C₂₈H₃₆FN₄O₃: 495.28 [M+H]⁺, found: 495.4.

***N*^α-Phenylacetyl-*N*^ε-acryloyl-L-lysine-4-(6-chloropyridinoyl)piperazide×TFA (13d)**



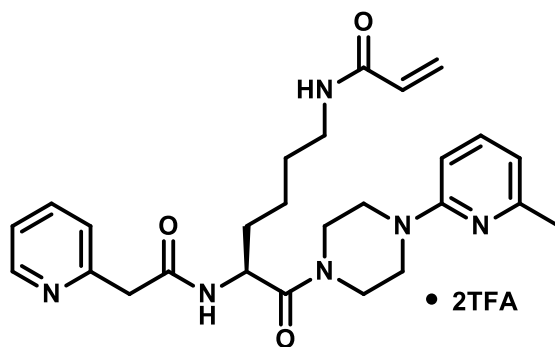
Compound **13d** (15 mg, 49%, colourless solid) was synthesised according to **GP VIII** using compound **5h** (0.05 mmol) and phenylacetyl chloride. $^1\text{H-NMR}$ (DMSO-*d*₆) δ =7.80 (t, $^3J=7.8$ Hz, 1H, H-4 of pyridine), 7.66 (dd, $^3J=7.4$ Hz, $^4J=3.3$ Hz, 1H, H-5 of pyridine), 7.42 (d, $^3J=8.0$ Hz, 1H, H-3 of pyridine), 7.39–7.28 (m, 3H; 3×H of phenyl), 7.28–7.23 (m, 2H, 2×H of phenyl), 6.66 (d, $^3J=7.9$ Hz, 1H, N $_{\alpha}$ H), 6.34–6.21 (m, 1H, CH=CHH), 6.17–5.99 (m, 2H, CH=CH₂, N $_{\epsilon}$ H), 5.63 (d, $^3J=10.2$ Hz, 1H, CH=CHH), 4.99–4.86 (m, 1H, C $_{\alpha}$ H), 3.98–3.51 (m, 10 H, 4×CH₂ of piperazine, CH₂-phenyl), 3.35–3.19 (m, 2H, C $_{\epsilon}$ H₂), 1.73–1.47 (m, 4H, C $_{\beta}$ H₂, C $_{\delta}$ H₂), 1.37–1.23 (m, 2H, C $_{\gamma}$ H₂), diffuse signals (partly in duplicate) due to the amide bonds on both sides of the piperazine ring; $^{13}\text{C-NMR}$ (DMSO-*d*₆) δ =171.76, 170.53/170.47, 166.45, 166.05/165.96, 153.31, 150.15, 140.07 (C-4 of pyridine), 134.32, 130.61 (CH=CH₂), 129.42 (2×CH of phenyl), 129.18 (2×CH of phenyl), 127.70 (C-4 of phenyl), 126.96 (CH=CH₂), 126.06 (C-3 of pyridine), 123.23/123.16 (C-5 of pyridine), 48.61 (C $_{\alpha}$), 47.27/47.02 (CH₂ of piperazine), 45.85/45.28 (CH₂ of piperazine), 43.65 (CH₂-phenyl), 42.76/42.56/42.53/42.01 (2×CH₂ of piperazine), 39.25 (C $_{\epsilon}$), 32.71 (C $_{\beta}$), 28.43 (C $_{\delta}$), 22.25 (C $_{\gamma}$); $^{19}\text{F-NMR}$ (DMSO-*d*₆) δ = -75.82 (s, TFA); MS (ESI⁺): *m/z* calculated for C₂₇H₃₃ClN₅O₄: 526.22 [M(³⁵Cl)+H]⁺, found: 526.3.

***N*^α-Phenylacetyl-*N*^ε-acryloyl-L-lysine-4-dansylpiperazidexTFA (13e)**



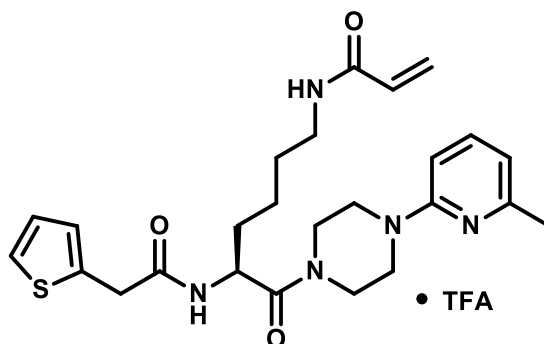
Compound **13e** (19 mg, 54%, yellow-green solid) was synthesised according to **GP VIII** using compound **5c** (0.05 mmol) and phenylacetyl chloride. **¹H-NMR** (DMSO-*d*₆) δ=8.54 (d, ³*J*=8.5 Hz, 1H, H of dansyl), 8.28 (d, ³*J*=8.7 Hz, 2H, H of dansyl, N_dH), 8.12 (dd, ³*J*=7.4 Hz, ²*J*=1.2 Hz, 1H, H of dansyl), 7.99 (t, ³*J*=5.6 Hz, 1H, N_εH), 7.67 (dd, ³*J*=8.5, 7.4 Hz, 1H, H of dansyl), 7.62 (dd, ³*J*=8.6, 7.7 Hz, 1H, H of dansyl), 7.28 (d, ³*J*=7.5 Hz, 1H, H of dansyl), 7.24-7.12 (m, 5H, H-2,3,4,5,6 phenyl), 6.16 (dd, ³*J*=17.1, 10.1 Hz, 1H, CH=CH₂), 6.03 (dd, ³*J*=17.1 Hz, ²*J*=2.4 Hz, 1H, CH=CHH), 5.53 (dd, ³*J*=10.0 Hz, ²*J*=2.4 Hz, 1H, CH=CHH), 4.61-4.50 (m, 1H, C_αH), 3.68-3.10 (m, 10H, 4×CH₂ of piperazine, CH₂-phenyl), 3.06-2.97 (m, 2H, C_εH₂), 2.83 (s, 6H, 2×CH₃), 1.60-1.09 (m, 6H, C_βH₂, C_γH₂, C_δH₂); **¹³C-NMR** (DMSO-*d*₆) δ=169.92, 169.66, 164.36, 151.28 (quart. C of dansyl), 142.67 (quart. C of dansyl), 136.20, 131.84 (CH=CH₂), 130.40 (CH of dansyl), 130.09 (CH of dansyl), 129.59 (quart. C of dansyl), 129.15 (quart. C of dansyl), 128.84 (2×CH of phenyl), 128.27 (CH of dansyl), 128.06 (2×CH of phenyl), 126.25 (C-4 of phenyl), 124.72 (CH=CH₂), 123.71 (CH of dansyl), 118.92 (CH of dansyl), 115.38 (CH of dansyl), 48.06 (C_αH), 45.44 (CH₂ of piperazine), 45.18 (CH₂ of piperazine), 45.05 (2×CH₃), 44.53 (CH₂ of piperazine), 41.80 (CH₂-phenyl), 41.12 (CH₂ of piperazine), 38.21 (C_ε), 31.10 (C_β), 28.72 (C_δ), 22.47 (C_γ); **¹⁹F-NMR** (DMSO-*d*₆) δ= -74.48 (s, TFA); MS (ESI⁺): *m/z* calculated for C₃₃H₄₂N₅O₅S: 620.29 [M+H]⁺, found: 620.4.

***N*^α-2-Pyridylacetyl-*N*^ε-acryloyl-L-lysine-4-(6-methylpyridin-2-yl)piperazide×2TFA (14a)**



Compound **14a** (27 mg, 64%, yellow oil) was synthesised according to **GP IX** using compound **5a** (0.06 mmol) and 2-pyridylacetic acid chloride. **¹H-NMR** (DMSO-*d*₆) δ=8.68 (d, ³*J*=4.6 Hz, 1H, H-6 of pyridine), 8.62 (d, ³*J*=7.8 Hz, 1H, N_αH), 8.16 (t, ³*J*=6.9 Hz, 1H, H-4 of pyridine), 8.05 (t, ³*J*=5.3 Hz, 1H, N_εH), 7.67 (d, ³*J*=7.9 Hz, 1H, H-3 of pyridine), 7.64–7.59 (m, 1H, H-4 of methylpyridine), 6.91–6.83 (m, 1H, H-3 of methylpyridine), 6.69 (d, ³*J*=7.0 Hz, 1H, H-5), 6.64 (d, ³*J*=7.3 Hz, 1H, H-5), 6.18 (dd, ³*J*=17.1, 10.1 Hz, 1H, CH=CH₂), 6.04 (dd, ³*J*=17.1 Hz, ²*J*=2.3 Hz, 1H, C=CHH), 5.54 (dd, ³*J*=10.0 Hz, ²*J*=2.3 Hz, 1H, C=CHH), 4.81–4.66 (m, 1H, C_αH), 3.94–3.83 (m, 2H, CH₂-pyridine), 3.74–3.43 (m, 8H, 4×CH₂ of piperazine), 3.16–3.07 (m, 2H, C_εH₂), 2.40 (s, 3H, CH₃), 1.74–1.62 (m, 1H, C_βHH), 1.62–1.50 (m, 1H, C_βHH), 1.49–1.37 (m, 2H, C_δH₂), 1.37–1.21 (m, 2H, C_γH₂); **¹³C-NMR** (DMSO-*d*₆) δ=169.94, 167.36, 164.44, 158.11 (q, ²*J*_{C,F}=35.8 Hz, CO of TFA), 131.83 (CH₂=C), 124.81 (CH₂=C), 112.71, 48.51 (C_α), 38.27 (C_ε), 31.27 (C_β), 28.85 (C_δ), 22.53 (C_γ), signals for 4×CH₂ of piperazine, CH₃, C-2,3,4,6 of methylpyridine/pyridine and 1×C-5 are not visible; **¹⁹F-NMR** (DMSO-*d*₆) δ= -74.69 (s, TFA); MS (ESI⁺): *m/z* calculated for C₂₆H₃₅N₆O₃: 479.28 [M+H]⁺, found: 479.3.

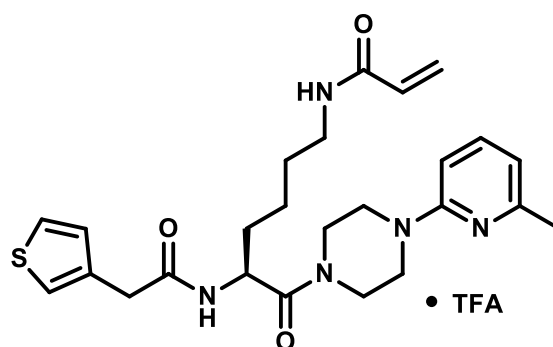
***N*^α-2-Thienylacetyl-*N*^ε-acryloyl-L-lysine-4-(6-methylpyridin-2-yl)piperazide×TFA (14b)**



Compound **14b** (21 mg, 59%, white solid) was synthesised according to **GP VIII** using compound **5a** (0.06 mmol) and 2-thienylacetyl chloride. **¹H-NMR** (DMSO-*d*₆) δ=8.43 (d, ³*J*=8.2 Hz, 1H, N_αH), 8.04 (t, ³*J*=4.8 Hz, 1H, N_εH), 7.72 (broad s, 1H, H-4 of pyridine), 7.33

(dd, $^3J=5.0$ Hz, $^4J=1.3$ Hz, 1H, H-5 of thiophene), 6.97–6.87 (m, 3H, H-3,4 of thiophene, H-3 of pyridine), 6.75–6.66 (m, 1H, H-5 of pyridine), 6.18 (dd, $^3J=17.1$, 10.1 Hz, 1H, $CH=CH_2$), 6.04 (dd, $^3J=17.1$ Hz, $^2J=2.3$ Hz, 1H, $C=CHH$), 5.54 (dd, $^3J=10.1$ Hz, $^2J=2.3$ Hz, 1H, $C=CHH$), 4.77–4.67 (m, 1H, $C_\alpha H$), 3.78–3.43 (m, 10H, $4\times CH_2$ of piperazine, CH_2 -thiophene), 3.15–3.02 (m, 2H, $C_\epsilon H_2$), 2.42 (s, 3H, CH_3), 1.74–1.60 (m, 1H, $C_\beta HH$), 1.59–1.48 (m, 1H, $C_\beta HH$), 1.48–1.35 (m, 2H, $C_\delta H_2$), 1.34–1.20 (m, 2H, $C_\gamma H_2$); ^{13}C -NMR (DMSO- d_6) δ =170.04, 168.78, 164.41, 137.53, 131.85 ($CH_2=C$), 126.51 (CH of thiophene), 126.05 (CH of thiophene), 124.78 ($CH_2=C$, C-5 of thiophene), 112.74 (C-5 of pyridine), 48.24 (C_α), 45.51 (CH_2 of piperazine), 45.11 (CH_2 of piperazine), 44.06 (CH_2 of piperazine), 40.87 (CH_2 of piperazine), 38.26 (C_ϵ), 36.12 (CH_2 -thiophene), 31.28 (C_β), 28.82 (C_δ), 22.52 (C_γ), signals for C-2,3,4,6 of pyridine are not visible; ^{19}F -NMR (DMSO- d_6) δ = -74.70 (s, TFA); MS (ESI $^+$): m/z calculated for $C_{25}H_{34}N_5O_3S$: 484.24 [M+H] $^+$, found: 484.2.

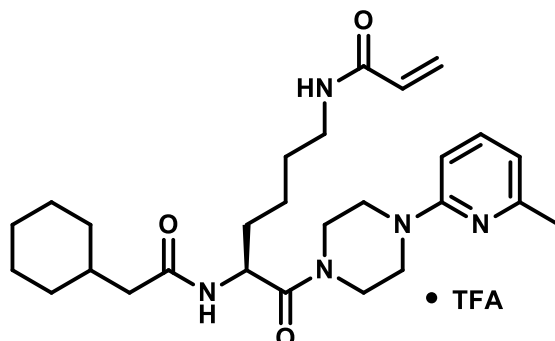
***N*^α-3-Thienylacetyl-*N*^ε-acryloyl-L-lysine-4-(6-methylpyridin-2-yl)piperazide×TFA (**14c**)**



Compound **14c** (21 mg, 60%, yellow oil) was synthesised according to **GP IX** using compound **5a** (0.06 mmol) and 3-thienylacetic acid. 1H -NMR (DMSO- d_6) δ =8.35 (d, $^3J=8.1$ Hz, 1H, $N_\alpha H$), 8.05 (t, $^3J=5.6$ Hz, 1H, $N_\epsilon H$), 7.75 (broad s, 1H, H-4 of pyridine), 7.43 (dd, $^3J=4.9$ Hz, $^4J=3.0$ Hz, 1H, H-5 of thiophene), 7.24 (dd, $^4J=2.9$, 1.1 Hz, 1H, H-2 of thiophene), 7.02 (dd, $^3J=4.9$ Hz, $^4J=1.2$ Hz, 1H, H-4 of thiophene), 6.95 (broad s, 1H, H-3 of pyridine), 6.73 (d, $^3J=7.0$ Hz, 1H, H-5 of pyridine), 6.19 (dd, $^3J=17.1$, 10.1 Hz, 1H, $CH=CH_2$), 6.04 (dd, $^3J=17.1$ Hz, $^2J=2.3$ Hz, 1H, $C=CHH$), 5.54 (dd, $^3J=10.1$ Hz, $^2J=2.3$ Hz, 1H, $C=CHH$), 4.76–4.66 (m, 1H, $C_\alpha H$), 3.76–3.42 (m, 10H, $4\times CH_2$ of piperazine, CH_2 -thiophene), 3.15–3.05 (m, 2H, $C_\epsilon H_2$), 2.43 (s, 3H, CH_3), 1.71–1.60 (m, 1H, $C_\beta HH$), 1.60–1.48 (m, 1H, $C_\beta HH$), 1.47–1.34 (m, 2H, $C_\delta H_2$), 1.33–1.20 (m, 2H, $C_\gamma H_2$); ^{13}C -NMR (DMSO- d_6) δ =170.23, 169.44, 164.42, 158.13 (q, $^2J_{C,F}=36.4$ Hz, CO of TFA), 136.05, 131.85 ($CH_2=C$), 128.64 (C-4 of thiophene), 125.61 (C-5 of thiophene), 124.77 ($CH_2=C$), 122.13 (C-5 of thiophene), 112.78 (C-5 of pyridine), 48.19 ($C_\alpha H$), 45.58 (CH_2 of piperazine), 45.21 (CH_2 of piperazine), 43.96 (CH_2 of piperazine), 40.84 (CH_2 of piperazine), 38.27 ($C_\epsilon H_2$), 36.67 (CH_2 -thiophene), 31.24 (C_β), 28.84 (C_δ), 22.56

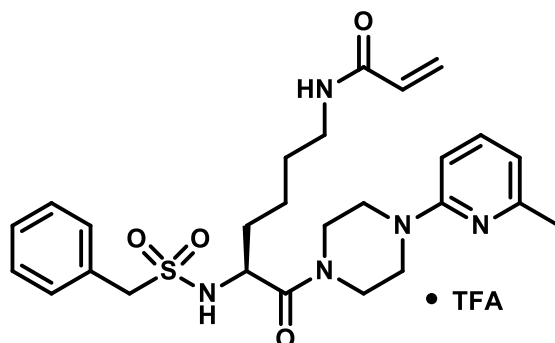
(C_γ), signals for CH₃ and C-2,3,4,6 of pyridine are not visible; ¹⁹F-NMR (DMSO-*d*₆) δ= -74.77 (s, TFA); MS (ESI⁺): m/z calculated for C₂₅H₃₄N₅O₃S: 484.24 [M+H]⁺, found: 484.2.

N^ε-Cyclohexylacetyl-N^ε-acryloyl-L-lysine-4-(6-methylpyridin-2-yl)piperazide×TFA (14d)



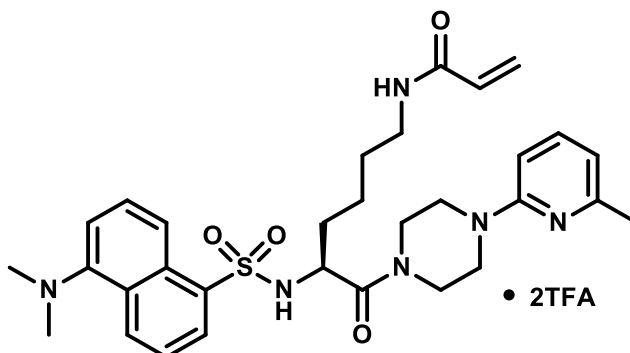
Compound **14d** (13 mg, 54%, yellow solid) was synthesised according to **GP VIII** using compound **5a** (0.04 mmol) and cyclohexylacetyl chloride. ¹H-NMR (DMSO-*d*₆) δ=8.11–8.03 (m, 2H, N_aH, N_eH), 7.68 (broad s, 1H, H–4 of pyridine), 6.89 (broad s, 1H, H–3 of pyridine), 6.69 (broad s, 1H, H–5 of pyridine), 6.18 (dd, ³J=17.1, 10.1 Hz, 1H, CH=CH₂), 6.04 (dd, ³J=17.1 Hz, ²J=2.3 Hz, 1H, C=CHH), 5.54 (dd, ³J=10.1 Hz, ²J=2.3 Hz, 1H, C=CHH), 4.75–4.66 (m, 1H, C_αH), 3.78–3.43 (m, 8H, 4×CH₂ of piperazine), 3.15–3.04 (m, 2H, C_εH₂), 2.41 (s, 3H, CH₃), 2.06–1.92 (m, 2H, CH₂-cyclohexyl), 1.71–0.81 (m, 17H, C_βH₂, C_γH₂, C_δH₂, 5×CH₂ of cyclohexyl, 1×CH of cyclohexyl); ¹³C-NMR (DMSO-*d*₆) δ=171.08, 170.32, 164.42, 158.04 (q, ²J_{C,F}=34.9 Hz, CO of TFA), 131.85 (CH₂=C), 124.79 (CH₂=C), 112.70 (C–5 of pyridine), 47.93 (C_α), 45.53 (CH₂ of piperazine), 45.08 (CH₂ of piperazine), 44.12 (CH₂ of piperazine), 42.84 (CH₂-cyclohexyl), 40.93 (CH₂ of piperazine), 38.29 (C_ε), 34.72 (CH of cyclohexyl), 32.55 (CH₂ of cyclohexyl), 32.42 (CH₂ of cyclohexyl), 31.15 (C_β), 28.82 (C_δ), 25.86 (CH₂ of cyclohexyl), 25.64 (CH₂ of cyclohexyl), 25.61 (CH₂ of cyclohexyl), 22.67 (C_γ), signals for CH₃ and C-2,3,4,6 of pyridine are not visible; ¹⁹F-NMR (DMSO-*d*₆) δ= -74.52 (s, TFA); MS (ESI⁺): m/z calculated for C₂₇H₄₂N₅O₃: 484.33 [M+H]⁺, found: 484.4.

***N*^α-Phenylmethanesulfonyl-*N*^ε-acryloyl-L-lysine-4-(6-methylpyridin-2-yl)piperazide×TFA (14e)**



Compound **14e** (8 mg, 32%, yellow solid) was synthesised according to **GP VIII** using compound **5a** (0.04 mmol) and phenylmethanesulfonyl chloride. **¹H-NMR** (DMSO-*d*₆) δ=8.05 (t, ³*J*=5.6 Hz, 1H, N_εH), 7.65 (broad s, 1H, H-4 of pyridine), 7.41–7.29 (m, 6H, 5×H of phenyl, N_αH), 6.85 (broad s, 1H, H-3 of pyridine), 6.68 (broad s, 1H, H-5 of pyridine), 6.18 (dd, ³*J*=17.1, 10.1 Hz, 1H, CH=CH₂), 6.02 (dd, ³*J*=17.1 Hz, ²*J*=2.3 Hz, 1H, C=CHH), 5.53 (dd, ³*J*=10.1 Hz, ²*J*=2.3 Hz, 1H, C=CHH), 4.36–4.24 (m, 2H, CH₂-phenyl), 4.24–4.15 (m, 1H, C_αH), 3.70–3.45 (m, 8H, 4×CH₂ of piperazine), 3.14–3.03 (m, 2H, C_εH₂), 2.40 (s, 3H, CH₃), 1.63–1.19 (m, 6H, C_βH₂, C_γH₂, C_δH₂); **¹³C-NMR** (DMSO-*d*₆) δ=170.09, 164.42, 158.00 (d, ²*J*_{C,F}=34.7 Hz, CO of TFA), 131.83 (CH₂=C), 130.84 (2×C of phenyl), 130.13 (C-1 of phenyl), 128.17 (2×C of phenyl), 127.94 (C-4 of phenyl), 124.77 (CH₂=C), 112.69 (C-5 of pyridine), 58.54 (CH₂-phenyl), 52.10 (C_α), 45.21 (CH₂ of piperazine), 44.92 (CH₂ of piperazine), 44.18 (CH₂ of piperazine), 41.04 (CH₂ of piperazine), 38.24 (C_ε), 32.28 (C_β), 28.79 (C_δ), 22.32 (C_γ), signals for CH₃ and C-2,3,4,6 of pyridine are not visible; **¹⁹F-NMR** (DMSO-*d*₆) δ= -74.47 (s, TFA); MS (ESI⁺): *m/z* calculated for C₂₆H₃₆N₅O₄: 514.25 [M+H]⁺, found: 514.2.

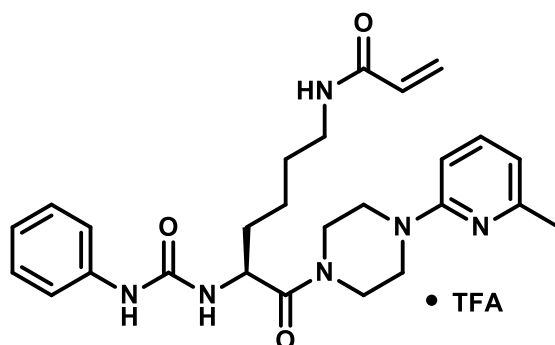
***N*^α-Dansyl-*N*^ε-acryloyl-L-lysine-4-(6-methylpyridin-2-yl)piperazide×TFA (14f)**



Compound **14f** (67 mg, 49%, yellow solid) was synthesised according to **GP VIII** using compound **5a** (0.19 mmol) and dansyl chloride. **¹H-NMR** (DMSO-*d*₆) δ=8.41 (d, ³*J*=8.5 Hz, 1H,

H of dansyl), 8.33 (d, $^3J=8.7$ Hz, 1H, H of dansyl), 8.25 (d, $^3J=8.9$ Hz, 1H, $N_\alpha H$), 8.13 (dd, $^3J=7.3$ Hz, $^4J=1.1$ Hz, 1H, H of dansyl), 7.95 (t, $^3J=5.5$ Hz, 1H, $N_\epsilon H$), 7.69 (broad s, 1H, H-4 of pyridine), 7.60–7.54 (m, 2H, 2×H of dansyl), 7.24 (d, $^3J=7.4$ Hz, 1H, H of dansyl), 6.83 (broad s, 1H, H-3 of pyridine), 6.70 (d, $^3J=7.5$ Hz, 1H, H-5 of pyridine), 6.15 (dd, $^3J=17.1$, 10.1 Hz, 1H, $CH=CH_2$), 6.01 (dd, $^3J=17.1$ Hz, $^2J=2.4$ Hz, 1H, $C=CHH$), 5.52 (dd, $^3J=10.0$ Hz, $^2J=2.4$ Hz, 1H, $C=CHH$), 4.19–4.09 (m, 1H, $C_\alpha H$), 3.56–3.10 (m, 8H, 4× CH_2 of piperazine), 2.93–2.82 (m, 2H, $C_\epsilon H_2$), 2.79 (s, 6H, 2× CH_3 of dansyl), 2.41 (s, 3H, CH_3), 1.52–1.34 (m, 2H, $C_\beta H_2$), 1.26–0.96 (m, 4H, $C_\gamma H_2$, $C_\delta H_2$); ^{13}C -NMR (DMSO- d_6) δ =169.20 (CON), 164.33 (CON $_\epsilon$), 158.29, 157.93, 150.93 (quart. C of dansyl), 136.32 (quart. C of dansyl), 131.81 ($CH_2=C$), 129.43, 129.14 (quart. C of dansyl), 128.83 (quart. C of dansyl), 128.32, 127.68, 124.75 ($CH_2=C$), 123.38, 119.63, 115.11, 112.78 (C-5 of pyridine), 51.75 (C_α), 45.21 (CH_2 of piperazine), 45.05 (2× CH_3 of dansyl), 44.73 (CH_2 of piperazine), 43.89 (CH_2 of piperazine), 40.65 (CH_2 of piperazine), 38.09 (C_ϵ), 31.70 (C_β), 28.41 (C_δ), 22.20 (C_γ), signals for CH_3 and C-3,4 of pyridine are not visible; ^{19}F -NMR (DMSO- d_6) δ = -74.74 (s, TFA); MS (ESI $^+$): m/z calculated for $C_{31}H_{41}N_6O_4S$: 593.29 [M+H] $^+$, found: 593.1.

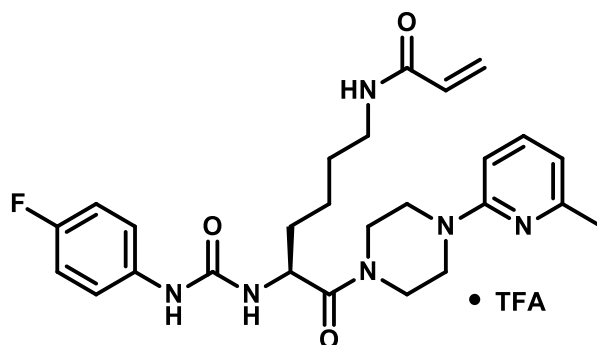
***N* $^\alpha$ -Phenylcarbamoyl-*N* $^\epsilon$ -acryloyl-L-lysine-4-(6-methylpyridin-2-yl)piperazide×TFA (**14g**)**



Compound **14g** (46 mg, 40%, white solid) was synthesised according to **GP VIII** using compound **5a** (0.19 mmol) and phenyl isocyanate. 1H -NMR (DMSO- d_6) δ =8.68 (s, 1H, NH-phenyl), 8.05 (t, $^3J=5.5$ Hz, 1H, $N_\epsilon H$), 7.67 (broad s, 1H, H-4 of pyridine), 7.36 (d, $^3J=8.3$ Hz, 2H, H-2,6 of phenyl), 7.21 (t, $^3J=7.9$ Hz, 2H, H-3,5 of phenyl), 6.89 (ps-t, $^3J=7.3$ Hz, 2H, H-4 of phenyl, H-3 of pyridine), 6.68 (d, $^3J=6.7$ Hz, 1H, H-5 of pyridine), 6.50 (d, $^3J=8.3$ Hz, 1H, $N_\alpha H$), 6.18 (dd, $^3J=17.1$, 10.1 Hz, 1H, $CH=CH_2$), 6.03 (dd, $^3J=17.1$ Hz, $^2J=2.3$ Hz, 1H, $C=CHH$), 5.52 (dd, $^3J=10.1$ Hz, $^2J=2.3$ Hz, 1H, $C=CHH$), 4.77–4.69 (m, 1H, $C_\alpha H$), 3.82–3.50 (m, 8H, 4× CH_2 of piperazine), 3.15–3.06 (m, 2H, $C_\epsilon H_2$), 2.40 (s, 3H, CH_3), 1.72–1.58 (m, 1H, $C_\beta H$), 1.56–1.26 (m, 5H, $C_\beta HH$, $C_\gamma H_2$, $C_\delta H_2$); ^{13}C -NMR (DMSO- d_6) δ =170.86 (CON), 164.42 (CON $_\epsilon$), 154.66 (CON $_\alpha$), 140.23 (C-1 of phenyl), 131.84 ($CH_2=C$), 128.67 (C-3,5 of phenyl), 124.76 ($CH_2=C$), 121.16 (C-4 of phenyl), 117.51 (C-2,6 of phenyl), 112.68 (C-5 of pyridine), 48.41

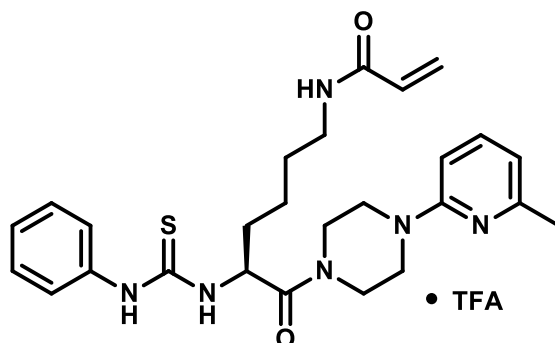
(C_α), 45.41 (CH₂ of piperazine), 44.98 (CH₂ of piperazine), 44.21 (CH₂ of piperazine), 40.94 (CH₂ of piperazine), 38.30 (C_ε), 32.27 (C_β), 28.87 (C_δ), 22.31 (C_γ), signals for CH₃ and C,2,3,4,6 of pyridine are not visible; ¹⁹F-NMR (DMSO-*d*₆) δ= -74.49 (s, TFA); MS (ESI⁺): *m/z* calculated for C₂₆H₃₅N₆O₃: 479.28 [M+H]⁺, found: 479.1.

N^α-4-Fluorophenylcarbamoyl-N^ε-acryloyl-L-lysine-4-(6-methylpyridin-2-yl)piperazide×TFA (14h)



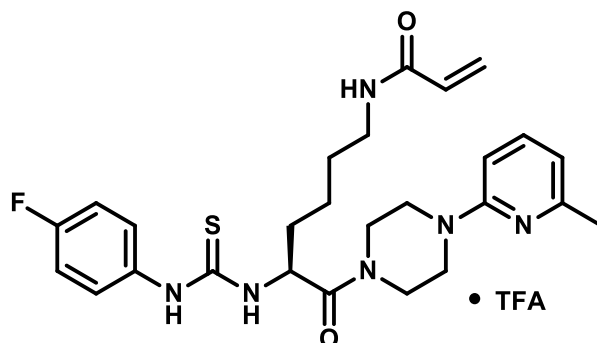
Compound **14h** (71 mg, 87%, white solid) was synthesised according to **GP VIII** using compound **5a** (0.13 mmol) and 4-fluorophenyl isocyanate. ¹H-NMR (DMSO-*d*₆) δ=8.72 (s, 1H, NH-phenyl), 8.05 (t, ³J=5.6 Hz, 1H, N_εH), 7.75 (broad s, 1H, H-4 of pyridine), 7.41–7.33 (m, 2H, H-2,6 of fluorophenyl), 7.05 (t, ³J_{H,H}=³J_{H,F}=8.9 Hz, 2H, H-3,5 of fluorophenyl), 6.97 (s, 1H, H-3 of pyridine), 6.73 (d, ³J=6.9 Hz, 1H, H-5 of pyridine), 6.49 (d, ³J=8.3 Hz, 1H, N_αH), 6.18 (dd, ³J=17.1, 10.1 Hz, 1H, CH=CH₂), 6.03 (dd, ³J=17.1 Hz, ²J=2.3 Hz, 1H, C=CHH), 5.53 (dd, ³J=10.1 Hz, ²J=2.3 Hz, 1H, C=CHH), 4.80–4.67 (m, 1H, C_αH), 3.84–3.54 (m, 8H, 4×CH₂ of piperazine), 3.17–3.05 (m, 2H, C_εH₂), 2.44 (s, 3H, CH₃), 1.70–1.58 (m, 1H, C_βHH), 1.58–1.19 (m, 5H, C_βHH, C_γH₂, C_δH₂); ¹³C-NMR (DMSO-*d*₆) δ=170.91 (CON), 164.43 (CON_ε), 158.29, 157.93, 156.91 (d, ¹J_{C,F}=237.3 Hz, C-4 of fluorophenyl), 154.71 (CON_α), 136.59 (d, ⁴J_{C,F}=2.2 Hz, C-1 of fluorophenyl), 131.84 (CH₂=C), 124.77 (CH₂=C), 119.09 (d, ³J_{C,F}=7.6 Hz, C-2,6 of fluorophenyl), 115.14 (d, ²J_{C,F}=22.1 Hz, C-3,5 of phenyl), 112.78 (C-5 of pyridine), 48.47 (C_α), 45.63 (CH₂ of piperazine), 45.19 (CH₂ of piperazine), 44.03 (CH₂ of piperazine), 40.84 (CH₂ of piperazine), 38.29 (C_ε), 32.20 (C_β), 28.88 (C_δ), 22.29 (C_γ); ¹⁹F-NMR (DMSO-*d*₆) δ= -74.77 (s, TFA), -122.37– -122.46 (m, F-4); MS (ESI⁺): *m/z* calculated for C₂₆H₃₄FN₆O₃: 497.27 [M+H]⁺, found: 497.1.

***N*^α-Phenylthiocarbamoyl-*N*^ε-acryloyl-L-lysine-4-(6-methylpyridin-2-yl)piperazide×TFA
(14i)**



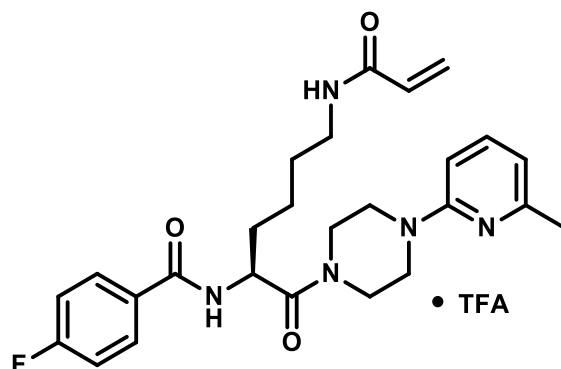
Compound **14i** (72 mg, 61%, colourless oil) was synthesised according to **GP VIII** using compound **5a** (0.19 mmol) and phenyl isothiocyanate. **¹H-NMR** (DMSO-*d*₆) δ=10.57 (s, 1H, NH-phenyl), 8.78 (broad s, 1H, NH-phenyl), 8.09 (t, ³*J*=6.0 Hz, 1H, N_H), 7.55–7.42 (m, 4H, H–4 of pyridine, 3×H of phenyl), 7.29–7.24 (m, 2H, 2×H of phenyl), 6.73 (d, ³*J*=8.5 Hz, 1H, H–3 of pyridine), 6.62 (d, ³*J*=7.2 Hz, 1H, H–5 of pyridine), 6.21 (dd, ³*J*=17.1, 10.1 Hz, 1H, CH=CH₂), 6.07 (dd, ³*J*=17.1 Hz, ²*J*=2.4 Hz, 1H, C=CHH), 5.57 (dd, ³*J*=10.0 Hz, ²*J*=2.4 Hz, 1H, C=CHH), 4.77–4.69 (m, 1H, C_αH), 3.82–3.50 (m, 8H, 4×CH₂ of piperazine), 3.15–3.06 (m, 2H, C_εH₂), 2.40 (s, 3H, CH₃), 1.89–1.78 (m, 1H, C_βHH), 1.78–1.68 (m, 1H, C_βHH), 1.52–1.35 (m, 4H, C_γH₂, C_δH₂); **¹³C-NMR** (DMSO-*d*₆) δ=182.38 (CS), 174.27 (CON), 164.47 (CON_ε), 158.00 (d, ²*J*_{C,F}=34.5 Hz, CO of TFA), 157.33, 155.48, 138.56 (C–4 of pyridine), 133.40 (C–1 of phenyl), 131.85 (CH₂=C), 128.79 (2×C of phenyl), 128.68 (2×C of phenyl), 128.55 (C–4 of phenyl), 124.79 (CH₂=C), 113.24 (C–5 of pyridine), 104.69 (C–3 of pyridine), 59.20 (C_α), 42.53 (CH₂ of piperazine), 42.44 (CH₂ of piperazine), 41.85 (CH₂ of piperazine), 41.81 (CH₂ of piperazine), 38.29 (C_ε), 30.48 (C_β), 28.70 (C_δ), 23.92 (CH₃), 21.48 (C_γ); **¹⁹F-NMR** (DMSO-*d*₆) δ= -74.33 (s, TFA); MS (ESI⁺): *m/z* calculated for C₂₆H₃₅N₆O₂S: 495.25 [M+H]⁺, found: 495.1.

***N*^α-4-Fluorophenylthiocarbamoyl-*N*^ε-acryloyl-L-lysine-4-(6-methylpyridin-2-yl)piperazide×TFA (**14j**)**



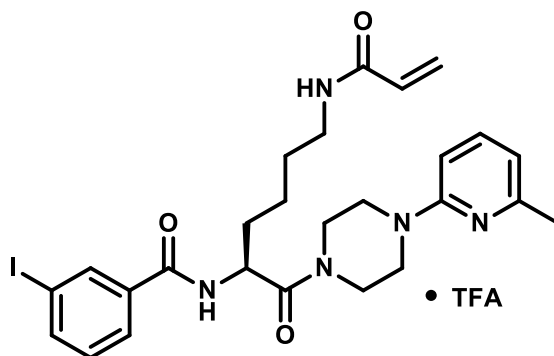
Compound **14j** (66 mg, 79%, white solid) was synthesised according to **GP VIII** using compound **5a** (0.13 mmol) and 4-fluorophenyl isothiocyanate. **¹H-NMR** (DMSO-*d*₆) δ=10.60 (s, 1 H, NH-phenyl), 8.80 (s, 1H, NH-phenyl), 8.09 (t, ³*J*=5.3 Hz, 1H, N_H), 7.55 (dd, ³*J*=8.4, 7.4 Hz, 1H, H-4 Pyridin), 7.34–7.30 (m, 4H, 4×H of fluorophenyl), 6.76 (d, ³*J*=8.5 Hz, H-3 of pyridine), 6.64 (d, ³*J*=7.3, 1H, H-5 of pyridine), 6.20 (dd, ³*J*=17.1, 10.1 Hz, 1H, CH=CH₂), 6.07 (dd, ³*J*=17.1 Hz, ²*J*=2.3 Hz, 1H, C=CHH), 5.57 (dd, ³*J*=10.0 Hz, ²*J*=2.4 Hz, 1H, C=CHH), 4.43–4.39 (m, 1H, C_αH), 3.74–3.67 (m, 4H, 2×CH₂ of piperazine), 3.24–3.09 (m, 6H, 2×CH₂ of piperazine, C_εH₂), 2.34 (s, 3H, CH₃), 1.89–1.68 (m, 2H, C_βH₂), 1.58–1.19 (m, 4H, C_γH₂, C_δH₂); **¹³C-NMR** (DMSO-*d*₆) δ=182.29 (CS of fluorophenyl), 174.24 (CON), 164.48 (CON_ε), 161.70 (d, ¹*J*_{C,F}=245.4 Hz, C-4 of fluorophenyl), 158.29, 157.94, 138.90 (C-4 of pyridine), 131.85 (CH₂=C), 131.01 (d, ³*J*_{C,F}=9.0 Hz, C-2,6 of fluorophenyl), 129.63 (d, ⁴*J*_{C,F}=3.0 Hz, C-1 of fluorophenyl), 124.81 (CH₂=C), 115.61 (d, ²*J*_{C,F}=22.8 Hz, C-3,5 of fluorophenyl), 113.28 (C-5 of pyridine), 105.01 (C-3 of pyridine), 59.23 (C_α), 42.50 (CH₂ of piperazine), 42.41 (CH₂ of piperazine), 41.96 (CH₂ of piperazine), 41.92 (CH₂ of piperazine), 38.29 (C_ε), 30.45 (C_β), 28.70 (C_δ), 23.65 (CH₃), 21.53 (C_γ); **¹⁹F-NMR** (DMSO-*d*₆) δ= -74.61 (s, TFA), -113.07– -113.18 (m, F-4); MS (ESI⁺): *m/z* calculated for C₂₆H₃₄FN₆O₂S: 513.24 [M+H]⁺, found: 513.1.

***N*^α-4-Fluorobenzoyl-*N*^ε-acryloyl-L-lysine-4-(6-methylpyridin-2-yl)piperazide×TFA (14k)**



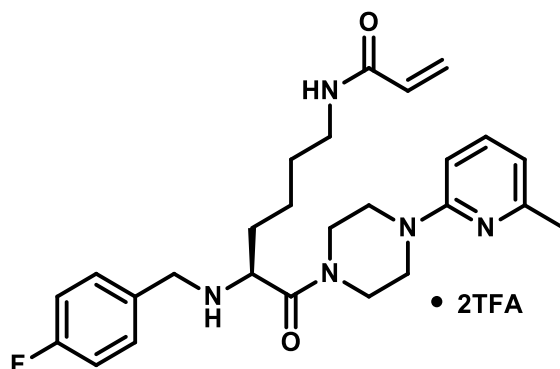
Compound **14k** (91 mg, 71%, rose oil) was synthesised according to **GP VIII** using compound **5a** (0.21 mmol) and 4-fluorobenzoyl chloride. **¹H-NMR** (DMSO-*d*₆) δ=8.67 (d, ³*J*=7.8 Hz, 1H, N_αH), 8.07 (t, ³*J*=5.6 Hz, 1H, N_εH), 7.97 (dd, ³*J*_{H,H}=8.9 Hz, ⁴*J*_{H,F}=5.5 Hz, 2H, H–2,6 of fluorobenzoyl), 7.75 (broad s, 1H, H–4 of pyridine), 7.29 (t, ³*J*_{H,H}=³*J*_{H,F}=8.9 Hz, 2H, H–3,5 of fluorobenzoyl), 6.98 (breites s, 1H, H–3 of pyridine), 6.73 (d, ³*J*=7.1 Hz, 1H, H–5 of pyridine), 6.18 (dd, ³*J*=17.1, 10.1 Hz, 1H, CH=CH₂), 6.03 (dd, ³*J*=17.1 Hz, ²*J*=2.3 Hz, 1H, C=CHH), 5.54 (dd, ³*J*=10.1 Hz, ²*J*=2.3 Hz, 1H, C=CHH), 4.93–4.85 (m, C_αH), 3.86–3.52 (m, 8H, 4×CH₂ of piperazine), 3.18–3.05 (m, 2H, C_εH₂), 2.43 (s, 3H, CH₃), 1.78–1.68 (m, 2H, C_βH₂), 1.52–1.29 (m, 4H, C_γH₂, C_δH₂); **¹³C-NMR** (DMSO-*d*₆) δ=170.31 (CON), 165.18, 164.38 (CON_ε), 163.95 (d, ²*J*_{C,F}=248.7 Hz, C–4 of fluorobenzoyl), 158.29, 157.93, 131.85 (CH₂=C), 130.30 (d, ⁴*J*_{C,F}=2.9 Hz, C–1 of fluorobenzoyl), 130.18 (d, ³*J*_{C,F}=9.0 Hz, C–2,6 of fluorobenzoyl), 124.77 (CH₂=C), 115.14 (d, ²*J*_{C,F}=21.7 Hz, C–3,5 of fluorobenzoyl), 112.74 (C–5 of pyridine), 49.30 (C_α), 45.65 (CH₂ of piperazine), 45.25 (CH₂ of piperazine), 44.04 (CH₂ of piperazine), 40.93 (CH₂ of piperazine), 38.26 (C_ε), 30.73 (C_β), 28.90 (C_δ), 22.93 (C_γ), signals for CH₃ and C-3,4 of pyridine are not visible; **¹⁹F-NMR** (DMSO-*d*₆) δ= -72.55 (s, TFA), -107.00– -107.14(m, F-4); MS (ESI⁺): *m/z* calculated for C₂₆H₃₃FN₅O₃: 482.26 [M+H]⁺, found: 482.2.

***N*^α-3-Iodobenzoyl-*N*^ε-acryloyl-L-lysine-4-(6-methylpyridin-2-yl)piperazidexTFA (14I)**



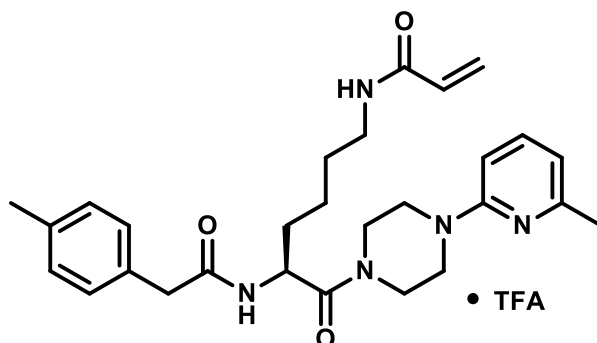
Compound **14I** (60 mg, 40%, yellow solid) was synthesised according to **GP IX** using compound **5a** (0.21 mmol) and 3-iodobenzoic acid. **¹H-NMR** (DMSO-*d*₆) δ=8.77 (d, ³*J*=7.9 Hz, 1H, N_αH), 8.26 (t, ⁴*J*=1.6 Hz, 1H, H-2 of iodobenzoyl), 8.07 (t, ³*J*=5.5 Hz, 1H, N_εH), 7.92–7.90 (m, 1H, H-4 of iodobenzoyl), 7.90–7.88 (m, 1H, H-6 of iodobenzoyl), 7.71 (broad s, 1H, H-4 of pyridine), 7.28 (t, ³*J*=7.8 Hz, H-5 of iodobenzoyl), 6.94 (broad s, 1H, H-3 of pyridine), 6.71 (d, ³*J*=6.6 Hz, 1H, H-5 of pyridine), 6.18 (dd, ³*J*=17.1, 10.1 Hz, 1H, CH=CH₂), 6.03 (dd, ³*J*=17.1 Hz, ²*J*=2.3 Hz, 1H, C=CHH), 5.54 (dd, ³*J*=10.1 Hz, ²*J*=2.3 Hz, 1H, C=CHH), 4.94–4.85 (m, C_αH), 3.83–3.48 (m, 8H, 4×CH₂ of piperazine), 3.17–3.06 (m, 2H, C_εH₂), 2.42 (s, 3H, CH₃), 1.78–1.67 (m, 2H, C_βH₂), 1.53–1.27 (m, 4H, C_γH₂, C_δH₂); **¹³C-NMR** (DMSO-*d*₆) δ=170.18 (CON), 164.65, 164.44, 158.59, 158.24, 157.88, 139.90 (C-4 of iodobenzoyl), 135.81 (C-2 of iodobenzoyl), 131.85 (CH₂=C), 130.44 (C-5 of iodobenzoyl), 127.01 (C-6 of iodobenzoyl), 124.77 (CH₂=C), 112.70 (C-5 of pyridine), 99.69, 94.58 (C-3 of iodobenzoyl), 49.32 (C_α), 45.54 (CH₂ of piperazine), 45.16 (CH₂ of piperazine), 44.09 (CH₂ of piperazine), 40.98 (CH₂ of piperazine), 38.25 (C_ε), 30.68 (C_β), 28.86 (C_δ), 22.91 (C_γ), signal for CH₃ is not visible; **¹⁹F-NMR** (DMSO-*d*₆) δ= -74.63 (s, TFA); MS (ESI⁺): *m/z* calculated for C₂₆H₃₃IN₅O₃: 590.16 [M+H]⁺, found: 590.2.

N^α-4-Fluorobenzyl-N^ε-acryloyl-L-lysine-4-(6-methylpyridin-2-yl)piperazide×2TFA (14m)



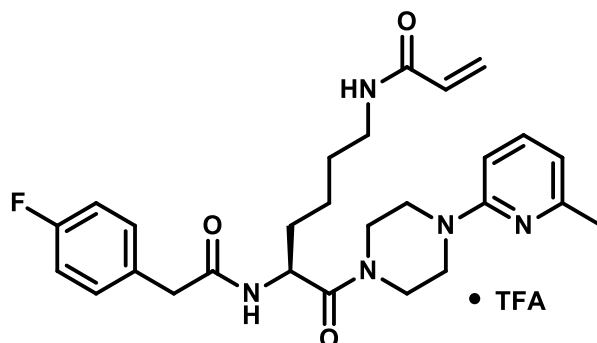
The synthesis was accomplished according to the general procedure for reductive alkylation described by Abdel-Magid and Mehrman⁴⁰. To a solution of compound **5a** (80.9 mg, 0.14 mmol, 1 eq.) in THF (10 mL) under N₂ atmosphere were added TEA (48 μL, 0.345 mmol, 2.5 eq.) and 4-fluorobenzaldehyde (13.8 μL, 0.13 mmol, 0.95 eq.) followe by the addition of sodium triacetoxyborohydride (40.9 mg, 0.19 mmol, 1.4 eq.). The reaction mixture was stirred for 24 h. 4-Fluorobenzaldehyde (13.9 μL, 0.13 mmol, 0.95 eq.) was added again and stirring was continued for 24 h. Subsequently, the solvent was removed *in vacuo*, the residue was dissolved in 3 M NaOH (10 mL) and extracted with ethyl acetate (3×20 mL). The organic phases were combined, dried over Na₂SO₄ and evaporated. The crude product was purified by preparative RP-HPLC. The product-containing fractions were combined and lyophilised to afford compound **14m** (9 mg, 9%) as a light yellow solid. **¹H-NMR** (DMSO-*d*₆) δ=9.28 (s, 1H, NH), 9.12 (s, 1H, NH), 8.05 (t, ³J=5.6 Hz, 1H, N_H), 7.58–7.46 (m, 3H, H–2,6 of fluorophenyl, H–4 of pyridine), 7.32–7.25 (m, 2H, H–3,5 of fluorophenyl), 6.73 (d, ³J=8.4 Hz, 1H, H–3 of pyridine), 6.61 (d, ³J=7.2 Hz, 1H, H–5 of pyridine), 6.16 (dd, ³J=17.1, 10.1 Hz, 1H, CH=CH₂), 6.00 (dd, ³J=17.1 Hz, ²J=2.3 Hz, 1H, C=CHH), 5.51 (dd, ³J=10.1 Hz, ²J=2.3 Hz, 1H, C=CHH), 4.52–4.43 (s, 1H, C_αH), 4.15–4.00 (m, 2H, CH₂-fluorophenyl), 3.67–3.46 (m, 8H, 4×CH₂ of piperazine), 3.20–3.03 (m, 2H, C_εH₂), 2.35 (s, 3H, CH₃), 1.87–1.71 (m, 2H, C_βH₂), 1.48–1.20 (m, 4H, C_γH₂, C_δH₂); **¹³C-NMR** (DMSO-*d*₆) δ=165.98, 164.50, 158.00 (q, ²J_{C,F}=34.1 Hz, CO of TFA), 132.74 (d, ³J_{C,F}=8.7 Hz, C–2,6 of fluorophenyl), 131.72 (CH₂=C), 127.52 (s), 124.89 (CH₂=C), 115.49 (d, ²J_{C,F}=21.7 Hz, C–3,5 of fluorophenyl), 112.70 (C–5 of pyridine), 55.76 (C_α), 48.69 (CH₂-fluorophenyl), 44.73 (CH₂ of piperazine), 44.43 (CH₂ of piperazine), 44.33 (CH₂ of piperazine), 41.48 (CH₂ of piperazine), 37.90 (C_ε), 29.43 (C_β), 28.88 (C_δ), 21.17 (C_γ), signals for C-1,4 of fluorophenyl, C-2,3,4,6 of pyridine and CH₃ are not visible; **¹⁹F-NMR** (DMSO-*d*₆) δ= -74.31 (s, TFA), -122.44– -112.56 (m, F-4); MS (ESI⁺): m/z calculated for C₂₆H₃₅FN₅O₂: 468.28 [M+H]⁺, found: 468.3.

***N*^α-4-Methylphenylacetyl-*N*^ε-acryloyl-L-lysine-4-(6-methylpyridin-2-yl)piperazide×TFA
(15a)**



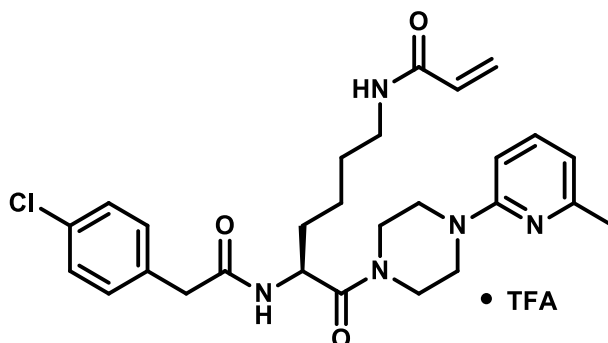
Compound **15a** (15 mg, 24%, white solid) was synthesised according to **GP IX** using compound **5a** (0.10 mmol) and 4-methylphenylacetic acid. **¹H-NMR** (DMSO-*d*₆) δ=8.34 (d, ³*J*=8.2 Hz, 1H, N_δH), 8.03 (t, ³*J*=5.3 Hz, 1H, N_εH), 7.63 (broad s, 1H, H-4 of pyridine), 7.14 (d, ³*J*=8.0 Hz, 2H, 2×H of methylphenyl), 7.07 (d, ³*J*=7.9 Hz, 2H, 2×H of methylphenyl), 6.79 (broad s, 1H, H-3 of pyridine), 6.66 (d, ³*J*=5.8 Hz, 1H, H-5 of pyridine), 6.18 (dd, ³*J*=17.1, 10.1 Hz, 1H, CH=CH₂), 6.04 (dd, ³*J*=17.1 Hz, ²*J*=2.3 Hz, 1H, C=CHH), 5.54 (dd, ³*J*=10.1 Hz, ²*J*=2.3 Hz, 1H, C=CHH), 4.73–4.65 (m, 1H, C_αH), 3.72–3.30 (m, 10H, 4×CH₂ of piperazine, CH₂-methylphenyl), 3.13–3.03 (m, 2H, C_εH₂), 2.38 (s, 3H, CH₃ of pyridine), 2.22 (s, 3H, CH₃ of phenyl), 1.71–1.59 (m, 1H, C_βHH), 1.58–1.47 (m, 1H, C_βHH), 1.46–1.35 (m, 2H, C_δH₂), 1.32–1.20 (m, 2H, C_γH₂); **¹³C-NMR** (DMSO-*d*₆) δ=170.07, 169.92, 164.40, 135.27, 133.25, 131.85 (CH₂=C), 128.81 (2×C of methylphenyl), 128.68 (2×C of methylphenyl), 124.74 (CH₂=C), 112.63 (C-5 of pyridine), 48.08 (C_α), 45.23 (CH₂ of piperazine), 44.83 (CH₂ of piperazine), 44.14 (CH₂ of piperazine), 41.56 (CH₂-methylphenyl), 40.98 (CH₂ of piperazine), 38.28 (C_ε), 31.30 (C_β), 28.81 (C_δ), 22.56 (C_γ), 20.57 (CH₃-phenyl), signals for C-2,3,4,6 and CH₃ of pyridine are not visible; **¹⁹F-NMR** (DMSO-*d*₆) δ= -74.43 (s, TFA); MS (ESI⁺): *m/z* calculated for C₂₈H₃₈N₅O₃: 492.30 [M+H]⁺, found: 492.3.

***N*^α-4-Fluorophenylacetyl-*N*^ε-acryloyl-L-lysine-4-(6-methylpyridin-2-yl)piperazide×TFA
(15b)**



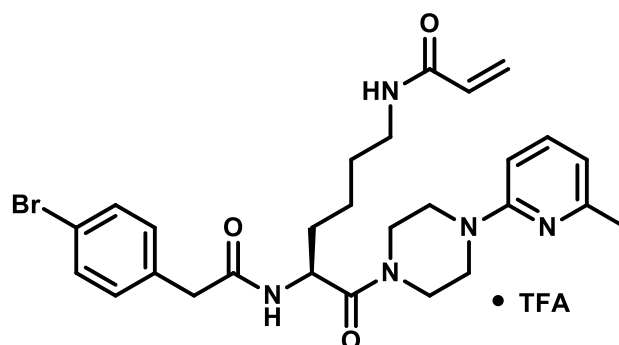
Compound **15b** (104 mg, 58%, rosy solid) was synthesised according to **GP IX** using compound **5a** (0.29 mmol) and 4-fluorophenylacetic acid. **¹H-NMR** (DMSO-*d*₆) δ=8.41 (d, ³*J*=8.2 Hz, 1H, N_δH), 8.04 (t, ³*J*=5.6 Hz, 1H, N_εH), 7.75 (broad s, 1H, H-4 of pyridine), 7.28 (dd, ³*J*_{H,H}=8.7 Hz, ⁴*J*_{H,F}=5.6 Hz, 2H, H-2,6 of fluorophenyl), 7.10 (t, ³*J*_{H,H}=³*J*_{H,F}=8.9 Hz, 2H, H-3,5 of fluorophenyl), 6.94 (broad s, 1H, H-3 of pyridine), 6.73 (d, ³*J*=6.9 Hz, 1H, H-5 of pyridine), 6.18 (dd, ³*J*=17.1, 10.1 Hz, 1H, CH=CH₂), 6.04 (dd, ³*J*=17.1 Hz, ²*J*=2.3 Hz, 1H, C=CHH), 5.54 (dd, ³*J*=10.0 Hz, ²*J*=2.3 Hz, 1H, C=CHH), 4.75–4.64 (m, C_αH), 3.78–3.38 (m, 10H, 4×CH₂ of piperazine, CH₂-fluorophenyl), 3.13–3.03 (m, 2H, C_εH₂), 2.43 (s, 3H, CH₃), 1.70–1.58 (m, 1H, C_βHH), 1.58–1.46 (m, 1H, C_βHH), 1.46–1.33 (m, 2H, C_δH₂), 1.31–1.17 (m, 2H, C_γH₂); **¹³C-NMR** (DMSO-*d*₆) δ=170.18, 169.72, 164.42 (CON_ε), 160.97 (d, ¹*J*_{C,F}=242.1 Hz, C-4 of fluorophenyl), 158.26, 157.90, 132.49 (d, ⁴*J*_{C,F}=3.0 Hz, C-1 of fluorophenyl), 131.85 (CH₂=C), 130.75 (d, ³*J*=8.0 Hz, C-2,6 of fluorophenyl), 124.77 (CH₂=C), 114.84 (d, ²*J*_{C,F}=21.1 Hz, C-3,5 of fluorophenyl), 112.78 (C-5 of pyridine), 99.34 (C-3 of pyridine), 48.18 (C_α), 45.56 (CH₂ of piperazine), 45.17 (CH₂ of piperazine), 43.95 (CH₂ of piperazine), 40.94 (CH₂-phenyl), 40.84 (CH₂ of piperazine), 38.26 (C_ε), 31.25 (C_β), 28.83 (C_δ), 22.55 (C_γ), signals for CH₃ and C-4 of pyridine are not visible; **¹⁹F-NMR** (DMSO-*d*₆) δ= -74.75 (s, TFA), -116.76–-116.96 (m, F-4); MS (ESI⁺): *m/z* calculated for C₂₇H₃₅FN₅O₃: 496.27 [M+H]⁺, found: 496.3.

***N*^α-4-Chlorophenylacetyl-*N*^ε-acryloyl-L-lysine-4-(6-methylpyridin-2-yl)piperazide×TFA
(15c)**



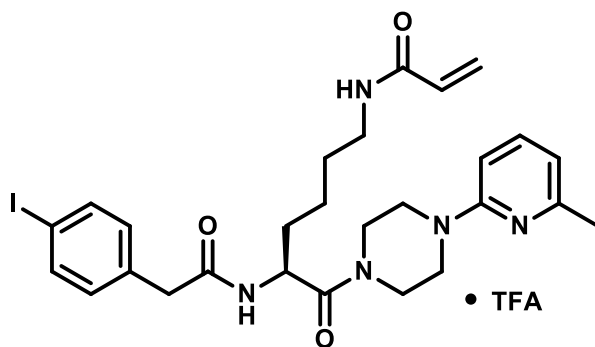
Compound **15c** (18 mg, 29%, white solid) was synthesised according to **GP IX** using compound **5a** (0.10 mmol) and 4-chlorophenylacetic acid. **¹H-NMR** (DMSO-*d*₆) δ=8.44 (d, ³*J*=8.1 Hz, 1H, N_αH), 8.05 (t, ³*J*=5.7 Hz, 1H, N_εH), 7.73 (t, ³*J*=8.0 Hz, 1H, H-4 of pyridine), 7.37–7.31 (m, 2H, 2×H of chlorophenyl), 7.30–7.24 (m, 2H, 2×H of chlorophenyl), 6.92 (d, ³*J*=8.5 Hz, 1H, H-3 of pyridine), 6.72 (d, ³*J*=7.2 Hz, 1H, H-5 of pyridine), 6.18 (dd, ³*J*=17.1, 10.1 Hz, 1H, CH=CH₂), 6.04 (dd, ³*J*=17.1 Hz, ²*J*=2.3 Hz, 1H, C=CHH), 5.54 (dd, ³*J*=10.1 Hz, ²*J*=2.3 Hz, 1H, C=CHH), 4.73–4.66 (m, 1H, C_αH), 3.69–3.40 (m, 10H, 4×CH₂ of piperazine, CH₂-chlorophenyl), 3.12–3.04 (m, 2H, C_εH₂), 2.42 (s, 3H, CH₃), 1.71–1.60 (m, 1H, C_βHH), 1.59–1.47 (m, 1H, C_βHH), 1.46–1.35 (m, 1H, C_δH₂), 1.32–1.19 (m, 2H, C_γH₂); **¹³C-NMR** (DMSO-*d*₆) δ=170.17, 169.49, 164.47, 135.36, 131.85 (CH₂=C), 131.10, 130.84 (2×C of chlorophenyl), 128.10 (2×C of chlorophenyl), 124.83 (CH₂=C), 112.80 (C-5 of pyridine), 48.24 (C_α), 45.55 (CH₂ of piperazine), 45.17 (CH₂ of piperazine), 44.00 (CH₂ of piperazine), 41.11 (CH₂-chlorophenyl), 40.87 (CH₂ of piperazine), 38.28 (C_ε), 31.25 (C_β), 28.84 (C_δ), 22.58 (C_γ), signals for CH₃ and C-2,3,4,6 of pyridine are not visible; **¹⁹F-NMR** (DMSO-*d*₆) δ= -74.67 (s, TFA); MS (ESI⁺): *m/z* calculated for C₂₇H₃₅ClN₅O₃: 512.24 [M(³⁵Cl)+H]⁺, found: 512.2.

***N*^α-4-Bromophenylacetyl-*N*^ε-acryloyl-L-lysine-4-(6-methylpyridin-2-yl)piperazide×TFA
(15d)**



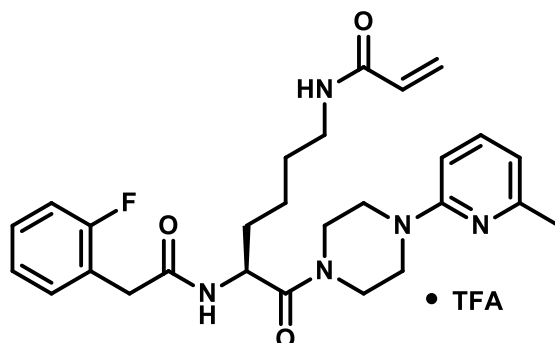
Compound **15d** (34 mg, 51%, white solid) was synthesised according to **GP IX** using compound **5a** (0.10 mmol) and 4-bromophenylacetic acid. **¹H-NMR** (DMSO-*d*₆) δ=8.44 (d, ³*J*=8.1 Hz, 1H, N_δH), 8.04 (t, ³*J*=5.6 Hz, 1H, N_εH), 7.73 (broad s, 1H, H-4 of pyridine), 7.47 (d, ³*J*=8.4 Hz, 2H, 2×H of bromophenyl), 7.21 (d, ³*J*=8.4 Hz, 2H, 2×H of bromophenyl), 6.93 (broad s, 1H, H-3 of pyridine), 6.72 (d, ³*J*=6.9 Hz, 1H, H-5 of pyridine), 6.18 (dd, ³*J*=17.1, 10.1 Hz, 1H, CH=CH₂), 6.04 (dd, ³*J*=17.1 Hz, ²*J*=2.3 Hz, 1H, C=CHH), 5.54 (dd, ³*J*=10.1 Hz, ²*J*=2.3 Hz, 1H, C=CHH), 4.74–4.66 (m, 1H, C_αH), 3.77–3.38 (m, 10H, 4×CH₂ of piperazine, CH₂-bromophenyl), 3.13–3.04 (m, 2H, C_εH₂), 2.43 (s, 3H, CH₃), 1.71–1.59 (m, 1H, C_βHH), 1.59–1.48 (m, 1H, C_βHH), 1.46–1.35 (m, 2H, C_δH₂), 1.32–1.18 (m, 2H, C_γH₂); **¹³C-NMR** (DMSO-*d*₆) δ=170.13, 169.37, 164.42, 158.12 (q, ²*J*_{C,F}=36.3 Hz, CO of TFA), 135.77 (C-1 of bromophenyl), 131.84 (CH₂=C), 131.21 (2×C of bromophenyl), 131.00 (2×C of bromophenyl), 124.77 (CH₂=C), 119.53 (C-4 of bromophenyl), 112.78 (C-5 of pyridine), 48.21 (C_α), 45.54 (CH₂ of piperazine), 45.14 (CH₂ of piperazine), 43.97 (CH₂ of piperazine), 41.15 (CH₂-bromophenyl), 40.86 (CH₂ of piperazine), 38.25 (C_ε), 31.24 (C_β), 28.83 (C_δ), 22.56 (C_γ), signals for CH₃ and C-2,3,4,6 of pyridine are not visible; **¹⁹F-NMR** (DMSO-*d*₆) δ= -74.76 (s, TFA); MS (ESI⁺): *m/z* calculated for C₂₇H₃₅BrN₅O₃: 556.19 [M(⁷⁹Br)+H]⁺, found: 556.2.

***N*^α-4-iodophenylacetyl-*N*^ε-acryloyl-L-lysine-4-(6-methylpyridin-2-yl)piperazide×TFA (X)**



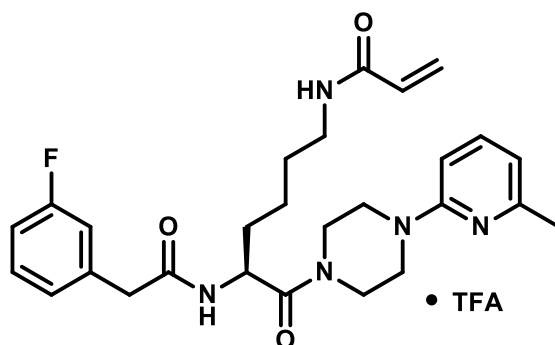
Compound **15e** (49 mg, 32%, light yellow solid) was synthesised according to **GP IX** using compound **5a** (0.21 mmol) and 4-iodophenylacetic acid. **¹H-NMR** (DMSO-*d*₆) δ=8.42 (d, ³*J*=8.1 Hz, 1H, N₆H), 8.04 (t, ³*J*=5.9 Hz, 1H, N₆H), 7.69 (broad s, 1H, H-4 of pyridine), 7.64 (d, ³*J*=8.3 Hz, 2H, H-3,5 of iodophenyl), 7.07 (d, ³*J*=8.3 Hz, 2H, H-2,6 of iodophenyl), 6.87 (broad s, 1H, H-3 of pyridine), 6.69 (d, ³*J*=6.9 Hz, 1H, H-5 of pyridine), 6.18 (dd, ³*J*=17.1, 10.1 Hz, 1H, CH=CH₂), 6.04 (dd, ³*J*=17.1 Hz, ²*J*=2.3 Hz, 1H, C=CHH), 5.54 (dd, ³*J*=10.1 Hz, ²*J*=2.3 Hz, 1H, C=CHH), 4.74–4.64 (m, C_αH), 3.73–3.36 (m, 10H, 4×CH₂ of piperazine, CH₂-iodophenyl), 3.15–3.04 (m, 2H, C_εH₂), 2.41 (s, 3H, CH₃), 1.70–1.59 (m, 1H, C_βHH), 1.58–1.47 (m, 1H, C_βHH), 1.47–1.33 (m, 2H, C_δH₂), 1.33–1.17 (m, 2H, C_γH₂); **¹³C-NMR** (DMSO-*d*₆) δ=170.07, 169.35, 164.41, 157.35, 152.70, 136.88 (C-3,5 of iodophenyl), 136.15 (C-1 of iodophenyl), 131.84 (CH₂=C), 131.40 (C-2,6 of iodophenyl), 124.77 (CH₂=C), 112.71 (C-5 of pyridine), 92.15 (C-4 of iodophenyl), 48.20 (C_α), 45.77 (CH₂ of piperazine), 44.90 (CH₂ of piperazine), 44.14 (CH₂ of piperazine), 41.29 (CH₂-iodophenyl), 40.90 (CH₂ of piperazine), 38.26 (C_ε), 31.26 (C_β), 28.83 (C_δ), 22.57 (C_γ), signals for CH₃ and C-3,4 of pyridine are not visible; **¹⁹F-NMR** (DMSO-*d*₆) δ= -74.52 (s, TFA); MS (ESI⁺): *m/z* calculated for C₂₇H₃₅IN₅O₃: 604.18 [M+H]⁺, found: 604.2.

***N*^α-2-Fluorophenylacetyl-*N*^ε-acryloyl-L-lysine-4-(6-methylpyridin-2-yl)piperazide×TFA
(15f)**



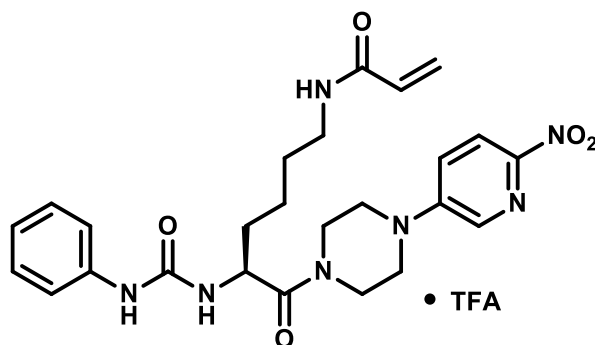
Compound **15f** (13 mg, 35%, colourless solid) was synthesised according to **GP IX** using compound **5a** (0.06 mmol) and 2-fluorophenylacetic acid. **¹H-NMR** (DMSO-*d*₆) δ=8.42 (d, ³*J*=8.1 Hz, 1H, N_αH), 8.06 (t, ³*J*=5.5 Hz, 1H, N_εH), 7.67 (broad s, 1H, H-4 of pyridine), 7.35-7.20 (m, 2H, 2×H of fluorophenyl), 7.17-7.08 (m, 2H, 2×H of fluorophenyl), 6.87 (broad s, 1H, H-3 of pyridine), 6.68 (d, ³*J*=6.7 Hz, 1H, H-5 of pyridine), 6.19 (dd, ³*J*=17.1, 10.1 Hz, 1H, CH=CH₂), 6.04 (dd, ³*J*=17.1 Hz, ²*J*=2.3 Hz, 1H, CH=CHH), 5.54 (dd, ³*J*=10.1 Hz, ²*J*=2.3 Hz, 1H, CH=CHH), 4.78-4.67 (m, 1H, C_αH), 3.82-3.34 (m, 10H, 4×CH₂ of piperazine/CH₂-fluorophenyl), 3.18-3.02 (m, 2H, C_εH₂), 2.40 (s, 3H, CH₃), 1.72-1.60 (m, 1H, C_βH), 1.60-1.49 (m, 1H, C_βH), 1.49-1.36 (m, 2H, C_δH₂), 1.35-1.19 (m, 2H, C_γH₂); **¹³C-NMR** (DMSO-*d*₆) δ=170.10 (CON), 168.78 (C_αCON), 164.43 (CON_ε), 160.54 (d, ¹*J*_{C,F}=244.3 Hz, C-2 of fluorophenyl), 158.04 (psd, ²*J*_{C,F}=35.4 Hz, C-1 of TFA), 131.86 (CH₂=C), 131.72 (d, ³*J*_{C,F}=4.5 Hz, CH of fluorophenyl), 128.55 (d, ³*J*_{C,F}=8.1 Hz, CH of fluorophenyl), 124.78 (CH₂=C), 124.10 (d, ⁴*J*_{C,F}=3.5 Hz, C-5 of fluorophenyl), 123.25 (d, ²*J*_{C,F}=15.9 Hz, C-1 of fluorophenyl), 114.95 (d, ²*J*_{C,F}=21.7 Hz, C-3 of fluorophenyl), 112.70, 48.29 (C_α), 45.40 (CH₂ of piperazine), 45.01 (CH₂ of piperazine), 44.13 (CH₂ of piperazine), 40.95 (CH₂ of piperazine), 38.29 (C_ε), 34.88 (CH₂-fluorophenyl), 31.27 (C_β), 28.85 (C_δ), 22.56 (C_γ), signals for CH₃ and C-2,3,4,6 of pyridine are not visible; **¹⁹F-NMR** (DMSO-*d*₆) δ= -74.48 (s, TFA), -117.26– -117.36 (m, F-2); MS (ESI⁺): *m/z* calculated for C₂₇H₃₅FN₅O₃: 496.27 [M+H]⁺, found: 496.4.

***N*^α-3-Fluorophenylacetyl-*N*^ε-acryloyl-L-lysine-4-(6-methylpyridin-2-yl)piperazide×TFA
(15g)**



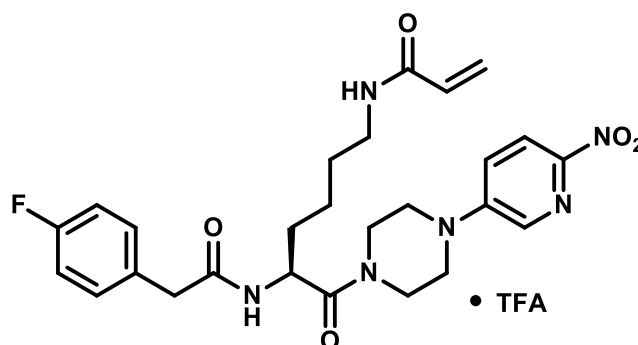
Compound **15g** (14 mg, 38%, colourless solid) was synthesised according to **GP IX** using compound **5a** (0.06 mmol) and 3-fluorophenylacetic acid. **¹H-NMR** (DMSO-*d*₆) δ=8.45 (d, ³*J*=8.1 Hz, 1H, N₆H), 8.05 (t, ³*J*=5.5 Hz, 1H, N₆H), 7.66-7.58 (m, 1H, H-4 of pyridine), 7.34-7.28 (m, Hz, 1H, H-5 of fluorophenyl), 7.13-7.06 (m, 2H, H-2,6 of fluorophenyl), 7.05-6.95 (m, 1H, H-4 of fluorophenyl), 6.87-6.76 (m, 1H, H-3 of pyridine), 6.66 (d, ³*J*=7.2 Hz, 1H, H-5 of pyridine), 6.18 (dd, ³*J*=17.1, 10.1 Hz, 1H, CH=CH₂), 6.03 (dd, ³*J*=17.1 Hz, ²*J*=2.3 Hz, 1H, CH=CH₂), 5.54 (dd, ³*J*=10.1 Hz, ²*J*=2.3 Hz, 1H, CH=CH₂), 4.77-4.65 (m, 1H, C_αH), 3.72-3.34 (m, 10H, 4×CH₂ of piperazine, CH₂-fluorophenyl), 3.19-3.03 (m, 2H, C_εH₂), 2.38 (s, 3H, CH₃), 1.71-1.60 (m, 1H, C_βHH), 1.59-1.48 (m, 1H, C_βHH), 1.47-1.33 (m, 2H, C_δH₂), 1.31-1.13 (m, 2H, C_γH₂); **¹³C-NMR** (DMSO-*d*₆) δ=170.05, 169.26, 164.40 (C_αCON, CON_α, CON_ε), 161.95 (d, ¹*J*_{C,F}=242.9 Hz, C-3 of fluorophenyl), 139.09 (d, ³*J*_{C,F}=7.8 Hz, C-1 of fluorophenyl), 131.83 (CH₂=C), 129.95 (d, ³*J*_{C,F}=8.5 Hz, C-5 of fluorophenyl), 125.11 (d, ⁴*J*_{C,F}=2.6 Hz, C-6 of fluorophenyl), 124.77 (CH₂=C), 115.69 (d, ²*J*_{C,F}=21.3 Hz, C-2 of fluorophenyl), 113.11 (d, ²*J*_{C,F}=20.7 Hz, C-4 of fluorophenyl), 112.66 (C-5 of pyridine), 48.21 (C_α), 45.29 (CH₂ of piperazine), 44.89 (CH₂ of piperazine), 44.14 (CH₂ of piperazine), 41.47 (CH₂-fluorophenyl), 40.97 (CH₂ of piperazine), 38.25 (C_ε), 31.26 (C_β), 28.80 (C_δ), 22.56(C_γ), signals for CH₃ and C-3,4 are not visible; **¹⁹F-NMR** (DMSO-*d*₆) δ= -74.30 (s, TFA), -113.86– -113.96 (m, F-3); MS (ESI⁺): *m/z* calculated for C₂₇H₃₅FN₅O₃: 496.27 [M+H]⁺, found: 496.4.

***N*^α-Phenylcarbamoyl-*N*^ε-acryloyl-L-lysine-4-(6-nitropyridin-3-yl)piperazide×TFA (17a)**



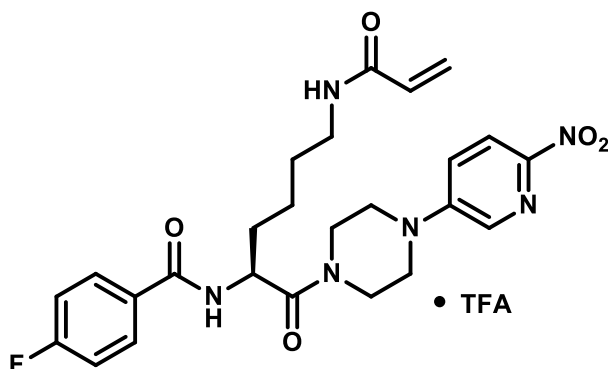
Compound **17a** (72 mg, 86%, yellow solid) was synthesised according to **GP VIII** using compound **5b** (0.16 mmol) and phenyl isocyanate. **¹H-NMR** (DMSO-*d*₆) δ=8.66 (s, 1H, NH-phenyl), 8.26 (d, ⁴*J*=3.0 Hz, 1H, H-2 of pyridine), 8.18 (d, ³*J*=9.2 Hz, 1H, H-5 of pyridine), 8.05 (t, ³*J*=5.6 Hz, 1H, N_HH), 7.48 (dd, ³*J*=9.3 Hz, ²*J*=3.1 Hz, 1H, H-4 of pyridine), 7.36 (dd, ³*J*=8.6 Hz, ⁴*J*=1.1 Hz, 2H, H-2,6 of phenyl), 7.26–7.14 (m, 2H, H-3,5 of phenyl), 6.92–6.87 (m, 1H, H-4 of phenyl), 6.50 (d, *J*=8.3 Hz, 1H, N_αH), 6.18 (dd, ³*J*=17.1, 10.1 Hz, 1H, CH=CH₂), 6.02 (dd, ³*J*=17.1 Hz, ²*J*=2.3 Hz, 1H, C=CHH), 5.54 (dd, ³*J*=10.1 Hz, ²*J*=2.3 Hz, 1H, C=CHH), 4.76–4.69 (m, 1H, C_αH), 3.82–3.51 (m, 8H, 4×CH₂ of piperazine), 3.16–3.07 (m, 2H, C_εH₂), 1.72–1.60 (m, 1H, C_βHH), 1.57–1.39 (m, 3H, C_βHH, C_δH₂), 1.39–1.26 (m, 2H, C_γH₂); **¹³C-NMR** (DMSO-*d*₆) δ=170.89 (CON), 164.41 (CON_ε), 154.65 (CON_α), 149.43, 146.85, 140.21, 133.52, 131.83 (CH₂=C), 128.66 (C-3,5 of phenyl), 124.76 (CH₂=C), 121.16, 120.63, 119.80, 117.52 (C-2,6 of phenyl), 48.38 (C_α), 46.03 (CH₂ of piperazine), 45.59 (CH₂ of piperazine), 43.98 (CH₂ of piperazine), 40.75 (CH₂ of piperazine), 38.29 (C_ε), 32.25 (C_β), 28.87 (C_δ), 22.32 (C_γ); **¹⁹F-NMR** (DMSO-*d*₆) δ= -74.82 (s, TFA); MS (ESI⁺): *m/z* calculated for C₂₅H₃₂N₇O₅: 510.25 [M+H]⁺, found: 510.1.

***N*^α-4-Fluorophenylacetyl-*N*^ε-acryloyl-L-lysine-4-(6-nitropyridin-3-yl)piperazide×TFA
(17b)**



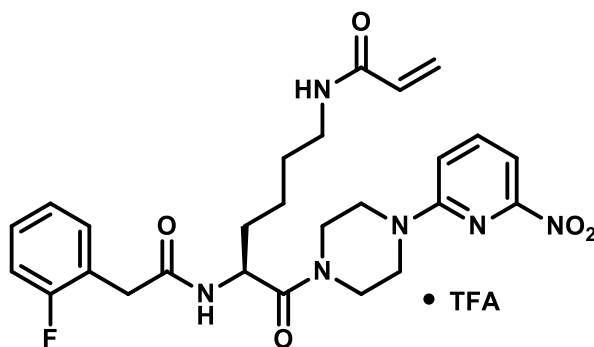
Compound **17b** (15 mg, 38%, yellow solid) was synthesised according to **GP IX** using compound **5b** (0.06 mmol) and 4-fluorophenyl acetic acid. **¹H-NMR** (DMSO-*d*₆) δ=8.42 (d, ³*J*=8.2 Hz, 1H, N_H), 8.23 (d, ⁴*J*=3.0 Hz, 1H, H-2 of pyridine), 8.17 (d, ³*J*=9.2 Hz, 1H, H-5 of pyridine), 8.03 (t, ³*J*=5.6 Hz, 1H, N_H), 7.45 (dd, ³*J*=9.3 Hz, ⁴*J*=3.0 Hz, 1H, H-4 of pyridine), 7.32–7.25 (m, 2H, H-2,6 of fluorophenyl), 7.12–7.05 (m, 2H, H-3,5 of fluorophenyl), 6.18 (dd, ³*J*=17.1, 10.1 Hz, 1H, CH=CH₂), 6.03 (dd, ³*J*=17.1 Hz, ²*J*=2.3 Hz, 1H, C=CHH), 5.54 (dd, ³*J*=10.1 Hz, ²*J*=2.3 Hz, 1H, C=CHH), 4.74–4.66 (m, 1H, C_αH), 3.76–3.29 (m, 10H, 4×CH₂ of piperazine, CH₂-fluorophenyl), 3.12–3.03 (m, 2H, C_εH₂), 1.72–1.59 (m, 1H, C_βHH), 1.59–1.47 (m, 1H, C_βHH), 1.46–1.34 (m, 2H, C_δH₂), 1.31–1.18 (m, 2H, C_γH₂); **¹³C-NMR** (DMSO-*d*₆) δ=170.08, 169.68, 164.39, 160.96 (d, ¹*J*_{C,F}=241.9 Hz, C-4 of fluorophenyl), 149.43, 146.87, 133.51 (C-2 of pyridine), 132.49 (d, ⁴*J*_{C,F}=3.0 Hz, C-1 of fluorophenyl), 131.84 (CH₂=C), 130.74 (d, ³*J*_{C,F}=7.9 Hz, C-2,6 of fluorophenyl), 124.75 (CH₂=C), 120.62 (C-4 of pyridine), 119.75 (C-5 of pyridine), 114.84 (d, ²*J*_{C,F}=21.1 Hz, C-3,5 of fluorophenyl), 48.10 (C_α), 45.96 (CH₂ of piperazine), 45.58 (CH₂ of piperazine), 43.89 (CH₂ of piperazine), 40.95 (CH₂-fluorophenyl), 40.76 (CH₂ of piperazine), 38.26 (C_ε), 31.26 (C_β), 28.82 (C_δ), 22.57 (C_γ); **¹⁹F-NMR** (DMSO-*d*₆) δ= -74.70 (s, TFA), -116.79– -116.88 (m, F-4); MS (ESI⁺): *m/z* calculated for C₂₆H₃₂FN₆O₅: 527.24 [M+H]⁺, found: 527.2.

***N*^α-4-Fluorobenzoyl-*N*^ε-acryloyl-L-lysine-4-(6-nitropyridin-3-yl)piperazide·TFA (17c)**



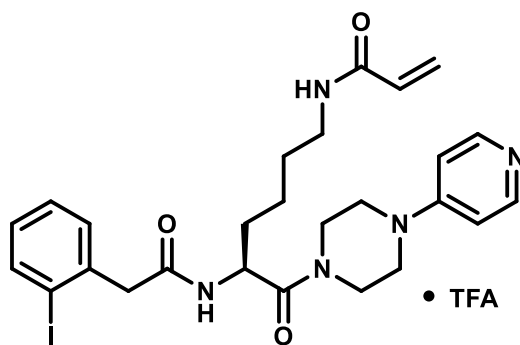
Compound **17c** (22 mg, 55%, yellow solid) was synthesised according to **GP VIII** using compound **5b** (0.06 mmol) and 4-fluorobenzoyl chloride. **¹H-NMR** (DMSO-*d*₆) δ=8.67 (d, ³*J*=7.8 Hz, 1H, N_H), 8.26 (d, ⁴*J*=3.0 Hz, 1H, H-2 of pyridine), 8.17 (d, ³*J*=9.2 Hz, 1H, H-5 of pyridine), 8.06 (t, ³*J*=5.6 Hz, 1H, N_H), 8.00–7.94 (m, 2H, H-2,6 of fluorophenyl), 7.48 (dd, ³*J*=9.3 Hz, ⁴*J*=3.1 Hz, 1H, H-4 of pyridine), 7.33–7.25 (m, 2H, H-3,5 of fluorophenyl), 6.18 (dd, ³*J*=17.1, 10.1 Hz, 1H, CH=CH₂), 6.03 (dd, ³*J*=17.1 Hz, ²*J*=2.3 Hz, 1H, C=CHH), 5.53 (dd, ³*J*=10.1 Hz, ²*J*=2.3 Hz, 1H, C=CHH), 4.94–4.84 (m, 1H, C_αH), 3.87–3.46 (m, 8H, 4×CH₂ of piperazine), 3.16–3.07 (m, 2H, C_εH₂), 1.79–1.67 (m, 2H, C_βH₂), 1.51–1.28 (m, 4H, C_γH₂, C_δH₂); **¹³C-NMR** (DMSO-*d*₆) δ=170.27, 165.12, 164.43, 163.93 (d, ¹*J*_{C,F}=248.8 Hz, C-4 of fluorophenyl), 149.45, 146.83, 133.51 (C-2 of pyridine), 131.84 (CH₂=C), 130.31 (d, ⁴*J*_{C,F}=2.9 Hz, C-1 of fluorophenyl), 130.18 (d, ³*J*_{C,F}=9.0 Hz, C-2,6 of fluorophenyl), 124.76 (CH₂=C), 120.59 (C-4 of pyridine), 119.79 (C-5 of pyridine), 115.12 (d, ²*J*_{C,F}=21.7 Hz, C-3,5 of fluorophenyl), 49.26 (C_α), 46.03 (CH₂ of piperazine), 45.63 (CH₂ of piperazine), 43.99 (CH₂ of piperazine), 40.85 (CH₂ of piperazine), 38.27 (C_ε), 30.75 (C_β), 28.89 (C_δ), 22.95 (C_γ); **¹⁹F-NMR** (DMSO-*d*₆) δ= -74.70 (s, TFA), -109.28 (tt, ³*J*_{H,F}=8.8 Hz, ⁴*J*_{H,F}=5.5 Hz, F-4); **MS** (ESI⁺): *m/z* calculated for C₂₅H₃₀FN₆O₅: 513.23 [M+H]⁺, found: 513.2.

***N*^α-2-Fluorophenylacetyl-*N*^ε-acryloyl-L-lysine-4-(6-nitropyridin-2-yl)piperazide×TFA (18)**



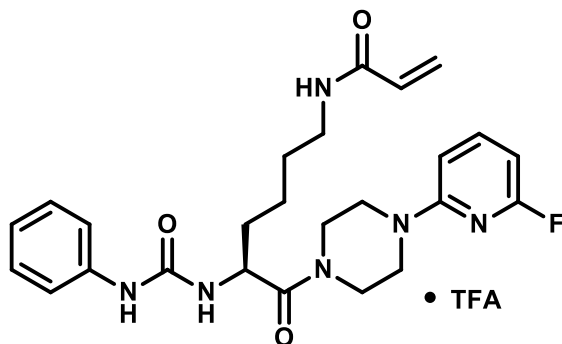
Compound **18** (27 mg, 86%, yellow solid) was synthesised according to **GP IX** using compound **5m** (0.05 mmol) and 2-fluorophenylacetic acid. ¹H-NMR (DMSO-*d*₆) δ=8.41 (d, ³*J*=8.1 Hz, 1H, N_δH), 8.04 (t, ³*J*=5.6 Hz, 1H, N_εH), 7.91 (dd, ³*J*=8.5, 7.6 Hz, 1H, H-4 of pyridine), 7.49 (d, ³*J*=7.5 Hz, 1H, H-5 of pyridine), 7.36-7.21 (m, 3H, H-3 of pyridine, 2×CH of fluorophenyl), 7.16-7.06 (m, 2H, 2×CH of fluorophenyl), 6.18 (dd, ³*J*=17.1, 10.1 Hz, 1H, CH=CH₂), 6.03 (dd, ³*J*=17.1 Hz, ²*J*=2.3 Hz, 1H, CH=CHH), 5.53 (dd, ³*J*=10.1 Hz, ²*J*=2.3 Hz, 1H, CH=CHH), 4.77-4.69 (m, 1H, C_αH), 3.72-3.48 (m, 10H, 4×CH₂ of piperazine, CH₂-fluorophenyl), 3.14-3.05 (m, 2H, C_εH₂), 1.73-1.61 (m, 1H, C_βHH), 1.60-1.50 (m, 1H, C_βHH), 1.48-1.37 (m, 2H, C_δH₂), 1.33-1.23 (m, 2H, C_γH₂); ¹³C-NMR (DMSO-*d*₆) δ=170.04, 168.74, 164.40 (C_αCON, CON_α, CON_ε), 160.52 (d, ¹*J*_{C,F}=244.2 Hz, C-2 of fluorophenyl), 157.23, 155.22, 141.03 (C-4 of pyridine), 131.85 (CH=CH₂), 131.71 (d, ⁴*J*_{C,F}=4.5 Hz, CH of fluorophenyl), 128.51 (d, ³*J*_{C,F}=8.1 Hz, CH of fluorophenyl), 124.73 (CH=CH₂), 124.08 (d, ³*J*=3.5 Hz, CH of fluorophenyl), 123.24 (d, ²*J*_{C,F}=16.0 Hz, C-1 of fluorophenyl), 114.92 (d, ²*J*_{C,F}=21.7 Hz, C-3 of fluorophenyl), 113.12 (C-3 of pyridine), 105.61 (C-5 of pyridine), 48.30 (C_αH), 44.42 (CH₂ of piperazine), 44.23 (CH₂ of piperazine), 43.99 (CH₂ of piperazine), 41.01 (CH₂ of piperazine), 38.28 (C_ε), 34.87 (CH₂-fluorophenyl), 31.31 (C_β), 28.82 (C_δ), 22.56 (C_γ); ¹⁹F-NMR (DMSO-*d*₆) δ= -74.84 (s, TFA), -117.25– -117.36 (m, F-2); MS (ESI⁺): *m/z* calculated for C₂₆H₃₂FN₆O₅: 527.24 [M+H]⁺, found: 527.3.

***N*^α-2-Iodophenylacetyl-*N*^ε-acryloyl-L-lysine-4-(pyridin-4-yl)piperazide×TFA (19)**



Compound **19** (64 mg, 63%, colourless oil) was synthesised according to **GP IX** using compound **5t** (0.14 mmol) and 2-iodophenylacetic acid. ¹H-NMR (CDCl₃) δ=8.31 (d, ³J=5.4 Hz, 2H, H-2,6 of pyridine), 7.86 (d, ³J=7.9 Hz, 1H, H of iodophenyl), 7.40–7.30 (m, 2H, 2×H of iodophenyl), 7.05–6.98 (m, 1H, H of iodophenyl), 6.88 (broad s, 2H, H-3,5 of pyridine), 6.56 (d, ³J=7.8 Hz, 1H, N_αH), 6.24 (d, ³J=16.8 Hz, 1H, CH=CHH), 6.16–6.03 (m, 2H, N_εH, CH=CH₂), 5.66 (d, ³J=10.2 Hz, 1H, CH=CHH), 4.93 (broad s, 1H, C_αH), 4.06–3.58 (m, 10H, 4×CH₂ of piperazine, CH₂-iodophenyl), 3.46–3.19 (m, 2H, C_εH₂), 1.80–1.21 (m, 6H, C_βH₂, C_γH₂, C_δH₂); MS (ESI⁺): m/z calculated for C₂₆H₃₃IN₅O₃: 590.16 [M+H]⁺, found: 590.3.

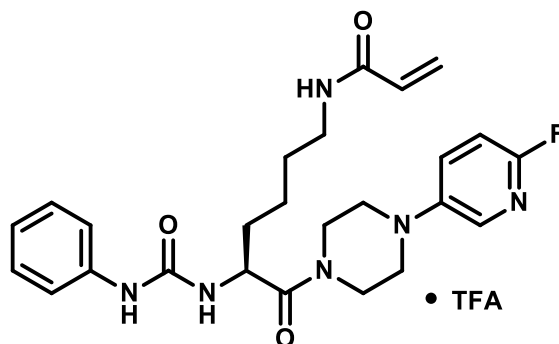
***N*^α-Phenylcarbamoyl-*N*^ε-acryloyl-L-lysine-4-(6-fluoropyridin-2-yl)piperazide×TFA (20a)**



Compound **20a** (49 mg, 49%, white solid) was synthesised according to **GP VIII** using compound **5d** (0.21 mmol) and phenyl isocyanate. ¹H-NMR (DMSO-*d*₆) δ=8.68 (s, NH-phenyl), 8.66 (s, 1H, NH-phenyl), 8.04 (t, ³J=5.5 Hz, 1H, N_εH), 7.70 (ps-q, J=8.3 Hz, 1H, H-4 of pyridine), 7.45 (dd, ³J=8.6 Hz, ²J=1.1 Hz, H-2,6 of phenyl), 7.36 (dd, ³J=8.6 Hz, ⁴J=1.1 Hz, H-2,6 of phenyl), 7.30–7.25 (m, 1H, H-3,5 of phenyl), 7.24–7.17 (m, 2H, H-3,5 of phenyl), 6.99–6.94 (m, H-4 of phenyl), 6.92–6.86 (m, H-4 of phenyl), 6.70 (dd, ³J_{H,H}=8.3 Hz, ⁵J_{H,F}=2.6 Hz, 1 H, H-3 of pyridine), 6.49 (d, ³J=8.3 Hz, 1H, N_αH), 6.31 (dd, ³J_{H,H}=7.7 Hz, ³J_{H,F}=2.7 Hz, H-5 of pyridine), 6.18 (dd, ³J=17.1, 10.1 Hz, 1H, CH=CH₂), 6.02 (dd, ³J=17.1 Hz, ²J=2.3 Hz, 1H, C=CHH), 5.51 (dd, ³J=10.1 Hz, ²J=2.3 Hz, 1H, C=CHH), 4.76–4.69 (m, 1H,

C_αH), 3.73–3.42 (m, 8H, 4×CH₂ of piperazine), 3.15–3.04 (m, 2H, C_εH₂), 1.71–1.58 (m, 1H, C_βHH), 1.56–1.37 (m, 3H, C_βHH, C_δH₂), 1.39–1.19 (m, 2H, C_γH₂), signals for H-2,3,4,5,6 and NH-phenyl appear in duplicate, probably due to potential atropisomers which originate from the hindered rotation around the N-phenyl bond⁵¹⁻⁵²; ¹³C-NMR (DMSO-*d*₆) δ=170.73 (CON), 164.40 (CON_ε), 161.96 (d, ¹J_{C,F}=233.4 Hz, C-6 of pyridine), 157.65 (d, ³J_{C,F}=15.8 Hz, C-2 of pyridine), 154.63 (CON_α), 142.71 (d, ⁴J_{C,F}=8.2 Hz, C-3 of pyridine), 140.24 (C-1 of phenyl), 139.69 (C-1 of phenyl), 131.83 (CH₂=C), 128.70 (d, ³J_{C,F}=8.4 Hz, C-4 of pyridine), 128.67 (C-3,5 of phenyl), 124.72 (CH₂=C), 121.76, 121.13 (C-4 of phenyl), 118.14 (C-2,6 of phenyl), 117.50, 103.60 (d, *J*=3.8 Hz), 95.65 (d, ²J_{C,F}=37 Hz, C-5 of pyridine), 48.40 (C_α), 44.61 (CH₂ of piperazine), 44.36 (CH₂ of piperazine), 44.14 (CH₂ of piperazine), 41.00 (CH₂ of piperazine), 38.29 (C_ε), 32.33 (C_β), 28.84 (C_δ), 22.28 (C_γ); ¹⁹F-NMR (DMSO-*d*₆) δ= -68.86 (d, ³J_{H,F}=9.0 Hz, F-6), -74.61 (s, TFA); MS (ESI⁺): *m/z* calculated for C₂₅H₃₂FN₆O₃: 483.25 [M+H]⁺, found: 483.1.

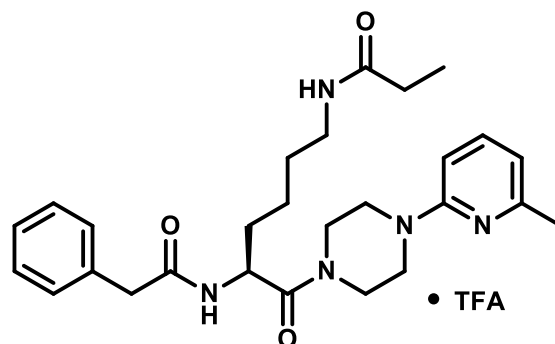
N^ε-Phenylcarbamoyl-N^ε-acryloyl-L-lysine-4-(6-fluoropyridin-3-yl)piperazide×TFA (20b)



Compound **20b** (79 mg, 67%, yellow solid) was synthesised according to **GP VIII** using compound **5j** (0.20 mmol) and phenyl isocyanate. ¹H-NMR (DMSO-*d*₆) δ=8.67 (s, 1H, NH-phenyl), 8.04 (t, ³J=5.6 Hz, 1H, N_εH), 7.85 (dd, ⁴J_{H,H}=2.8 Hz, ⁵J_{H,H}=1.7 Hz, 1H, H-2 of pyridine), 7.63 (ddd, ³J_{H,H}=9.1 Hz, ⁴J_{H,F}=7.1 Hz, ⁴J_{H,H}=3.2 Hz, 1H, H-4 of pyridine), 7.36 (dd, ³J=8.6 Hz, ⁴J=1.0 Hz, 2H, H-2,6 of phenyl), 7.26–7.17 (m, 2H, H-3,5 of phenyl), 7.05 (dd, ³J_{H,H}=9.0 Hz, ³J_{H,F}=3.5 Hz, 1H, H-5 of pyridine), 6.89 (t, ³J=7.3 Hz, 1H, H-4 of phenyl), 6.48 (d, ³J=8.4 Hz, 1H, N_αH), 6.17 (dd, ³J=17.1, 10.1 Hz, 1H, CH=CH₂), 6.02 (dd, ³J=17.1 Hz, ²J=2.3 Hz, 1H, C=CHH), 5.52 (dd, ³J=10.1 Hz, ²J=2.3 Hz, 1H, C=CHH), 4.77–4.68 (m, 1H, C_αH), 3.99–3.45 (m, 6H, 2×CH₂ of piperazine, CH₂-phenyl), 3.23–3.05 (m, 6H, 2×CH₂ of piperazine, C_εH₂), 1.71–1.57 (m, 1H, C_βHH), 1.56–1.38 (m, 3H, C_βHH, C_δH₂), 1.37–1.26 (m, 2H, C_γH₂); ¹³C-NMR (DMSO-*d*₆) δ=170.55 (CON), 164.41 (CON_ε), 156.94 (d, ¹J_{C,F}=228.5 Hz, C-6 of pyridine), 154.63 (CON_α), 145.30 (d, ⁴J_{C,F}=3.9 Hz, C-3 of pyridine), 140.23 (C-1 of phenyl), 134.08 (d, ³J_{C,F}=15.2 Hz, C-2 of pyridine), 131.84 (CH₂=C), 129.69 (d, ³J_{C,F}=7.4 Hz, C-4 of pyridine), 128.67 (C-3,5 of phenyl), 124.75 (CH₂=C), 121.15 (C-4 of phenyl), 117.51 (C-2,6

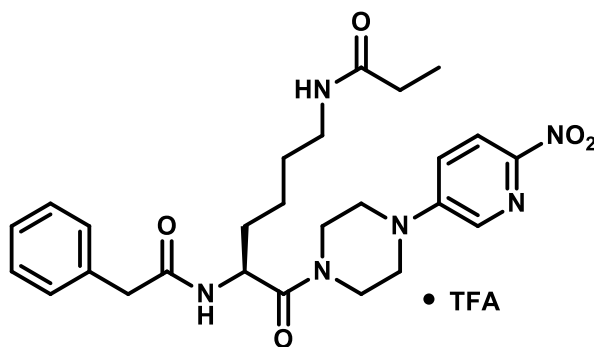
of phenyl), 109.09 (d, $^2J_{C,F}=39.6$ Hz, C-5 of pyridine), 48.90 (CH₂ of piperazine), 48.41 (CH₂ CH₂ of piperazine), 48.31 (C_α), 44.62 (CH₂ CH₂ of piperazine), 41.10 (CH₂ CH₂ of piperazine), 38.31 (C_ε), 32.36 (C_β), 28.86 (C_δ), 22.32 (C_γ); **¹⁹F-NMR** (DMSO-*d*₆) δ= -80.10 (s, F-6), -74.48 (s, TFA); MS (ESI⁺): m/z calculated for C₂₅H₃₂FN₆O₃: 483.25 [M+H]⁺, found: 483.1.

N^α-Phenylacetyl-N^ε-propionyl-L-lysine-4-(6-methylpyridin-2-yl)piperazide×TFA (21a)



Compound **21a** (5 mg, 4%, colourless solid) was synthesised according to **GP VIII** using compound **5z** (0.17 mmol) and phenylacetyl chloride. **¹H-NMR** (DMSO-*d*₆) δ=7.80 (t, $^3J=7.8$ Hz, 1H, H-4 of pyridine), 7.37-7.20 (m, 4H, H-2,3,5,6 of phenyl), 6.98 (d, $^3J=5.6$ Hz, 1H, N_αH), 6.82 (d, $^3J=8.5$ Hz, 1H, H-3 of pyridine), 6.71 (d, $^3J=7.0$ Hz, 1H, H-5 of pyridine), 6.60 (s, 1H, N_εH), 4.93-4.78 (m, 1H, C_αH), 4.04-3.49 (m, 10H, 4×CH₂ of piperazine, CH₂-phenyl), 3.26-3.10 (m, 2H, C_εH₂), 2.60 (s, 3H, -CH₃), 2.26-2.14 (m, 2H, -CH₂-CH₃), 1.77-1.42 (m, 4H, C_βH₂, C_δH₂), 1.38-1.23 (m, 2H, C_γH₂), 1.11 (t, $^3J = 7.3$ Hz, 3H, -CH₂-CH₃); **¹³C-NMR** (DMSO-*d*₆) δ=175.65, 171.67, 170.90 (C_αCON, CON_α, CON_ε), 153.59, 150.82, 144.46 (C-4 of pyridine), 134.68, 129.35 (2×CH of phenyl), 128.96 (2×CH of phenyl), 127.42 (C-4 of phenyl), 114.17 (C-5 of pyridine), 109.32 (C-3 of pyridine), 48.89 (C_α), 46.90 (CH₂ of piperazine), 46.61 (CH₂ of piperazine), 44.31 (CH₂ of piperazine), 43.31 (CH₂-phenyl), 41.17 (CH₂ of piperazine), 39.14 (C_ε), 32.13 (C_β), 29.44 (-CH₂-CH₃), 28.67 (C_δ), 22.33 (C_γ), 19.50 (-CH₃), 10.11 (-CH₂-CH₃); **¹⁹F-NMR** (DMSO-*d*₆) δ= -75.89 (s, TFA); MS (ESI⁺): m/z calculated for C₂₇H₃₈N₅O₃: 483.30 [M+H]⁺, found: 480.3.

***N*^α-Phenylacetyl-*N*^ε-propionyl-L-lysine-4-(6-nitropyridin-3-yl)piperazide×TFA (21b)**



Compound **21b** (75 mg, 41%, yellow solid) was synthesised according to **GP VIII** using compound **5aa** (0.28 mmol) and phenylacetyl chloride. **¹H-NMR** (DMSO-*d*₆) δ=8.40 (d, ³*J*=8.3 Hz, 1H, N_αH), 8.22 (d, ⁴*J*=3.0 Hz, 1H, H-2 of pyridine), 8.17 (d, ³*J*=9.2 Hz, 1H, H-5 of pyridine), 7.67 (t, ³*J*=5.4 Hz, 1H, N_εH), 7.44 (dd, ³*J*=9.3 Hz, ⁴*J*=3.1 Hz, 1H, H-4 of pyridine), 7.28-7.24 (m, 4H, H-2,3,5,6 of phenyl), 7.19-7.14 (m, 1H, H-4 of phenyl), 4.73-4.65 (m, 1H, C_αH), 3.76-3.28 (m, 10H, 4×CH₂ of piperazine, CH₂-phenyl), 3.02-2.92 (m, 2H, C_εH₂), 2.03 (q, ³*J*=7.6 Hz, 2H, -CH₂-CH₃), 1.71-1.59 (m, 1H, C_βHH), 1.58-1.45 (m, 1H, C_βHH), 1.41-1.30 (m, 2H, C_δH₂), 1.29-1.17 (m, 2H, C_γH₂), 0.96 (t, ³*J* = 7.6 Hz, 3H, -CH₂-CH₃); **¹³C-NMR** (DMSO-*d*₆) δ=172.58, 170.11, 169.77 (C_αCON, CON_α, CON_ε), 149.42 (C-6 of pyridine), 146.86 (C-3 of pyridine), 136.35 (C-1 of phenyl), 128.94 (2×CH of phenyl), 128.12 (2×CH of phenyl), 126.29 (C-4 of phenyl), 120.63 (C-4 of pyridine), 119.77 (C-5 of pyridine), 48.11 (C_α), 45.95 (CH₂ of piperazine), 45.60 (CH₂ of piperazine), 43.87 (CH₂ of piperazine), 41.94 (CH₂-phenyl), 40.77 (CH₂ of piperazine), 38.14 (C_ε), 31.29 (C_β), 28.96 (C_δ), 28.48 (-CH₂-CH₃), 22.53 (C_γ), 9.97 (-CH₂-CH₃); **¹⁹F-NMR** (DMSO-*d*₆) δ= -74.73 (s, TFA); MS (ESI⁺): *m/z* calculated for C₂₆H₃₅N₆O₅: 511.27 [M+H]⁺, found: 511.2.

References

- (1) Edman, P. Method for Determination of the Amino Acid Sequence in Peptides. *Acta Chem. Scand.* **1950**, *4*, 283-293.
- (2) Edman, P. On the Mechanism of the Phenyl Isothiocyanate Degradation of Peptides. *Acta Chem. Scand.* **1956**, *10*, 761-768.
- (3) Rulev, A. Y. Aza-Michael reaction: achievements and prospects. *Russ. Chem. Rev.* **2011**, *80*, 197-218.
- (4) Bharatam, P. V.; Amita, A. G.; Kaur, D. Theoretical studies on S-N interactions in sulfonamides. *Tetrahedron* **2002**, *58*, 1759-1764.
- (5) Baldauf, C.; Günther, R.; Hofmann, H.-J. Conformational properties of sulfonamido peptides. *J. Mol. Struct. (THEOCHEM)* **2004**, *675*, 19-28.
- (6) Nyasse, B.; Grehn, L.; Ragnarsson, U.; Maia, H. L. S.; Monteiro, L. S.; Leito, I.; Koppel, I.; Koppel, J. Synthesis and cathodic cleavage of a set of substituted benzene-sulfonamides including the corresponding tert-butyl sulfonyl-carbamates: pKa of sulfonamides. *J. Chem. Soc., Perkin Trans. 1* **1995**, 2025-2031.
- (7) Gennari, C.; Longari, C.; Ressel, S.; Salom, B.; Mielgo, A. Synthesis of chiral vinylogous sulfonamidopeptides (vs-peptides). *Eur. J. Org. Chem.* **1998**, 945-959.
- (8) Vaidyanathan, G.; Zalutsky, M. R. Preparation of N-succinimidyl 3-[¹²⁵I]iodobenzoate: an agent for the indirect radioiodination of proteins. *Nat. Protoc.* **2006**, *1*, 707-713.
- (9) Hauser, C.; Wodtke, R.; Löser, R.; Pietsch, M. A fluorescence anisotropy-based assay for determining the activity of tissue transglutaminase. *Amino Acids* **2017**, *49*, 567-583.
- (10) Schrödinger Release 2015-2016: Maestro, S., LLC, New York, NY, 2015-2016.
- (11) Accelrys Software Inc., D. S. M. E., Release 3.5, San Diego: Accelrys Software Inc. 2012.
- (12) Hansch, C.; Leo, A.; Hoekman, D., *Exploring QSAR: Hydrophobic, Electronic, and Steric Constants*, American Chemical Society, USA, **1995**, pp. 217-304.
- (13) Charton, M. Steric Effects. I. Esterification and Acid-Catalyzed Hydrolysis of Esters. *J. Am. Chem. Soc.* **1975**, *97*, 1552-1555.
- (14) Scheler, W., *Grundlagen der allgemeinen Pharmakologie*, VEB Gustav Fischer Verlag, Jena, **1989**, pp. 312-334.
- (15) Hansch, C.; Leo, A., *Exploring QSAR Fundamentals and Applications in Chemistry and Biology*, American Chemical Society, USA, **1995**, pp. 69-96.
- (16) Hansch, C.; Leo, A., *Exploring QSAR Fundamentals and Applications in Chemistry and Biology*, American Chemical Society, USA, **1995**, pp. 97-124.
- (17) Wolf, S.; Haase-Kohn, C.; Lenk, J.; Hoppmann, S.; Bergmann, R.; Steinbach, J.; Pietzsch, J. Expression, purification and fluorine-18 radiolabeling of recombinant S100A4: a potential probe for molecular imaging of receptor for advanced glycation endproducts in vivo? *Amino Acids* **2011**, *41*, 809-820.
- (18) Reissenweber, B.; Mosch, B.; Pietzsch, J. Experimental hypoxia does not influence gene expression and protein synthesis of Eph receptors and ephrin ligands in human melanoma cells in vitro. *Melanoma Res.* **2013**, *23*, 85-95.
- (19) <http://www.acdlabs.com/products/percepta/predictors/logp/> (24.01.2018)
- (20) <http://www.acdlabs.com/products/percepta/predictors/pka/> (24.01.2018)
- (21) <http://www.acdlabs.com/products/percepta/predictors/logd/> (24.01.2018)
- (22) Cobas, C.; Dominguez, S.; Larin, N.; Iglesias, I.; Geadá, C.; Seoane, F.; Sordo, M.; Monje, P.; Fraga, S.; Cobas, R.; Peng, C.; Garcia, J. A.; Goebel, M.; Vaz, E., *MestReNova 6.1.1-6384*, Mestrelab Research S.L., **2010**.
- (23) Yin, J.; Buchwald, S. L. Palladium-catalyzed intermolecular coupling of aryl halides and amides. *Org. Lett.* **2000**, *2*, 1101-1104.
- (24) Bergbreiter, D. E.; Osburn, P. L.; Li, C. Soluble polymer-supported catalysts containing azo dyes. *Org. Lett.* **2002**, *4*, 737-740.
- (25) Grogna, M.; Cloots, R.; Luxen, A.; Jérôme, C.; Desreux, J.-F.; Detrembleur, C. Design and synthesis of novel DOTA(Gd3+)-polymer conjugates as potential MRI contrast agents. *J. Mater. Chem.* **2011**, *21*, 12917.
- (26) Stefanowicz, P.; Siemion, I. Z. Reactivity of N-hydroxysuccinimide esters. *Pol. J. Chem.* **1992**, *66*, 111-118.
- (27) Bonnitich, P. D.; Bayly, S. R.; Theobald, M. B.; Betts, H. M.; Lewis, J. S.; Dilworth, J. R. Nitroimidazole conjugates of bis(thiosemicarbazone)64Cu(II) - Potential combination agents for the PET imaging of hypoxia. *J. Inorg. Biochem.* **2010**, *104*, 126-135.
- (28) Wityak, J.; Prime, M. E.; Brookfield, F. A.; Courtney, S. M.; Erfan, S.; Johnsen, S.; Johnson, P. D.; Li, M.; Marston, R. W.; Reed, L.; Vaidya, D.; Schaertl, S.; Pedret-Dunn, A.; Beconi, M.; Macdonald, D.; Muñoz-Sanjuan, I.; Dominguez, C. SAR Development of Lysine-Based Irreversible Inhibitors of Transglutaminase 2 for Huntington's Disease. *ACS Med. Chem. Lett.* **2012**, *3*, 1024-1028.
- (29) *CRC Handbook of Chemistry and Physics, 84th Edition*, CRC Press, Boca Raton, **2003**, pp. 6/180-6/183.
- (30) Gattner, M. J.; Vrabel, M.; Carell, T. Synthesis of epsilon-N-propionyl-, epsilon-N-butyryl-, and epsilon-N-crotonyl-lysine containing histone H3 using the pyrrolysine system. *Chem. Commun.* **2013**, *49*, 379-381.
- (31) Pavia, M. R.; Taylor, C. P.; Lobbestael, S. J. 6-Alkyl-N,N-Disubstituted-2-Pyridinamines as Anticonvulsant Agents. *J. Med. Chem.* **1989**, *32*, 1237-1242.

- (32) Swanson, D. M.; Dubin, A. E.; Shah, C.; Nasser, N.; Chang, L.; Dax, S. L.; Jetter, M.; Breitenbucher, J. G.; Liu, C.; Mazur, C.; Lord, B.; Gonzales, L.; Hoey, K.; Rizzolio, M.; Bogenstaetter, M.; Codd, E. E.; Lee, D. H.; Zhang, S. P.; Chaplan, S. R.; Carruthers, N. I. Identification and biological evaluation of 4-(3-trifluoromethylpyridin-2-yl)piperazine-1-carboxylic acid (5-trifluoromethylpyridin-2-yl)amide, a high affinity TRPV1 (VR1) vanilloid receptor antagonist. *J. Med. Chem.* **2005**, *48*, 1857-1872.
- (33) Sashuk, V.; Schoeps, D.; Plenio, H. Fluorophore tagged cross-coupling catalysts. *Chem. Commun.* **2009**, 10.1039/b820633c 770-772.
- (34) Stauffer, S. R.; Hartwig, J. F. Fluorescence resonance energy transfer (FRET) as a high-throughput assay for coupling reactions. Arylation of amines as a case study. *J. Am. Chem. Soc.* **2003**, *125*, 6977-6985.
- (35) Prante, O.; Tietze, R.; Hocke, C.; Lober, S.; Hubner, H.; Kuwert, T.; Gmeiner, P. Synthesis, radiofluorination, and in vitro evaluation of pyrazolo[1,5-a]pyridine-based dopamine D4 receptor ligands: discovery of an inverse agonist radioligand for PET. *J. Med. Chem.* **2008**, *51*, 1800-1810.
- (36) Zulli, A. L.; Aimone, L. D.; Mathiasen, J. R.; Gruner, J. A.; Raddatz, R.; Bacon, E. R.; Hudkins, R. L. Substituted phenoxypropyl-(R)-2-methylpyrrolidine aminomethyl ketones as histamine-3 receptor inverse agonists. *Bioorg. Med. Chem. Lett.* **2012**, *22*, 2807-2810.
- (37) Verma, S. K.; Acharya, B. N.; Kaushik, M. P. Imidazole-catalyzed monoacylation of symmetrical diamines. *Org. Lett.* **2010**, *12*, 4232-4235.
- (38) Wang, L. X.; Zhou, X. B.; Xiao, M. L.; Jiang, N.; Liu, F.; Zhou, W. X.; Wang, X. K.; Zheng, Z. B.; Li, S. Synthesis and biological evaluation of substituted 4-(thiophen-2-ylmethyl)-2H-phthalazin-1-ones as potent PARP-1 inhibitors. *Bioorg. Med. Chem. Lett.* **2014**, *24*, 3739-3743.
- (39) Oh, S. J.; Lee, K. C.; Lee, S. Y.; Ryu, E. K.; Saji, H.; Choe, Y. S.; Chi, D. Y.; Kim, S. E.; Lee, J.; Kim, B. T. Synthesis and evaluation of fluorine-substituted 1H-pyrrolo[2,3-b]pyridine derivatives for dopamine D4 receptor imaging. *Bioorg. Med. Chem.* **2004**, *12*, 5505-5513.
- (40) Abdel-Magid, A. F.; Mehrman, S. J. A review on the use of sodium triacetoxyborohydride in the reductive amination of ketones and aldehydes. *Org. Process Res. Dev.* **2006**, *10*, 971-1031.
- (41) Audouze, K.; Nielsen, E. O.; Olsen, G. M.; Ahning, P.; Jorgensen, T. D.; Peters, D.; Liljefors, T.; Balle, T. New Ligands with Affinity for the $\alpha 4 \beta 2$ Subtype of Nicotinic Acetylcholine Receptors. Synthesis, Receptor Binding, and 3D-QSAR Modeling. *J. Med. Chem.* **2006**, *49*, 3159-3171.
- (42) Bach, T. B.; Jensen, A. A.; Petersen, J. G.; Sorensen, T. E.; Della Volpe, S.; Liu, J.; Blaazer, A. R.; van Muijlwijk-Koezen, J. E.; Balle, T.; Frolund, B. Exploration of the molecular architecture of the orthosteric binding site in the $\alpha 4 \beta 2$ nicotinic acetylcholine receptor with analogs of 3-(dimethylamino)butyl dimethylcarbamate (DMABC) and 1-(pyridin-3-yl)-1,4-diazepane. *Eur. J. Med. Chem.* **2015**, *102*, 425-444.
- (43) Keenan, M.; Chaplin, J. H.; Alexander, P. W.; Abbott, M. J.; Best, W. M.; Khong, A.; Botero, A.; Perez, C.; Cornwall, S.; Thompson, R. A.; White, K. L.; Shackelford, D. M.; Koltun, M.; Chiu, F. C.; Morizzi, J.; Ryan, E.; Campbell, M.; von Geldern, T. W.; Scandale, I.; Chatelain, E.; Charman, S. A. Two analogues of fenarimol show curative activity in an experimental model of Chagas disease. *J. Med. Chem.* **2013**, *56*, 10158-10170.
- (44) Grotjahn, D. B.; Lev, D. A. A general bifunctional catalyst for the anti-Markovnikov hydration of terminal alkynes to aldehydes gives enzyme-like rate and selectivity enhancements. *J. Am. Chem. Soc.* **2004**, *126*, 12232-12233.
- (45) Hintermann, L.; Xiao, L.; Labonne, A. A general and selective copper-catalyzed cross-coupling of tertiary Grignard reagents with azacyclic electrophiles. *Angew. Chem. Int. Ed. Engl.* **2008**, *47*, 8246-8250.
- (46) Henrion, G.; Chavas, T. E.; Le Goff, X.; Gagosz, F. Biarylphosphonite gold(I) complexes as superior catalysts for oxidative cyclization of propynyl arenes into indan-2-ones. *Angew. Chem. Int. Ed. Engl.* **2013**, *52*, 6277-6282.
- (47) Debien, L.; Braun, M. G.; Quiclet-Sire, B.; Zard, S. Z. Tri- and tetrasubstituted functionalized vinyl sulfides by radical allylation. *Org. Lett.* **2013**, *15*, 6250-6253.
- (48) Klapars, A.; Buchwald, S. L. Copper-catalyzed halogen exchange in aryl halides: an aromatic Finkelstein reaction. *J. Am. Chem. Soc.* **2002**, *124*, 14844-14845.
- (49) Louërât, F.; Gros, P.; Fort, Y. First selective lithiation of pyridylpiperazines: straightforward access to potent pharmacophores. *Tetrahedron* **2005**, *61*, 4761-4768.
- (50) Hesse, S.; Kirsch, G. Palladium-Catalyzed C-C Bond Formation from β -Chloroacroleins in Aqueous Media. *Synthesis* **2001**, *5*, 755-758.
- (51) Adler, T.; Bonjoch, J.; Clayden, J.; Font-Bardia, M.; Pickworth, M.; Solans, X.; Sole, D.; Vallverdu, L. Slow interconversion of enantiomeric conformers or atropisomers of anilide and urea derivatives of 2-substituted anilines. *Org. Biomol. Chem.* **2005**, *3*, 3173-3183.
- (52) Clayden, J.; Lemiegre, L.; Pickworth, M.; Jones, L. Conformation and stereodynamics of 2,2'-disubstituted N,N'-diaryl ureas. *Org. Biomol. Chem.* **2008**, *6*, 2908-2913.